CLINAM

European Foundation for Clinical Nanomedicine

14/2023

Basel, October 8 – 11

POSTER SESSION

POSTER

Amy Barton Alston

Pragmatic challenges in using in silico modeling to evaluate the pharmacokinetics of iron-carbohydrate products

Amy Alston, PharmD, MS, Beat Flühmann, PhD, Reinaldo Digigow, PhD
CSL Vifor, Glattbrugg, Switzerland

INTRODUCTION

- Intravenous iron-carbohydrate complexes are a heterogenous class of nanomedicines whose critical quality attributes (CQAs) have not been fully established.
- Despite being used in clinical practice for decades, the *in vivo* biodisposition profiles and mechanisms of biodegradation of the iron-carbohydrate complexes after uptake into the mononuclear phagocytic system are not established.
- The lack of mechanistic understanding of both plasma pharmacokinetics (PK) and tissue distribution prevents current application of physiologically-based PK (PBPK) modeling (Figure 1).
- **There are three fundamental challenges** that need to be addressed before predictive PBPK models can be developed and applied; **1)** the lack of assays to quantitatively measure the serum concentration of intact iron nanoparticles and unbound iron species. **2)** PBPK models need to include several parameters to describe iron-carbohydrate nanoparticle metabolism that are yet to be completely defined. **3)** modeling is further complicated by the lack of traditional receptor/enzyme interactions, iron is stored and released based on the individual's own iron homeostasis.
- The known parameters of bioavailability, distribution, metabolism, and excretion for iron-carbohydrate products will be reviewed and challenges that currently prevent the direct application of PBPK or other in silico modeling techniques will be discussed.

Figure 1. A general physiologically based PK model

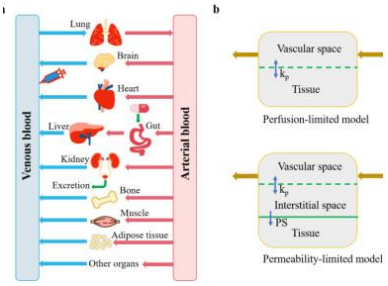

Figure 2. Hypothesized bioprocessing of iron-carbohydrate complexes

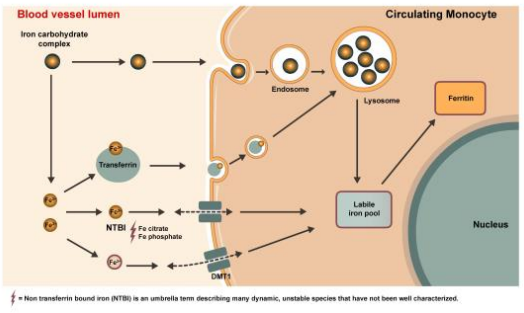

The fundamental challenge to developing PBPK models for iron-carbohydrate nanoparticles is that there is not a fully validated assay to accurately measure nanoparticle-bound iron after intravenous administration.

Click for Full-Text Article

CSL Vifor

ABSORPTION (BIOAVAILABILITY)

There is no validated method to measure nanoparticle-bound iron:

- Clinical iron indices currently used to evaluate plasma PK profiles of iron-carbohydrate products only measure the total serum iron (TI) or transferrin-bound iron (TBI).
- *These assays cannot distinguish between nanoparticle-derived iron in the serum versus endogenous iron.*

DISTRIBUTION

Serum iron concentrations do not accurately reflect of nanoparticle-bound iron biodistribution:

- Serum iron or iron carbohydrate nanoparticle concentration do not accurately represent tissue biodistribution.
- Methods to evaluate tissue biodistribution include radio-labeling the iron moiety or evaluating pre-clinical species
- *However, translation of these data to humans, is unknown.*

METABOLISM

The mechanism of biodegradation is not established for iron-carbohydrate nanoparticles:

- Intravenous iron-carbohydrate complexes do not exhibit a classical drug-enzyme interaction that facilitates the breakdown of the drug into water-soluble species for excretion.
- However, the rate and extent of the biodegradation process are specific to each unique iron-carbohydrate product specific.[1] Not all available IV iron products have detailed PK studies available.
- As **Figure 2** depicts, the iron-carbohydrate nanoparticles are opsonized by peripheral blood macrophages which is influenced by each iron-carbohydrate nanoparticle's size, morphology and surface characteristics.
- *The rate constants (k) for distribution to key pharmacological compartments are not established and therefore not available for modelling.*

EXCRETION

Iron is typically highly conserved and recycled and therefore minimal excretion is predicted after intravenous dosing:

- Excretion is not anticipated to be a key parameter in PBPK models.

Garbowski et al. 2021 https://haematologica.org/article/view/haematol.2020.250803

Anti-tumor Efficacy of PEGylated Liposomal Doxorubicin Targeted with CREKA Peptide in Murine Melanoma Model

CLINAM European Foundation for Clinical Nanomedicine

Kimia Rahmati [a], Mohammad Mashreghi [a], Mahmoud Reza Jaafari [a b c], Leila Arabi [a b]*

Mashhad University of Medical Sciences

a Nanotechnology Research Center, School of Pharmacy, Mashhad University of Medical Sciences, Mashhad, Iran
b Department of Pharmaceutical Nanotechnology, School of Pharmacy, Mashhad University of Medical Sciences, Mashhad, Iran
c Biotechnology Research Center, School of Pharmacy, Mashhad University of Medical Sciences, Mashhad, Iran
*Corresponding/ Presenting Author: leilaa.arabi@gmail.com, Arabil@mums.ac.ir

INTRODUCTION

In this study, we try to increase the therapeutic efficacy of PEGylated Liposomal Doxorubicin (PLD) formulation to melanoma tumor cells and reduce its side effects by CREKA linear pentapeptide (Cys-Arg-Glu-Lys-Ala). CREKA is a "tumor- homing peptide", which targets overexpressed fibrin and fibrin-fibronectin complexes found in tumor, vasculature stroma, and also myocardial ischemia-reperfusion and atherosclerosis (1).

STUDY DESIGN AND METHODOLOGY

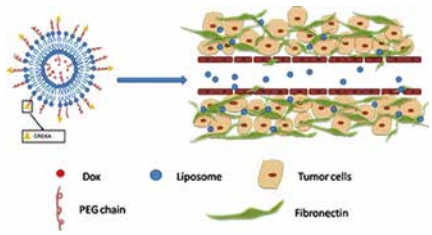

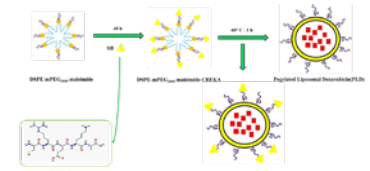

CREKA peptide was linked to DSPE-mPEG2000-maleimide phospholipid through thioether linkage. The targeted micelles with 50, 100, 200 and 400 peptide ligands, post-inserted into the preformed PLD.

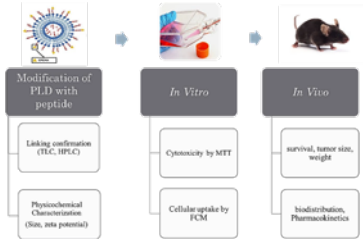

RESULTS

Characteristics of CREKA-PLD and non-targeted PLD. Each value represents Mean±SD (n = 3)

Formulation	Z-average (nm) ±SD	Zeta potential (mV)±SD	PDI±SD
PLD	89.58±19.21	-17±9.48	0.069±0.023
PLD-50	87.10±15.42	-13.5±10.3	0.169±0.0305
PLD-100	101.4±20.03	-11.4±7.07	0.17±0.037
PLD-200	97.07±16.48	-13.4±9.04	0.140±0.0045
PLD-400	105.8±27.01	-11.8±9.82	0.124±0.0452

In vitro cellular uptake of CREKA-PLD, PLD and free doxorubicin in B16F10 cell line at 4 °C (A) and at 37 °C (B). The interactions of targeted formulations with cells have not changed significantly compared to PLD (P≤0.05).

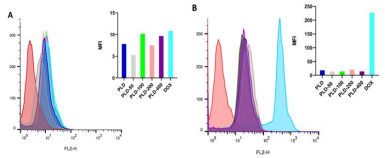

In vitro cytotoxicity effect (IC50) of CREKA-PLD, PLD, and free doxorubicin against B16F10 cells after different exposure times (3h and 6h) Data represented as µg/ml±SD (n=3). The presence of the peptide increased the toxicity of the formulations

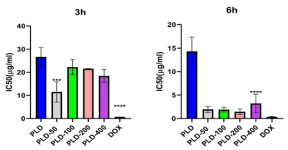

Therapeutic efficacy of CREKA-PLD, PLD in female C57BL6 mice bearing B16F10 melanoma tumor after I.v. administration of a single dose of 10 mg/kg doxorubicin on day 8 after tumor inoculation. Average tumor volume, and survival curve (n = 4, mean ± S.E.M.). CREKA-PLD treatment significantly improved the overall survivals compare to PLD (log-rank). The longest survival period, the largest decrease in tumor size and drug accumulation at the tumor site (P≤0.05) were observed in formulations with 400 ligands (PLD-400).

In animal studies (biodistribution and survival analysis) in melanoma model in C57BL/6 mice, no significant difference was observed in the distribution of targeted formulations in peripheral tissues (after 24h). However, targeted formulations with 400 ligands (PLD-44) increased drug accumulation in the tumor tissue of mice.

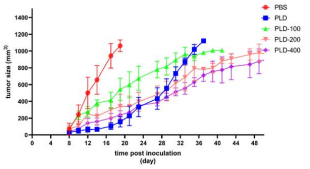

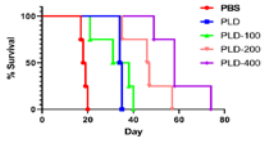

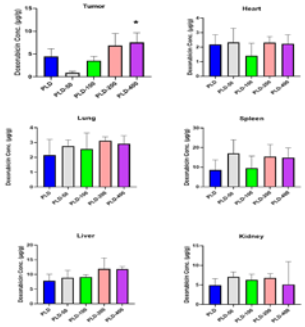

Therapeutic efficacy data of CREKA-PLD, PLD in mice bearing melanoma.

GROUPS	PBS	PLD	PLD-100	PLD-200	PLD-400
TTE (Days ± SD)	18±1.06	35±0.45	33±7.44	46±7.73	60±9.06
TGD%	0	88.15	76.92	150.83	226.65
MST (Day)	18.5	34.5	34.5	46.5	58
ILS%	0	86.48	86.48	151.35	213.51

Pharmacokinetic parameters using non-compartmental methods in mice bearing melanoma

GROUPS	PLD	PLD-100	PLD-200	PLD-400
t1/2 (h)	18.88	28.38	23.95	19.07
AUC 0-t(µg/ml²·h)	1410.17	1330.35	1413.51	1228.9
MRT (h)	26.24	40.89	35.09	27.78
Cl ((mg/kg)/(µg/ml)/h	0.004	0.003	0.003	0.005

CONCLUSION

Overall, the results of this study showed that the use of CREKA peptide to decorate PLDs could result in the effective tumor regression and prolonged survival in C57BL/6 mice bearing B16F10 melanoma. CREKA peptide-modified nanoplatforms can achieve a "specific distribution" , "homing", and "retention" of the loaded drugs at the target position and improve treatment efficiency.

REFERENCES

1- Zhang N, Ru B, Hu J, Xu L, Wan Q, Liu W, et al. Recent advances of CREKA peptide-based nanoplatforms in biomedical applications. Journal of Nanobiotechnology. 2023;21(1):77-.

Andreas Åslund

NaDeNo – Unleashing the potential of hard-to-deliver drugs

Andreas K. O. Åslund[1], Astrid Hyldbakk[1,2], Sofie Snipstad [1,2,3,4], Karianne Giller Fleten[5], Kjersti Flatmark[5], Annbjørg Eide Falck[3], Ýrr Mørch[1,3]

[1]SINTEF Industry, [2]Norwegian University of Science and Technology, [3]NaDeNo Nanoscience AS, [4]Cancer Clinic, St. Olav's Hospital, [5]Oslo University Hospital/The Norwegian Radium Hospital

Medical Need

The peritoneum is a common location for cancer metastases, typically originating from colorectal, gastric and ovarian cancer. Due to a lack of early symptoms, **peritoneal metastasis** is often diagnosed late with very poor survival rates. There are no standard treatments for this disease[1].

Current treatment strategies		Current challenges
Surgical resection	→	Unable to remove all tumors
Intravenous chemotherapy	→	High systemic toxicity
Hyperthermic intraperitoneal chemotherapy (HIPEC)	→	Fast clearance from the peritoneum, 70-80% relapse

Our Solution

- A drug delivery system of polymeric nanoparticles encapsulating chemotherapy for **local administration** in the peritoneum.
- The nanoparticles are designed to encapsulate large amounts of hydrophobic small molecule drugs without the need of chemical drug modification.
- The particles degrade over time and release their payload in a controlled manner.
- Our lead candidate is a preclinical stage proprietary nanoformulation of the potent cancer chemotherapeutic drug cabazitaxel.

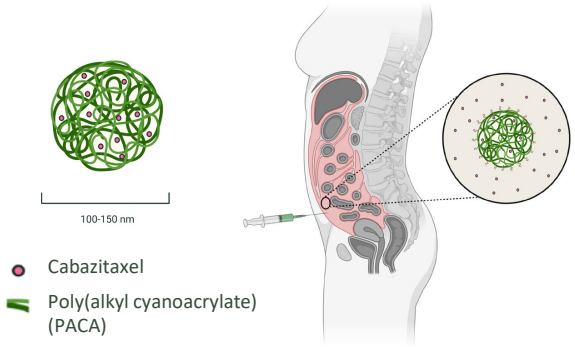

Results

We have performed studies in mouse models of peritoneal metastasis showing[2]:

- Sustained drug release
- Long drug retention time
- Reduced side effects
- Tumor-specific accumulation
- High treatment efficacy

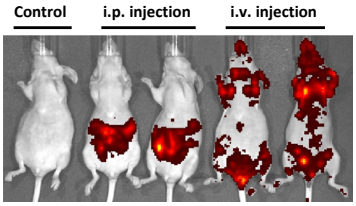

Intraperitoneal (i.p) vs intravenous (i.v.) injections of fluorescently labelled polymeric nanoparticles showing an even and restricted intraperitoneal distribution of nanoparticles, combined with long retention time (1 hr post injection).

Tumor specific drug accumulation in a mouse model of peritoneal metastasis originating from human ovarian cancer. Organs/tumor harvested 2 hrs post i.p administration. N=10, *P< .05, **P< .01, ****P< .0001.

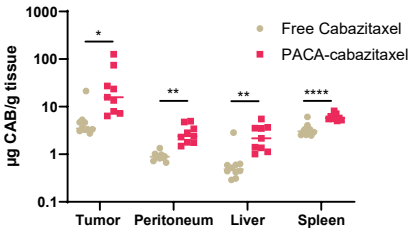

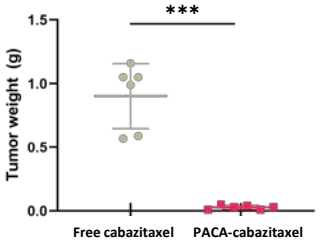

Significant treatment effect in a mouse model of peritoneal metastasis originating from ovarian cancer. The mice were treated with a single intraperitoneal injection. Tumor weight at study end (day 38), N=6, ***P< .001.

References

1. Cortés-Guiral, D. *et al. Nature Reviews Disease Primers* 7, 91 (2021)
2. Hyldbakk, A. *et al. Nanomedicine: Nanotechnology, Biology and Medicine* 48, 102656 (2023)

Funding

This work was supported by the Research Council of Norway and the Norwegian Cancer Society.

NaDeNo SINTEF Oslo University Hospital CLINAM European Foundation for Clinical Nanomedicine

DEVELOPING A PLATFORM FOR FUTURE TREATMENT OF MULTIDRUG-RESISTANT MICROBIAL INFECTIONS

Andreas K.O. Åslund[1], Anne Tøndervik[1], Guro Kruge Nærdal[1], Sabina Strand[1], Kristin Degnes[1], Joanna Empel[2], Hansjörg Götzke[3], Geir Klinkenberg[1]
[1] SINTEF AS, Department for Biotechnology and Nanomedicine, Trondheim, Norway; [2] National Medicines Institute, Warsaw, Polen; [3] NanoTag Biotechnologies, Göttingen, Germany. E-mail: leadtotreat-project@sintef.no

Introduction: The treatment of bacterial infections on a global scale is facing the enormous challenge of rapidly increasing occurrence of antimicrobial resistance (AMR). It is estimated that up to 1.27 million deaths were the direct result of AMR in 2019[1] Many promising lead compounds with high activities and wide therapeutic windows have failed to progress to clinical trials due to poor solubility, protein adsorption or other difficulties in formulation (i.e. low drugability).

The primary objective of LeadtoTreat is to develop a flexible, targeted nanoparticle system for delivery of synergistic antimicrobial treatments, demonstrated with methicillin resistant *Staphylococcus aureus* (MRSA) targeting nano-formulations of difficult-to-formulate drug candidates towards MRSA bacterial infections.

Results

- Lead compound MBL-AB01 was discovered during marine bioprospecting activities.
- MBL-AB01 has 50-100x higher activity against MRSA than vancomycin (unpublished data)
- Due to its very low drugability, MBL-AB01 is dependent on nanoformulation
- Encapsulation in polyphosphazenes (POPZ) gives high antimicrobial activity and low cytotoxicity (Figure 1)

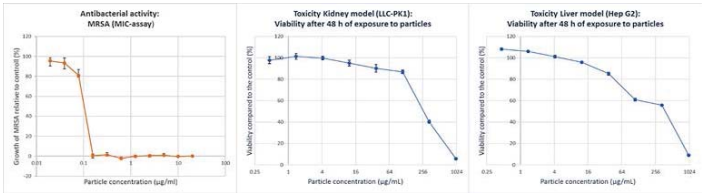

Figure 1: *In vitro MIC of MBL-AB01 containing POPZ nanoformulation for MRSA (ATCC 43300) compared to in vitro cytotoxicity in two cell lines (LLC-PK1, kidney model and HepG2, liver model) for the same formulation.*

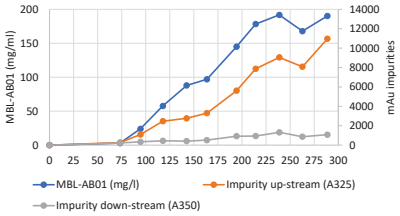

Figure 2: *Production of MBL-AB01*

Production of MBL-AB01

The MBL-B01 producing strain belonged to the rare Actinobacterium *Actinoalloteichus*. Starting with a very low production of MBL-AB01 in the wild type isolate, the yield of MBL-AB01 was improved by classical mutagenesis and medium screening. The volumetric yield of MBL-AB01 under controlled conditions reached 193 mg/L while the ratio of unwanted impurities were reduced (Figure 2).

Synergy screen

An initial synergy screen to look for synergetic combinations of antibiotic/antibiotic and antibiotic/potentiator has been performed (Figure 3).

- Score matrices indicate potential synergies (green) between antibiotics and potentiators
- Synergies mainly found for combinations including vancomycin and MBL-AB01
- MBL-AB01 shows synergy with ticlopidine and disulfiram for two of the strains

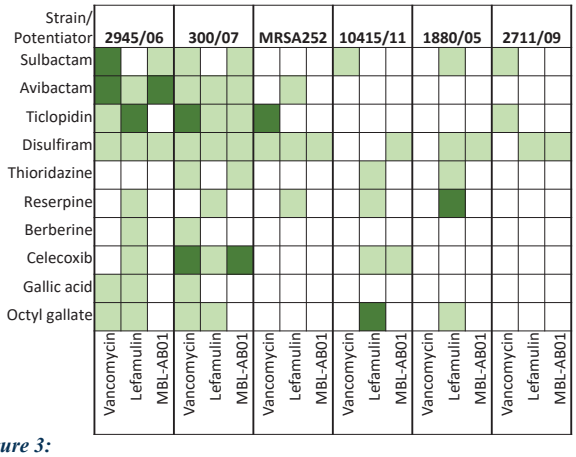

Figure 3:
Synergetic screen of antibiotics and potentiators. Cells in light green indicate potential synergetic effect, cells in dark green indicate stronger potential for synergetic effect.

Production of Nanobodies

- Three immunization campaigns performed in alpacas using three inactivated MRSA strains
- Nanobodies have been produced and purified in small scale *in vitro*
- Validation of nanobody candidates in ELISA and cell-based assays is ongoing

Conclusion

- MBL-AB01 has been produced for use in the project
- The first synergy screen reveals synergetic combinations between MBL-AB01 and potentiators
- Nanobodies for MRSA targeting have been identified

European Innovation Council
LeadtoTreat has received funding from the European Innovation Council (EIC) under grant agreement No 101046941. The EIC receives support from the European Union's Horizon Europe research and innovation programme.

Reference: 1. Murray, C. L. J. *et al. Lancet* 2022, 399, 10325, 629

Dynamics of biodegradation of iron carbohydrates in macrophages, a clue to understand their therapeutic effect

Vanesa Ayala-Nunez[1], Alexandra Rippl[1], Stephanie Eitner[1], Vera Kissling[1], Amy E. Barton Alston[2], Reinaldo Digigow[2], Beat Flühmann[2], Peter Wick[1]

[1] Swiss Federal Laboratories for Materials and Science and Technology (Empa), St. Gallen, Switzerland

[2] CSL Vifor, Glattbrugg, Switzerland

Introduction

- **Iron-carbohydrate complexes** are the standard of care to treat severe iron deficiencies. Post-IV injection, these nanomedicines are cleared from blood circulation and can be found in the liver and spleen, mainly in macrophages.
- The mechanism on how human macrophages perform this process is not fully understood. The why and how different iron-carbohydrate formulations trigger different physiological responses is also not known.

Objective

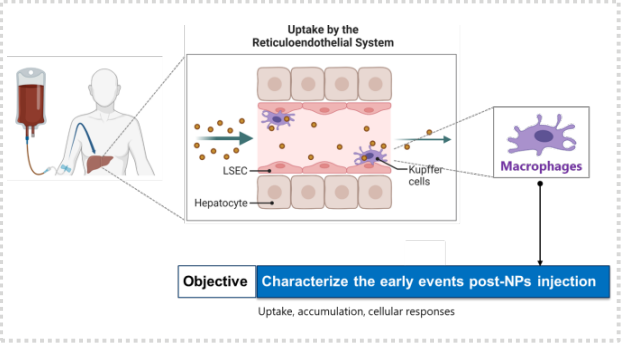

Results

Different iron carbohydrates have different uptake rates

Although the type of responses to iron sucrose (IS), ferric carboxymaltose (FCM), and iron isomaltoside-1000 (IIM) were similar, each nanoparticle formulation had a specific dynamic profile. For example, IS had a faster internalization rate compared to FCM and IIM.

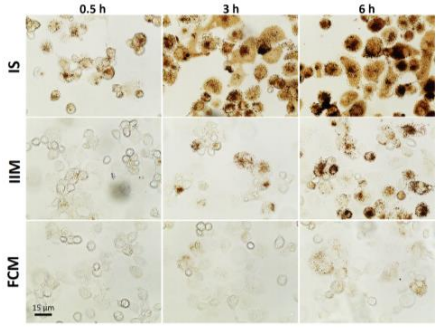

Macrophages derived from THP-1 cells were treated with 1800 µM of the indicated iron carbohydrate nanoparticles. After 0.5 h, 3 h and 6 h of treatment, the cells were washed and stained with Pearl's Prussian Blue and Diaminobenzidine. The brown coloration indicates the presence of Fe^{3+}.

Internalization of the nanoparticles was mediated by the endolysosomal system

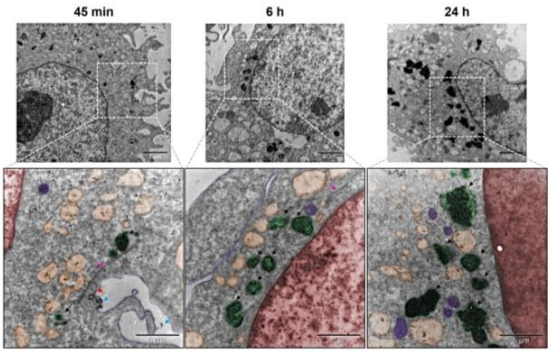

Primary human M2 macrophages were treated with 1800 µM of IS for 45 min, 6 h and 24 h. The cells were then fixed and processed for TEM analysis. The images show lysosomes containing iron nanoparticles at the different treatment time points. Red: nucleus, blue outline: plasma membrane, violet: mitochondria, orange: endosomes, green/black arrows: iron nanoparticles in lysosomes, blue arrows: iron particles outside of cell, red arrow: endocytic process, pink arrow: ER.

Conclusions

- Our results illustrate the impact that the physicochemical properties can have on the biological properties of these nanomedicines.
- Our data show how human macrophages, a key player in the iron metabolism, effectively use these nanomedicines as a source of iron and convert it in bioavailable iron (e.g. ferric iron bound to ferritin) that can later be released to blood and be used in the bone marrow for hematopoiesis.

Iris Batalha

Nanobiotics for mycobacterial infections: 'It's the little things that matter the most'

Iris L. Batalha [1,2,3,*], Audrey Bernut [4], Mark Welland [2], R. Andres Floto [3]

** Email: ibatalha@ibecbarcelona.eu*

[1] *Institute for Bioengineering of Catalonia (IBEC), Barcelona Institute of Science and Technology (BIST), Barcelona, Spain*
[2] *Nanoscience Centre, Department of Engineering, University of Cambridge, Cambridge, United Kingdom*
[3] *Molecular Immunity Unit, Department of Medicine, University of Cambridge, Cambridge, United Kingdom*
[4] *Dept. of Infection, Immunity & Cardiovascular Disease, Bateson Centre, University of Sheffield, Sheffield, United Kingdom*

BACKGROUND: Deaths caused by infections from antibiotic-resistant bacteria are expected to skyrocket over the next decades, with a staggering 10 million deaths per year projected for 2050. Infections by intracellular pathogens, such as *M. tuberculosis (Mtb)*, which have adapted to outsmart the host immune system and use it as shelter, are particularly difficult to treat and eradicate. Antibiotic-polymer conjugate nanoparticles provide a viable solution by enabling targeted drug release and reducing the dosing frequency and overall systemic toxicity. However, despite of improved pharmacokinetic and pharmacodynamic profiles, the clinical translation of polymer-drug conjugates has been primarily hampered by their physicochemical heterogeneity, failing to meet GMP guidelines. We report a smart multi-drug delivery vehicle, which allows the simultaneous incorporation of both hydrophilic (isoniazid; INH) and hydrophobic (clofazimine; CFZ) antibiotics at high concentrations and their targeted delivery to both intracellular and granuloma-resident mycobacteria *in vivo* in an infected zebrafish model.

THE POLYMER

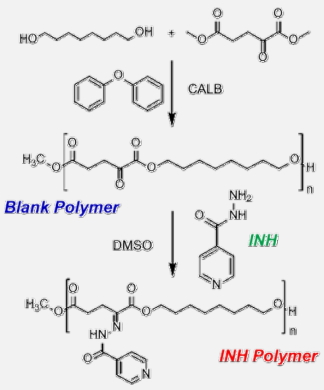

THE NANOBIOTICS

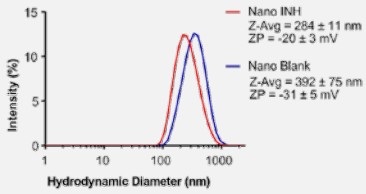

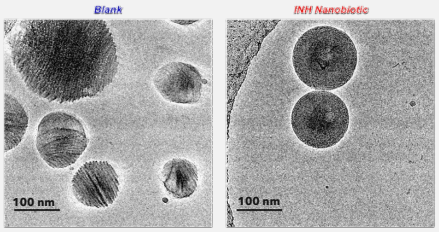

MACROPHAGE MOBILISATION *IN VIVO*

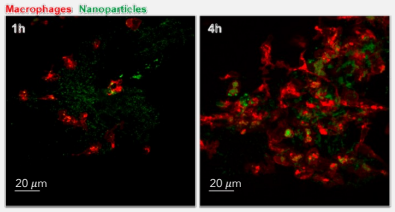

NANOBIOTIC ACCUMULATION IN GRANULOMAS AND MYCOBACTERIAL CORDS

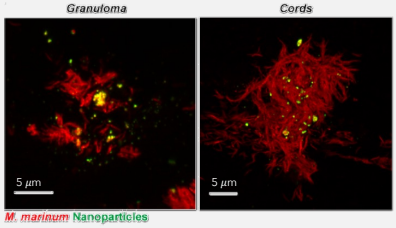

BACTERIAL KILLING AND REDUCTION IN GRANULOMA

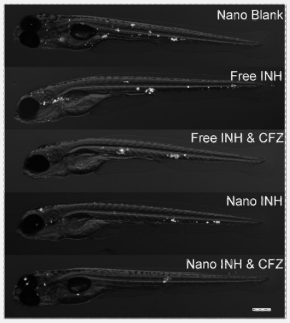

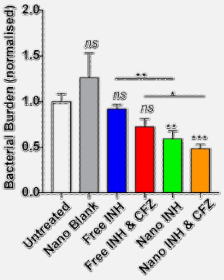

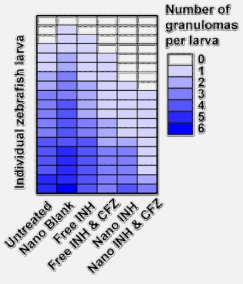

CONCLUSIONS

- Nanobiotics composed of INH-conjugated polymer and encapsulated CFZ presented **lack of toxicity, dose responsiveness, and improved therapeutic efficacy** in the treatment of mycobacterial when compared to free drugs.
- Nanoparticles were able to efficiently penetrate mycobacterial cords and granulomatous lesions – shielded regions of difficult access by free drugs, improving the therapeutic effect.
- **Synthetic simplicity and versatility: (1)** the drug is directly conjugated to the polymer without the need for any further chemical modifications; **(2)** the drug-polymer bond is acid-labile, allowing site-specific drug release; **(3)** the polymer itself is hydrolysable facilitating excretion; and **(4)** polymer size can be tuned without affecting the high drug loading capacity, since there is one drug conjugation site per monomeric unit of polymer.

ACKOWLEDGEMENTS

- Rosetrees Trust Interdisciplinary Prize 2015
- Fellowship from 'La Caixa' Foundation (ID 100010434) and from the European Union's Horizon 2020 research and innovation programme under the Marie Skłodowska-Curie grant agreement No 847648. The fellowship code is LCF/BQ/PI21/11830004.

REFERENCES: Batalha, I.L. et al. (2019) Journal of Controlled Release, 314, 116–124.

universität freiburg

Antimicrobial peptides:
lipid clustering and leaky fusion in PG/PE model vesicles

Katharina Beck[1], Janina Nandy[1,2], Nicolas Färber[3,4], Maria Hoernke[1,5], Heiko Heerklotz[1,6]

[1] Institute of Pharmaceutical Sciences, University of Freiburg, Germany
[2] Research Group Biophysics, Research Center Borstel - Leibniz Lung Center, Germany
[3] Experimental Physics I, Institute of Physics, University of Augsburg, Germany
[4] Physiology, Institute of Theoretical Medicine, University of Augsburg, Germany
[5] Physical Chemistry, Martin-Luther-University Halle (S.), Germany
[6] Leslie Dan Faculty of Pharmacy, University of Toronto, Canada

INTRODUCTION

Membrane-active antimicrobial peptides are a promising approach to combat growing antibiotic resistance. We focus on the effects of trivalent cyclic hexapeptides on model membranes. The antimicrobial activity of cR_3W_3 has been demonstrated [Junkes 2011].

To analyse the mechanism of action, we investigate the effects of the peptide on binary model vesicles containing negatively charged phosphatidylglycerol (POPG) and zwitterionic phosphatidylethanolamine (POPE) lipids. This also revealed the limitations of this commonly used model system.

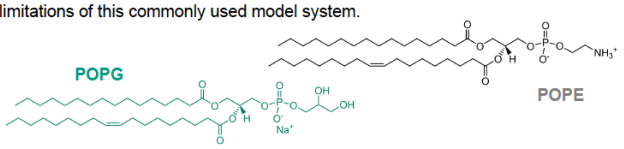

CONCLUSION

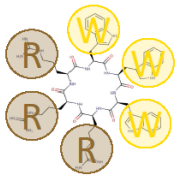

cR_3W_3
MIC*(E.coli)* = 11 µM

- → cR_3W_3 binds strongly to negatively charged model membranes and induces all-or-none vesicle leakage. This is consistent with its antimicrobial activity and selectivity.
- → cR_3W_3 induces electrostatic lipid clustering or lateral segregation of PG/PE mixtures with saturated or unsaturated lipids.
- → cR_3W_3 causes vesicle aggregation and fusion, making model membrane data difficult to interpret. Leaky fusion is mainly responsible for the observed vesicle leakage, limiting extrapolation to biological systems.

VESICLE LEAKAGE – Calcein fluorescence

Time-correlated single photon counting was used to quantify the vesicle leakage exploiting the lifetimes of the self-quenching dye calcein [Patel 2009].

- → cR_3W_3 induces all-or-none leakage.

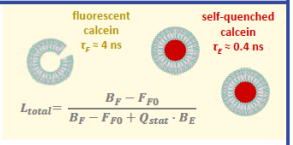

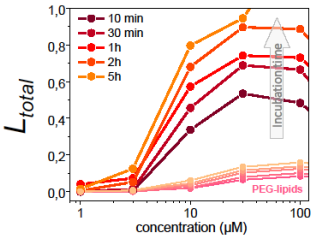

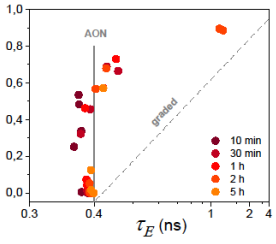

- → Vesicle leakage is caused primarily by leaky fusion [Beck 2023].
- → cR_3W_3 induces more leakage in PG/PE vesicles compared to PG/PC vesicles.

LIPID CLUSTERING – Laurdan fluorescence

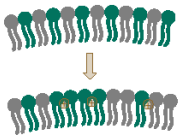

Antimicrobial hexapeptides induce DSC-detectable electrostatic lipid clustering in saturated DPPG/DPPE vesicles [Finger2015].

Laurdan fluorescence spectroscopy was used to quantify lipid phase transitions in model membranes, to examine unsaturated POPG/POPE lipid membranes [Färber 2022].

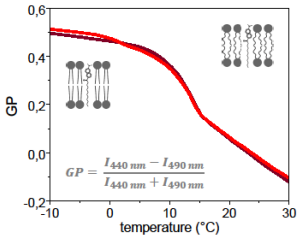

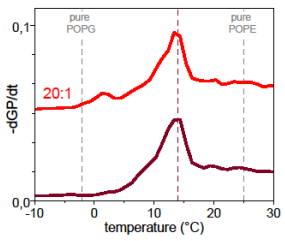

- → cR_3W_3 induces lipid clustering also in unsaturated POPG/POPE lipid vesicles.
- → Non-ideal mixing of PG/PE may be enhanced by cR_3W_3 [Navas 2005].

VESICLE AGGREGATION

Particle size and size distribution (PDI) were determined with dynamic light scattering (DLS).

- → cR_3W_3 induces visible vesicle aggregation of negatively charged membranes.
- → Vesicle aggregation and fusion lead to further problems during spectroscopic analyses and cause various artefacts.
- → Vesicle aggregation and fusion can be prevented by PEG-lipids.

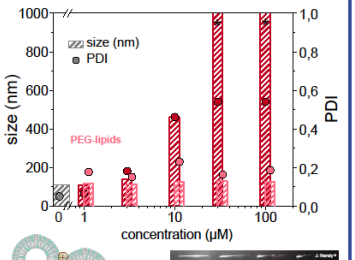

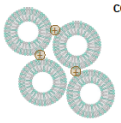

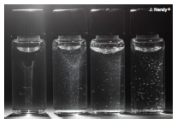

VESICLE FUSION

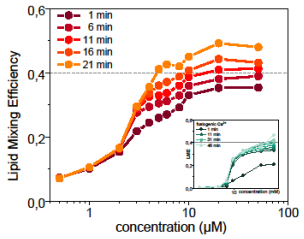

Förster resonance energy transfer (FRET) between PE-NBD and PE-Rhodamine B was used to quantify the Lipid Mixing Efficiency (LME) and to assess vesicle fusion [Shi 2022].

- → cR_3W_3 has fusogenic properties.
- → PG/PE membranes are biased towards fusion.

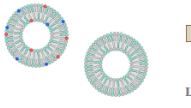

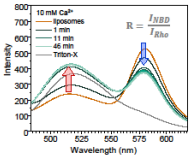

K. Beck et al. Soft Matter 19.16 (2023): 2919-2931.
C. Junkes et al. European Biophysics Journal 40.4 (2011): 515-528.
N. Färber et al. Biochimica et Biophysica Acta (BBA)-Biomembranes 1864.1 (2022): 183794.
S. Finger et al. Biochimica et Biophysica Acta (BBA)-Biomembranes 1848.11 (2015): 2998-3006.
B. Navas et al. Biochimica et Biophysica Acta (BBA)-Biomembranes 1716.1 (2005): 40-48.
S. Shi et al. Langmuir 38.7 (2022): 2379-2391. & Nanoscale Advances 4.23 (2022): 5109-5122.

DFG Deutsche Forschungsgemeinschaft

katharina.beck@pharmazie.uni-freiburg.de

Karina Benderski

Development and characterization of a syngeneic fibrotic hepatocellular carcinoma model

Karina Benderski[1], Paul Schneider[2], Panayiotis Kordeves[1] Federica De Lorenzi[1], Twan Lammers[1], Alexandros Marios Sofias[1], Leonard Kaps[2]

[1] Department of Nanomedicine and Theranostic, Institute for Experimental Molecular Imaging, University Hospital RWTH Aachen, Aachen, Germany; [2] First Department of Medicine , University Medical Center, Mainz, Germany

Development of a hepatocellular carcinoma model

Hepatocellular Carcinoma (HCC) accounts for 90% of all primary liver tumors [1]. Cirrhosis, due to chronic organ damage, is characterized by a massive accumulation of scared tissue in the liver and is the most frequent risk factor for HCC [2] [3]. But incidences of HCC are also increasingly observed in patients with metabolic-associated steatohepatitis (MASH) without cirrhosis [4]. Common murine models for HCC are lengthy and tumor load tends to be heterogeneous as tumor induction takes around 20 weeks and less than 50% of mice bear tumors [5]. In this work, we introduce a rapid and easy-to-handle injection model for HCC in cirrhotic and non-cirrhotic livers, which recapitulates histological and molecular key features of HCC in patients [6]. RNA-Seq analysis of HCC cells used in this work, namely Dt81Hepa 1-6, revealed that HCC hub genes (AFP, MCM3, SPATS2, NT5DC2, MCM6) were significantly upregulated and tumor cells showed a distinct clustering compared to healthy hepatocytes (Fig. 1a). For the non-cirrhotic model, mice were intrasplenically injected with Dt81-Hepa 1-6 tumor cells (HCC cells), while for the cirrhotic model, mice were gavaged with profibrogenic CCl4 for 6 weeks prior tumor cell inoculation. (Fig. 1b). After 4 weeks, inoculated mice developed tumors exclusively in their livers. Interestingly, livers of the cirrhotic group had a significantly higher tumor load as indicated by higher liver weights (2.5-fold) and morphometric readouts of liver sections compared to non-cirrhotic mice (Fig. 1c).

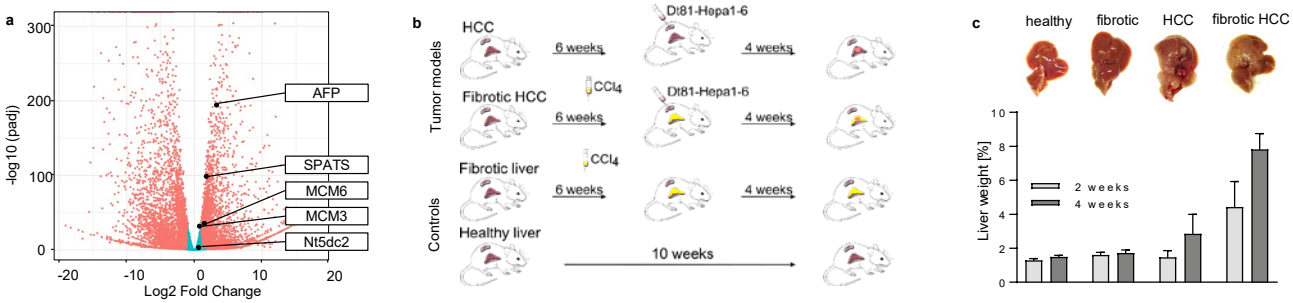

Figure 1. Development and initial assessment of HCC mouse models. (a) Dt81Hepa1-6 cells were sequenced and HCC keygenes were found to be upregulated. **b)** The HCC model was generated by intrasplenic injection of Dt81 Hepa-1-6 cells. The fibrotic HCC model was generated by CCl_4 administration for 6 weeks and subsequent injection of Dt81Hepa-1-6 cells. Livers from healthy mice or mice only administrated with CCl_4 were used as controls. **(c)** Liver weight revealed tumor formation by substantial liver weight increase as compared to control livers. Furthermore, livers from cirrhotic tumor group had a higher tumor load as compared to livers from the non-cirrhotic tumor group.

Analysis of the liver vs tumor microenvironment

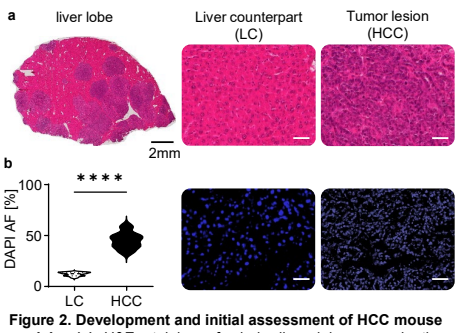

Figure 2. Development and initial assessment of HCC mouse models. (a) H&E staining of whole liver lobes reveals the difference between tumor lesions and the adjacent liver counterpart. **(b)** Quantification of cell density in tumor lesions versus non-malignant liver counterpart (scale bar = 50 µm).

Clinical Relevance

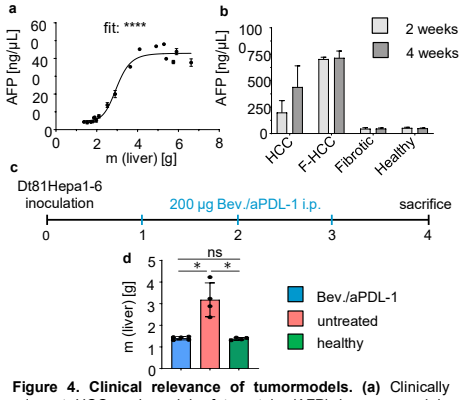

Figure 4. Clinical relevance of tumormodels. (a) Clinically relevant HCC-marker alpha-fetoprotein (AFP) is expressed in sera of tumor-bearing mice and correlates with liver weight and tumorburden. **(b)** Fibrotic HCC mice displayed higher AFP concentrations after 2 weeks. **(c)** Experimental outline for Bevacicumab/anti-PDL1 treatment. **(d)** Standard first-line medication against HCC inhibited development of tumor lesions.

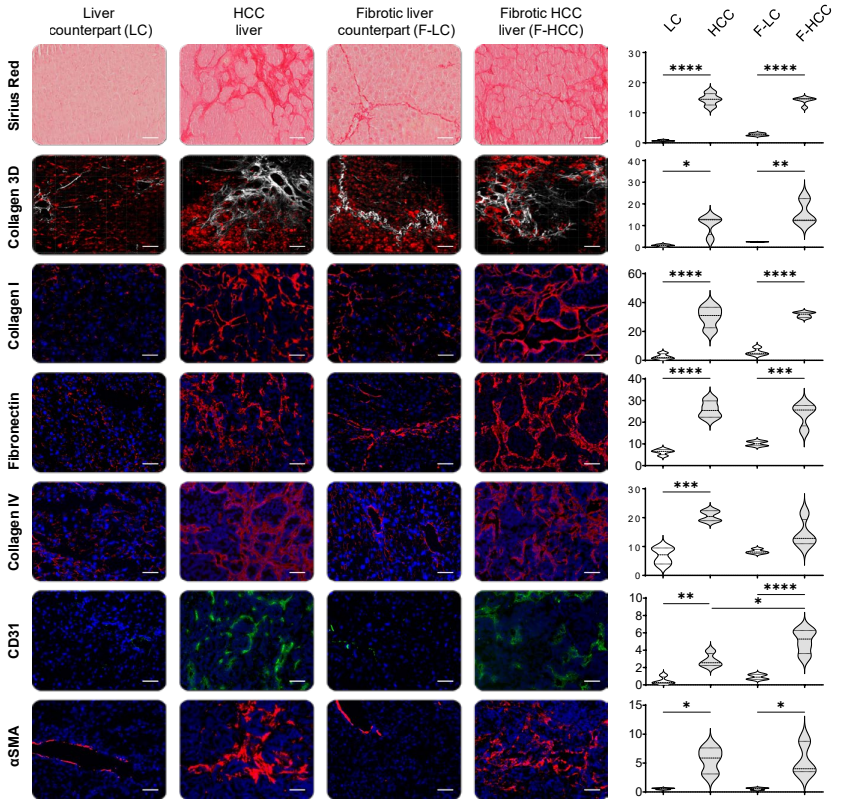

Figure 3. Quantification and analysis of liver ECM and vascular markers. A strong overexpression of ECM and vascular components was observed for HCC and fibrotic HCC, in comparison to their respective non-malignant liver counterparts. Compared to the surrounding tissue of HCC, the surrounding tissue of fibrotic HCC exhibits an overexpression of various ECM components, showcasing the ability of CCl_4 to provoke fibrotic reactions in livers. No change in vascular markers was observed between healthy and fibrotic livers. (scale bars = 50 µm; violin plots are expressed as area fraction % or volume fraction % for 2D microscopy and 3D multiphoton microscopy respectively).

Conclusions

We present two easy-to-handle murine models for HCC with high relevance for translational research. The two models resulted in robust cancer development and were proven more time-efficient in comparison to current models. Furthermore, CCl4 administration along with HCC cell injection caused a fibrotic HCC model, which resembles how cirrhosis-derived HCC manifests in humans. The models reflect characteristics of human HCC and showed a positive antitumor response to AtezoBev.

References: [1] Llovet et al., Nat. Rev. Dis. Primers, 2021 [2] Sofias#, De Lorenzi# et al., Adv. Drug Deliv. Rev., 2021 [3] Kaps et al., Cells, 2020. [4] Xuancheng Xie et al, Nature Scientific Reports, 2022 [5] Galle et al., J. Hepatol, 2018. [6] Lacoste, Raymond et al., PLOS one, 2017.

Sven Borgos

Polyethylene glycol (PEG) as a broad applicability marker for LC-MS/MS-based biodistribution analysis of nanomedicines

Astrid Hyldbakk[1,2], Terkel Hansen[1], Sjoerd Hak[1,3], Sven Even Borgos[1]

[1]Department of Biotechnology and Nanomedicine, SINTEF Industry, Trondheim, Norway
[2] Department of Physics, Norwegian University of Science and Technology (NTNU), Trondheim, Norway
[3] Department of Circulation and Medical Imaging, Norwegian University of Science and Technology (NTNU), Trondheim, Norway

Contact: sven.e.borgos@sintef.no

The challenge

Nanoencapsulation is frequently used to improve biodistribution and pharmacokinetics of drugs. But most of the time, only the drug is quantified as a proxy for distribution of the nanoparticle, which is not itself measured due to analytical challenges. This does not properly account for the drug release, which determines the *active* concentration of the drug. The result is a – potentially severely – incomplete understanding of the drug pharmacokinetic, toxicity and efficacy.

The idea

Conjugation to polyethylene glycol (PEG) is widely used to improve stability and circulation time of nanomedicines, as well as antibody drugs. Quantification of the PEG could provide a near-ideal marker for the nanoparticle carrier, since PEG is:

- Non-endogenous, yielding very low background signal
- Metabolically inert and chemically stable
- Easily detected by mass spectrometry with good sensitivity after hydrolysis

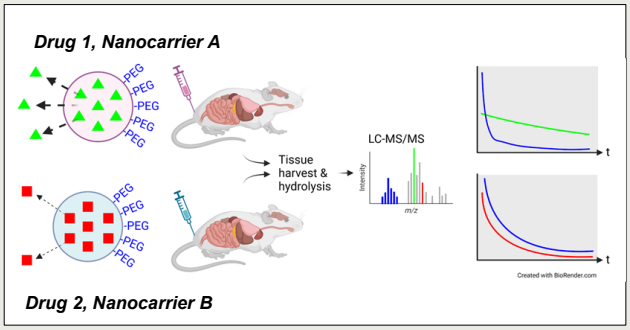

Conceptual overview of the method and output. Mass spectrometry (LC-MS/MS) is used to quantify both nanocarrier material (as PEG) and drug with high specificity, selectivity and sensitivity in all relevant organs.

The strengths of the method

PEG is covalently conjugated to different components of the nanocarrier. After administration *in vivo*, organs are extracted and completely hydrolyzed in strong acid. This also releases the PEG from its chemical conjugate. Thus, the method is:

- Robustly and completely extracting the PEG from all tissue types and blood
- Releasing the PEG from a wide range of conjugates (Figure 2), enabling one analytical method for virtually all PEG-containing systems
- Maximising LC-MS/MS sensitivity by degrading other components that could interfere analytically, such as proteins

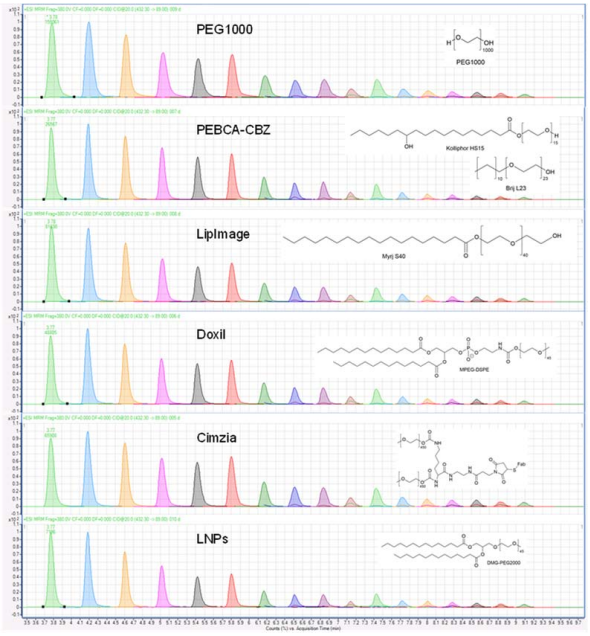

Figure 2: *LC-MS/MS chromatograms of PEGylated compounds after H_2SO_4 hydrolysis. Horizontal axis shows retention time (minutes) and vertical axis shows signal intensity (counts). PEBCA-CBZ, Poly(ethylbutyl cyanoacrylate) nanoparticles with cabazitaxel; LipImage, solid lipid nanoparticles with IR780-oleyl; Doxil®, liposomal doxorubicin; Cimzia, PEGylated antibody, LNPs, lipid nanoparticles for nucleic acid delivery. The corresponding PEGylated compounds are shown as inserts.*

Novel insight on *in vivo* behavior

Detection of *both* the nanocarrier and the drug enables direct assessment and comparison of drug release *in vivo*. This is crucial to determine the actual, bioactive drug concentrations in organs.

We applied the method to biodistribution studies of two nanomedicines, one polymeric and one lipidic (Figure 3) and could show fundamental differences in both biodistribution and what appears to be *in vivo* release kinetics of the encapsulated compounds.

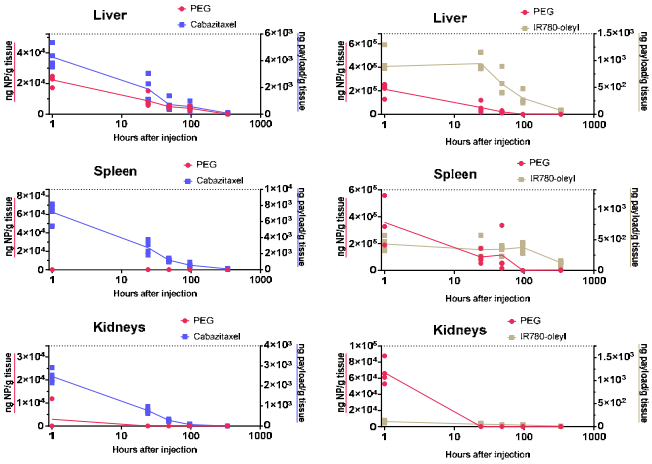

Figure 3: *Measured concentrations in a selection of organs as function of time after administration, of nanocarrier material (as PEG, red) and encapsulated payload (blue, brown) for two different nanomedicines injected IV in mice. Left: PEBCA-CBZ, Poly(ethylbutyl cyanoacrylate) nanoparticles loaded with anti-cancer drug cabazitaxel (blue). Right: LipImage, solid lipid nanoparticles with the near-IR dye IR780-oleyl (brown).*

Conclusions

The novel method is a robust, versatile and generic approach for biodistribution analysis of PEGylated therapeutics that can provide a detailed understanding of various critical aspects of the in vivo behavior of PEGylated nanomedicines, such as drug release and particle stability.

ETH zürich | SIB Swiss Institute of Bioinformatics | CSL Vifor | Empa Materials Science and Technology

Uncovering the dynamics of cellular responses induced by iron-carbohydrate complexes in human macrophages using quantitative proteomics and phosphoproteomics

Jonas Bossart[1,2,3], **Alexandra Rippl**[1], **Amy E. Barton Alston**[4], **Beat Flühmann**[4], **Reinaldo Digigow**[4], **Marija Buljan**[1,2], **Vanesa Ayala-Nunez**[1], **Peter Wick**[1]

[1] Empa, Particles-Biology Interactions Laboratory, St. Gallen, Switzerland
[2] Swiss Institute of Bioinformatics, Lausanne, Switzerland
[3] Department of Health Sciences and Technology, ETH Zurich, Zurich, Switzerland
[4] CSL Vifor, Glattbrugg, Switzerland

INTRODUCTION

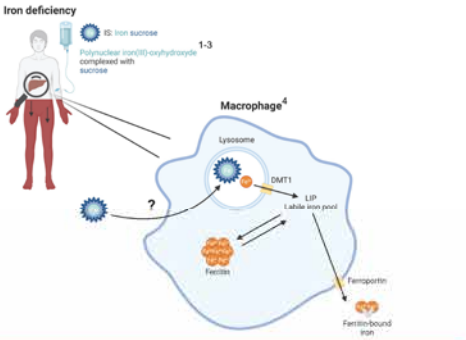

APPROACH

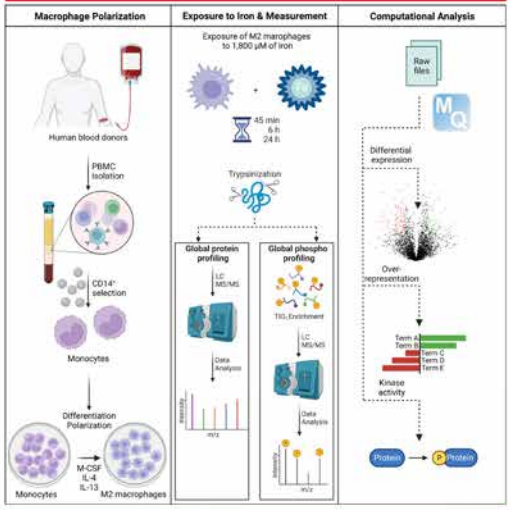

CONCLUSIONS

- IS is taken up as complete particles and dissociated iron ions
- Internalized iron is stored and released as ferritin
- Exposure to IS induces signs of a M2 polarization loss
- Cells successfully adapt to increased iron availability
  - Prevention of ferroptosis
- Further biological validation experiments necessary
- Omics approaches have potential to innovate mechanistic studies for complex drugs and to screen nanomedicines

References
1. Funk F. et al., Int. J. Mol. Sci., 2022
2. Nikravesh N. et al., Nanomedicine:NBM, 2020
3. Krupnik L. et al., Unpublished manuscript, 2023
4. Arsiwala T. et al., Int. J. Mol. Sci., 2022
5. Labonte A.C. et al., Mol. Cells., 2014
6. Patel S. et al., Front. Immunol., 2021
7. Chen P.-H. et al., Cell Death Differ., 2020
8. Chen P.-H. et al., Cell Death Dis., 2021

This study is under review.

Funding: This work was financed by CSL-Vifor.
Acknowledgements: We would like to express our gratitude to the members of the FGCZ for technical assistance, measurements, and discussions.
Icons: Icons were created with biorender.com.

RESULTS

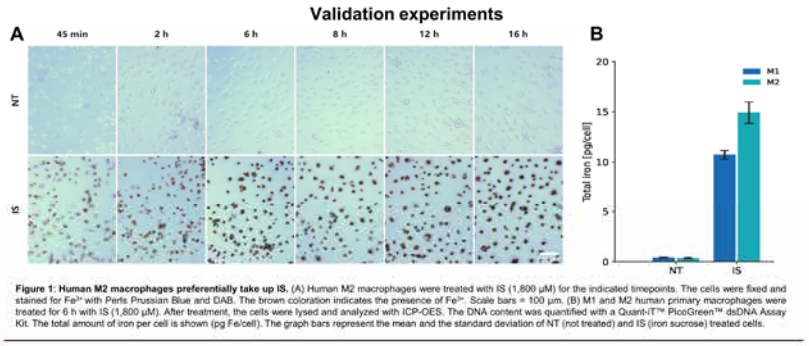

Figure 1: Human M2 macrophages preferentially take up IS. (A) Human M2 macrophages were treated with IS (1,800 µM) for the indicated timepoints. The cells were fixed and stained for Fe^{3+} with Perls Prussian Blue and DAB. The brown coloration indicates the presence of Fe^{3+}. Scale bars = 100 µm. (B) M1 and M2 human primary macrophages were treated for 6 h with IS (1,800 µM). After treatment, the cells were lysed and analyzed with ICP-OES. The DNA content was quantified with a Quant-iT™ PicoGreen™ dsDNA Assay Kit. The total amount of iron per cell is shown (pg Fe/cell). The graph bars represent the mean and the standard deviation of NT (not treated) and IS (iron sucrose) treated cells.

Molecular changes

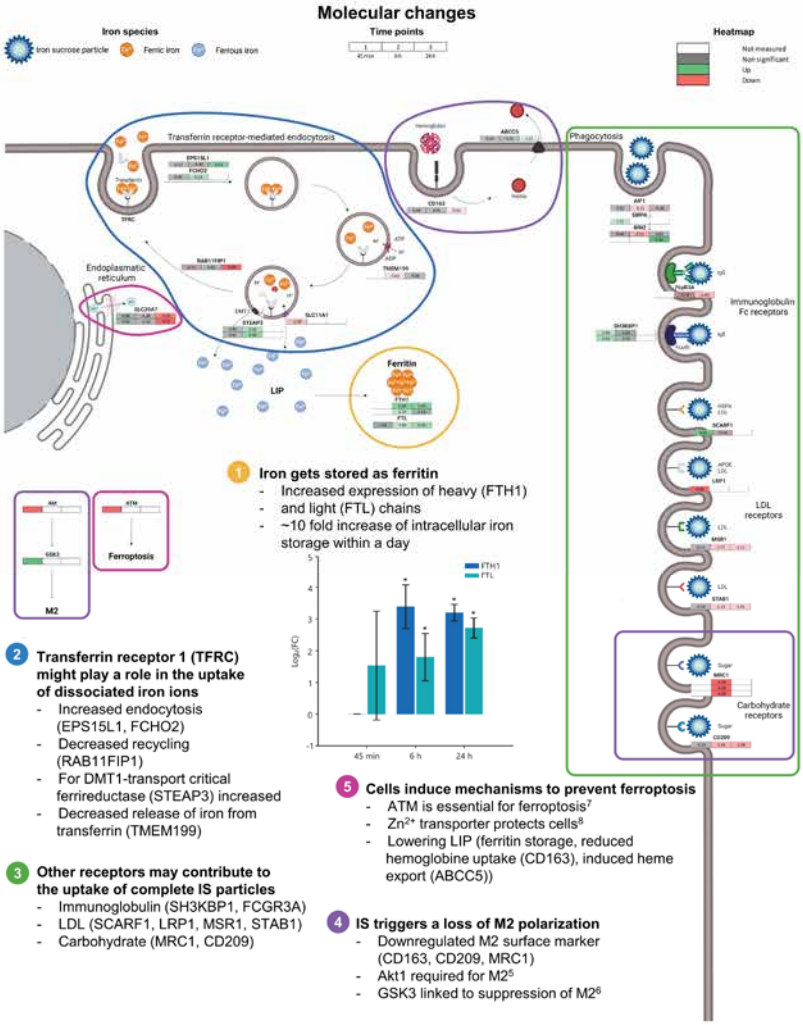

1 Iron gets stored as ferritin
- Increased expression of heavy (FTH1)
- and light (FTL) chains
- ~10 fold increase of intracellular iron storage within a day

2 Transferrin receptor 1 (TFRC) might play a role in the uptake of dissociated iron ions
- Increased endocytosis (EPS15L1, FCHO2)
- Decreased recycling (RAB11FIP1)
- For DMT1-transport critical ferrireductase (STEAP3) increased
- Decreased release of iron from transferrin (TMEM199)

3 Other receptors may contribute to the uptake of complete IS particles
- Immunoglobulin (SH3KBP1, FCGR3A)
- LDL (SCARF1, LRP1, MSR1, STAB1)
- Carbohydrate (MRC1, CD209)

4 IS triggers a loss of M2 polarization
- Downregulated M2 surface marker (CD163, CD209, MRC1)
- Akt1 required for M2[5]
- GSK3 linked to suppression of M2[6]

5 Cells induce mechanisms to prevent ferroptosis
- ATM is essential for ferroptosis[7]
- Zn^{2+} transporter protects cells[8]
- Lowering LIP (ferritin storage, reduced hemoglobine uptake (CD163), induced heme export (ABCC5))

Visit us at www.curevac.com

STABILIZATION OF MRNA VACCINES BY UTILIZING DRYING TECHNOLOGIES

Roland Böttger, Dennis Krieg, Livia Palmerston Mendes, Paula Muresan, Vusala Ibrahimova, Salvatore Cinquerrui, Gemma Navarro, Patrick Baumhof
CureVac SE, Tübingen, Germany

1. Introduction: mRNA vaccines have shown to be suitable for tackling emerging pandemics due to their rapid development process, superior efficacy, and favorable safety profile. However, further maturation of mRNA technologies will be required to be competitive with other modalities on the regular pharmaceutical market. A significant drawback of the currently marketed mRNA products is their low stability requiring storage at negative temperatures, implying challenges in their transport and distribution, while consequently increasing costs. The development of dry mRNA presentations has potential to increase stability and could enable storage at refrigerated or even ambient temperatures. Here, we investigated novel LNPs with improved stability to enable drying and storage at ambient conditions without loss of vaccination efficiency.

2. CureVac's Proprietary mRNA-LNP Delivery Platform

- Proprietary ionizable lipids with distinct features
- Novel structural lipids
- Proprietary non-PEG-Lipids stabilize the particle against aggregation
- Cholesterol

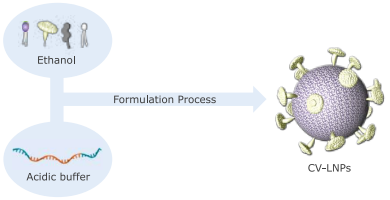

Characteristics of CureVac's prophylactic mRNA-LNPs:

Diameter (Z-Ave) = 45-120 nm
Polydispersity (PDI) < 0.2
Encapsulation (EE) > 90 %
TNS pKa > 6.5
Ionizable lipid logP > 18

3. New CV-LNP with High Vaccination Efficacy

Frozen liquid

- Vaccination with RAV-G mRNA-LNP (0.25 µg) in mice
- CV-LNP produce consistent virus neutralizing titers (VNTs)
- Stimulates robust T-cell response
- Efficacy comparable to commercially utilized LNP composition (Example)

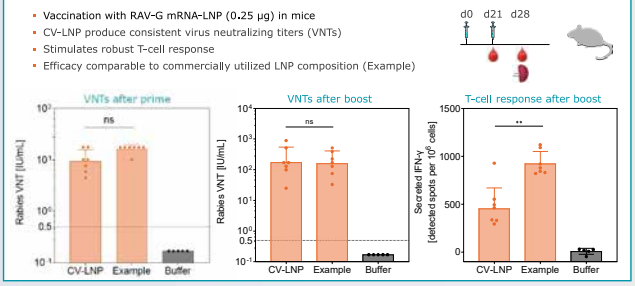

4. Stability After Freeze/Thaw at Low Concentration

Unfrozen
1 freeze/thaw

- mRNA-LNPs show colloidal instability when frozen at low concentrations often requiring distribution in multi-dose vials at higher concentration and dilution prior administration.
- Example LNP show increased size when frozen at concentrations < 200 µg/mL
- Significant increase in size for CV-LNP seen only upon freezing at very low concentrations < 50 µg/ml

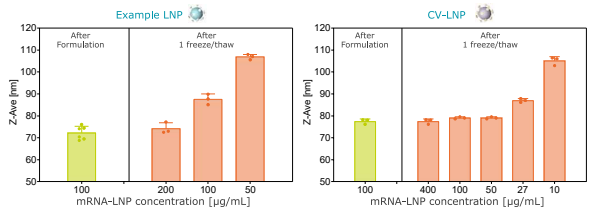

5. Development of Lyophilized LNP

Frozen liquid
Lyophilized

- PpLuc-RNA formulated in CV-LNP and lyophilized
- Modest increase in size observed
- PDI increase requires further optimization
- No alteration of morphology
- No significant decrease in EE
- No impact on RNA integrity
- Comparable *in vitro* transfection efficiency
- No dependency on the mRNA-LNP concentration

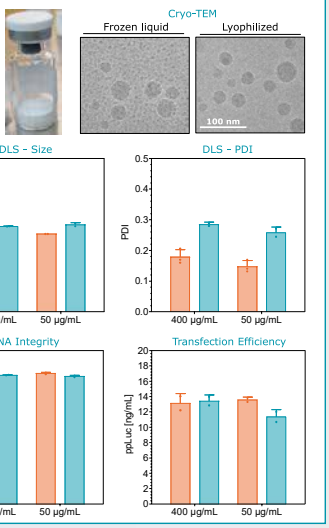

6. Improved Stability of Lyophilized LNP

2-8°C 25°C 40°C
Frozen liquid (-80°C)

- RAV-G mRNA formulated in CV-LNP, lyophilized at 50 µg/mL and stored at different temperatures.
- After lyophilization, modest increase in size and PDI. No further alteration after storage. No alteration of EE.
- Subtle reduction of RNA integrity after lyophilization. At 2-8°C no further decrease, at 25°C modest decrease within specifications and at 40°C considerable RNA degradation.
- Lyophilized CV-LNP can be stored at ambient conditions without compromising physicochemical properties for at least 12 weeks. The study will be extended to test long-term stability including potency monitoring.

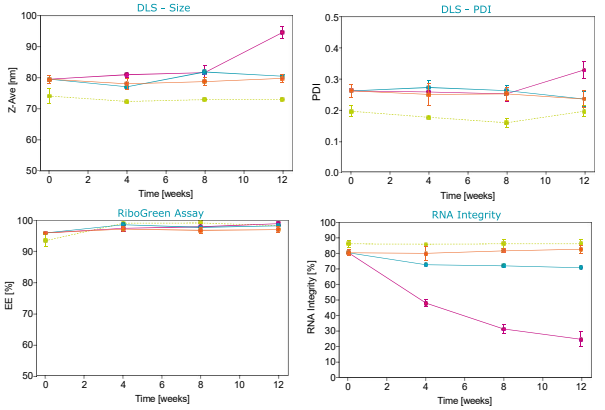

7. Lyophilization Retains Vaccination Efficiency

Frozen liquid
Lyophilized

- Vaccination with RAV-G mRNA-LNP (0.25 µg) in mice
- Lyophilization of CV-LNP at 50 µg/mL retains virus neutralizing titers and robust T-cell response compared to frozen-stored liquid material
- The CV-LNP could enable dry single-dose mRNA vaccine presentations for long-term storage at ambient temperatures

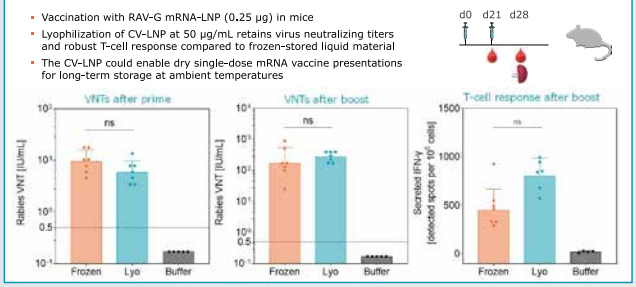

8. Conclusion: It was found that specific lipid excipients are preferred to stabilize LNPs against stress associated with dilution and drying. An optimal LNP composition could be lyophilized and stored at ambient conditions with minimal change of physicochemical parameters and vaccination efficiency. Drying is a promising strategy to overcome stability issues and could help increase opportunities for mRNA medicines on the post-pandemic drug market.

Acknowledgements

Technology - Formulation and Process Development teams at CureVac

Further readings:

1. Lutz *et al.*, *npj Vaccines*, 2017
2. Buschmann, *et al.*, *Vaccines*, 2021
3. Schoenmaker, *et al.*, *International Journal of Pharmaceutics* , 2021
4. Hasset *et al.*, *Mol Ther Nucleic Acids*. 2019

All data presented: Preliminary and unclean data

Correspondence should be addressed to:
roland.boettger@curevac.com

Danielle Brain

Assessment of cell phenotype and gene expression changes, following repeat exposure to the NRTIs FTC, 3TC and long acting polymer linear poly(FTC) – relevance to subcutaneous administration of long-acting therapeutics

Danielle Brain[1,2], Faye Hern[2,3], Christopher David[1,2] Anika Shakhil[2,3], Chung Liu[2,3], Steve Rannard[2,3], Andrew Owen[2] and Neill Liptrott[1,2].

[1]Immunocompatibility Group, Department of Pharmacology and Therapeutics, Institute of Systems and Molecular Biology, University of Liverpool, Liverpool, UK.
[2]Centre of Excellence for Long-acting Therapeutics (CELT), Department of Pharmacology and Therapeutics, Institute of Systems and Molecular Biology, University of Liverpool, Liverpool, UK.
[3]Department of Chemistry, School of Physical Sciences, University of Liverpool, Liverpool, UK.

Introduction

- HIV treatment requires chronic administration of antiretrovirals to suppress viral replication, with no current cure (1).
- Due to the lack of "forgiveness" in current antiretroviral regimens, in terms of viral breakthrough, long-acting antiretroviral medication can help to improve adherence to medication, resulting in better treatment outcomes (2).
- Currently, the nucleoside reverse-transcriptase inhibitors (NRTIs), emtricitabine (FTC) and lamivudine (3TC), are being explored for use in long-acting delivery.
- A key question in this type of delivery is, with long-acting antiretrovirals, does repeated, and long-term, exposure to these drugs alter the functional capacity of human immune cells.
- Linear poly(FTC) is a long-acting polymeric prodrug of FTC, which is designed to be delivered subcutaneously as an implant that releases FTC slowly over time (3).
- It is important to assess its immunocompatibility with subcutaneous space relevant immune cell types. MUTZ-3 cells represent a useful model with which to study these interactions (4).

Repeated Exposure of the cell lines to FTC and 3TC

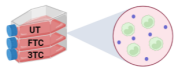

- **Cells in culture** - THP-1, MUTZ-3, CEM, or KU812
- **Drug molecule** - FTC (1.8 µg/mL), 3TC (2 µg/mL), or Linear poly(FTC) (20 µg/mL)

- Repeat exposure of the cell lines to FTC or 3TC was carried out for 7 weeks and cells were passaged twice weekly.

Cell Health Assessments

- CellROX™ Green reagent used to detect ROS levels.
- ThiolTracker™ Violet used to detect reduced glutathione levels.
- JC-1 reagent used to measure mitochondrial membrane potential.

Exposure of Cells to Positive Controls and Marker Expression Analysis

- Cells were treated with positive controls depending on the cell type.
  - THP-1 = LPS
  - MUTZ-3 = LPS or Resiquimod (R848)
  - KU812 = C5a or Calcium ionophore
  - CEM = PHA
- Cells were stained with antibodies for specific activation markers depending on the cell line tested.

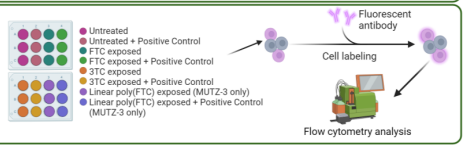

Gene Expression Assessment

- MUTZ-3 cells only, cells treated with R848
- RNA isolated
- Gene expression changes assessed using the metabolic pathways panel on the nCounter Pro Analysis system.

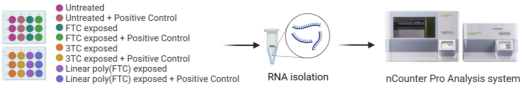

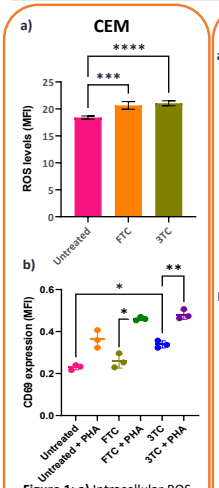

Figure 1: a) Intracellular ROS. **b)** CD69 expression.

- Intracellular **ROS levels were significantly higher** in the FTC- and 3TC-cultured cells, than the untreated cells (P= <0.001 and P < 0.0001 respectively).
- No significant differences were seen for the reduced glutathione levels or the mitochondrial membrane potential for either the FTC- or 3TC-cultured cells.
- When compared to the Untreated cells, the **3TC-cultured cells** showed a significantly **lower CD69 expression** (P = <0.05).

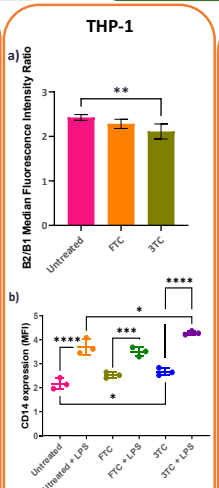

Figure 2: a) Mitochondrial membrane potential. **b)** CD14 expression.

- 3TC-cultured cells demonstrated a significantly **lower MMP** (P= <0.01).
- When compared to the untreated, **3TC-treated** cells showed a significantly **higher expression of CD14** (P= <0.05). When compared to the LPS-treated cells, the **3TC-cultured LPS-treated cells showed significantly higher CD14 expression** (P = <0.05).

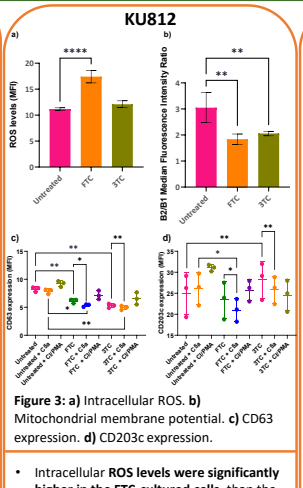

Figure 3: a) Intracellular ROS. **b)** Mitochondrial membrane potential. **c)** CD63 expression. **d)** CD203c expression.

- Intracellular **ROS levels were significantly higher in the FTC-cultured cells**, than the untreated cells (P= <0.0001).
- FTC- and 3TC-cultured cells displayed a **significantly lower MMP** (P= <0.01).
- When compared to the **FTC- and 3TC-cultured C5A-treated cells, the C5A-treated cells showed a significantly lower or higher CD63 expression respectively** (P = <0.01). When compared to the untreated cells, the **FTC- and 3TC-cultured cells showed a significantly lower or higher CD63 expression respectively** (P = <0.01).
- **3TC-cultured cells** in comparison with the Untreated cells showed significantly **higher CD203c expression** (P = <0.05). **FTC-cultured C5A-treated** cells when compared to C5A-treated cells showed significantly **lower CD203c** expression (P< 0.05).

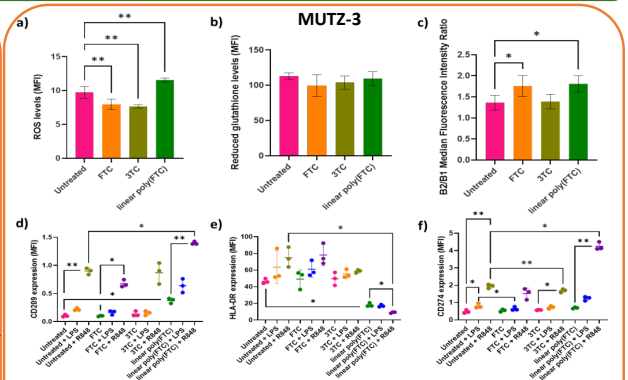

Figure 4: a) Intracellular ROS **b)** Reduced glutathione **c)** Mitochondrial membrane potential. **d)** CD209 expression. **e)** HLA-DR expression. **f)** CD274 expression.

- Intracellular **ROS levels were significantly lower in the FTC- and 3TC-cultured cells**, however **higher in the Linear poly(FTC)-cultured cells,** when compared to the untreated cells (P= <0.01).
- FTC- and Linear poly(FTC)-cultured cells displayed a **significantly higher MMP** (P= <0.05).
- **Linear poly(FTC)**-cultured cells showed a significantly **higher CD209 and significantly lower HLA-DR expression** when compared to the untreated (P<0.05).
- **Linear poly(FTC)-cultured R848 treated** cells had a significantly **higher CD209 and CD274** expression, however a significantly **lower HLA-DR** expression when compared to the R848 treated cells (P<0.05).
- **HLA-DR expression is significantly lower in the Linear poly(FTC)-cultured R848 treated cells** compared to the Linear poly(FTC)-cultured cells.

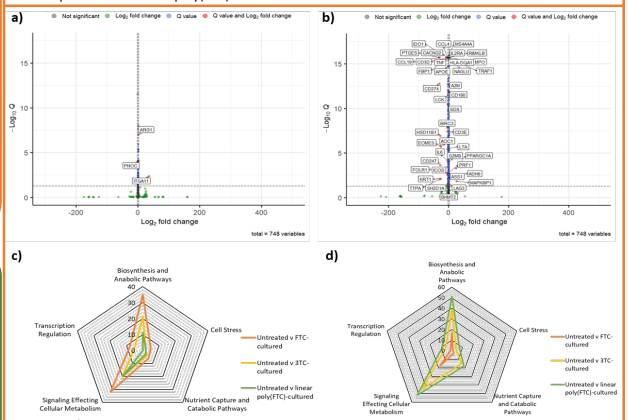

Figure 5: a) Significant gene expression changes when FTC-cultured R848 treated cells were compared to R848 treated cells (q<0.05). **b)** Significant gene expression changes when linear poly(FTC)-cultured R848 treated cells were compared to R848 treated cells (q<0.05). **c)** Number of that had a higher expression. **d)** Number of genes that had a lower expression.

- Only **3 genes** showed significantly altered gene expression when the **FTC-cultured cells treated with R848 were compared to the R848 treated cells**.
- **Many genes** showed altered expression when **linear poly(FTC)-cultured cells treated with R848 were compared to the R848 treated cells**.

Conclusions

- Cell line specific and treatment specific responses were seen for the FTC- and 3TC- cultured cells.
- Responses to linear poly(FTC) in the MUTZ-3 cell line were marker specific, this is interesting as it indicates there is some activation, but also some inhibition of marker responses as a result of the cells sensing linear poly(FTC).
- Reduced expression of CCL4, TNF and CCL19 in the linear poly(FTC)-cultured R848 treated cells could suggest reduced activation of these cells.
- FTC exposure results in a greater profile of genes with higher expression, whereas linear poly(FTC) exposure results in a greater profile of genes with lower expression, this suggests there is a complex relationship between these three treatments and the effect on the cells, it is important to next understand the phenotype more clearly as the mRNA levels don't necessarily translate into increased protein levels, as was seen for CD274.
- Metabolic processes of these cultured cells should be explored further to better understand the consequences.
- Previously efavirenz and lopinavir have led to lower glucose uptake and caused bioenergetic modifications to cells, it would be useful to explore this to determine if FTC, 3TC and linear poly(FTC) alter these profiles (5).
- These results have, potential, consequences for the development of future long-acting implants as they show possible effects of repeat exposure to antiretrovirals that may be used in such preparations and polymers of these antiretrovirals, and highlight the requirement for early assessment of biocompatibility, as highlighted elsewhere (6).

References

1.Ruelas, Debbie S. and Warner C. Greene, *An Integrated Overview of HIV-1 Latency.* Cell, 2013. **155**(3): p. 519-529.
2.Chandiwana, N.C., et al., *Impact of long-acting therapies on the global HIV epidemic.* AIDS, 2021. **35**(Supplement 2).
3.Shakil, A., et al., *Linear and branched polymer prodrugs of the water-soluble nucleoside reverse-transcriptase inhibitor emtricitabine as structural materials for long-acting implants.* Journal of Materials Chemistry B, 2022. **10**(23): p. 4395-4404.
4.Groell, F., et al., *Hydrogels in three-dimensional dendritic cell (MUTZ-3) culture as a scaffold to mimic human immuno competent subcutaneous tissue.* Int J Pharm, 2018. **544**(1): p. 297-303.
5.Heaton, B.J., et al., *Exposure of human immune cells, to the antiretrovirals efavirenz and lopinavir, leads to lower glucose uptake and altered bioenergetic cell profiles through interactions with SLC2A1.* Biomed Pharmacother, 2022. **150**: p. 112999.
6.Su, J.T., et al., *A Subcutaneous Implant of Tenofovir Alafenamide Fumarate Causes Local Inflammation and Tissue Necrosis in Rabbits and Macaques.* Antimicrobial Agents and Chemotherapy, 2020. **64**(3): p. e01893-19.

Thomas Bruckdorfer

From Bioengineering to Surface Modification

A Conceptual Overview of Linkerology® Methodologies

Thomas Bruckdorfer[1,2,4] , Stefan Kubick[4], Raimund Maier[1], Sandra Miklos[3], Karin Rustler[1], Haixiang Zhang[2]

[1] Iris Biotech GmbH, Adalbert-Zoellner-Str. 1, 95615 Marktredwitz, Germany, www.iris-biotech.de
[2] Iris Biotech Laboratories GmbH, Adalbert-Zoellner-Str. 1, 95615 Marktredwitz, Germany
[3] Cfm Oskar Tropitzsch GmbH, Adalbert-Zoellner-Str. 1, 95615 Marktredwitz, Germany
[4] B4 PharmaTech GmbH, Am Sandwerder 16, 14109 Berlin, Germany, www.b4pt.com

Abstract

Conjugating highly potent small molecules to vastly target specific biomolecules (e.g. antibodies, single-chain, nanobodies) or other carriers has become a modern and sophisticated approach, particularly in the field of cancer therapy. As a result, the list of antibody-drug conjugates (ADCs) in clinics continues to grow. The choice of a linker for selective and site-specific control of payload release remains the major goal as premature release of a highly toxic payload would have fatal side-effects. Here we focus on preparing two different classes of carriers for subsequent conjugation with the appropriate technology: (a) engineering biomolecules by cell-free synthesis and (b) treating plastic surfaces with plasma.

Cell-free synthesis (CFS) has attracted attention as a simple and controllable method for direct manipulation of protein expression to facilitate the synthesis of so far challenging or even inaccessible biomolecules, such as cytotoxic proteins, including site-specifically labeled proteins and protein-drug conjugates, or other complex membrane proteins. By using a lysate based on eukaryotic insect cells (*Spodoptera frugiperda* 21, Sf21), endogenous endoplasmic reticulum-derived structures (microsomes) are retained, enabling native-like protein maturation. The modular addition of protein-coding plasmids to the CFS allows a straightforward and defined study of protein assembly.

Plasma technology allows to equip inert polymers such as polyethylene (PE), polystyrene (PS), polytetrafluoroethylene (PTFE), or co-polymers thereof with functional groups like amine or carboxylate enabling further conjugations and applications.

Bioengineering *via* cell-free Synthesis

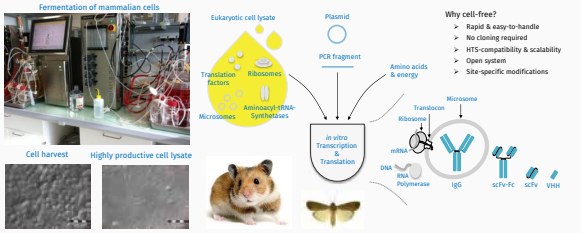

- Syntheses of cytotoxic proteins, including site-specifically labeled proteins and protein-drug conjugates.
- Synthesis of complex membrane proteins.
- Post-translational modifications are feasible in eukaryotic cell-free systems (signal peptide cleavage, glycosylation, phosphorylation, lipid modifications)

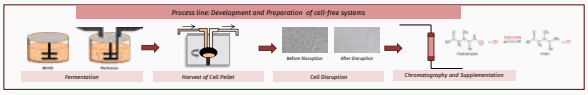

The entire process for the production of cell-free systems, starts with the fermentation in 30L fermenters, goes through cell disruption to lysate purification and supplementation. No genetically modified organisms are produced in the entire process of lysate production from cultured cell lines. The protein production itself is also free from the generation of genetically modified organisms and can therefore be carried out in any technical environment, even without an S1 or S2 laboratory.
A DNA or RNA template can be added directly to the open cell-free system. Protein synthesis is completed within 60-90 minutes in the batch format, achieving protein yields in the range of 10µg/ml to 100µg/ml. In dialysis-based systems, protein yields in excess of 1000µg/ml can be achieved within 24 hours.

Empowering Properties of Drug Products by Conjugation to Suitable Vectors, Carriers or Particles

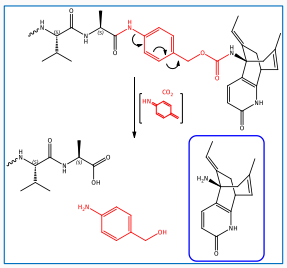

Huperzine A, bearing primary amino function, conjugated with Val-Ala-PAB linker undergoes self-immolative fragmentation in the presence of cathepsin B.

Carrier	Conjugation Chemistry
Metal surface	Affinity of sulfur to gold and silver
Metal oxide	Chelat formation
Silicates	Affinity of silicon and oxygen
Carbon: • Nanotubes • Fullerenes	Nitrenen addition via photoactivation of perfluoroarylazides
Plastic polymers: • Teflon • Polyethylene • Polystyrene • Latex	Ammonia or acrylic acid plasma followed by amide bond formation
Biopolymers: • Peptides • Proteins • Antibodies • Single Chain • Nanobodies • Camelides • Oligonucleotides • Aptamers	Thioether formation with maleimide Disulfide bond formation Acylation of Amines His-Tag acylation Click conjugation (CuCAAC, SPAAC, IEDDA) Enzyme supported conjugation: HaloTag® CLIP-Tag™ SNAP-Tag® Sequence dependent conjugation (Sortase)

Cleavage	Fragmentation	Functionality of Natural Product
Enzymatic hydrolysis: • Val-Ala • Val-Cit • Phe-Lys • Gly-Phe-Leu-Gly • Ala-Leu-Ala-Leu • Cyclobutyl-Ala • Cyclobutyl-Cit • Glucuronic acid Reduction Acidic hydrolysis	*p*-Aminobenzyl *p*-Hydroxybenzyl Oxathiolone Dimethylimidazolidinone	Primary & secondary amines Tertiary amines Alcohols Phenols Carboxylic acids

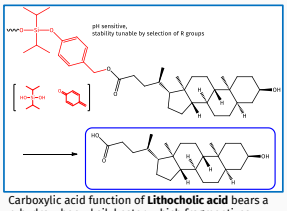

Carboxylic acid function of **Lithocholic acid** bears a *p*-hydroxybenzyl silyl ester, which fragmentizes under acidic conditions. Its stability can be adapted by exchanging *iso*-propyl against other residues.

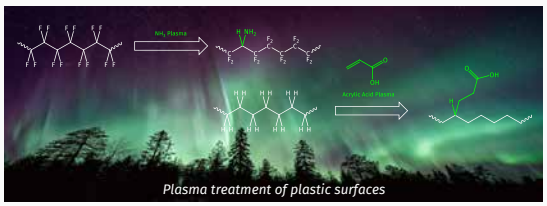

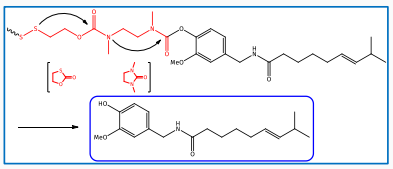

Capsaicin, bearing an alcohol function, conjugated with disulfide and DMAE linker undergoes self-immolative fragmentation under reductive conditions.

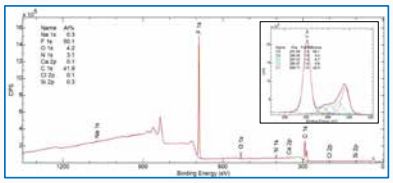

Surface analytics by **XPS** provides quantitative information about elemental composition down to 10 nm; deconvolution of high resolution spectra delivers information about oxidation and binding state.

Irreversible enzyme labeling with His-Tag, HaloTag®, CLIP-Tag™, SNAP-Tag®

Click

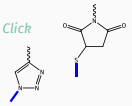

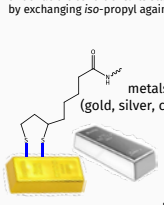

Photoactivation of perfluoroarylazides

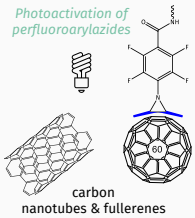

Plasma treatment with NH_3 or acrylic acid

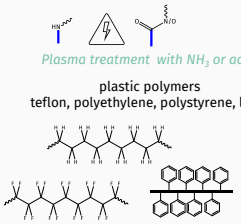

enzymatic acylation

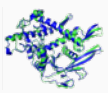

Antibodies (150 kDa)
scFv (30 kDa)
Nanobodies (15 kDa)
Camelides (90 kDa)

References:

[1] Antibody–drug conjugates: Recent advances in linker chemistry; Z. Su, D. Xiao, F. Xie, L. Liu, Y. Wang, S. Fan, X. Zhou and S. Li; *Acta Pharmaceutica Sinica B* 2021; https://doi.org/10.1016/j.apsb.2021.03.042
[2] Disulfide-Based Self-Immolative Linkers and Functional Bioconjugates for Biological Applications; Z. Deng, J. Hu and S. Liu; *Macromol Rapid Commun* 2020; **41**: e1900531; https://doi.org/10.1002/marc.201900531
[3] Linker Technologies for Antibody–Drug Conjugates; B. Nolting; *Antibody-Drug Conjugates L. Ducry* 2013; **1045**: 71–100; https://doi.org/10.1007/978-1-62703-541-5_5
[4] "The essentials of the "Green Deal" of the European Commission"; Green Facts. Green Facts, 7 January 2020.

Marion Casanova

Modular self-assembling dendrimer nanosystems as potent antibacterial candidates against antibiotics-resistant bacteria and biofilms

Marion Casanova,[a] Dinesh Dhumal,[a] Bar Maron,[b] Einav Malach,[b] Domenico Marson,[c] Erik Laurini,[c] Sabrina Pricl,[c,d] Zvika Hayouka,[b*] Ling Peng [a*]

[a] Centre Interdisciplinaire de Nanoscience de Marseille (CINaM), UMR 7325 CNRS, , Aix Marseille Univ, Marseille, France.
[b] Institute of Biochemistry, Food Science and Nutrition, The Robert H. Smith Faculty of Agriculture, Food and Environment, The Hebrew University of Jerusalem, Israel.
[c] MolBNL@UniTS, DEA, University of Trieste, Trieste, Italy.
[d] Department of General Biophysics, University of Lodz, Lodz, Poland.

mails: marion.casanova@univ-amu.fr; ling.peng@univ-amu.fr

The alarming increase and prevailing nature of antibiotic resistance urge for new antibacterial agents, in particular those differing substantially from conventional antibiotics.[1] In this context, amphiphilic dendrimers[2] bearing different functionalities are emerging as a promising new paradigm to combat bacterial AMR with a low likelihood of generating resistance.[3].

Chemical modulations

a. Hydrophobic tail
b. Generations
c. Terminal functions

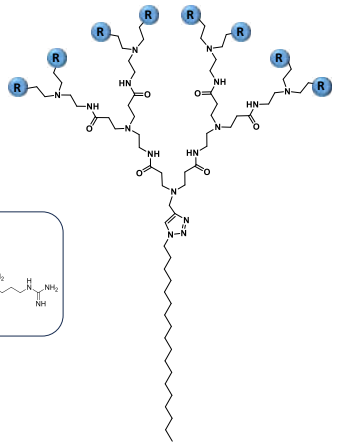

Self-assembling dendrimer nanosystems

Mimic natural antimicrobial peptides
enhanced stability and cooperative multivalency

Antimicrobial resistance & Severe nosocomial infections

(*Escherichia coli, Staphylococcus aureus, Pseudomonas aeruginosa*)

Dendrimer structure variation	Hydrophobic chain	Generation	Surface functionality	MIC [μg mL⁻¹] S. aureus	MRSA	E. coli	P. aeruginosa
Hydrophobic tail	No chain	2	Primary amine	—[a]	—[a]	>85	>64
	C_{10}	2	Primary amine	64	—[a]	1	3
	C_{16}	2	Guanidine	11.85	11.85	2.96	11.85
	No chain	2	Guanidine	>384.86	>384.86	21.8	87.21
Hydrophobic tail length	C_6	2	Primary amine	>500	>500	>500	—[a]
	C_{12}	2	Primary amine	15	15	60	—[a]
	C_{16}	2	Primary amine	5	8	10	—[a]
Generation dependence	C_{16}	3	Primary amine	3.9	—[a]	7.8	—[a]
	C_{16}	2	Primary amine	1.95	—[a]	3.9	—[a]
	C_{16}	1	Primary amine	3.9	—[a]	3.9	—[a]
Terminal functionality	C_{16}	3	Primary amine	6	6	6	6
	C_{16}	3	Tertiary amine	63	42	6	65
	C_{16}	3	Guanidine	200	>200	200	100
	C_{16}	3	Carboxylic acid	100	75	100	>200

[a] not available
MIC (minimum inhibitory concentration): lowest concentration required to inhibit 90% of bacterial growth, and value given in μg.mL⁻¹

Amphiphilic nature
antibacterial effect

Amine terminals
large spectrum activities

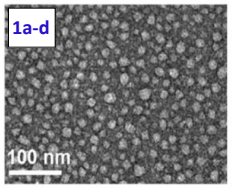

Transmission electron microscopy (TEM) images of the supramolecular nanomicelles

Dendrimer	CMC[a] (μM)	Particle size[b] (nm)	Zeta potential (mV)
1a	15	14 ± 2	+35
1b	17	17 ± 4	+23
1c	35	15 ± 3	+40
1d	4	10 ± 2	−13

Dendrimer	Cytotoxicity IC_{50}[c] (μM) L929[d]	HEK 293[e]	Hemolysis IC_{50}[f] (μM) RBC[g]
1a	>200	196	100
1b	>200	>200	100
1c	177	67	50
1d	>200	>200	>250

[a] CMC: critical micelle concentration
[b] Particle size: average values calculated with 300 nanoparticles measured in the TEM images
[c] Cytotoxicity-IC50: concentration of a dendrimer required for 50% inhibition of cell growth.
[d] L929: fibroblast cells; [e] HEK293: human embryonic kidney cell.
[f] Hemolysis-IC50: concentration required for lysis of 50% red blood cells; [g] RBC: red blood cells.

Small and stable
nanomicelles

Cooperative and multivalent interaction

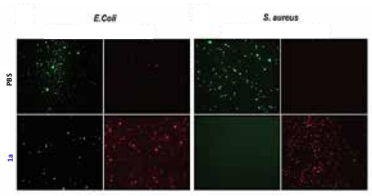

Studies on the live and dead bacterial cells and their membrane integrity and morphology upon treatment. Fluorescent microscopic imaging of live and dead cells of E. coli and S. aureus upon treatment with 1a. Live and dead cells were stained using SYTO9 and propidium iodide respectively.

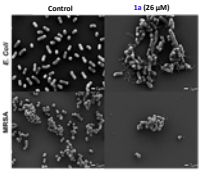

Scanning electron microscopic (SEM) images of E. coli and MRSA bacterial membrane surfaces upon treatment with 1a.

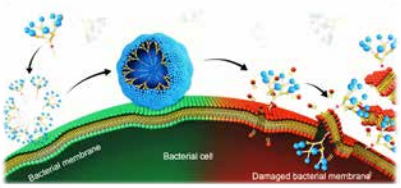

Cartoon illustration of the antibacterial activity shown by amphiphilic dendrimers via membrane adsorption, self-assembling, interaction, insertion, disintegration and disruption

Positive surface charges
Membrane disruption

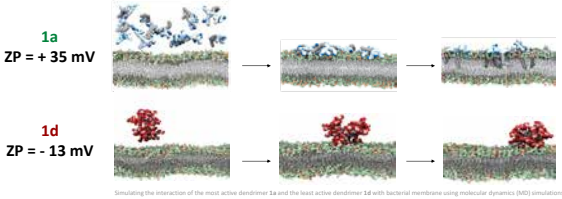

Simulating the interaction of the most active dendrimer **1a** and the least active dendrimer **1d** with bacterial membrane using molecular dynamics (MD) simulations

Multifuntional self-assembling dendrimer nanosytems against neuropathologies

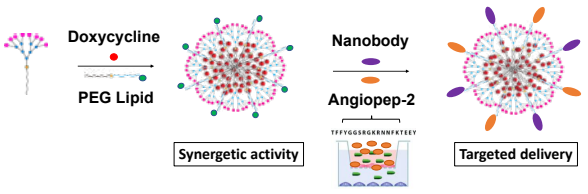

BBB transcytosis by recognizing
LRP-1 expressed on endothelial cells

Decreased "time to kill" compared to free drug
≈ 14% of BBB crossing

co-deliver antibiotics to cross BBB for targeted delivery

Our study presents a novel concept for generating potent antibacterial candidates and offers a new perspective for combatting antibacterial resistance.

1. U. Theuretzbacher et al., *Nat. Rev. Microb.*, **2020**, *18*, 275-85.
2. C. Galanakou et al., *Biomater. Sci.*, **2023**, *11*, 3379–3393.
3. D. Dumal et al., *Nanoscale*, **2022**, *14*, 9286–9296.
4. K. Nian et al, *ACS Infect. Dis.* **2023**, *submitted*.

Noemi Stefania Csaba

A MULTI-STAGE PULMONARY DRUG DELIVERY SYSTEM BASED ON SPOROPOLLENIN

S. Robla[1,2], L. Valverde-Fraga[1], C. Remuñán-López[1], S. Sánchez[1], R. Ambrus[2], N. Csaba,[1*]
1. School of Pharmacy - Center for Research in Molecular Medicine and Chronic Diseases (CIMUS), University of Santiago de Compostela, Spain
2. School of Pharmacy, Institute of Pharmaceutical Technology and Regulatory Affairs, University of Szeged, Szeged, Hungary
* noemi.csaba@usc.es

Tuberculosis (TB) is a life-threatening disease and a main cause of death worldwide. Current treatments consist of the systemic administration of combinations of antibiotics in high doses and for long periods. These therapeutic regimens are associated with severe side effects and high rates of drug resistance. To overcome these problems, this study aims at developing a micro/nano system for the improved delivery of antibiotics, with potential application in local, mucosal delivery.

METHODS

1 CHAMOMILE POLLEN PURIFICATION

Natural pollen | Purified pollen | Loaded with Ncs

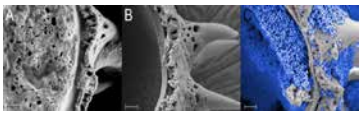

Fig. 1: Scanning electron micrographs of chamomile pollen **A**. Natural pollen. **B**. Purified pollen. **C**. Purified pollen loaded with nanoparticles of 200 nm. Bars represents 1 µm. (Nanoparticles are artificially coloured to enhance contrast).

2 FORMULATION AND CHARACTERIZATION OF POLYMERIC NANOCAPSULES

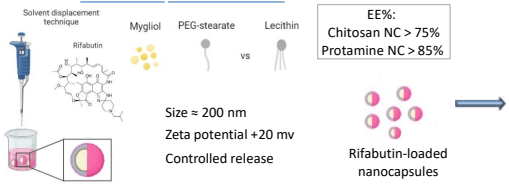

EE%:
Chitosan NC > 75%
Protamine NC > 85%

Size ≈ 200 nm
Zeta potential +20 mv
Controlled release

Rifabutin-loaded nanocapsules

3 LOADING OF POLLEN GRAINS WITH NANOCAPSULES

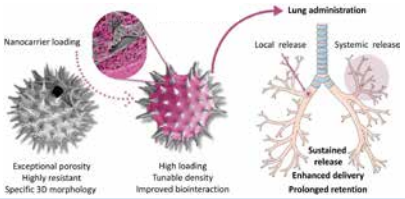

IN VITRO MECHANISTIC STUDIES

Lung cells and macrophages were cultured in a microfluidic system, to better mimic dynamic in vivo conditions.

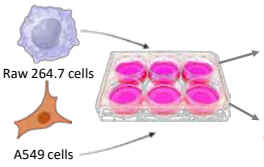

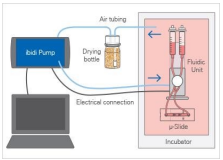

EFFICACY STUDIES

Antimicrobial susceptibility tests were performed according to the EUCAST guidelines using the mycobacterium species *M. phlei* (fast-growing) and *M. smegmatis* (slow-growing).

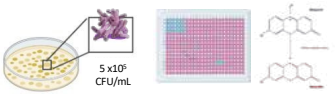

AERODYNAMIC CHARACTERIZATION

Pollen-NC dry powder formulations were evaluated for their lung deposition using the Andersen Cascade Impactor according to Ph. Eur.

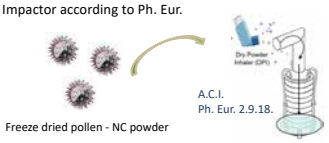

RESULTS

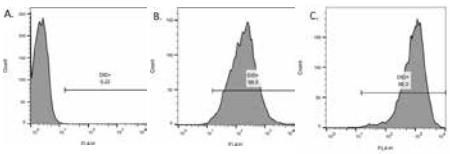

Figure 2: FACS histograms of A549 cells: control (A), treated with chitosan nanocapsules (B) and protamine nanocapsules (c)

Uptake studies were performed in lung cells and macrophages, showing efficient NC internalization (> 90%) in the cytoplasmic region of both cell types (**Fig 2** and **3**).

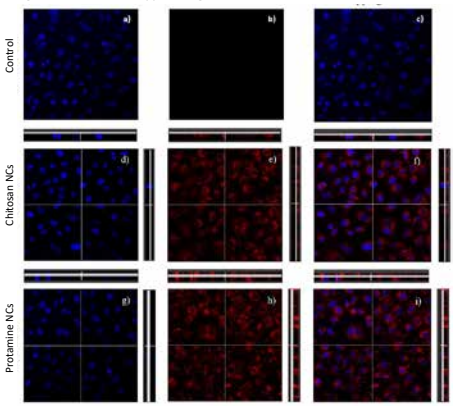

Figure 3: Confocal microscopy images of A549 cells: control: without nanocapsules (a-c), with chitosan nanocapsules (d-f) and protamine nanocapsules (g-i), with corresponding z stacks aligned to the right and above. Red channel (DiD): nanocapsules; Blue channel (DAPI): cell nuclei.

Purified pollen grains had high loading capacity for chitosan and protamine nanocapsules, as shown by confocal microscopy (**Fig 4**).

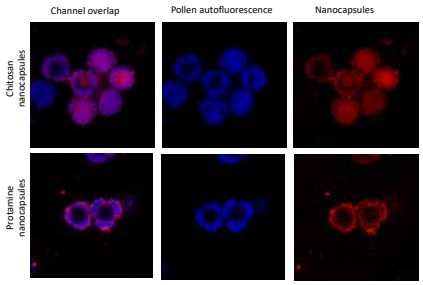

Figure 4. Confocal image of purified pollen grains loaded with nanocapsules. Blue channel: purified pollen grains; Red channel: nanocapsules labelled with DiD

Pollen grains were able to interact with cells and were retained beyond 4 hours under continuous flow **(Fig.5).** Under the same conditions, nanocapsules were washed out and the observed fluorescence was negligible.

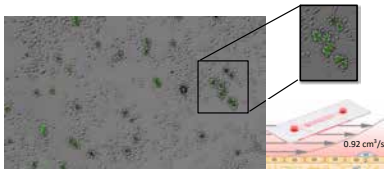

Figure 5: Fluorescence microscopy image of A549 cells grown in µ-Slide I channel slides, 4 h after the perfusion with purified pollen grains. Green channel: purified pollen grains

Efficacy studies indicated complete inhibition of growth both in *M. phlei* and *M. smegmatis*, within the expected susceptibility range of Mycobacterium (≤0.25–16 mg/L).

	Protamine NC	Chitosan NC	Free rifabutin
MIC (mg/L)	0.25	0.25	0.25
IC50 (mg/L)	0.15	0.11	0.11

Table 1. Minimum inhibitory concentrations (MIC) and half-maximal inhibitory concentrations (IC50) values in mg/L of rifabutin-loaded chitosan and protamine nanocapsules in Mycobacteria

The formulation showed 100% emission of dose from the inhaler and notable accumulation at the different stages of the lung (**Fig. 6A**). In addition, the 15% of the rifabutin dose was also detected in the pulmonary region (**Fig. 6B**).

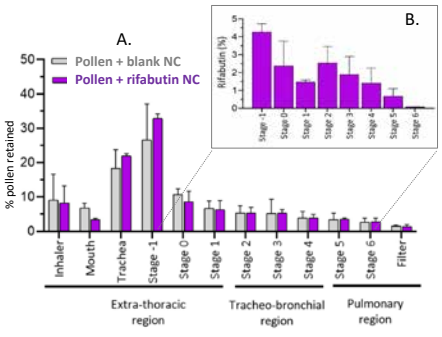

Figure. 6. Percentage of purified pollen, unloaded and loaded with rifabutin NCs (A) and quantification of rifabutin deposited in the different stages (B) upon in vitro aerodynamic evaluation by the Andersen Cascade Impactor. (mean ± SD, n =3.)

CONCLUSIONS

Drug loaded nanocapsules were efficiently loaded into purified pollen grains for enhanced mucointeraction. In vitro studies showed efficient internalization while maintaining cellular integrity. The system can be converted into a ready-to-use inhalable dry powder formulation and can efficiently deliver intact rifabutin. Overall, this platform could be an interesting candidate as a mucosal delivery system for the local treatment of infectious diseases.

References:
1. Robla et. al. Eur J. Pharm Sci 185 (2023) 106442
2. Valverde et. al. Eur. J. Pharm. Sci. 187 (2023) 106484
3. Ageitos et. al. Polymers, 13 (2021) 2094

EUROPEAN UNION
EUROPEAN REGIONAL DEVELOPMENT FUND
GOBIERNO DE ESPAÑA MINISTERIO DE CIENCIA E INNOVACION
(PID2019-107500RB-I00)

Nonspherical Microbubbles for Drug Delivery to Brain

Anshuman Dasgupta[1,2], Tao Sun[2,3], Roberto Palomba[4], Fabian Kiessling[1], Paolo Decuzzi[4], Nathan McDannold[3], Samir Mitragotri[2], Twan Lammers[1]

[1] Department of Nanomedicine and Theranostics, Institute for Experimental Molecular Imaging, RWTH Aachen University Clinic, Aachen, Germany.
[2] John A. Paulson School of Engineering and Applied Sciences (SEAS), Harvard University, Cambridge, USA..
[3] Brigham and Women's Hospital, Harvard Medical School, Boston, USA.
[4] Istituto Italiano di Tecnologia, Genova, Italy.

INTRODUCTION

Microbubbles (MB) are 1-10 µm-sized gas-filled vesicles which are used for ultrasound (US) imaging and drug delivery applications. To enhance MB performance, several physicochemical features have been systematically optimized over the years, including size, surface chemistry and shell rigidity. Shape is a feature that has thus far never been studied. MB are naturally spherical in shape due to surface tension. Here we created rod-shaped MB and demonstrate that these non-spherical MB outperform spherical MB in US-mediated drug delivery to the brain.

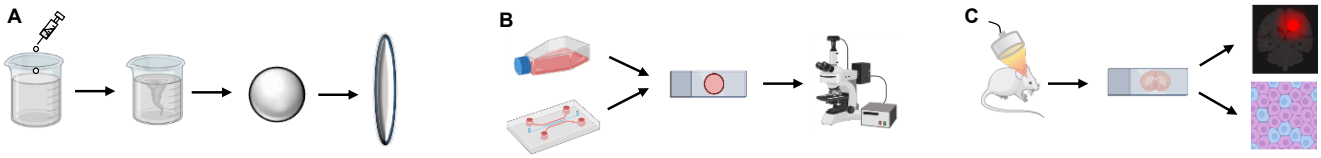

Figure 1. Study setup. (A) Spherical MB were produced by anionic polymerization of butylcyanoacrylate. Rod-shaped MB were produced by linearly stretching the spherical Mb above their Tg and cooling them down to rom temperature. (B) Rod-shaped MB were tested with regards to their phagocytosis, binding and margination propensity. (C) Rod-shaped MB were i.v. administered to evaluate their ability to permeate the BBB.

RESULTS

Rod-shaped MB

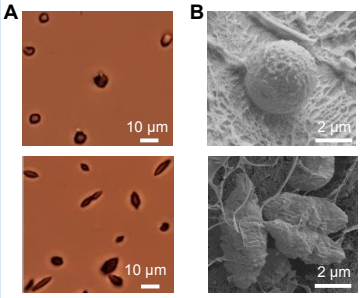

Figure 2. Engineering nonspherical MB. (A) Bright-field and (B) cryo-SEM confirm the spherical and anisotropic shape of the MB formulations.

Rods efficiently marginate

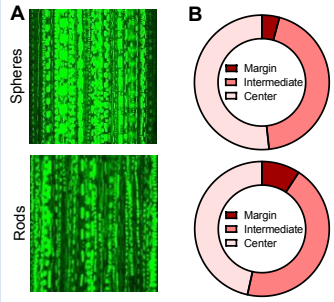

Figure 3. Margination. (A) Upon injection fluorophore-labelled MB, rods flowed closer to the channel walls (B) Percentage of rod-shaped MB flowing in the margin was doubled.

Rods circulate longer

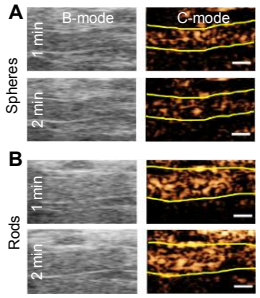

Figure 4. Circulation. (A-B) B-mode and C-mode US imaging of the aorta demonstrating that contrast of rod-shaped MB decreases less rapidly.

Rods improve drug delivery

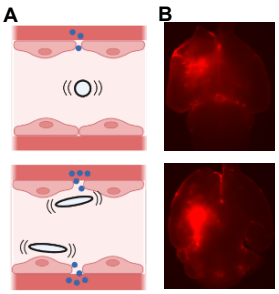

Figure 5. BBB permeation. (A-B) As a result of enhanced margination and circulation, rod-shaped MB improve BBB permeation upon FUS exposure.

TfR rod-shaped MB

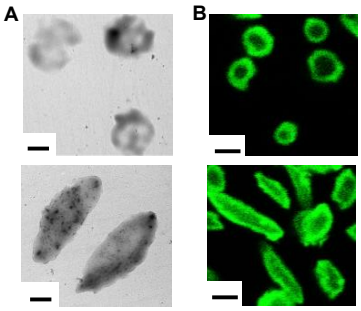

Figure 6. Engineering transferrin-targeted nonspherical MB. (A) TEM and (B) confocal confirm the spherical and anisotropic shape of the MB formulations.

TfR rods bind to brain endothelium

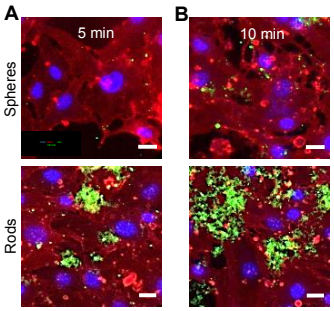

Figure 7. Binding to bEnd.3 cells. (A-B) After 5 and 10 min post incubation, transferrin-targeted rods bind efficiently to brain endothelium bEnd.3 cells.

TfR rods bind to BBB

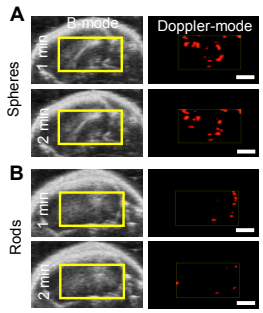

Figure 8. BBB Binding. (A-B) US imaging indicating that the power-doppler contrast of anti-TfR rods decreases faster.

TfR rods boost drug delivery

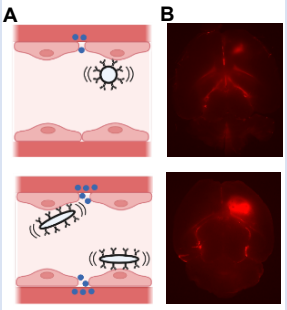

Figure 9. BBB permeation. (A-B) As a result of enhanced binding, anti-TfR rods improve FUS-assisted BBB permeation.

CONCLUSIONS

Nonspherical MB outperform spherical MB by presenting with enhanced margination, prolonged circulation, strong binding to BBB, and improved FUS-mediated BBB permeation.

ACKNOWLEDGEMENTS

This work was supported by EuroNanoMed-III: NSC4DIPG, DFG: GRK/RTG2375, NIH: R01 EB033307 John A. Paulson School of Engineering and Applied Scienced at Harvard University.

CONTACT

Email: adasgupta@ukaachen.de
Twitter: @Anshu_Dasgupta
Mobile: +4915730911539
Residence: Aachen, Germany

IL-12 delivery through immunostimulatory nanoparticles enhances inflammatory response for glioblastoma treatment

Flávia Sousa[1], Barbara Rother-Rutishauser[1], Alke Petri-Fink[1]
[1]Adolphe Merkle Institute, University of Fribourg, 1700 Fribourg, Switzerland
E-mail: flavia.sousa@unifr.ch

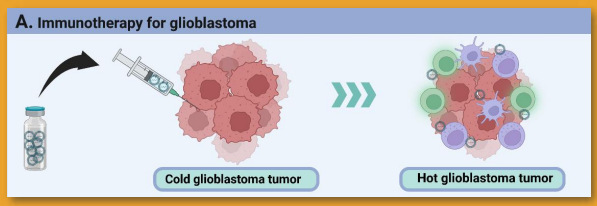

In the last decade, interleukin 12 (IL-12) has been studied as one of the most potent cytokines for anti-cancer immunotherapy because it stimulates the interferon-γ production, decreases the angiogenesis and changes the cancer microenvironment from one that contains T_H0 and M2-type phenotype macrophages to one richer in T_H1 cells and inflammatory M1-type macrophages (1-2). However, the anticancer cytokine IL-12 cannot be used as a systemic cancer treatment due to its excessive toxicity, instability and short half-life (3). In this study, IL-12 was formulated and encapsulated into polymeric nanoparticles to modulate the TAM landscape.

MATERIALS AND METHODS

Immunostimulatory nanoparticles were produced by double-emulsion technique and IL-12 was encapsulation.

Nanoparticle size, PdI and Zeta Potential were obtained with DLS.

Nanoparticle morphology was observed with Scanning Electron Microscopy and Transmission Electron Microscopy.

In vitro assays were done with Glioblastoma cancer cells (U87) and murine macrophages (J774A.1).

For the immunomodulation evaluation, ELISA, qPCR and FACS were used.

RESULTS AND DISCUSSION

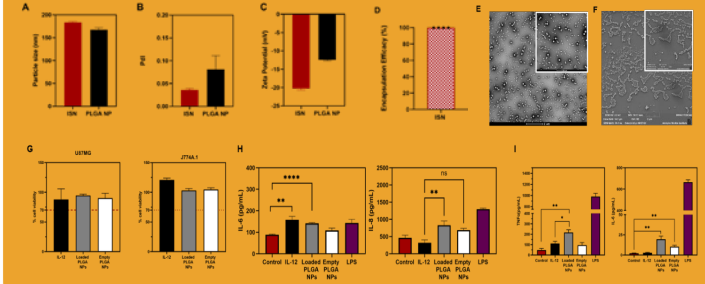

Figure 1. Preliminary results of stimulatory nanoparticles. Size distribution of nanoparticle vaccine were analyzed by (A) particle size, (B) PdI, (C) zeta potential. (D) Encapsulation efficacy of IL-12 within the nanoparticle vaccine. Morphology of the nanoparticles were analyzed by (E) transmission electron microscopy (TEM) and (F) scanning electron microscopy (SEM). Scale bar: 2 µm. Cell viability of U87MG (GBM cancer cell line) and J774A.1 (mouse macrophage cell line) after 24h of incubation with nanoparticle vaccine was evaluated by LDH (G). ELISA analysis of IL-6 and IL-8 production in culture supernatants of human U87MG with the indicated treatments. (I) ELISA analysis of TNF-α and IL-6 production in culture supernatants of J774A.1 macrophages with the indicated treatments. All data are presented as means ± SEM. Graphs represent pooled data from at least three independent experiments.

- Immunostimulatory nanoparticle vaccine has an average particle size around 180 nm, a PdI of 0.05 and a negative zeta potential (-20 mV).
- *In vitro* data also show that the nanoparticle vaccine was not toxic for GBM cancer cells (U87MG cell line) or mouse macrophages (J774A.1 cell line).
- Nanoparticles simulated the production of pro-inflammatory cytokines (IL-6, IL-8) in GBM cancer cells and macrophages (TNF-α and IL-6), suggesting possible modulation of the TAM landscape.
- The same behavior was also observed by mRNA expression measured by RT-PCR for the cytokines IL-8 and IL-6, where PLGA nanoparticle vaccine increased the production of pro-inflammatory cytokines.

CONCLUSION

These data indicate that PLGA nanoparticle cointaining IL-12 is an effective drug delivery platform for glioblastoma treatment. To compare the interaction between GBM cancer cells and macrophages, *in vivo* work will be done further.

1. Chiocca EA et al. Science Translational Medicine. 2019;11(505):eaaw5680. 2. Lasek W et al. 2014;63(5):419-35. 3. Leonard JP et al.. Blood. 1997;90(7):2541-8.

FLÁVIA SOUSA
Adolphe Merkle Institute
University of Fribourg
Switzerland
flavia.sousa@unifr.ch

Sander De Weerd

Engineering and characterization of biomimetic nanoparticles (BNPs) in leukemia.

Sander de Weerd[1,2,3], Emma Ruiter[1], Jan-Jacob Schuringa[2], Wouter Roos[3], Anna Salvati[1]

1 Department of Nanomedicine and Drug Targeting, Groningen Research Institute of Pharmacy, University of Groningen, A. Deusinglaan 1, 9713 AV Groningen, The Netherlands,
2 Department of Experimental Hematology, University Medical Center Groningen, University of Groningen, Groningen, The Netherlands,
3 Moleculaire Biofysica, Zernike Instituut, Rijksuniversiteit Groningen, Groningen, The Netherlands.

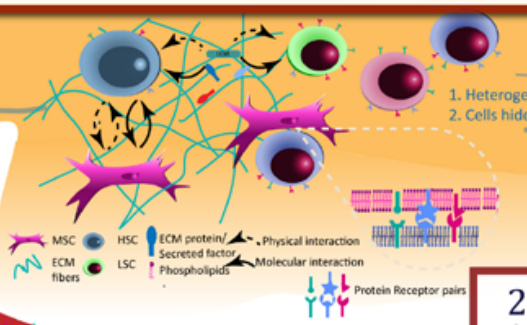

university of groningen

Sander de Weerd
0625116978
s.weerd.de@rug.nl

1. Optimization Membrane Extraction

1.1 Pressure and method

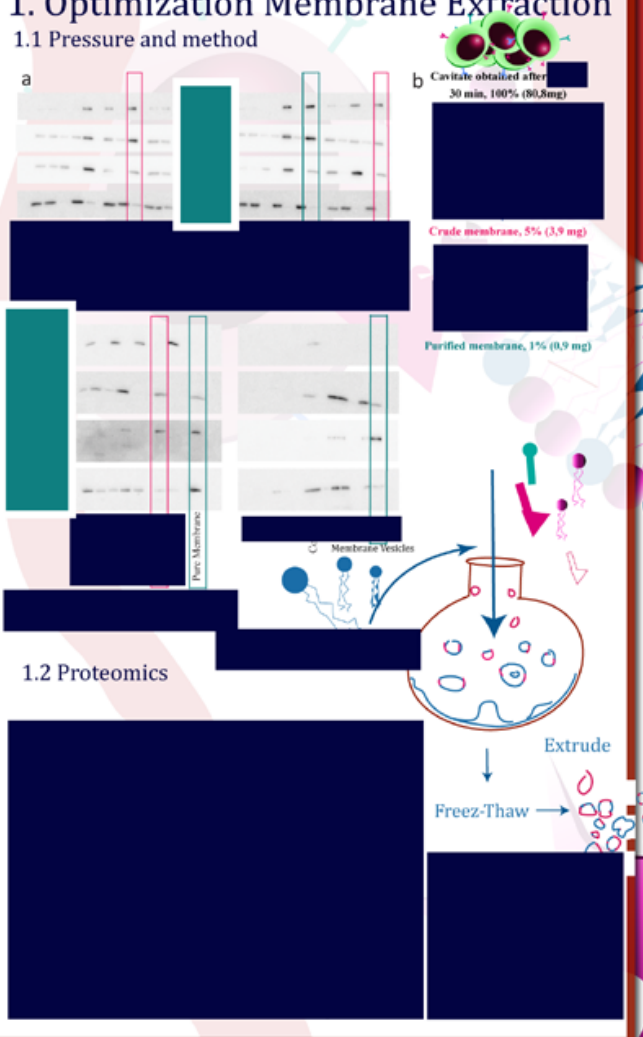

1.2 Proteomics

2. Particle Characterization

2.1 Dynamic Light Scattering (DLS)

2.1 AFM

3. Cell uptake kinetics (flow cytometry)

3.1 Membrane purity

4. Highlights

- Purity of membrane extract influences uptake
- BNPs are more rigid.
- This workflow can be tailored for the generation of BNPs from any cell.

Mareike Deuker

Interaction of anti-PEG antibodies with PEG

Mareike F. S. Deuker [a], Volker Mailänder [b,a], Svenja Morsbach*[a] and Katharina Landfester [a]

[a] Max Planck Institute for Polymer Research, Ackermannweg 10, 55128 Mainz, Germany.
[b] Department of Dermatology, University Medical Center of the Johannes Gutenberg-University Mainz, Langenbeckstrasse 1, 55131 Mainz, Germany

UNIVERSITÄTSmedizin. MAINZ

SFB 1066

MAX PLANCK INSTITUTE FOR POLYMER RESEARCH

INTRODUCTION

anti-PEG antibodies enrich in the protein corona of PEGylated NCs and could mitigate the stealth effect of PEG

- poly(ethylene glycol) (PEG) reduces unspecific protein adsorption and prolongs the nanocarrier (NC) circulation time (stealth effect)[1]
- administration of PEGylated NCs leads to an accelerated blood clearance via anti-PEG antibodies and might cause acute severe allergic reactions[2]
- proteins bound to the NC surface (protein corona) affect the NC's identity as recognized by cells[3]

1. study of anti-PEG antibodies in healthy individuals among the German population using an enzyme linked immunosorbent assay (ELISA)
2. enrichment of anti-PEG antibodies in the protein corona of PEGylated silica nanocapsules (SiNCs)
3. the cellular uptake of PEGylated NCs with varying amounts of bound anti-PEG antibodies

1. PLASMA SCREENING

Plasma screening to analyze the anti-PEG antibody concentration and prevalence in a sample of the German population (n = 500)

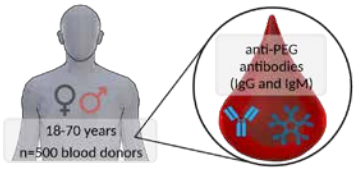

High anti-PEG antibody prevalence and concentration throughout population

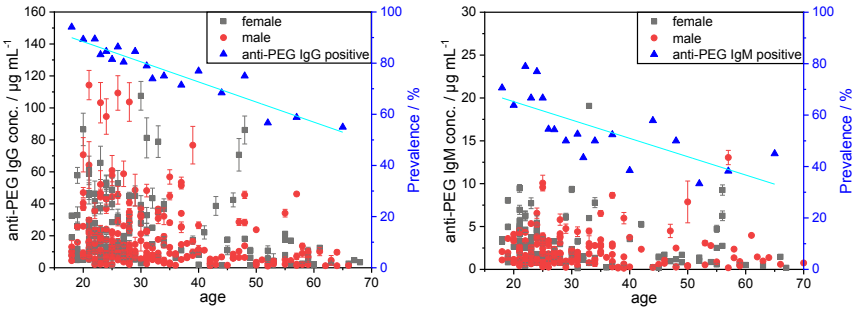

2. PROTEIN CORONA

The protein corona is the biological coating of the NC that determines its biological identity as recognized by cells. The accumulation of anti-PEG antibodies in the protein corona can be analyzed via various techniques.

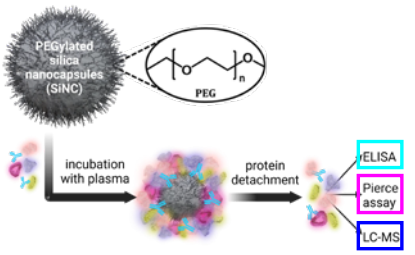

anti-PEG IgG antibodies enrich in the protein corona of PEGylated SiNC

Influence of PEG chain length and density on anti-PEG antibody concentration in the protein corona without PEG (CTACl as surfactant), increasing PEG density (low, medium, high), and PEG chain length (n=25 to n=80)

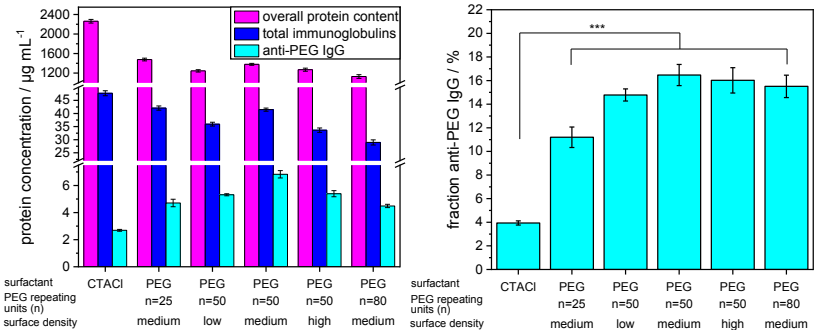

3. CELL UPTAKE

Cellular uptake of SiNC with increasing anti-PEG IgG concentration in the protein corona
Uptake in THP-1 (human) and RAW 264.7 (murine) macrophages

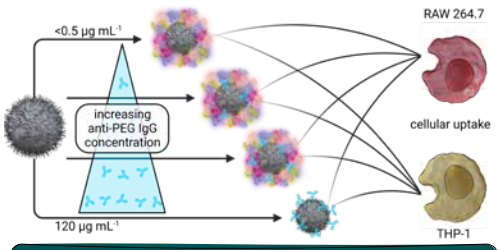

Cell uptake in macrophages increases with anti-PEG IgG concentration

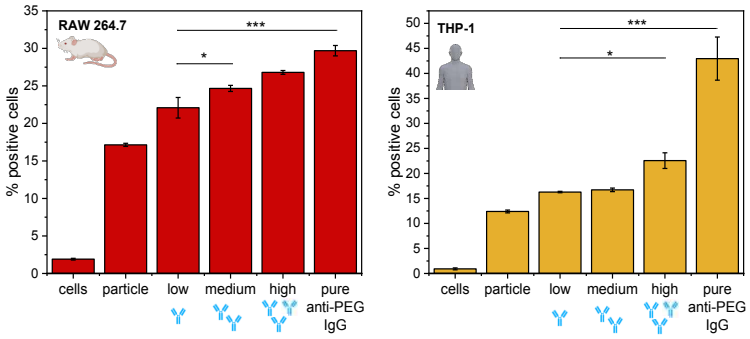

CONCLUSION

1. **High prevalence of anti-PEG IgG and IgM throughout all blood donor samples.**
2. **Enrichment of anti-PEG antibodies in the protein corona of PEGylated NCs compared to non-PEGylated NCs.**
3. **Cell uptake in macrophages increases with the anti-PEG antibody concentration in the protein corona.**

DOI: https://doi.org/10.1039/D3NH00198A

EXPRESSION OF CYTOKINES IN PBMC AND SPIKE PROTEIN CODING mRNA IN VARIOUS TISSUES OF THE PIG AFTER COMIRNATY VACCINATION: POTENTIAL MECHANISMS OF LONG TERM ADVERSE EVENTS

László Dézsi[1,2], Tamás Bakos[1], Gábor Kökény[3], Csaba Révész[3], Petra Berényi[1,2], Tamás Mészáros[1,2], Gergely Kozma[1,2], Béla Merkely[4], Tamás Radovits[4] and János Szebeni[1,2]

[1]Nanomedicine Research and Education Center, Department of Translational Medicine, Semmelweis University, Budapest, Hungary
[2]SeroScience Ltd., Budapest, Hungary
[3] Department of Translational Medicine, Semmelweis University, Budapest, Hungary
[4]Heart and Vascular Center, Semmelweis University, Budapest, Hungary

Introduction

A small, but important percentage of people immunized with mRNA-containing liposomal (LNP-mRNA) vaccine(s) developed allergy-like symptoms shortly after vaccination, occasionally leading to severe hypersensitivity reactions (HSRs) or even to death. It mimicked HSRs of i.v. administered nanomedicines called complement (C) activation-related pseudoallergy (CARPA). In our recent studies, we investigated CARPA-like reactions after administration of Pfizer's Comirnaty (CMT), an LNP-mRNA vaccine using a naturally hypersensitive porcine CARPA model. We have shown that CMT administration induced HSRs showing all characteristic properties of CARPA. Since the mass vaccination campaign a decent number of people produced long-term adverse events. Its mechanism is yet unknown but in various cells and tissues the presence of spike protein (SP) coding mRNA or SP per se suspected. In our present experiments, the expression of COVID-related cytokines and SP-coding mRNA after CMT injection are studied.

Materials and Methods

Pigs: Domestic pigs (20-25 kg) were sedated with ketamine/xylazine (10 and 2 mg/kg, respectively) and anesthetized by isoflurane (2-3%) in O2 flow. In spontaneously ventilating animals, the pulmonary arterial pressure (PAP) was measured using a Swan-Ganz catheter introduced into the pulmonary artery via the right external jugular vein, while systemic arterial pressure (SAP) and heart rate (HR) were measured in the femoral artery. The left femoral vein was cannulated for blood sampling. Test agents were injected in bolus (~30 sec) via the left external jugular vein. Hemodynamic changes and ECG were continuously monitored using an AD Instruments (ADI) PowerLab System. Mean PAP, SAP, HR and ECG data were evaluated by the ADI LabChart software.

Blood sampling: Blood samples of 2 ml, each were collected from the pigs before (time 0), and at pre-determined time points (1-3-5-15-30 min) after the injection. Samples were collected into K3-EDTA blood tubes, of which samples for TXB2 analysis were containing indomethacin. Aliquots of 100 µl blood were drawn into tubes with K3-EDTA for hematological analysis, performed by an Abacus (Diatron) analyzer. Blood was centrifuged at 1500 rpm for 10 min at 4 °C, and plasma was stored at -80 °C until analysis.

Thromboxane B2 levels: Plasma TXB2 (the stable metabolite of plasma TXA2) levels were measured with an ELISA kit (Cayman Chemicals).

PBMC and tissue sample analysis: After administration of CMT, serial blood samples were taken to measure blood cell changes, cytokine gene transcription in peripheral blood mononuclear cells (PBMC) and blood levels of inflammatory cytokines, using qPCR and ELISA. At the end of the study tissue samples were taken from multiple organs (incl. heart and kidney) for histological and SP-coding mRNA sequence analysis.

Test items: Repeated doses of 5x of the human dose of CMT vaccine (HVD) were given three-times as an i.v. or i.m. bolus injection. As positive control for CARPA zymosan (0.1 mg/kg) was used.

Results – part 1

Administration of **CMT** i.v. in the porcine CARPA model resulted in acute symptoms of HSRs. In some cases, already by the the first dose anaphylaxis, while at repeated administration self-induced tolerance (tahyphylaxis) could be observed.

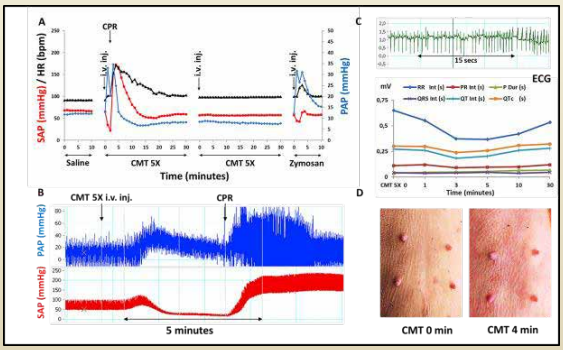

Figure 1: Original recordings of the hemodynamic, ECG and skin reactions**.** Anaphylaxis and tachyphylaxis in a pig repeatedly injected with 5x HVD of CMT followed by an injection of zymosan. TXB2 changes correlated well with PAP changes (not shown). **Fig. 1A–C. A** Mean pulmonary arterial pressure (PAP, blue), systemic arterial pressure (SAP, red), and heart rate (HR, black) changes during the whole experiment. **B** Real-time pulse pressure recording of the reaction during the initial 10 min. CPR - cardiopulmonary resuscitation. **C top**: a 25 s ECG recording during the reaction showing arrhythmia, and **C bottom**: changes of ECG parameters after the administration of CMT. **Fig. 1D.** Photographs of baseline (CMT 0) and skin flushing caused by Comirnaty at 4 min (CMT 4 min) after i.v. injection.

Conclusions

This study investigates the short and long term immune reactive properties of Comirnaty (CMT), an LNP-mRNA type vaccine. CMT administration induced HSRs showing all characteristic properties of CARPA. In addition, COVID-related cytokine- and SP-coding mRNA expression could be observed. This phenomenon may be a contributing factor to the long term events after HSRs to CMT and potentially other mRNA vaccines.

Outlook

We are just finishing a two-month chronic arm of this study where SP expression upon CMT is studied in various tissues. A positive outcome could further support our hypothesis on long term adverse effects of CMT, which would be like „re-infection" with COVID.

Results – part 2

In 10 of 15 pigs acute changes were followed. Similarly, to previous findings a transient increase in PAP, accompanied by TXA2 release and other hemodynamic and blood cell changes as SAP elevation, granulocytosis, lymphopenia, and thrombocytopenia were observed. Three pigs developed anaphylactic shock that required resuscitation. Repeated dosing had variable outcome, with or without tachyphylaxis. In some cases, skin flush was also observed (data not shown). In 5 pigs the study of chronic changes in the above parameters incl. SP expression is ongoing.

In PBMC COVID-related cytokines (IL1RA, CXCL10, TNFα) mostly elevated, with individual variations. SP-coding mRNA expression could also be observed in cardiac and renal tissue 6 h after the 1st CMT injection with similar variability.

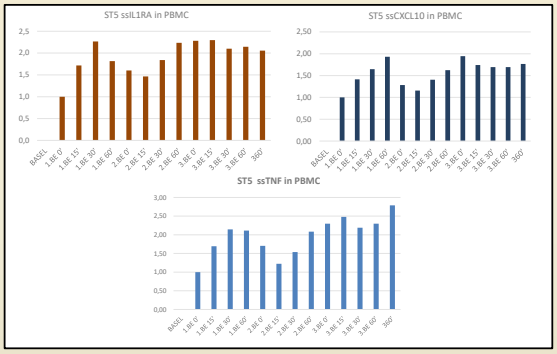

Figure 2: Changes in COVID-19 infection-related cytokines IL1RA (**top left**). CXCL10 (**top right**) and TNFα (**bottom**) in PBMC isolated from a pig (ST5) with a time course following three-times repeatedly injected with 5x HVD of CMT up to 6 hrs. Columns show fold changes in cytokines at baseline (BASEL) and at 0, 15, 30 and 60 min after each injection (1BE, 2BE, 3BE are 1st, 2nd and 3rd injections, respectively.

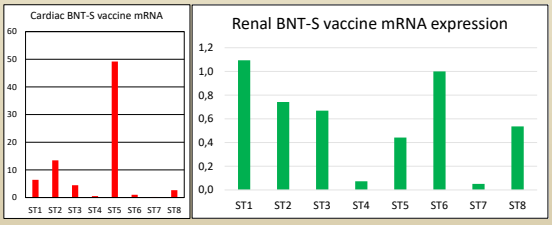

Figure 3: Expression of SP-coding mRNA sequence (BNT-S) at 6 hrs following CMT administration in heart and kidney samples from eight pigs (ST1-ST8). Columns show fold changes compared with samples with no vaccination.

Supported by the European Union Horizon 2020 projects 825828 "Expert" and 952520 "Biosafety", as well as the National Research, Development and Innovation Office of Hungary under the Investment in the Future funding scheme (2020-1.1.6-JÖVŐ-2021-00013), and a Semmelweis University Grant (STIA-KFI-2022).

Laura Dietz

Forming of a Protein Corona on Extracellular Vesicles increases Uptake into Immune Cells

Laura Dietz[1,2*], Jennifer Oberländer[1,2*], Ana Mateos-Maroto[2], Jenny Schunke[1,2], Michael Fichter[1,2], Eva-Maria Krämer-Albers[3], Katharina Landfester[2], Volker Mailänder[1,2]
(*shared first)

[1] Department of Dermatology, University Medical Center Mainz, Langenbeckstraße 1, 55131 Mainz, Germany
[2] Max Planck Institute for Polymer Research, Ackermannweg 10, 55128 Mainz, Germany
[3] Institute of Developmental Biology and Neurobiology, Johannes Gutenberg University of Mainz, Mainz, Germany

MAX PLANCK INSTITUTE FOR POLYMER RESEARCH

ABSTRACT

Extracellular vesicles (EV) have attracted much attention as novel nanotherapeutic recently and first clinical trials are ongoing. Similar to synthetic nanotherapeutics, EVs acquire a protein corona upon contact with biological fluids that likely influences their biodistribution, cell targeting and in consequence therapeutic efficacy. Unlike for synthetic nanotherapeutics, little is known about the influence of the EVs' protein corona on any of these processes. Therefore, we aimed to compare the influence of a protein corona on EVs directly to the protein corona on engineered liposomes. First, we analyze the influence of the protein corona on EV uptake into human monocytes and compare it with the influence on the uptake of engineered liposomes. Further, we use a proteomic approach in order to analyze the protein composition of the EVs themselves and the protein composition of a human blood plasma protein corona around EVs. The increased uptake of EVs in presence of a protein corona can be attributed to the presence of complement system proteins in the protein corona. Our results demonstrate the relevance of the protein corona for EV uptake, which will aid their use in therapeutic applications.

PRODUCTION AND LABELLING OF EVS

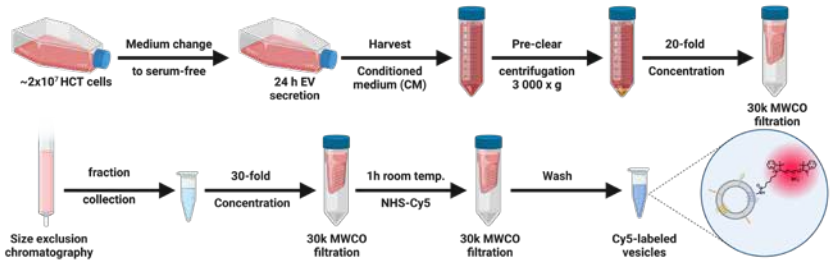

- EVs were produced under serum-free conditions from HCT 116 cells and isolated by size exclusion chromatography (SEC)
- EV preparation was characterized by cryo-TEM and mass spectrometry (exosome marker CD81 and CD9 identified) (not shown)
- Hydrodynamic diameter: ~200 nm
- Fluorescent labeling performed with NHS-Cy5 reacting to primary amines of surface proteins

LABELLING OF LIPOSOMES

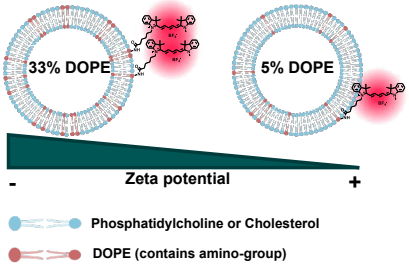

- Prepared with Phosphatidylcholine, cholesterol and varying amount of DOPE by thin film hydration and extrusion
- Hydrodynamic diamter: ~200 nm
- Fluorescent labeling performed with NHS-Cy5 reacting to primary amine of DOPE head group

PROTEIN CORONA OF HCT 116-DERIVED EVS

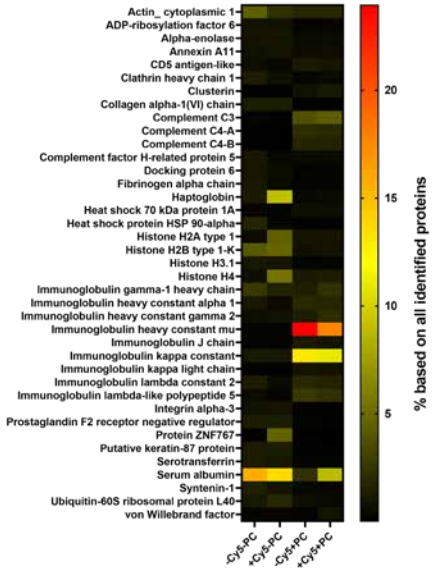

- Protein corona prepared by incubation of EVs or liposomes in human citrate plasma 37°C for 1 h
- Protein corona was not detached from EVs, proteins enriched in protein corona sample are considered EV protein corona proteins
- Main EV corona proteins found: **complement proteins C3** and **C4**, **immunoglobulin heavy constant μ** and **κ constant**
- Main EV corona proteins have opsonizing properties → enhance uptake by immune cells

UPTAKE IN IMMUNE CELLS

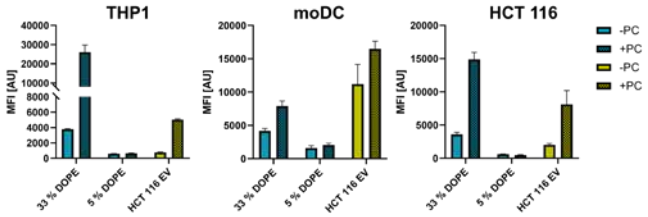

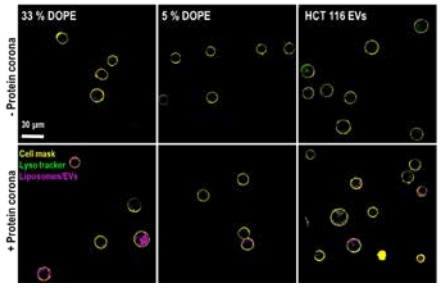

- Protein corona prepared by incubation of EVs or liposomes in human citrate plasma 37°C for 1 h
- MFI values were calibrated according fluorescence intensity with and without protein corona
- In human monocytic cell line (THP1), primary monocyte-derived dendritic cells (moDC) and HCT 116 cells, uptake of EVs and 33%-DOPE liposome was enhanced by adsorption of a protein corona
- For fluorescence microscopy, HCT 116 cells were incubated with vesicle amounts calibrated according to fluorescence intensity
- Boost of cell uptake after adsorption of a protein corona was also observed in fluorescence micrographs for all vesicles

Conclusion

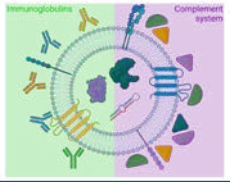

- Uptake of liposomes and EVs is enhanced by adsorption of a human blood plasma-derived protein corona
- EV protein corona was enriched with opsonizing proteins like immunoglobulins and complement proteins that can be responsible for enhanced uptake
- Liposome protein corona was enriched with immunoglobulins but also contained dysopsonizing proteins like apolipoproteins
- Supports emerging theory that EV protein corona is integral part of EV functionality
- Stealth modifications needed for EVs to unravel full potential as drug delivery platform and nanotherapeutic

Contact: dietzl@mpip-mainz.mpg.de
This work was supported by the Max Planck Graduate Center
All figures were created with BioRender.com

Max Planck Graduate Center mit der Johannes Gutenberg-Universität

Philip Dreier

PEG Lipid Isomerization as a Selective Tool against Anti-PEG Antibody Recognition in Lipid Nanoparticles

P. Dreier[a], R. Matthes[a], D. Göbel[b], T. Endres[c] and H. Frey*[a]

[a]Johannes Gutenberg University, Department of Chemistry, 55128 Mainz, Germany

[b]Evonik Operations GmbH, Rodenbacher Chaussee 4, 63457 Hanau-Wolfgang, Germany

[c]Evonik Operations GmbH, Kirschenallee, 64293 Darmstadt, Germany

CLINAM European Foundation for Clinical Nanomedicine

Abstract

In the last decades, poly(ethylene glycol) (PEG) has been established as the most relevant pharmaceutical polymer in modern nanomedicine. Despite several advantages, an increasing number of studies has led to concerns related to the presence of anti-PEG antibodies (APA) in a constantly growing part of the population, diminishing the desired effect of PEGylation. We present isomerization of PEG as an efficient approach to inhibit APA interaction while preserving PEG´s main advantages and structure in lipid nanoparticle formulations.

Fundamental Concept

Lipid Characterization

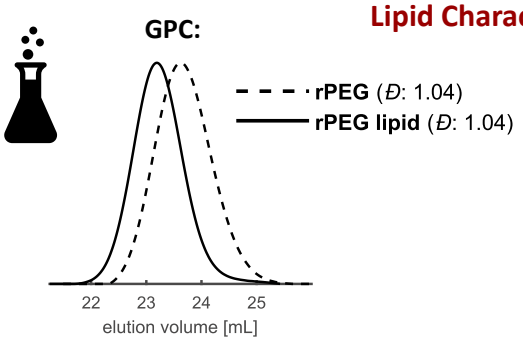

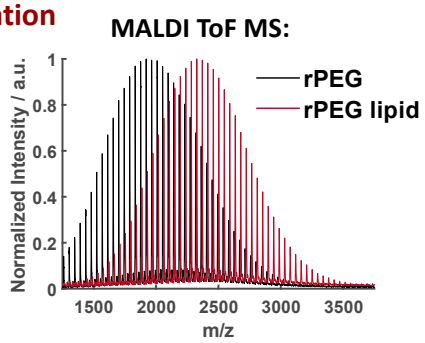

ELISA Studies

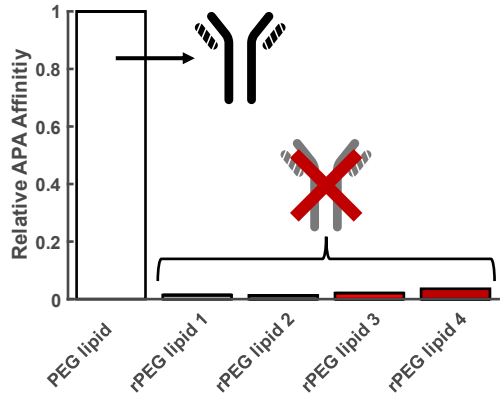

Lipid Nanoparticle Formulations

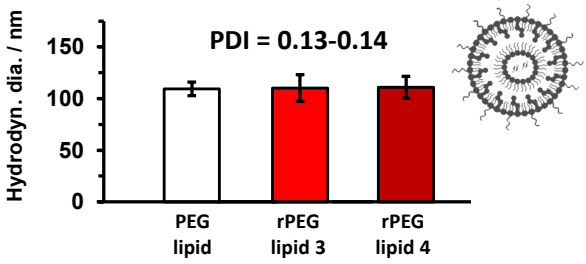

Transfection Assays

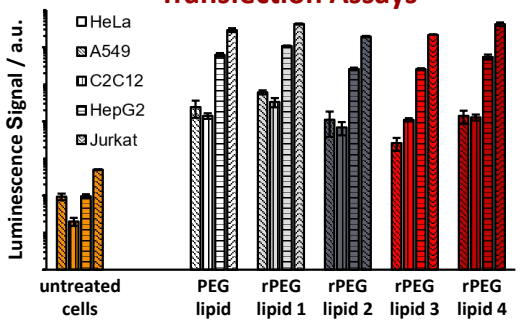

Summary

- well-defined rPEG lipid structures
- well-defined rPEG lipid nanoparticles
- high transfection efficiencies
- efficient inhibition of APA interaction

Aroa Duro

PEG alternatives based on bioinspired polymers with shielding properties as Lipid Nanoparticle (LNP) components

A. Duro-Castano, R. Miravet-Martí, S. Alonso, I. García, P. Martínez, G. Sogorb, L. Herrera, J. García, S. Esteban, V. J. Nebot

CURAPATH

PEG problem and Curapath's bioinspired alternatives

PEG-lipid conjugates are commonly applied in the formulation of the most successful nucleic acid delivery systems: lipid nanoparticles (LNPs) [1]. Indeed, PEG-shielded LNPs have positioned as key non-viral vectors for gene delivery with BioNTech/Pfizer and Moderna/ /NIAID mRNA COVID-19 vaccines leading the way [2,3]. However, the extensive use of PEG in marketed products has raised concerns related to immunogenicity and loss of efficiency of PEG-containing medicines due to the production of anti-PEG antibodies which clear PEGylated excipients from the bloodstream (Accelerated Blood Clearance, ABC) [4]. To overcome this, at Curapath we work with a portfolio of proprietary bioinspired alternatives to PEG based on polypeptides and polypeptoids. Examples are the conjugate PSar-succ-tocopherol conjugate or diol modified PGA-lipid conjugates that have analogue solubility, macromolecular properties and interactions with water compared to PEG, with a wide and versatile terminus group functionality for (bio)conjugation [5].

Curapath's PEG Alternatives for Shielding Lipids

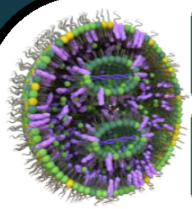

Ionizable Lipid *(neutral/protonated)*
Aids in the encapsulation of nucleic acids through electrostatic interactions

Cholesterol
Decreases permeability of the LNP and enhances its stability

Nucleic Acid *(e.g. mRNA)*
Encodes protein of interest

'Helper' Lipid
Improves LNP stability and fusogenicity

PEG-Lipid
Prevents non-specific protein absorption, particle aggregation and controls LNP size

PEG Alternatives
PSar, PGA-Diol, Biocompatible, endogenous building blocks, overcome PEG immunogenicity

Controlled synthesis and scale-up

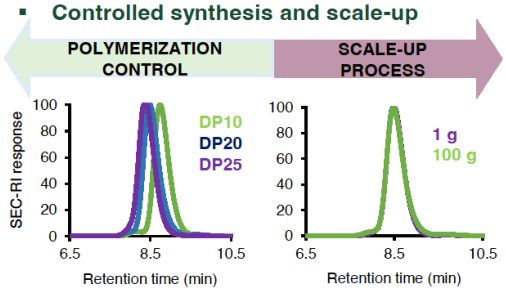

✓ These PEG alternatives have been produced and scaled up in technical batches and with demonstrated batch-to-batch reproducibility and QC compliance.

Formulation process development

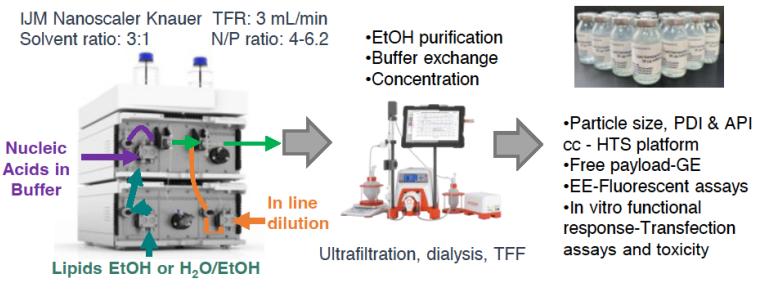

LNP characterization

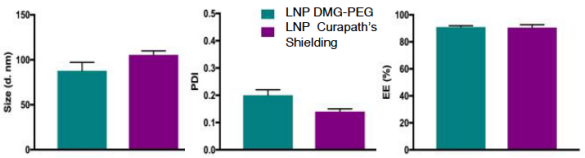

✓ Stable formulations with adequate encapsulation efficiencies, suitable physic-chemical properties and good reproducibility are obtained when tuning the % of lipid-shielding using a commercially validated method.

In vitro functional response

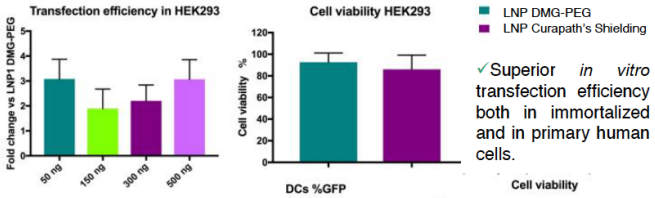

✓Superior *in vitro* transfection efficiency both in immortalized and in primary human cells.

In vivo performance

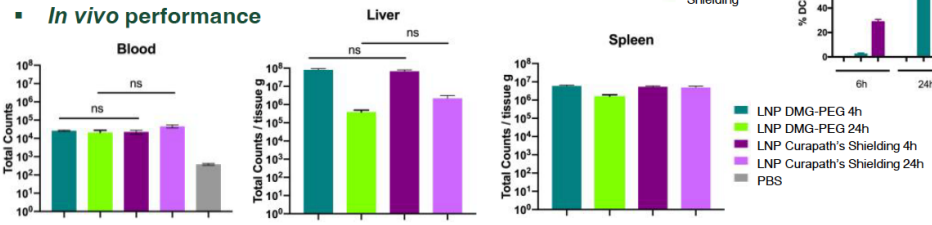

✓*In vivo* transfection of LNPs containing mRNALuc. Non-significant differences against Benchmark when i.v. injected in Balb/c mice confirming that PEG can be replaced without affecting performance.

Conclusions

✓Our PEG-free alternatives when formulated in LNPs lead to stable formulations with suitable QC, superior transfection *in vitro* and comparable *in vivo* performance to that of Benchmark PEG-formulations. Envisaging what is ahead in the current nucleic acid delivery landscape, Curapath has engineered a library of different PEG replacement alternatives with the aim to not only overcome PEG drawbacks but to confer different surface features to help build the next generation LNPs.

References

[1] Hou et al . Nature Rev Materials, 2021 6(12): 1078-1094
[2] Anderson et al. N Engl J Med 2020; 383:2427-2438
[3] Polack et al. N Engl J Med 2020; 383:2603-2615
[4] Ishida and Kiwada, Int J Pharm 2008; 354:56–62
[5] Huesmann et al. Polymer 2015; 67:240–248

Acknowledgements

- CIPF for In vivo studies
- KNAUER partnership
- Torres Quevedo Funding from Spanish National plan for Scientific and Technical Research and Innovation

Find out more about our end-to-end services and catalogue products at www.curapath.com
Curapath-Precision polymers & lipid nanoparticles for drug delivery

Sara Elsafy

Continuous Manufacturing of PEGylated Liposomes: Tailoring Sizes for Diverse Clinical Applications

Sara El-Safy, Twan Lammers, Josbert M. Metselaar

Institute for Experimental Molecular Imaging, RWTH Aachen University Clinic, 52074, Aachen, Germany

Email: selsafy@ukaachen.de

INTRODUCTION

Liposomes are lipid-based vesicles extensively utilized in pharmaceutical industries for drug delivery. However, large-scale production is impeded by expensive and time-consuming batch methods, leading to batch-to-batch variability, which ultimately influences liposome sizes. This is of utmost importance as liposome size significantly impacts in-vivo bio-distribution, accumulation, and uptake behaviour. To overcome these challenges we developed a continuous flow manufacturing setup using milli-fluidics to enable large-scale production of liposomes with uniform, reproducible sizes.

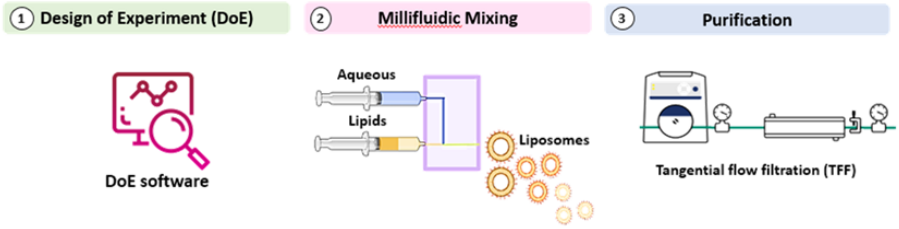

Figure 1. Outlines liposomal preparation, characterization and purification

RESULTS

DESIGN OF EXPERIMENT

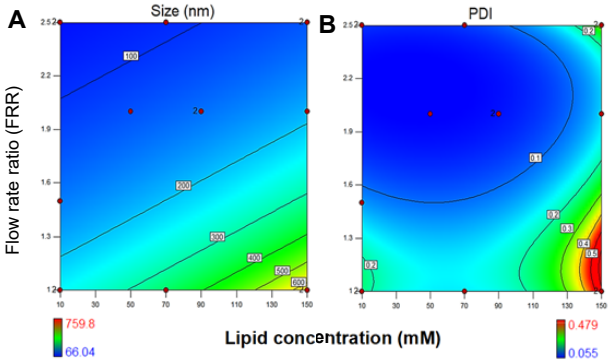

Figure 2. Heat maps demonstrating the effect of lipid concentration (mM) and flow rate ratio (FRR) (vol/vol) on both liposomes' (A) size and (B) PDI. Results show that our system allows for a broad size variation (80-200nm) with PDI below 0.15.

MICROFLUIDIC MIXING

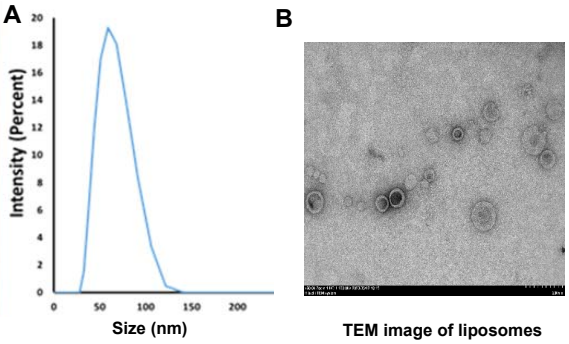

Figure 3. Liposomes size and morphological analysis measured using A) DLS and B) TEM, respectively.

PURIFICATION

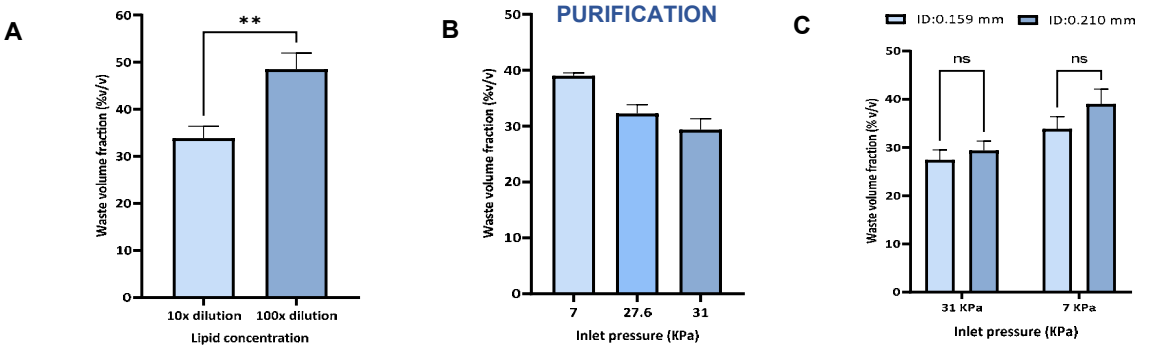

Figure 4. The effect of A) sample dilution and B) inlet pressure and C) filter outlet diameter on the cleaning efficiency of the filtration.

CONCLUSION

The lipid concentration and FRR were identified as the critical process parameters to be controlled in order to achieve the desired size. For the TFF module in the CFM set-up, high sample dilution, low inlet pressure and small outlet diameter maximized cleaning efficacy. These results demonstrate the versatility of our CFM to produce nano-medicines for different clinical applications to meet both market and individual needs.

REFERENCES

1. Sheybanifard M, Guerzoni LPB, Omidinia-Anarkoli A, et al., *Lab Chip*. 23(1):182-194, 2022.

2.Costa AP, Xu X, Khan MA, Burgess DJ, *Pharm Res*. 33(2):404-416, 2016.

Asmaa Said Sayed Elshafei

DMOG-induced vascular promotion primes the tumor microenvironment to improve tumor-targeted drug delivery

Asmaa Said ElShafei[1], Diana Möckel[1], Elena Rama[1], Anshuman Dasgupta[1], Fabian Kiessling[1], Twan Lammers[1]

[1] Institute for Experimental Molecular Imaging (ExMI), RWTH Aachen University Clinic, Aachen, Germany

E-Mail: aelshafei@ukaachen.de

Introduction and Methods

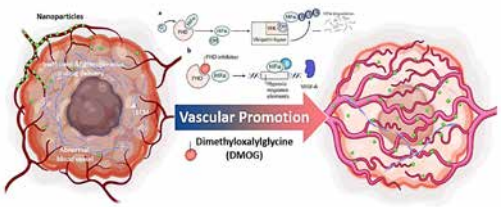

Figure 1: The schematic overview visually illustrates the study's principles and methods.

Effective drug delivery to tumors is one of the most complicated steps in cancer therapy, owing particularly to barriers in the tumor microenvironment (TME), such as aberrant vasculature and excessive stroma [1]. Inducing vascular promotion is a promising strategy for overcoming this challenge with a one-size-fits-all solution. We here used the prolyl hydroxylase domain inhibitor dimethyloxalylglycine (DMOG) [2], which promotes tumor blood vessel formation via upregulation of hypoxia inducible factor (HIF) and vascular endothelial growth factor (VEGF) signaling, to enhance tumor-targeted drug delivery.

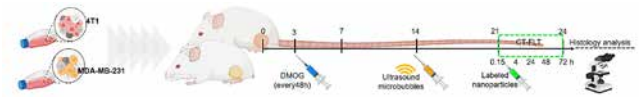

Results

4T1 Mouse TNBC

DMOG induces endothelium activation

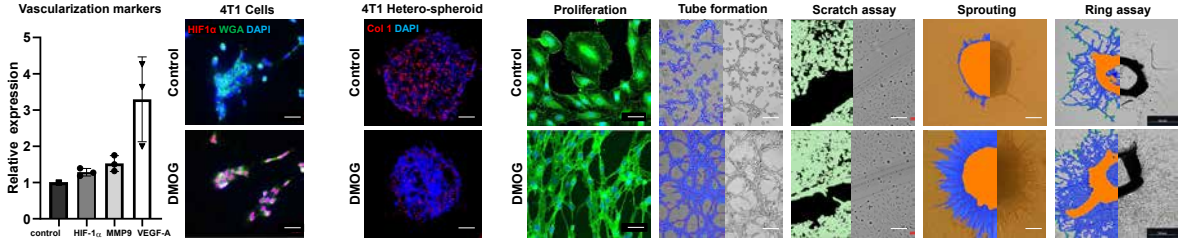

Figure 2: DMOG recognizes multiple steps of vascularization processes. It upregulates the expression of VEGF-A and MMP9 in 4T1 cells without affecting HIF expression. However, immunofluorescence images reveal that DMOG promotes the stability and nuclear translocation of HIF-1α in 4T1 cells. Additionally, DMOG effectively reduces collagen1 signal levels in 3D 4T1 hetero-spheroids. Furthermore, DMOG supernatant enhances endothelial cell proliferation[d]. Notably, DMOG treatment in the endothelial tube formation assay increases the covered area, number of tubes, and loops formed. Moreover, the scratch wound healing assay demonstrates accelerated cell migration upon DMOG treatment. Lastly, DMOG exhibits increased vascular sprouting in the aortic ring assay.

DMOG modifies TME

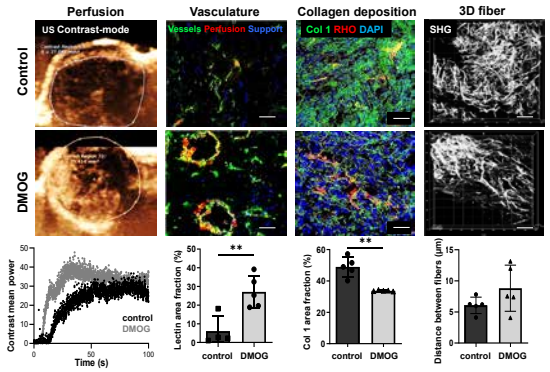

Figure 3: CEUS images showed impressive improvements in tumor vascularization and perfusion in the DMOG-treated group. Immunofluorescence analysis confirmed a substantial increase in vessel perfusion and a notable decrease in collagen 1 deposition compared to the control group. Additionally, the second harmonic generation (SHG) analysis revealed an increase in both fiber thickness and the inter-fiber space.

DMOG enhances NP tumor delivery

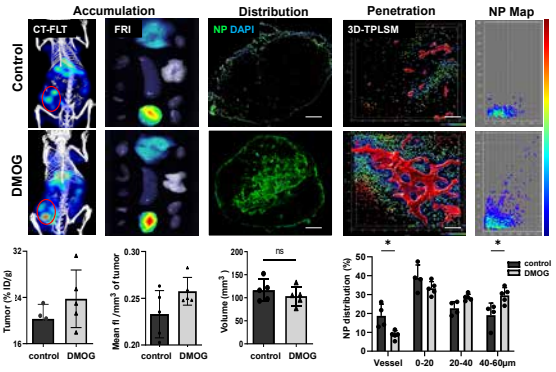

Figure 4: The 3D CT-FLT images showed increased accumulation of Cy7-labelled nanoparticles (NP), supported by 2D-FRI analysis of harvested tumors. Vectra overview images displayed a more uniform NP distribution in the DMOG-treated group. Furthermore, measurements of 3D NP-to-vessel distances indicated deep penetration of labelled NP. Additionally, the 3D NP intensity distribution map revealed enhanced micro-distribution of NP.

MDA-MB-231 Human TNBC

MDA-MB-231 TNBC human model validated the impact of DMOG

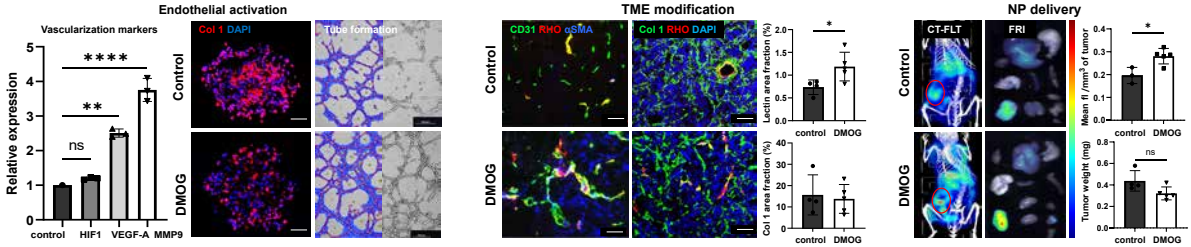

Figure 5 : DMOG treatment boosts vascularization marker gene expression, reduces collagen1 deposition in hetero-spheroids, and activates HUVECs. DMOG significantly promotes functionality and maturity of tumor blood vessels and slightly decreases collagen deposition in MDA-MB-231 tumors. DMOG treatment significantly increases labelled NP accumulation without affecting tumor volume compared to the control.

Conclusion

- DMOG-induced vascular promotion is a stepping stone in the tumor microenvironment (TME) transformation.
- DMOG-induced vascular promotion may provide a one-size-fits-all solution to improve the accumulation and penetration of drugs.
- Combining the DMOG-based vascular promotion with advanced (nano-, chemo- and/or immuno-) therapeutic agents may improve treatment outcomes.

References:

[1] Wong P et al, Cancer Cell 2015
[2] Ojha et al, Adv Drug Deliv Rev 2017
[3] Mpekris F et al, PNAS 2020
[4] Nelson B, Nat Chem Biol 2018

Acknowledgement: This work is supported by the German Academic Exchange Service (DAAD) and the European Research Council (ERC): Meta-targeting # 864121.

Polymeric Nanoparticles: high throughput screening for finding the right polymer for the required genetic material

Esteban-Pérez, S.; Dolz-Pérez, I.; Garcia-Garcia, J.; Herrera, L.; Colprim-Martínez, C.; Sogorb, G.; García, I.; Duro-Castano, A.; Nebot V. J.

CURAPATH

Curapath's polymer manufacturing for gene therapy solutions

Gene therapy has emerged as a versatile technique with the potential to treat a wide range of human diseases [1]. The vector used to carry genetic material across tissue-, organ-, and cell-associated barriers is a critically important component of this therapeutic modality. The transport and delivery of genetic material to a desired site of action remains a challenging prospect, with problems primarily relating to the physicochemical features of genetic material (i.e., hydrophilicity, high negative charge, and instability). The chosen vector must protect the genetic payload and enhance delivery to the desired subcellular site of action. Vectors must be chosen/designed to overcome various intracellular and extracellular barriers of differing nature and complexity, depending on the specific disease/disorder and the preferred administration route. Polymer based NVVs can deliver a wide range of nucleic acid cargo sizes and possess both flexible manufacturing processes and safe toxicity profiles. Under certain conditions, electrostatic interaction of polymeric NVVs and nucleic acids results in the formation of the so-called polyplexes that are well-defined solid-like colloidal polymeric nanoparticles (PNPs) [2;3].

Curapath's Polymeric Nanoparticles (PNPs)

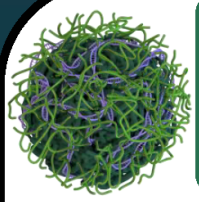

Polycationic polymer

Promotes the complexation with the genetic material by electrostatic interactions of the charges

Shielding polymer

Prevents non-specific protein absorption, particle aggregation and controls PNP size

Nucleic Acid *(e.g. mRNA)*

Encodes protein of interest or modulates genetic expression

Controlled synthesis and scale-up

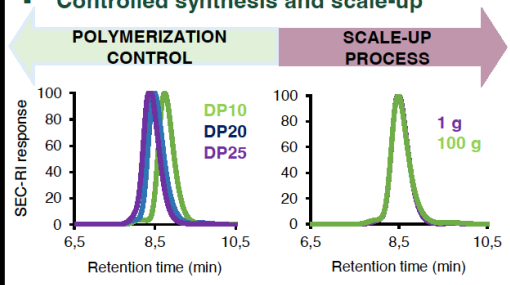

✓ Curapath polycationic and shielding polymer have been produced and scaled up in technical batches and with demonstrated batch-to-batch reproducibility and QC compliance.

Formulation process development

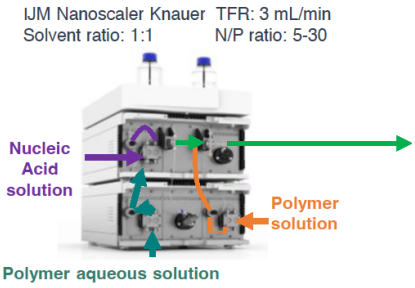

•Particle size, PDI & API cc - HTS platform
•Free payload-GE
•EE-Fluorescent assays
•In vitro functional response-Transfection assays and toxicity

Final PNP QC

High Throughput Screening of formulations

Instrument	Samples/Week	Volume (mL)	Concentration Range (mg/mL)	Min. API Amount Needed (µg)	Analytical Parameters
Herringbone	40	0.1 - 1	0.01 - 0.8	1	1- Size and polydispersity 2- Encapsulation efficiency 3- API concentration 4- API Integrity 5- Free API 6- In-vitro efficacy
T-Mixer	40	0.1 - 1	0.01 - 0.8	1	
NanoScaler	25	1 - 5,000	0.01 - 0.8	10	
Manual*	160	0.05 - 0.5	0.01 - 0.8	0.5	

✓Curapath screening services allow a high number of formulations characterized per week and an agile characterization functionality relationship stablishment

PNPs HTS characterization

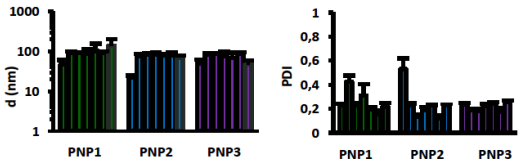

✓ Stable formulations with adequate particle size and PDI has been obtained and maintained it particle size for 28 days.

In vitro functional response

✓Superior *In vitro* transfection of PNPs containing Luc-coding genetic material. The structure modification relationship leads to a rise of *in vitro* transfection efficiency

C5 Complement activation in Human serum

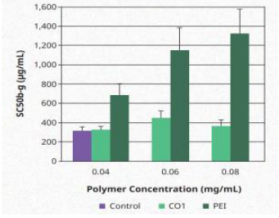

✓C5 Complement activation in human serum has demonstrated that Curapath ionizable polymer (C01) is less immunogenic than PEI in a dose-response manner

Conclusions

✓Curapath has stablished a HTS platform combining their end-to-end services. On one hand, the chemistry team has developed several polymers with high reproducibility and quality parameters. On the other hand, the formulation team has been able to prepare an elevated number of formulations in order to find out the best candidate as non viral transfection vector. Moreover, the holistic approach pursued by Curapath involving CMC and QA teams have provided a robust scalable process.

References

[1] Wirth, Thomas et al. Gene vol. 525,2 (2013): 162-9.
[2] Zu, Hui, and Danchen Gao. The AAPS journal vol. 23,4 78. 2 Jun. 2021
[3] Li, Qianwen et al. Nanomaterials (Basel, Switzerland) vol. 7,6 122. 27 May. 2017.

Acknowledgements

- CIPF for In vivo studies
- KNAUER partnership
- Torres Quevedo Funding from Spanish National plan for Scientific and Technical Research and Innovation

Find out more about our end-to-end services and catalogue products at www.curapath.com
Curapath-Precision polymers & lipid nanoparticles for drug delivery

Nicolas Färber

Measuring lipid order to assess cell membrane permeability, lipid nanoparticle stability and membrane drug interaction

Nicolas Färber[1,2], Sophie Mauritz[2], Anna Nolde[2], Julian Schäfer[1], Jonas Reitler[1], Christoph Westerhausen[1,2,3]

Contact: faerbnic@gmail.com, christoph.westerhausen@gmail.com

[1]Experimental Physics I, Institute of Physics, University of Augsburg, Germany
[2]Physiology, Institute of Theoretical Medicine, University of Augsburg, Germany
[3]Center for NanoScience (CeNS), Ludwig-Maximilians-Universität Munich, Germany

Prepare your sample with a solvatochromic probe or Add a solvatochromic probe after sample preparation

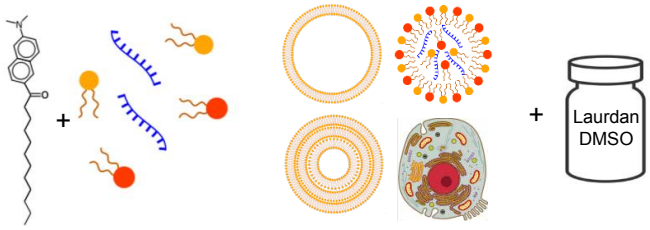

Laurdan, Lipids, Cholesterol, RNA, …

Vesicles, Lipid Nano Particles, Cell membranes, … [1]

Measure fluorescence spectra and calculate order parameter

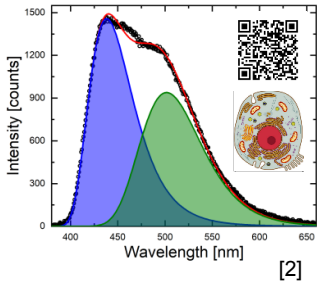

[2]

$A_{green} \propto I_{disordered}$

$A_{blue} \propto I_{ordered}$

$$GP = \frac{I_{ordered} - I_{disordered}}{I_{ordered} + I_{disordered}}$$

$GP \propto$ lipid order

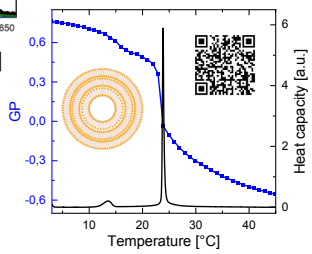

Be part of a pilot project and rent a LISO for free

Use the Lipid State Observer (LISO) for easy analysis

- Measure from -60°C to 90°C
- In standard reaction tubes
- With small sample volume: 260µl
- In situ temperature measurement
- Precision: 0.1K
- Automated data analysis

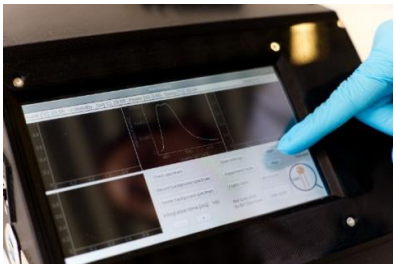

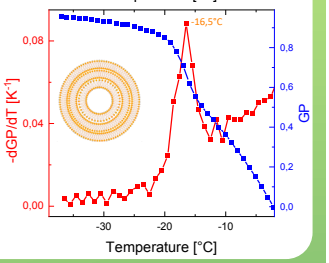

Lipid nanoparticle stability

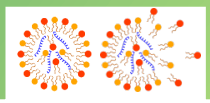

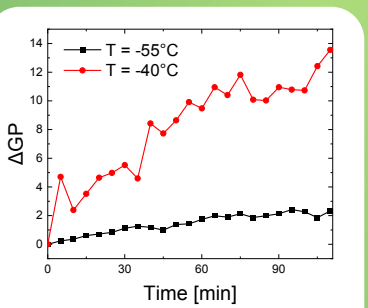

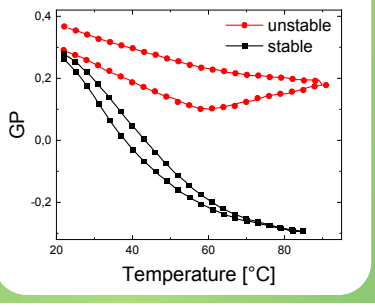

Cell membrane drug interaction

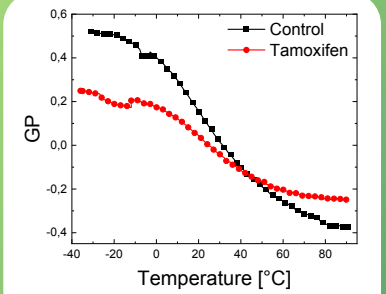

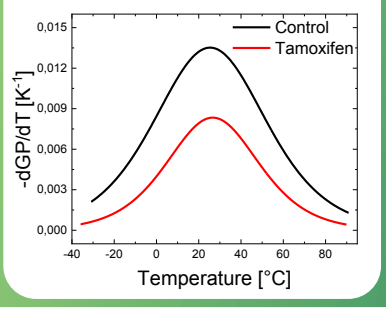

Cell membrane permeability

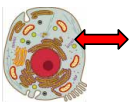

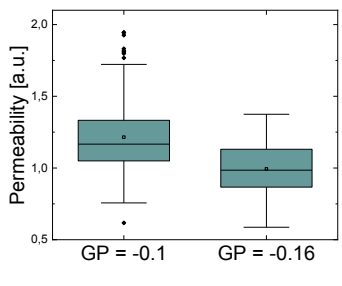

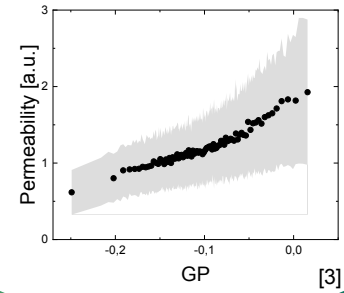

[3]

[1] Färber N, Neidinger S, Westerhausen C. Cell Membrane State, Permeability, and Elasticity Assessment for Single Cells and Cell Ensembles. Cell Viability Assays Methods Protoc., Springer; 2023
[2] Färber N, Westerhausen C. Broad lipid phase transitions in mammalian cell membranes measured by Laurdan fluorescence spectroscopy. Biochim Biophys Acta - Biomembr 2022;1864:183794
[3] Färber N, Reitler J, Schäfer J, Westerhausen C. Transport Across Cell Membranes is Modulated by Lipid Order. Adv Biol 2023:2200282

Alexander Fuchs

Cationic Polymer Nanogels for Nucleic Acid Delivery

Julius-Maximilians-
UNIVERSITÄT WÜRZBURG

Fakultät für Chemie und Pharmazie
MAKROMOLEKULARE CHEMIE

Alexander Fuchs[1], Christian Czysch[2] and Lutz Nuhn[1,*]

1: Institut für Funktionswerkstoffe und Biofabrikation, Lehrstuhl für Makromolekulare Chemie, Julius-Maximilians-Universität, Würzburg.
2: Max-Planck-Institut für Polymerforschung, Mainz.

Fully hydrophilic nanoparticles (nanogels) made of degradable synthetic diblock copolymers are a versatile system for nucleic acid (RNA, DNA) delivery. The transport platform may be used as an adjuvant for cancer immunotherapy. For this the nanogels can be loaded with immune stimulating nucleic acids such as the Toll-like receptor agonists CpG-ODN (TLR9) and Poly-(I:C) (TLR3).

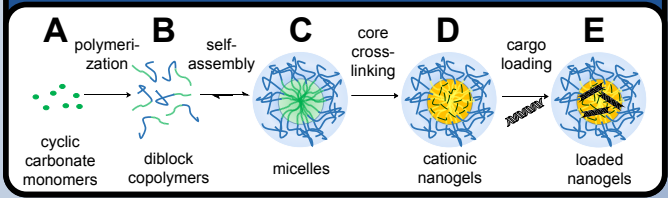

A one-step synthesis of reactive monomer

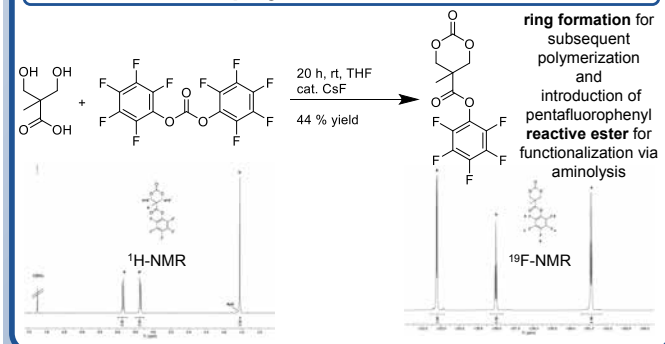

ring formation for subsequent polymerization and introduction of pentafluorophenyl **reactive ester** for functionalization via aminolysis

B cationic ring opening polymerization

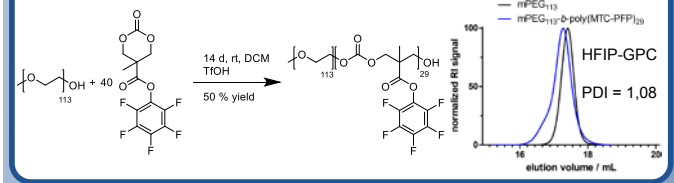

C self-assembly of micelles in alcohol

sonication of polymer in ethanol leads to micelle formation

added **water content** and a **heating step** increase micelle lifetime

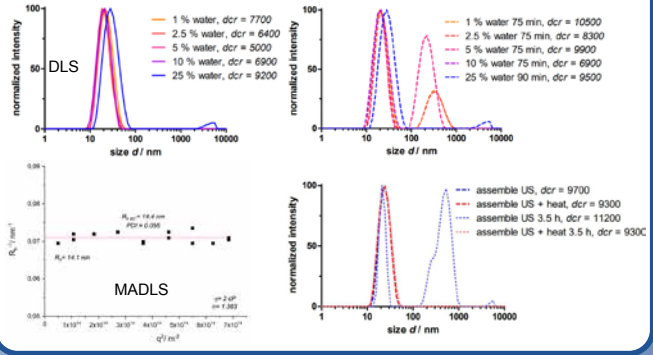

D core cross-linking forms cationic nanogels

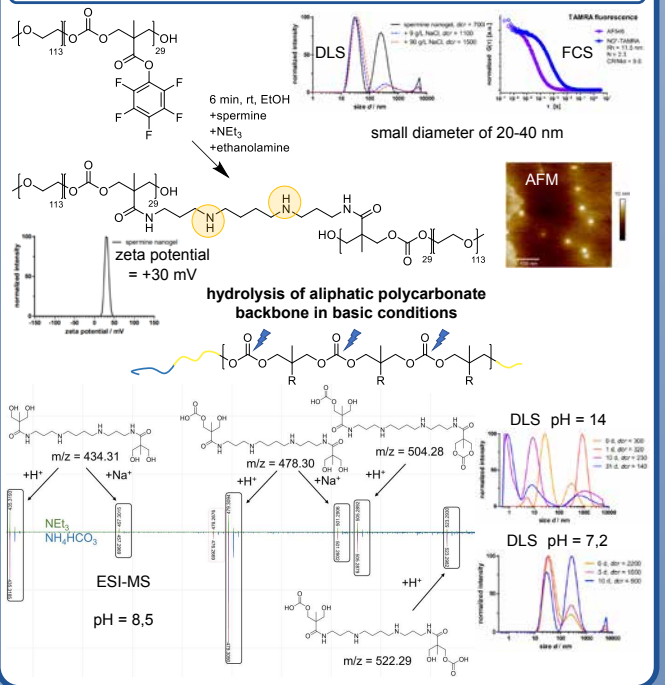

E electrostatic loading of RNA/DNA cargo

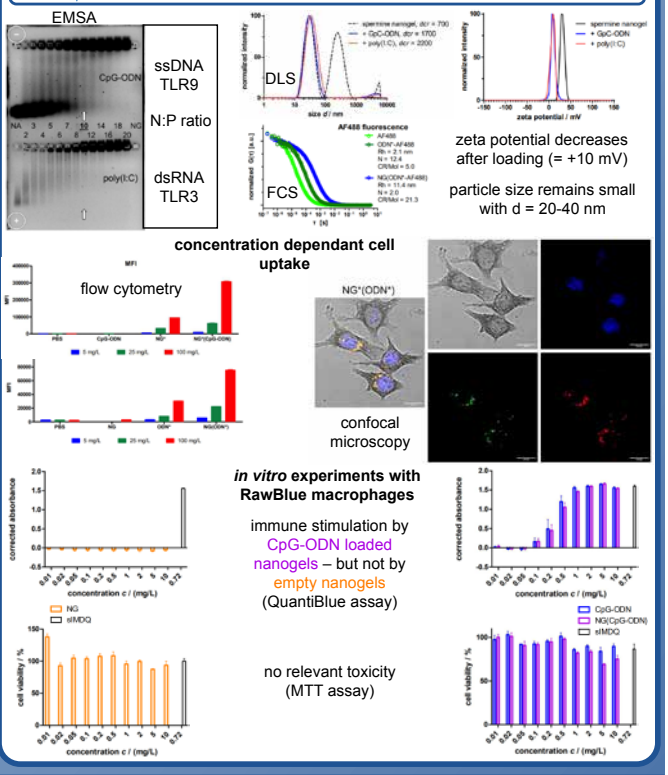

Julius-Maximilians-
UNIVERSITÄT WÜRZBURG
www.chemie.uni-wuerzburg.de/mmc/
alexander.fuchs@uni-wuerzburg.de
@nuhnlab
@NuhnLab

DFG Deutsche Forschungsgemeinschaft
Emmy Noether-Programm DFG
JG|U
SFB 1066
FCI FONDS DER CHEMISCHEN INDUSTRIE

Fabian Fuß

Evolving Polyethylene glycol: Evading Immune Recognition by Isomerization of PEG

Fabian Fuß[a*], Philip Dreier[a], Rebecca Matthes[a], Matthias Bros[b] and Holger Frey[a]

[a]Department of Chemistry, Johannes Gutenberg University, D-55128 Mainz, Germany, [b]Universitätsmedizin, Johannes Gutenberg-Universität Mainz

Introduction

PEG represents an essential building block to modern nanomedical applications ranging from chronic diseases to cancer therapy.[1] Nevertheless, reports about increasing prevalence of anti-PEG antibodies and related heavy immune reactions raise growing concerns about the efficiency and safety of PEGylated therapeutics.[2–4] Regarding the importance of PEGylation, especially for modern nanomedicine, the occurring immunogenicity of PEG urges for alternatives to PEG in medical applications.

In this work, we were aiming on preserving the underlying polyether class of PEG while altering the polymers architecture. This is achieved *via* random AROP of EO with glycidyl methyl ether (GME). The resulting constitutional isomers of PEG consist of polar GME repeating units which serve as statistical mutations of the highly regular PEG structure. This modifies the epitope of the anti-PEG antibodies beyond recognition while the beneficial properties of PEG are maintained. P(EO-*co*-GME) demonstrates a hydrophilicity comparable to PEG while showing low toxicity and no immunogenicity. Anti-PEG ELISA with backbone- and endgroup-specific antibodies confirm a reduction and complete elimination of antibody recognition with increasing GME content.

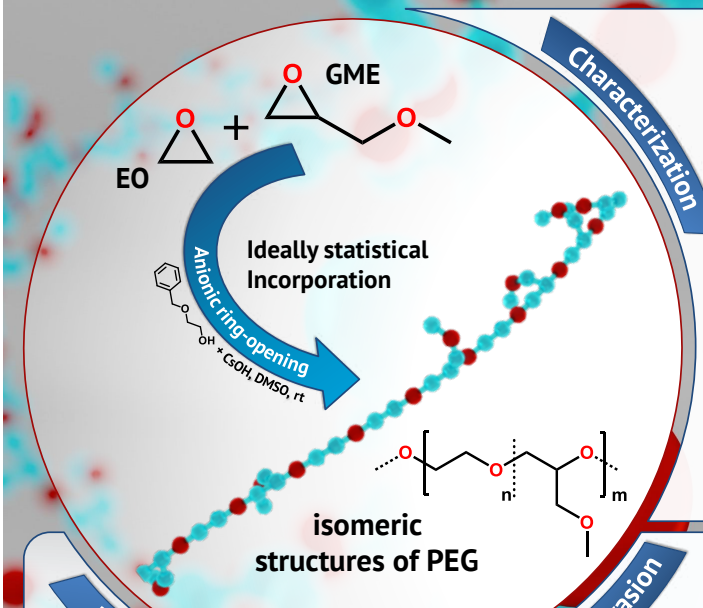

Characterization

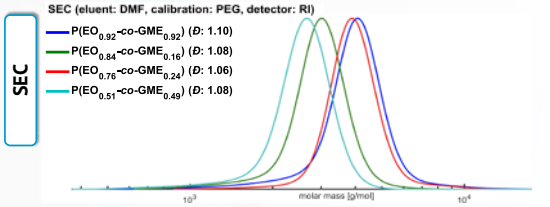

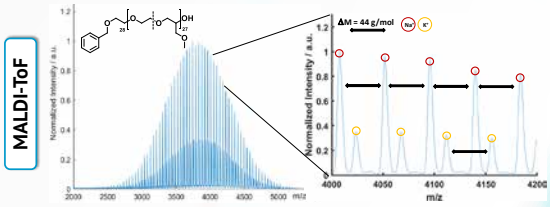

Biocompatibility

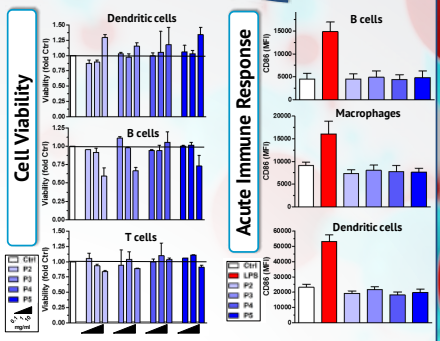

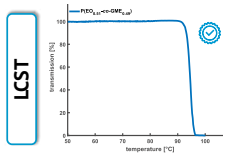

- Low toxicity
- Non-immunogenic
- Highly hydrophilic

Immune Evasion

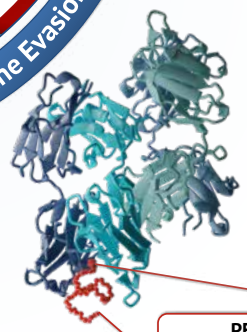

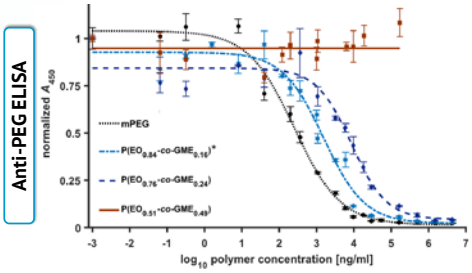

PEG-epitope: 16 consecutive EO units[5]

Interruption by GME side chains

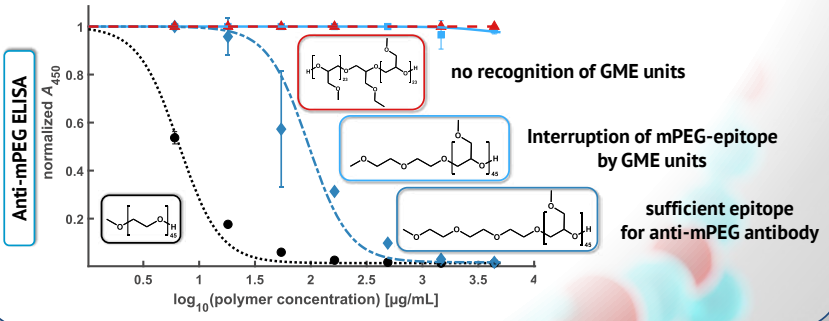

- no recognition of GME units
- Interruption of mPEG-epitope by GME units
- sufficient epitope for anti-mPEG antibody

Conclusion

- highly controlled polymerization well defined polyethers
- Ideally statistical copolymerization of EO and GME
- fully biocompatible
- no recognition by anti-PEG or anti-mPEG antibodies

References

(1) Ryan Cross. *C&EN Global Enterp* **2021** (Volume 99, Issue 8).
(2) Pasut *et al.*; *Elsevier*, **2020**, ISBN: 9780444640819.
(3) Chang *et al. Nature communications* **2017**, *8* (1), 522. DOI: 10.1038/s41467-017-00622-4.
(4) Hershfield *et al. Arthritis research & therapy* **2014**, *16* (2), R63. DOI: 10.1186/ar4500.
(5) Lai, Jacobs *et al., The Protein Data Bank* **2020**, https://doi.org/10.2210/pdb6VL9/pdb

fafuss@uni-mainz.de

JG|U THE FREY GROUP

erc

CLINAM
European Foundation for Clinical Nanomedicine
Switzerland

14/2023

Han Gao

Han Gao[1, 2 *], Shiqi Wang[2], Qiang Long[3], Ruoyu Cheng[1, 2], Artturi Koivuniemi[2], Zehua Liu[2], Xiaofeng Ye[3], Hélder A. Santos[1,2]

[1] Department of Biomedical Engineering, W.J. Kolff Institute for Biomedical Engineering and Materials Science, University Medical Center Groningen/University of Groningen, Ant. Deusinglaan 1, 9713 AV Groningen, The Netherlands

[2] Drug Research Program, Division of Pharmaceutical Chemistry and Technology, Faculty of Pharmacy, University of Helsinki, FI-00014 Helsinki, Finland

[3] Department of Cardiovascular Surgery, Ruijin Hospital, Shanghai Jiao Tong University School of Medicine, Shanghai 200020, China

*e-mail: h.gao@umcg.nl

INTRODUCTION

RNA interference (RNAi) represents the next-generation treatment strategy for a myriad of indications. As a result of their advantages in biosafety, non-immunogenicity and economic feasibility, non-viral synthetic nanoparticles (NPs) have drawn attention as vectors to deliver RNAi molecules, including small interfering RNAs (siRNAs). In general, an ideal targeted siRNA delivery system should hold the following features: (i) efficient siRNA encapsulation efficacy to prevent its degradation under blood circulation; (ii) precise targeting properties to avoid off-target gene silencing; and (iii) efficient endosome escape capability to allow the siRNA reaching the cytosol. To fulfill these requirements, the development of targeted siRNA delivery nanosystem with maximally simplified synthetic scheme is desired. Herein, a virus-mimicking polysaccharide nanocomplex was developed which showed membrane destabilization behavior and macrophage targeting capability. Significant enhanced accumulation level of EEPG nanocomplex was observed in cardiac lesion site, indicating its exclusive targeting capability for ischemic heart diseases. Altogether, these findings suggest the designed EEPG nanocomplex is favorable for siRNA delivery, which might have translational potential as a versatile platform in inflammation-related diseases.

AIMS

1. To design a versatile polysaccharide-based nanoplatform for gene delivery.
2. To optimize the release of siRNA during endocytosis by endosomolytic polymer.
3. To develop viral mimicry nanocomplex with precise targeting capability.

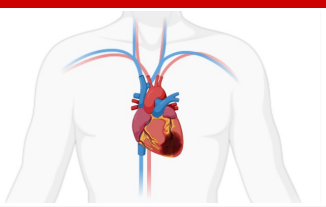

RESULTS

EVALUATION *IN VITRO*, *IN SILICO* AND *IN VIVO*

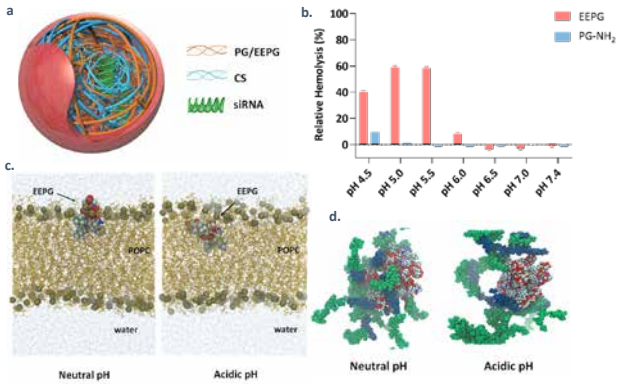

Figure 1. Endosomolytic activity of the synthesized polymer EEPG.
a. Schematic illustration of the formation of polysaccharide-based siRNA delivery system. **b.** Hemolytic behavior of EEPG and PG-NH_2. **c, d.** Molecular dynamic simulation of CEEPG NPs at acidic and neutral pH. Data are presented as mean ± SD of three independent measurements.

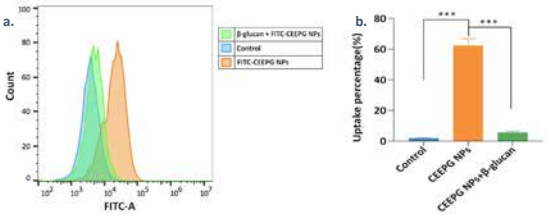

Figure 2. Targeting capability of the developed CEEPG NPs.
a. Flow cytometry analysis. b. Quantitative cellular uptake

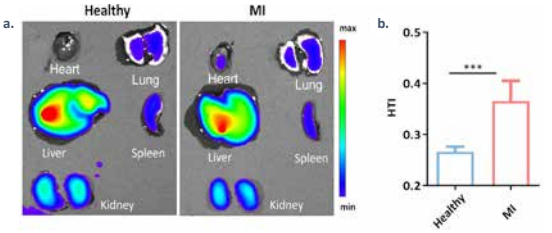

Figure 3. Biodistribution of Cy7-CEEPG NPs in MI murine model.
a. *In vivo* biodistribution analysis. b. Quantitative Heart targeting index (HTI)

CONCLUSIONS AND FUTURE PERSPECTIVES

- We successfully designed and fabricated a pH-responsive polysaccharide-based nanocomplex with endosomal membrane destabilization capability.
- The developed CEEPG NPs displayed precise targeting capability towards Dectin-1 receptor.
- Significant enhanced accumulation level of EEPG nanocomplex is observed in cardiac lesion site.

FUTURE WORK

Therapeutic application of EEPG based nanomedicine for cardiac diseases.

ACKNOWLEDGEMENTS

Barbara Graefen

JOHANNES GUTENBERG UNIVERSITÄT MAINZ

JGU UNIVERSITÄTSmedizin. HAUTKLINIK MAINZ

SFB 1066

Modulation of the tumor microenvironment via pH-regulating liposomes

B. Graefen[1,2], J. Krehan[2,3], A. Walther[2,3], A. Tuettenberg[1,2,4]

[1]Department of Dermatology, University Medical Center, Mainz
[2]Collaborative Research Center (SFB) 1066, Johannes Gutenberg-University, Mainz
[3]Department of Chemistry, Johannes Gutenberg-University, Mainz
[4]Research Center for Immunotherapy, University Medical Center, Mainz

FZI Forschungs-Zentrum für Immuntherapie

INTRODUCTION

Extracellular pH (pH_e) in the tumor microenvironment (TME) in malignant melanoma is ~ 7.0 while about ~7.4 in healthy skin tissue [1]. Acidification in the tumor is a consequence of high metabolic rates, reduced blood flow and regulated proton transport by intra- and extracellular pH sensors [2]. In addition, acidic pH_e enhances the invasive behavior of human melanoma cells [3].[b]

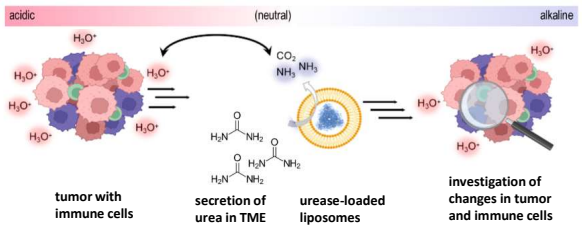

Macrophages (Mph) get subverted into potent pro-tumor agents called **tumor-associated-macrophages (TAM)**. High TAM density is associated with poor prognosis and has been demonstrated for malignant melanoma [4]. These TAM share characteristics with M2-type-mph (non classical, anti-inflammatory, tolerogenic) and serve as a model system for repolarization. Due to the plasticity M2-Mph can be repolarized (based on their environment) to M1-Mph (classical, pro-inflammatory) which show anti-tumor effects [5].

It has been shown:

- tumor cells secret urea into the TME [6]
- urease (enzyme) converts urea to two molecules ammonia (NH_3) and carbon dioxide
- ammonia (pK_a = 9.24 in water) has a potent impact on increasing the pH_e

AIM

- raise pH_e in the TME
- investigate changes in pro-tumorogenic immune cells (M2-Mph) and tumor cells

METHODS

monocyte-derived macrophages[b]

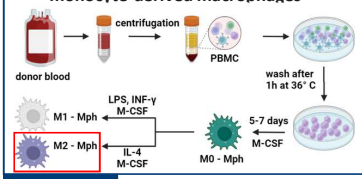

adjustment of pH in buffer free cell culture media[a,b,c]

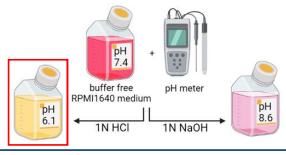

nanocarrier and controls[b]

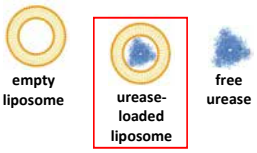

different cancer cell lines[b,c]

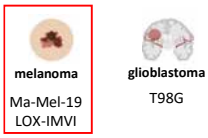

RESULTS

acidic pH_e decreases M1-Mph viability

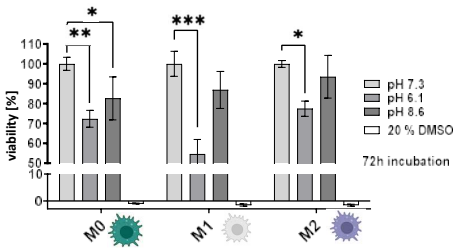

Resazurin assays performed after 72h incubation with media of pH 6.1, 7.3 and 8.6 with M0-, M1-, and M2-Mph. Absorbance was recorded with a microplate reader with N=3. 20% DMSO was used as a dead-control.[b,d]

liposomes are low cytotoxic compared to formed NH_3 in Ma-Mel-19 cells

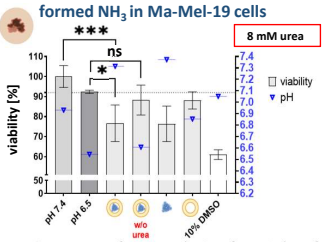

Resazurin assay of Ma-Mel-19 after 24h of incubation. Medium (pH 6.5) was treated with 5vol% urease-loaded liposomes (with or without urea), empty liposomes or free urease or pH 7.4 control and 10% DMSO dead control. pH_e were measured after assay with pH meter.[b,d]

acidic pH decreases proliferation in T98G glioblastoma cells

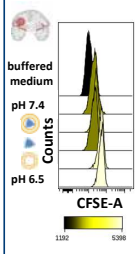

T98G cells were stained in CFSE dye prior plating. After attachment medium was changed by buffered medium, pH 7.4, 5vol% urease loaded liposomes/ free urease/ empty liposomes and pH 6.5. CFSE counts were measured with Flow Cytometer after 48h. Higher CFSE-signals shows a lower proliferation.[b,e]

CFSE = carboxyfluorescein succinimidyl ester

acidic pH_e causes lower energetic changes in M2-Mph

urease-loaded liposomes partially restore energy rate in LOX-IMVI

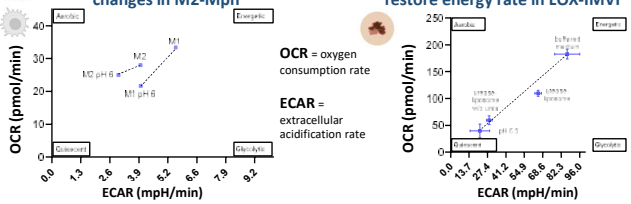

OCR = oxygen consumption rate

ECAR = extracellular acidification rate

OCR and ECAR were measured with Seahorse Cell Mito Stress assay, with M0-Mph (left graph) or LOX-IMVI malignant melanoma cells (right graph). M0-Mph (n=3) were polarized to M1- and M2-Mph for 48h. Subsequently the Mph or tumor cells were treated with normal buffered RPMI medium or buffer free pH 6.0 (Mph) / pH 6.5 (LOX-IMVI) and urease-loaded liposomes with or without urea in the medium (LOX-IMVI) and incubated for 24h.[b,d,f]

urease-loaded liposomes and production of NH_3 decrease M0-Mph viability

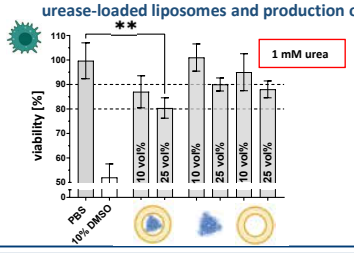

Resazurin assay performed at pH 7.4 with M0-Mph after 24h. Treatment was with 10 or 25 vol% of free urease, urease-loaded liposomes or empty liposomes. Absorbance was recorded with microplate reader with N=3. 10% DMSO was used as a dead-control and PBS was used as untreated vehicle control.[b,d]

SUMMARY

in Mph:

- acidic pH_e does affect Mph viability
- acidic pH_e causes lower energy changes in M2-Mph
- urease-loaded liposome formed NH_3 decrease Mph viability
- M1-Mph are more affected by acidic pH_e

in tumor cells:

- urease-liposomes restore energy changes from acidic pH_e
- urease-liposomes show low cytotoxicity compared to NH_3
- acidic pH_e decreases tumor cell proliferation

FUTURE DIRECTIONS

- functional assays to investigate Mph phenotype
- changes in mRNA levels of M1-/M2-Mph
- investigation of self-regulated nanocapsules
- *in vivo* targeting experiments with nanocarriers

REFERENCES [1] Hao et al., 2018; [2] Damaghi et al., 2013; [3] Martínez-Zaguilán et al., 1996; [4] Bröcker et al., 1988; [5] Abdullah et al., 2015; [6] Keshet et al. 2018;

[a] Supplemented with 1% human plasma, 1% GlutaMax and 0.2% primocin for Mph or 10% FBS instead of plasma for tumor cells; [b] Figures were created with BioRender; [c] Commercially available; [d] Graphs were created with GraphPad Prism Version 9. Data were analyzed by one-way ANOVA. A P-value of ≤ 0.05 is considered to be significant (denoted by *), ≤ 0.01 is denoted by **, ≤ 0.001 is denoted by ***, ≤ 0.0001 is denoted by ****; [e] Obtained fcs files were processed with the web based program Cytobank Community; [f] Data were measured with a Seahorse XF HS Mini Analyzer.

Serra Gurcan

Well Characterized Lipid Nanoparticle Library Accelerates Development of Next Generation Genomic Medicine

Serra Gurcan[1] (Presenting Author), Nikita Jain[1] (Corresponding Author), Sedigheh Nazaripour[1], Zhengyu Chen[1], Suraj Abraham[1], Leanna Yee[1], Sams Sadat[1], Gayatri Mehar Namala[1], Sijo Chemmannur[1], Kobe Tickner[1], Malathi Anantha[1],Ruchi Sharma[1], Srinivas Abbina[1], Seetalakshmi Thambatti[1], Vinay Mayya[1], Emily Soon[1], Jay Paquette[1], Anitha Thomas[1]

[1]Precision Nanosystems ULC, Vancouver, Canada

Contact us at:
Precision NanoSystems, Vancouver, BC, Canada
info@precision-nano.com

Introduction

- FDA approval of ONPATTRO® by Alnylam, Comirnaty® by BioNTech/Pfizer and Spikevax® by Moderna and the various clinical trials with mRNA-based drugs or vaccines have provided momentum to further develop lipid nanoparticle (LNP) based genetic medicines.
- Ionizable amino lipids are a major constituent of LNPs for delivering nucleic acid therapeutics, and thus ionizable lipids with high encapsulation efficiency, high endosomal release that are non-toxic are essential for efficient clinical translation.
- The scarcity of ionizable lipids that are suitable for development of vaccines, cell and gene therapies continues to be a problem in advancing many potential therapeutic/vaccine candidates to the clinic.

Methods and Results

1. Non-Viral Delivery Systems Enable Cell Therapy

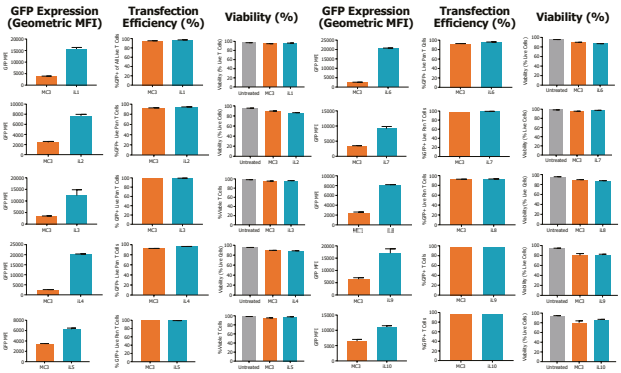

- MC3 – Ionizable lipid, an excipient in FDA approved Onpattro™, was used as benchmark lipid for comparative evaluation of potency of proprietary PNI lipids
- Higher GFP MFI and comparable transfection efficiency relative to MC3 was observed with PNI lipids
- Cell viability was >90% as compared to untreated cells

2. Proprietary LNPs Enable Erythropoietin Production *in vivo*

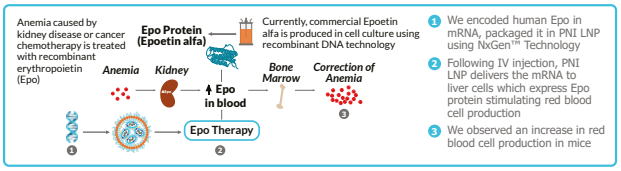

a. EPO Expression levels from LNPs Prepared with Different Ionizable Lipids

b. Hematocrit Results Comparing LNPs Prepared with Different Ionizable Lipids

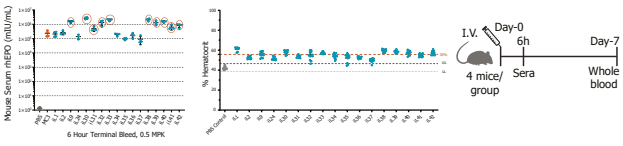

- EPO-encoded mRNA-LNP showed significant EPO expression levels at 6h in C57BL/6 mice following i.v administration of 0.5 mg/kg dose
- Post 7 days injection, EPP encoded mRNA LNP treated female C57BL/6 mice demonstrated ~20–40% increase in Hematocrit levels

3. Proprietary LNPs Towards Developing Self-Amplifying mRNA (saRNA) Vaccines

How do saRNA-LNP vaccines work?

1. saRNA is enzymatically synthesized *in vitro* from a DNA template
2. saRNA is delivered in a LNP formulation, to cytoplasm of host cells
3. saRNA self-amplifies, produces multiple copies of mRNA in the target cells and expresses vaccine antigen.

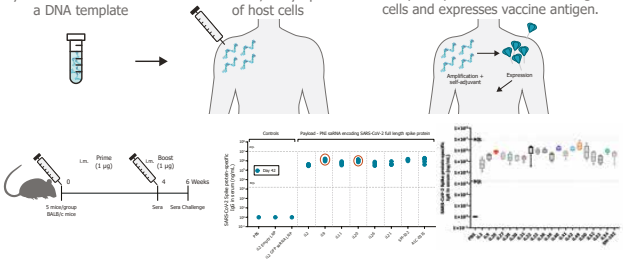

- The analysis for SARS CoV-2 spike protein specific antibodies, post two weeks boost (day 42), confirmed that many of the PNI lipids showed similar expression compared to clinically demonstrated SM-102 and ALC-0315.

Objectives

- Demonstrate cell therapy applications for proprietary lipids using GFP encoded mRNA and compare their transfection with clinically approved lipid Dlin-MC3-DMA (MC3) in human primary T cells.
- Demonstrate protein replacement applications for proprietary lipids using EPO encoded mRNA and their potency comparison with clinically approved Dlin-MC3-DMA in mice.
- Display PNI proprietary lipids for vaccine applications using self-amplifying RNA encoding for SARS-CoV-2 spike protein in comparison to SM-102 and ALC-0315 in mice.
- Showcase the PNI proprietary lipids for gene editing applications *in vivo.*
- Illustrate the safety and tolerability of PNI proprietary LNPs in mice.

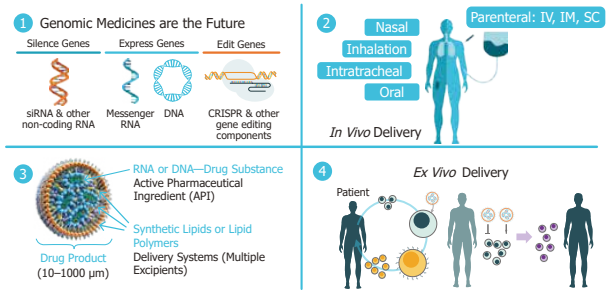

4. Novel Ionizable Lipids for Gene Editing Applications

a. TTR CRISPR Gene Editing – Preliminary Data with PNI Delivery System

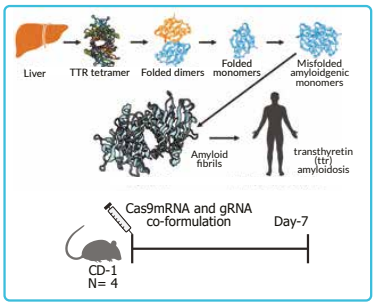

- A life-threatening genetic disease, caused by progressive accumulation of misfolded transthyretin (TTR) protein in tissues of nerves and heart
- Polyneuropathy & Myopathy can be resulted
- Leads to cardiovascular disorders
- Preliminary results show more than 75% reduction in TTR protein levels with majority of tested lipids with one injection (3 mg/Kg)

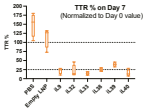

b. Base Editing - PCSK9 Knock Down - Preliminary Data with PNI Delivery system

- Caused by mutations in LDLR, PCSK9, and or APOB genes
- Two missense mutations in PCSK9 were associated with an autosomal dominant form of hypercholesterolemia
- Gain-of-function variants of PCSK9 reduces LDLR levels in liver, thereby inducing hypercholesterolemia - higher LDL cholesterol levels in plasma

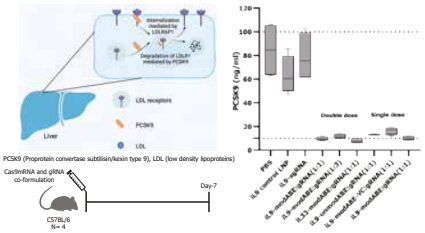

5. Tolerability of Proprietary LNP Administered IV in Mice

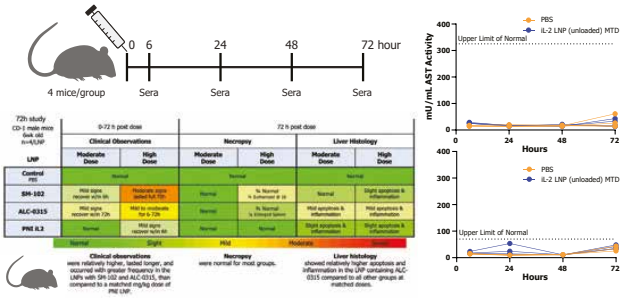

Conclusion

- Non-viral lipid nanoparticle delivery systems show significant promise in the field of genomic medicine.
- Precision NanoSystems has developed a proprietary ionizable lipid library comprising more than 100 lipids with diverse pKa for different applications including cell therapy, protein replacement, gene therapy and RNA vaccine.
- The Precision NanoSystems lipid technology enables the targeted delivery of nucleic acids to specific cells and tissues and can help to accelerate the development of genomic medicines for a wide-range of diseases.

Performance of a novel high-throughput nanoparticle formulation set-up

Sjoerd Hak[1], Alicja Molska[1], Francesca Roda[2,3], Anders Brunsvik[1], Jeremie Parot[1], Sven Even Borgos[1]

[1]SINTEF Industry, Department of Biotechnology and Nanomedicine, Trondheim, Norway
[2] Clinical and Experimental Medicine, University of Modena and Reggio Emilia, Modena, Italy
[3] Nanotech Lab, TE.FAR.T.I., Department of Life Sciences, University of Modena and Reggio Emilia, Modena, Italy

Aim

Development of novel nanoformulations delivering therapeutics to specific tissues and cells is a challenging endeavour and often based on extensive and costly nanoparticle library screening. High-throughput (HT) nanoparticle synthesis and characterization will enable more cost-effective and efficient nanomedicine development. We present a new HT flow-mixing based nanoparticle synthesis set-up consisting of commercially available liquid chromatography instruments and microfluidic chips. We demonstrate that the set-up provides highly reproducible and high-quality nanoparticle formulations.

The set-up

We have assembled and custom-programmed commercial high-end liquid chromatography and online analytical modules into a HT nanoparticle formulation set-up, which we call the HT-mixer (**Figure 1**). The set-up allows for automated formulation, miniaturization (<100 µL per nanoparticle batch), and dramatically increases the speed of manufacture (~3 minutes per batch).

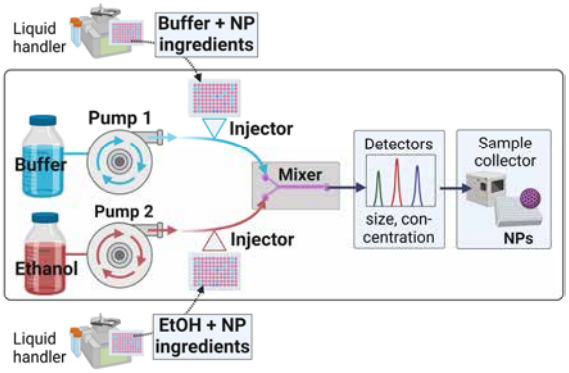

Figure 1: *High-throughput nanoparticle formulation set-up (biorender).*

To characterize plug-flow, we injected different dyes in the organic and aqueous channel. Absorption (in-line UV-detector) at 210 nm indicated asynchronous injection of the dyes (**Figure 2A**), confirmed by UV absorption spectra (**Figure 2B**). Tuning injection timepoints resulted in the desired synchronous injections in the two channels (**Figure 2C**).

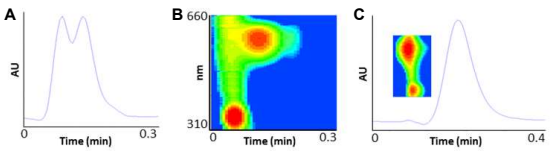

Figure 2: *Plug-flow characterization using in-line UV detector and coumarin (λ_{max}: 350 nm) injection in the organic and nile red (λ_{max}: 580) in the aqueous channel.*

Benchmarking of nanoparticle size

We prepared oil-in-water emulsions and mRNA-LNPs with the same microfluidic chip (Darwin microfluidics, product #: LFT-012.00-4264) in the HT-mixer and in a set-up with syringe pumps.

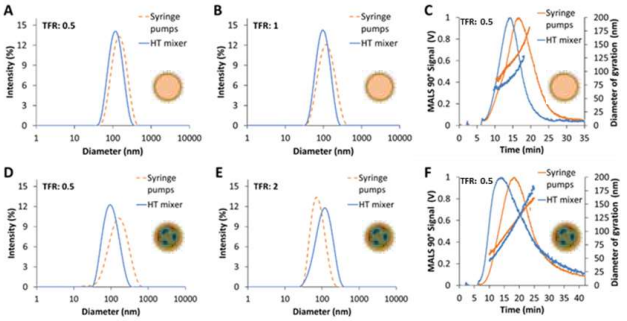

Figure 3. A-C*: Dynamic light scattering (DLS) (**A, B**) and multidetector field flow fractionation (MD-FFF, **C**) for emulsions, **D-F:** DLS (**D,E**) and MD-FFF (**F**) for mRNA-LNPs. TFR: Total flow rate (ml/min).*

Oil-in-water emulsions consisted of Miglyol 812 N and DSPC:Cholesterol:PEG2000-DSPE at molar ratios 57:33:10. mRNA-LNPs were prepared at pH 4 using D-Lin-MC3-DMA:DSPC:cholesterol:PEG2000-DMG at molar ratios 50:10:38.5:1.5 and N/P of 6. Batch size was only 50 to 100 µL. Emulsions prepared with the HT-mixer were consistently smaller than the ones prepared with the syringe pump set-up. Nevertheless, both emulsions and mRNA-LNPs from the HT-mixer were reproducible in size, see **Figure 3** and **Table 1.**

Table 1: *Summary of various produced nanoparticle batches.*

NP type	Mixer set-up	organic : aqueous flow rate ratio	Total flow rate (ml/min)	Final lipid concentration (mM)	DLS Z-AVG (nm)	DLS PdI (a.u.)	MD-FFF Diameter of gyration (nm)
Emulsion	Syringe	1:3	1	2	107	0.17	105
Emulsion	Syringe	1:3	1	2	111	0.15	112
Emulsion	HT mixer	1:3	1	2	76	0.08	64
Emulsion	HT mixer	1:3	1	2	88	0.14	80
Emulsion	Syringe	1:3	0.5	2	128	0.17	n.a.
Emulsion	Syringe	1:3	0.5	2	130	0.18	150
Emulsion	HT mixer	1:3	0.5	2	108	0.16	n.a.
Emulsion	HT mixer	1:3	0.5	2	109	0.14	90
mRNA-LNP	HT mixer	1:3	0.5	2.5	84	0.21	80
mRNA-LNP	HT mixer	1:3	0.5	2.5	91	0.18	85
mRNA-LNP	HT mixer	1:3	1	2.5	87	0.24	78
mRNA-LNP	HT mixer	1:3	1	2.5	97	0.23	67
mRNA-LNP	HT mixer	1:3	2	2.5	103	0.22	85
mRNA-LNP	HT mixer	1:3	2	2.5	108	0.21	82

Conclusion and outlook

We realized automated nanoparticle production at 3 minutes per 50-100 µL batch. Combined with, 1) liquid robotic handlers to prepare organic and aqueous solutions of nanoparticle ingredients, and 2) in-line characterization (in-line sizing in progress), this will allow us to formulate and characterize nanoparticles in a high-throughput fashion.

Contact: sjoerd.hak@sintef.no

Hajira Banu Haroon

Modulation of immune response through dendrimer functionalisation

DIRNANO
Directing the immune response through designed nanomaterials
H2020-MSCA-ITN-2020

Newcastle University

Hajira Banu Haroon [a,b], Pedro Veloso Maghalaes [c], Emanuele Papini [c], Jørn B. Christensen [d], Dmitri Simberg [e,f], Panagiotis N. Trohopoulos [g], S. Moein Moghimi [a,b,e]

[a] School of Pharmacy, Newcastle University, Newcastle upon Tyne NE1 7RU, UK, [b] Translational and Clinical Research Institute, Faculty of Health and Medical Sciences, Newcastle University, Newcastle upon Tyne NE2 4HH, UK, [c] Department of Biomedical Sciences, University of Padua, Padua 35121, Italy, [d] Department of Chemistry, University of Copenhagen, Frederiksberg C, Denmark, [e] Colorado Center for Nanomedicine and Nanosafety, University of Colorado Anschutz Medical Center, Aurora, CO, USA, [f] Translational Bio-Nanosciences Laboratory, The Skaggs School of Pharmacy and Pharmaceutical Sciences, Department of Pharmaceutical Sciences, University of Colorado Anschutz Medical Campus, Aurora, CO, USA, [g] CosmoPHOS Ltd, Thessaloniki, Greece

Introduction

Many nanoparticles depending on their physicochemical properties (including size, shape, and surface characteristics) activate complement system, an integral part of innate immune system that render nanoparticles susceptible to phagocytosis by immune cells like polymorphonuclear leukocytes and tissue macrophages [1].

Recently, we showed dendrimers evade complement activation due to Angstrom-scale spacing arrangement (the ASSA phenomenon) of their surface functional motifs [2].

Considering this, we hypothesize immune cells might also respond differently to nanoparticles that display surface ligands/functional groups in ASSA arrangement.

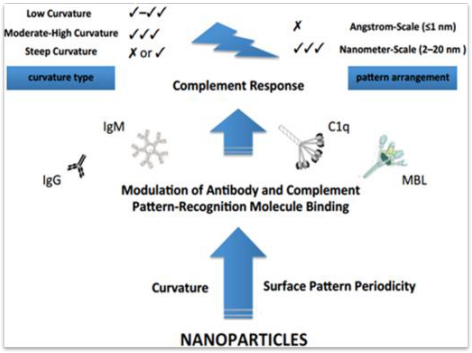

Methods

- The study involved functionalisation of polymeric nanoparticles with a library of fully characterized dendrimers.
- Assessment of surface properties with a wide range of state-of-the-art biophysical modalities like DLS, NTA, SEM, XPS, and FTIR, and modulation of immune responses through assessment of serum protein deposition by shot-gun proteomics and macrophage challenge.

Results and Discussion

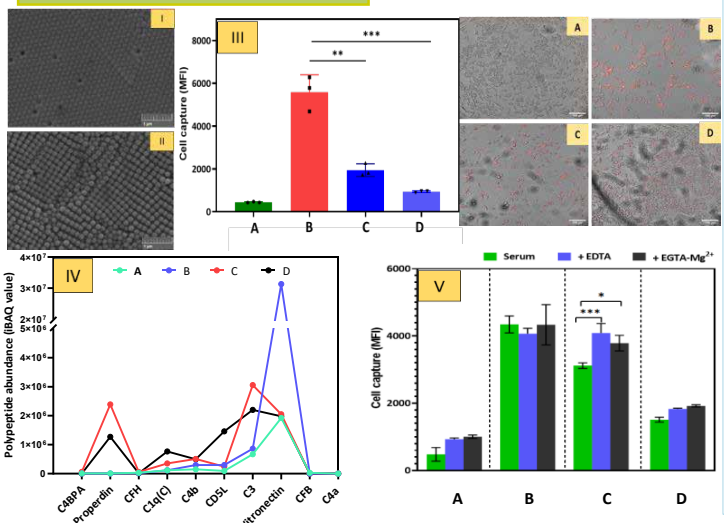

Figure: I and II – SEM image of non-functionalised and dendrimer functionalised NPs showing hexagonal and cuboidal arrangements, respectively.

III - Capture intensity of non-functionalized and dendrimer-functionalised NPs by human macrophages after 3h incubation at 37 °C and their associated confocal images. The data points represent mean ± s.d (n=3), analyzed by two-sided unpaired t-test, statistical significance compared with non-functionalised NPs (***p = 0.0006; **p = 0.0019)

IV - Proteomics analysis of selected complement proteins on NPs. Shot-gun and label-free quantification of complement proteins from protein corona of NPs after incubation in untreated HS.

V - Capture intensity NPs by human macrophages after 3h incubation at 37 °C in the presence of chelating agents (10 mM EGTA/2mM $MgCl_2$ or 10 mM EDTA) respectively. The data points represent mean ± s.d (n=3), analysed by one-way ANOVA followed Tukey-Kramer multiple comparison, statistical significance compared with respective particles in the absence of chelating agents in the same HS sample (***p = 0.001 – 0.005; *p = 0.05 -0.1).

(A – Untreated/ HS, B – non-functionalised NPs, C, and D Type I and Type II dendrimer functionalised NPs)

- Characterization of NPs through biophysical modalities confirmed the functionalisation of NPs with dendrimers, an example of this is the altered arrangement or packing behavior of NPs post dendrimer functionalisation as seen in SEM
- Results from shot-gun proteomics revealed deposition of complement proteins as seen in the figure IV, but same particles when fed to the macrophages, showed lesser uptake of dendrimer functionalised NPs (both type I and II dendrimers) than non-functionalised NPs indicating that protein deposition does not affect macrophage uptake of these NPs. Additionally, capture is Ca^{2+}/Mg^{2+} insensitive

Conclusion

Overall, the results of the study conclude that precision surface patterning with dendrimers can control and modulate immune responses.

References

[1] Moghimi SM, Haroon HB, Yaghmur A, Simberg D, Trohopoulos PN. Nanometer- and angstrom-scale characteristics that modulate complement responses to nanoparticles. J Control Release. 2022 Sep 27;351:432-443. doi: 10.1016/j.jconrel.2022.09.039. Epub ahead of print. PMID: 36152807.

[2] L.P. Wu, M. Ficker, M., J.B. Christensen, D. Simberg, P.N. Trohopoulos, S.M. Moghimi, Dendrimer end-terminal motif-dependent evasion of human complement and complement activation through IgM hitchhiking, Nat. Commun. 12: 4858

Acknowledgement- The study is funded by the European Union's Horizon 2020 programme funded under H2020-EU.1.3. – Excellent Science – Marie Skłodowska-Curie Actions, grant agreement ID. 956544 **(DIRNANO: Directing the Immune Response through Designed Nanomaterials).**

Adrian Hauck

Julius-Maximilians-
UNIVERSITÄT
WÜRZBURG

Fakultät für Chemie und Pharmazie
MAKROMOLEKULARE
CHEMIE

Dual pH-Degradable Polymeric Micelles for Potential Immuno Drug Delievery

Adrian Hauck,[1] Patric Komforth,[2]
Christian Czysch,[2] Judith Stickdorn,[2]
Simon Van Herck,[3] und **Lutz Nuhn**[1,*]

1: Institut für Funktionswerkstoffe und Biofabrikation, Lehrstuhl für Makromolekulare Chemie, Julius-Maximilians-Universität Würzburg
2: Max-Planck-Institut für Polymerforschung Mainz 3: College of Engineering, Cornell University, Ithaka (NY), USA

Highly potent small-molecule immuno drugs often lead to serious side effects when administered directly. To optimize the pharmacological properties of small molecule active ingredients, nanocarrier systems can play a decisive role.

Among other polymer-based nanoparticles, polymeric micelles are of particular interest. They allow a simple preparation of polymer-drug-formulations, using the solvent evaporation method.

Here we present the preparation of dual pH degradable polymeric micelles for the transport of active ingredients. Starting from the synthesis and characterization of a novel aliphatic carbonate-based acid labile monomer, we perform the preparation of homo and block copolymers. The latter can be used for the formulation of polymeric micelles. These structures were further characterized and successfully used in in vitro experiments, demonstrating their cell uptake and extraordinary ability to transport the highly immune stimulatory TLR7/8 agonist CL075 yielding a controllable stimulation of the cells immune system.

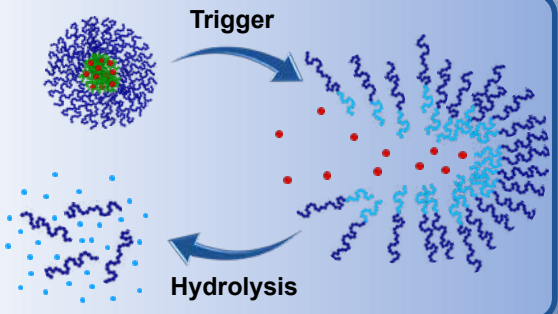

Nanoparticle Guided Drug Administration

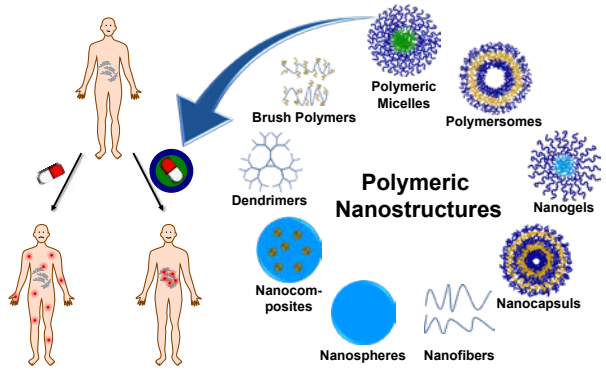

Nanoparticle Formulation and Decay

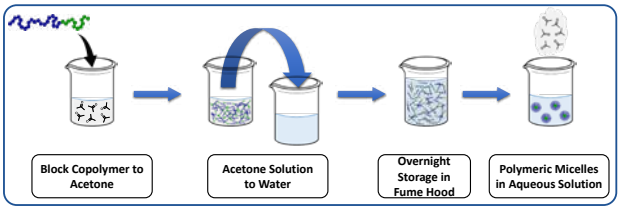

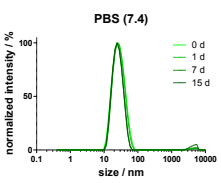

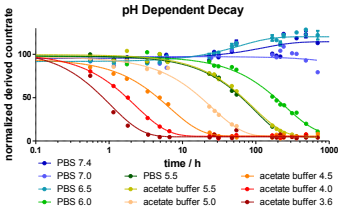

Monomer Synthesis

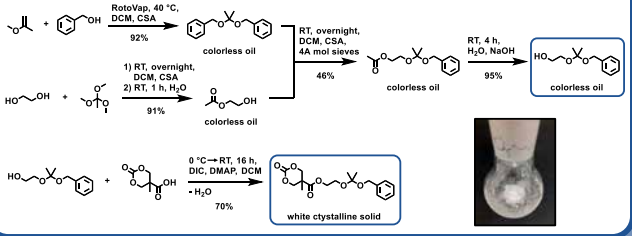

Ring Opening Polymerization to Block Copolymers

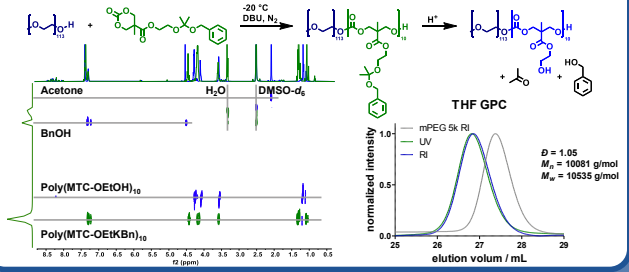

Cell Uptake and Drug Delivery

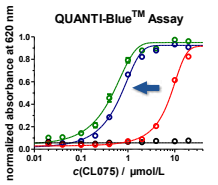

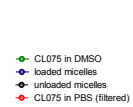

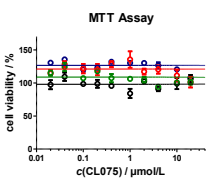

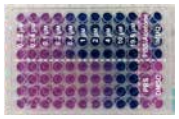

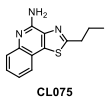

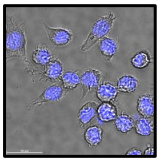

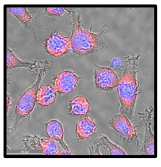

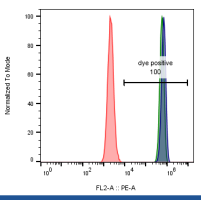

Weitere Infos: www.chemie.uni-wuerzburg.de/mmc
Kontakte: adrian.hauck@uni-wuerzburg.de
@NuhnLab @nuhnlab

UNI WÜ DFG Deutsche Forschungsgemeinschaft Emmy Noether-Programm DFG SFB 1066 FCI FONDS DER CHEMISCHEN INDUSTRIE

Beth Heaton

Investigating the immunological responses of hepatic and immune cells linked to the bioretention of iron oxide nanoparticles

Bethany J. Heaton, Doaa Mohamed and Neill J. Liptrott

Immunocompatibility Group, Department of Pharmacology and Therapeutics, Institute of Systems, Molecular and Integrative Biology, The University of Liverpool, Liverpool, UK; Centre of Excellence for Long-Acting Therapeutics (CELT), Department of Pharmacology and Therapeutics, Institute of Systems, Molecular and Integrative Biology, The University of Liverpool, UK

BACKGROUND

Super paramagnetic iron oxide nanoparticles (SPIONs) are being investigated for application in hyperthermia treatments. Nanoparticle physicochemical characteristic diversity presents a challenge to their immunocompatibility assessment which, combined with a lack of immune-competent tissue models, hampers development.

Our current work highlights cell-type specific responses to nanoparticles, underpinned by altered bioenergetics, that may define conditions and processes for the development of immune-competent tissue models. This highlights the need to first assess such responses in mono-culture to determine exposure-response relationships over extended periods of time.

We have assessed the responses of human immune and liver parenchymal cells, supported by physiologically based pharmacokinetic modelling (PBPK) (Figure 5). Detailed bioretention of SPIONs in the liver to a panel of pattern recognition receptor ligands and SPIONs, with varying surface chemistry, enabled development of appropriate immune-competent tissue models.

EXPERIMENTAL APPROACH

All cells were maintained in complete growth medium (THP-1: RPMI-1640 supplemented with 10% FBS; Hep G2: DMEM supplemented with 10% FBS) and maintained at 37°C, 5% CO_2. All studies were undertaken in the cell lines and as such cannot precisely represent complex physiological systems.

Cytotoxicity assessments: (MTT/LDH) The concentrations of SPIONs used in subsequent experiments were of non-cytotoxic concentrations, observed responses were not a consequence of cell death.

Responses of the human immune and liver parenchymal cells to experimental SPIONs and immunostimulatory ligands: THP-1 and Hep G2 cells at $5x10^5$ cells/mL were exposed to ligands and SPIONs for 2-, 4-, and 24-hours. Following incubation, responses were measured via a 6-plex Human Premixed Luminex assay or CellROX green.

Bioenergetic assessment, on THP-1 and Hep G2 cells, utilised the Agilent Seahorse ATP Rate Assay: cells were pre-treated with the CAR and PEG SPIONs, and ligands, for 24 hours prior to running a XF Real-Time ATP Rate Assay, which measures the rate of ATP production from glycolysis and mitochondria simultaneously in live cells.

Statistical analysis was performed using GraphPad Prism 8.3 software. Statistical significance was evaluated using a one-way ANOVA test. A P value <0.05 was considered statistically significant.

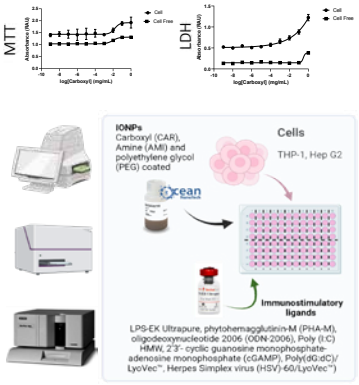

Secretion of bioactive molecules from model cell line, in response to immunostimulation

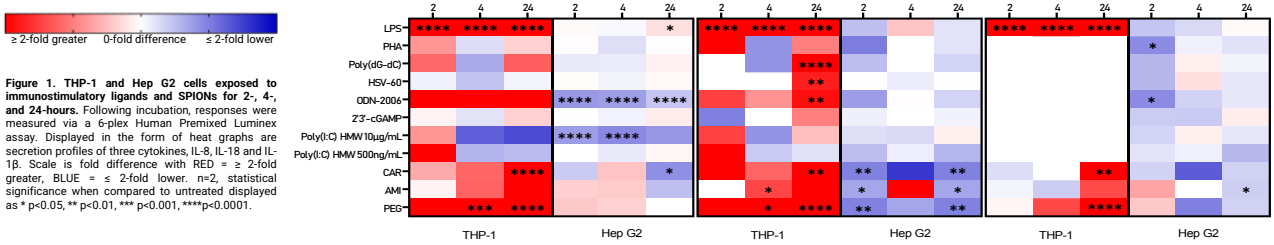

Figure 1. THP-1 and Hep G2 cells exposed to immunostimulatory ligands and SPIONs for 2-, 4-, and 24-hours. Following incubation, responses were measured via a 6-plex Human Premixed Luminex assay. Displayed in the form of heat graphs are secretion profiles of three cytokines, IL-8, IL-18 and IL-1β. Scale is fold difference with RED = ≥ 2-fold greater, BLUE = ≤ 2-fold lower. n=2, statistical significance when compared to untreated displayed as * p<0.05, ** p<0.01, *** p<0.001, ****p<0.0001.

IL-8 secretion is significantly lower after treatment with different SPIONs and ligands in Hep G2 cells, for example, the CAR coated SPION at 24 hours significantly lowered the secretion of IL-8 (1.78-fold, p=0.0114). **IL-8 secretion is significantly greater after treatment with different SPIONs and ligands in THP-1 cells**, such as stimulation with LPS (2 hours = 690.50-fold, 4 hours = 390.49-fold, 24 hours = 235.12-fold) (p=<0.0001).

IL-18 secretion was unaltered by ligands, however the SPIONs had significant effects in Hep G2 cells. CAR at 2 (1.97-fold) and 24 hours (1.98-fold) (p=0.002), AMI at 2 and 24 hours (1.55-fold, p=0.0233) and PEG at 2 and 24 hours (1.98-fold, p=0.002) lead to significantly lower secretion. **SPIONs caused significantly higher secretion, beginning at 4 hours in THP-1 cells**. Both AMI (3.45-fold, p=0.209) and PEG (6.50-fold, p=0.029) exposure increased **IL-18** secretion, which was further inflated with PEG at 24 hours (PEG = 40.14-fold, p=<0.0001). CAR at 24 hours also significantly raised the levels of **IL-18** secretion (23.00-fold, p=0.0027).

IL-1β secretion is significantly lower when treated with PHA in Hep G2 cells (1.87-fold, p=0.015) and ODN-2006 (1.85-fold, p= 0.015) at 2 hours. AMI also significantly lowers **IL-1β** secretion at 24 hours (1.25-fold, p=0.0489) in Hep G2 cells. **IL-1β** secretion is significantly greater when stimulated with LPS in THP-1 cells (2 hours = 141.14-fold, 4 hours = 91.50-fold, 24 hours = 17.97-fold) (p=<0.0001) and also when treated with CAR (3.24-fold, p=0.0016) and PEG (1.71-fold, p=<0.0001) at 24 hours.

Change in ATP rate production in THP-1 and Hep G2 cells following treatment with CAR and PEG SPIONS

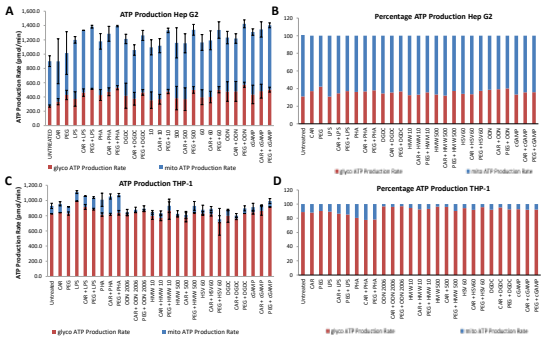

Figure 2. ATP production rate assessment on THP-1 and Hep G2 cells following 24-hour incubation with immunostimulatory ligands, CAR and PEG. (**A**) ATP production in Hep G2 cells (**B**) Percentage of ATP production in Hep G2 cells when compared to untreated (**C**) ATP production in THP-1 cells (**D**) Percentage of ATP production in THP- cells when compared to untreated. Graphs displayed as an average (n=4) ± SD. Blue bars displaying ATP produced via oxidative phosphorylation and red bars displaying ATP produced via glycolysis.

- Immune stimulation, in both THP-1s and Hep G2s, resulted in a greater total rate of ATP production with LPS.
- CAR and PEG SPIONs increase the ATP production rate within the Hep G2 cells (Figure 2A), yet have little effect on the THP-1 cells (Figure 2C).
- There is a clear difference in the baseline bioenergetics between THP-1 and Hep G2 cells in that the source of ATP production across the two cell lines differs, with THP-1s favouring glycolysis and Hep G2s favouring oxidative phosphorylation (Figure 2B, D).

ROS production in THP-1 cells in response to treatment with immunostimulatory ligands and SPIONs

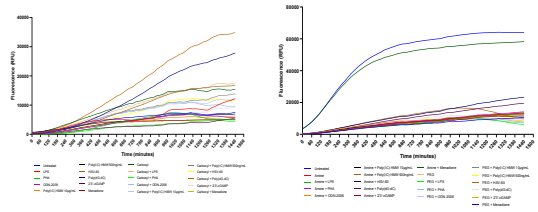

Figure 3. Cell stress assessment of immune cells to experimental materials. Kinetic measurements of reactive oxygen species generation in THP-1 cells in response to immunostimulatory ligands and SPIONs over 24 hours. Responses were measured via CellROX green. Results are displayed in the form of smooth line fluorescent readings, n=4.

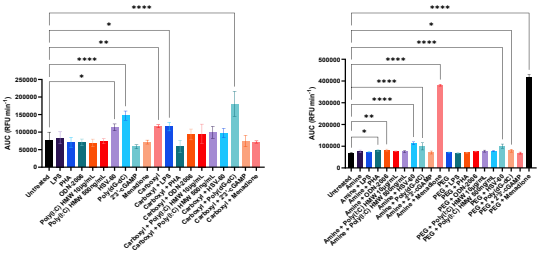

Figure 4. Area Under the Curve (AUC) calculations following ROS assessment of immune cells. AUC of kinetic measurements of reactive oxygen species generation in THP-1 cells in response to immunostimulatory ligands and SPIONs over 24 hours. Data displayed as average of n=4 ± SD. Statistical significance when compared to untreated displayed as * p<0.05, ** p<0.01, *** p<0.001, ****p<0.0001.

- ROS production (measured via CellROX green) showed via kinetic 24-hour measurements differed in response to immunostimulatory ligands and SPIONs (Figure 3)
- THP-1 cells treated with a ligands and SPIONs showed significant increase in AUC than untreated control cells (Figure 4). For example, cells treated with Poly(dG-dC) significantly increased the AUC by 1.94-fold, which was further increased by the addition of CAR (+Poly(dG-dC)) to 2.37-fold when compared with the untreated (p = <0.0001) when compared to the untreated.

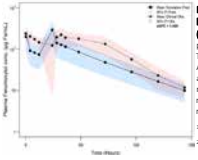

Figure 5. Plasma ferumoxytol log concentration after two consecutive IV bolus administered of 510 mg (24 hours apart) in healthy human subjects (n=100). The blue shaded area represents the simulation prediction results performed by physiologically based pharmacokinetic (PBPK) modelling approach. The red shaded area represents the clinical data obtained from pai et al 2010 [1]. Absolute average fold error (AAFE) for simulated conc. vs. clinical was within an acceptable 2-fold limit with a score of 1.069. One of key parameters in the PBPK model that influenced ferumoxytol retention in plasma is the macrophage/intracellular uptake in RES organs, the implemented in-vitro uptake rate (0.9 pg/day) obtained from Sharkey et al 2017 [2].

1.Pai, A.B., et al., *Plasma pharmacokinetics of two consecutive doses of ferumoxytol in healthy subjects.* Clin Pharmacol Ther, 2010. 88(2): p. 237-42.
2.Sharkey, J., et al., *Functionalized superparamagnetic iron oxide nanoparticles provide highly efficient iron-labeling in macrophages for magnetic resonance-based detection in vivo.* Cytotherapy, 2017. 19(4): p. 555-569.

SUMMARY Dependent on the cell type, conditions, and time of exposure, there are varying results for cytokine secretion, ROS production, and the bioenergetic profiling of the cells. The SPIONs induced pro-inflammatory cytokines in cell lines observed in monoculture, and further work will incorporate the use of co-culture for the assessment of cell-lines.

The cell bioenergetic assessments returned surprising results which indicates a need for additional work to determine the impact of the SPIONs in these cell lines. Going forward, we plan to assess the impact of long-term exposure on cellular responses to the SPIONs over a period of 7 days, looking deeper into cellular responses to identify whether the cells display senescence associated phenotypes after prolonged exposure.

Human Glioma Orthotopic Model

Manasa Manjunath Hegde[1], Jayant S. Goda[2], Srinivas Mutalik[3], and Bola Sadashiva Satish Rao[1*]

1. Manipal School of Life Sciences, Manipal Academy of Higher Education (MAHE), Manipal - 576 104, Karnataka, India, 2. Advanced Centre for Treatment, Education and Research in Cancer (ACTREC), Tata Memorial Centre, Kharghar, Navi Mumbai - 410 210, Maharashtra, India, 3. Manipal College of Pharmaceutical Sciences, MAHE, Manipal - 576 104, Karnataka, India.

INTRODUCTION

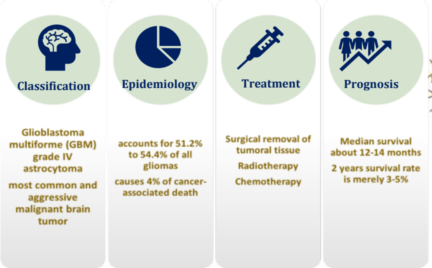

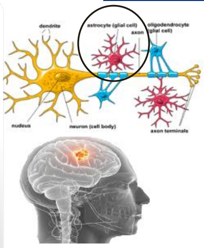

Origin of glioblastoma

- Several limiting factors including the blood-brain barrier, the highly invasive nature of gliomas, and drug resistance challenges with delivering therapeutic agents specifically to the tumour cells, make it difficult to treat malignant gliomas and results in a poor prognosis.
- To deliver targeted payloads with favourable pharmacokinetics and take benefit of cellular targeting for increased specificity, and enhanced effectiveness, nano-based therapeutic compounds are now in extensive use.
- In the present investigation, dual drug-loaded multifunctional liposomes were engineered with a combination of standard anticancer drug, Temozolomide (TMZ) and a chemosensitizer O6-Benzylguanine (O6-BG) along with ligand transferrin to bypass the blood-brain barrier as well as with a glioma tumour cell (U-87 MG Luc+) surface targeting moiety, anti-integrin antibody for targeted drug delivery aiming for an efficacious targeted delivery to the tumour in an intracerebral glioma model.

METHODOLOGY

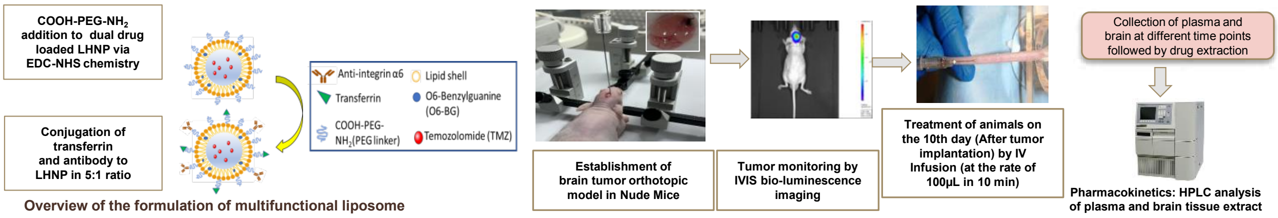

Overview of the formulation of multifunctional liposome

RESULTS

Physicochemical characterization of multifunctional NPs

Nanocarrier	Size (nm)	Zeta potential (mV)	PDI	Entrapment efficiency (%)	Drug loading (%)
Unconjugated LP	182 ± 5.0	-32± 5.0	0.423± 0.082	TMZ – 39.7± 2.0 O6-BG- 71.6± 2.0	4.6± 2.0 8.7± 2.0
Transferrin/Ab conjugated LPs	196± 5.0	-29± 5.0	0.528± 0.051	TMZ –36.3± 2.0 O6-BG- 69.4± 2.0	3.8± 2.0 7.6± 2.0

Table 1: Physicochemical characteristics of unconjugated and conjugated liposome loaded with dual drugs

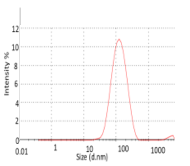

Fig. 1: Representative image showing the particle size distribution

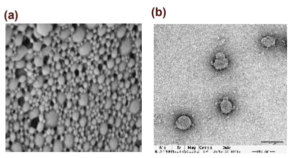

Fig. 2: Representative (a) SEM and (b) TEM images transferrin & anti-Integrin conjugated liposome showing well dispersed particles

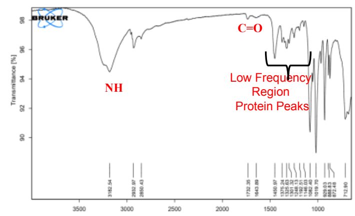

Fig. 3: FTIR spectra showing formation of amide linkage between Lipids and NH2-PEG-COOH with a C=O stretch at 1732.35 cm^{-1} and NH stretch at 3182.54 cm^{-1} indicating the formation of amide (CO-NH) bond, low frequency spectra of nanocomposite showing region of dual proteins

Determination of cellular uptake of Liposomes

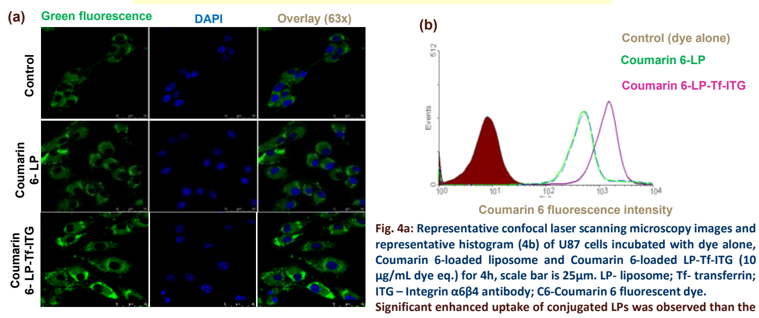

Fig. 4a: Representative confocal laser scanning microscopy images and representative histogram (4b) of U87 cells incubated with dye alone, Coumarin 6-loaded liposome and Coumarin 6-loaded LP-Tf-ITG (10 µg/mL dye eq.) for 4h, scale bar is 25µm. LP- liposome; Tf- transferrin; ITG – Integrin α6β4 antibody; C6-Coumarin 6 fluorescent dye. Significant enhanced uptake of conjugated LPs was observed than the unconjugated LPs facilitating the receptor mediated endocytosis

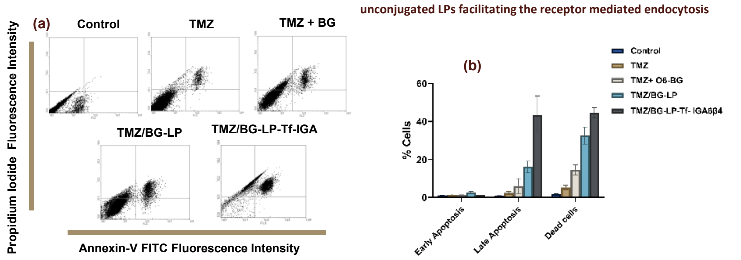

Fig. 5: Representative FACS a) dot-plot and b) histogram for U87 MG cells stained with Annexin V-FITC/ PI staining for after treatment with pure drugs and drug-loaded liposome for 72 h. Sustained release of drug leading to early and late apoptosis after various treatments

Establishment of the orthotopic glioblastoma mouse model

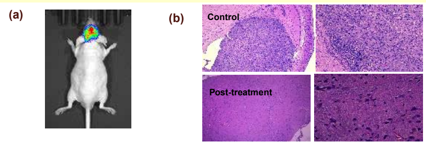

Fig 6: Representative images showing developed intracerebral tumor determined by (a) Bioluminescence imaging, (b) histopathology (H & E staining) section of untreated tumor and T+BG-LP-Tf/ITG treated brain

Pharmacokinetic profile of TMZ and formulations in blood & brain

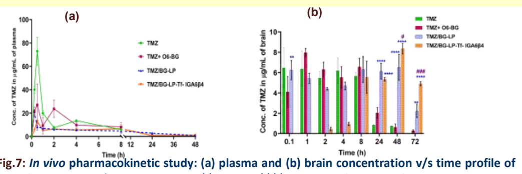

Fig.7: *In vivo* pharmacokinetic study: (a) plasma and (b) brain concentration v/s time profile of Data is represented as mean ± SD, **p<0.01, ****p <0.0001 in comparison to TMZ+O6-BG; .#p<0.05, .###p<0.001 in comparison to TMZ+BG-LP. T+BG-LP-Tf-ITG showed sustained drug release with significant drug uptake in brain with negligible plasma distribution

CONCLUSION & FUTURE PROSPECTS

- We developed multifunctional dual drug loaded (TMZ & O6-BG) liposomes tagged with transferrin to bypass BBB and specifically target stem cells in intracerebral glioma tumor by conjugation of anti-integrin antibody so as to enhance therapeutic efficacy.
- The use of Integrin antibody as tumor targeting moiety has been demonstrated the effective localization of liposomes inside the tumor cells.
- *In vitro* studies displayed that developed liposomes were able to reach the tumor cells and effectively cause cell death via cell cycle arrest and by irreversible DNA damage leading to apoptosis.
- The developed formulation (TMZ/BG-LP-Tf-IGA) showed a maximum uptake in brain and longer retention time for enhanced drug availability specifically to the tumor cells.
- Present work opens up a dual drug approach for treating highly resistant brain tumors in an efficient and feasible way.

ACKNOWLEDGMENT

We thank MAHE and Manipal School of Life Sciences for the infrastructure and also, to DST-SERB (EMR/2016/007782), Government of India, New Delhi for providing fellowship as well as research support to the first author. We thank ACTREC, Mumbai for facilitating small animal imaging facility The First author highly appreciate and acknowledge the support of CLINAM Foundation.

REFERENCES

- Prabhu, S., Goda, J.S., Mutalik, S., Mohanty, B.S., Chaudhari, P., Rai, S., Udupa, N., and Rao, B.S.S. (2017). A polymeric temozolomide nanocomposite against orthotopic glioblastoma xenograft: tumor-specific homing directed by nestin. Nanoscale 9, 10919–10932
- Riaz, M.K., Riaz, M.A., Zhang, X., Lin, C., Wong, K.H., Chen, X., Zhang, G., Lu, A., and Yang, Z. (2018). Surface Functionalization and Targeting Strategies of Liposomes in Solid Tumor Therapy: A Review. Int J Mol Sci 19

Surface-functionalized human serum albumin for modulating tumor microenvironment

Lifan Hu, Darijan Schüler, Seah Ling Kuan, Tanja Weil

1. Introduction

The altered metabolic biology, is a hallmark of cancer cells that support their activities and malignant properties. Warburg effect indicates that cancer cells tend to undergo glycolysis rather than oxidative phosphorylation (OXPHOS), even in aerobic environment, resulting in tumor immunosuppressive environment. Consequently, cancer metabolism has emerged as a vital area in cancer research to develop new treatment that are more effective. Nowadays, some small molecule inhibitors have been developed but shortcomings from these therapies such as limited stability, toxic side effects from non-specific targeting also need to be addressed. Herein, we develop a protein-based carrier that can be selectively uptaken in acidic environment of aggressive cancer.

2. Cancer metabolism inhibitors

Target	Metabolism inhibitor
Hexokinase-II	2-DG 3-bromopyruvate
GLUTs	Silibinin Cytochalasin B
MCT-1, MCT-2	AZD3965 AR-C155858
OXPHOS	Metformin Phenformin Lonidamine
PDK	Dichloroacetate
LDH	GSK28387808A FX11

Table 1. Targeting sites and inhibitors in cancer metabolism pathways. Limitations: limited stability, off-target toxic side effects.

3. Surface-functionalized HSA

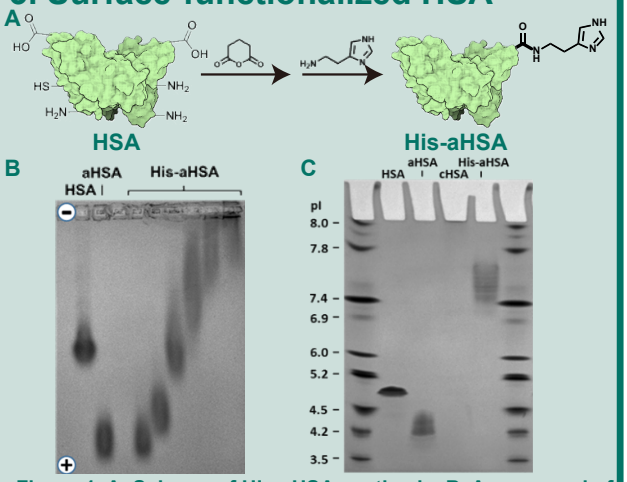

Figure 1. A. Scheme of His-aHSA synthesis. B. Agarose gel of HSA, aHSA, His-aHSA (depended on different n(Imidazole)). C. Isoelectric focusing gel of HSA, aHSA, cHSA, His-aHSA.

4. pH-dependent cell upatke

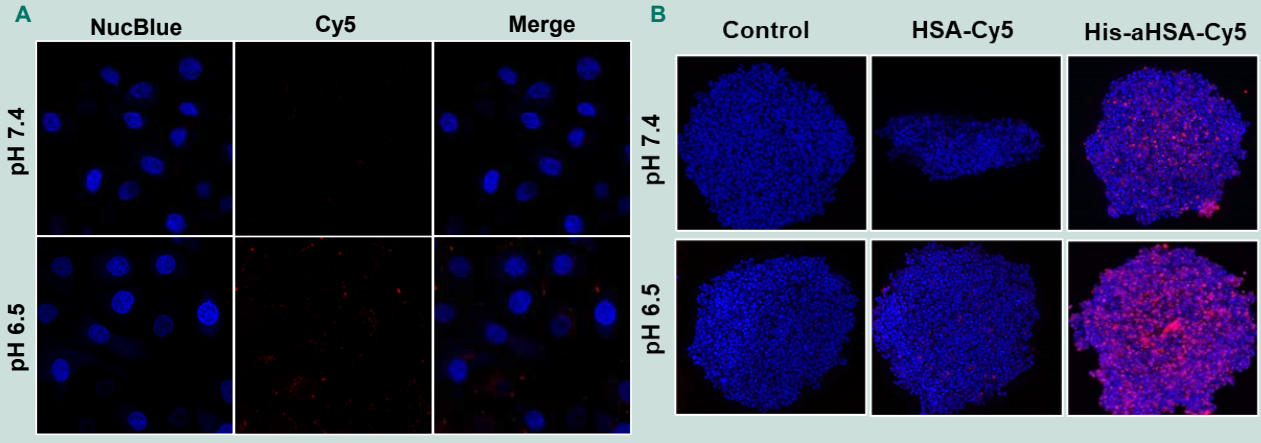

Figure 2. Confocal Microscopy images of pH-depended uptake. A. Cell uptake of His-aHSA-Cy5 on MDA-MB-231 cells under different pH environments. B. Cell uptake of HSA-Cy5 and His-aHSA-Cy5 on MDA-MB-231 spheroids under different pH environments.

4. References

- R.J. DeBerardinis, N.S. Chandel, Fundamentals of cancer metabolism, Sci Adv, 2 (2016) e1600200.
- Stine ZE, Schug ZT, Salvino JM, Dang CV. Targeting cancer metabolism in the era of precision oncology. Nat Rev Drug Discov. 2022 Feb;21(2):141-162.

Nicole Martina Hutter

Multicomponent Supramolecular Platform for the Design of Glycoconjugate Antitumor Vaccines

SFB 1066

Nicole Hutter[1], Isabelle Silvestre[2], Jessica Erlenbusch[1], Moritz Urschbach[1], Riem Attariya[2], David Straßburger[1], Natascha Stergiou[2], Tobias Bopp[2], Edgar Schmitt[2], Pol Besenius[1]
[1] Department of Chemistry, Johannes Gutenberg-University Mainz, Germany, [2] Institute of Immunology, University Medical Center Mainz, Germany

Abstract

Classical synthetic vaccine approaches commonly utilize immunogenic carrier proteins of biological origin to immobilize antigens or haptens. These bioconjugation approaches suffer from problems like low reproducibility and poor characterizability of the products. Deviations in the antigen loading are inevitable and may cause issues in biomedical applications. An ideal fully synthetic vaccine should only contain chemically well-defined molecules that are bound in a controlled and multivalent manner onto the carrier.
Supramolecular polymers are a promising scaffold for the presentation of antigenic structures to the immune system due to the dynamic nature of the underlying polymerization process.[1] Each monomer can be individually functionalized and comprise a targeting structure,[2] immunostimulant or antigen. Simple mixing in aqueous solution results in the formation of co-polymers which harbor all desired features on their surface and are able to trigger an antigen-specific humoral immune response.
We present the synthesis and immunological evaluation of a novel modular and fully synthetic antitumor vaccine. The supramolecular platform is employed for versatile multivalent presentation of different epitopes and capable of inducing a strong immune response directed against tumor-associated MUC1, comprising a Tn and 2,3-ST antigen, in C57BL/6 mice.

Nanoplatform For Vaccine Development

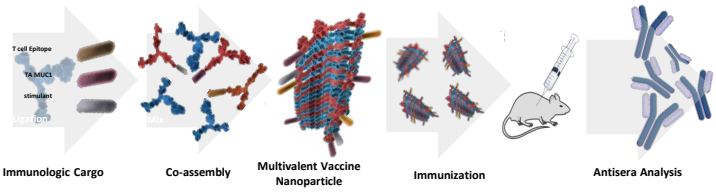

The human immune system is a powerful machinery, evolutionary specialized on recognizing and eliminating nano-scaled pathogens of viral, bacterial or xenobiotic origin. For the design of fully synthetic vaccines, supramolecular polymers can serve as well-defined scaffold to present relevant tumor-associated structures to immune cells on their surface. Bioorthogonality of the conjugation chemistry enables convenient, "last step" attachment of relevant pharmacological structures which was successfully demonstrated for peptidic B-cell and T-cell epitopes as well as heterocyclic immunostimulants. No effects of cytotoxicity or immunogenicity of the self-assembling scaffold were seen in the mouse model. The fact that each monomer bears only one cargo gives the chemists full control on the total amount of active ingredients in the vaccine. Blending diversely loaded monomers with different functional moieties and subsequent copolymerization in physiological media is a promising and modular approach to construct multivalent fully synthetic antitumor vaccines.

Self-Assembling Peptide Motifs

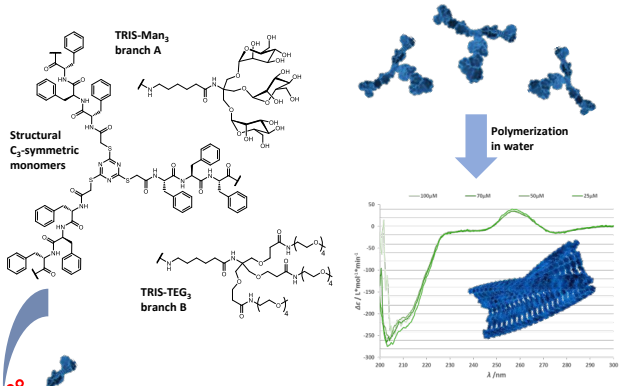

Triazine branched nonaphenylalanine based monomers bearing tetra(ethylenglycol) or mannose functionalized solubilizing dendrons direct supramolecular polymerization into anisotropic particles up to 300 nm in length.[4] The structures are characterized *via* CD-spectroscopy and TEM.

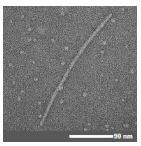

TEM, neg. stain, 10 µM in H_2O

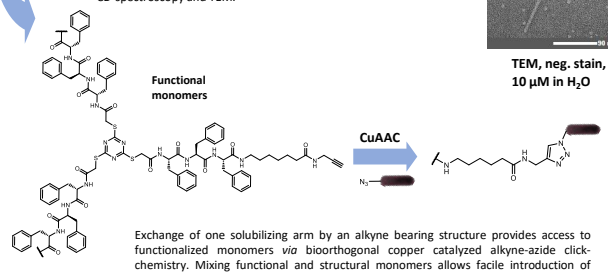

Exchange of one solubilizing arm by an alkyne bearing structure provides access to functionalized monomers *via* bioorthogonal copper catalyzed alkyne-azide click-chemistry. Mixing functional and structural monomers allows facile introduction of biologically active compounds, such as immunogenic epitopes, stimulants or dyes into self-assembled structures.

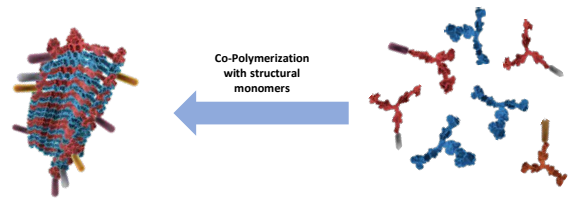

Mucin 1 Glycopeptide

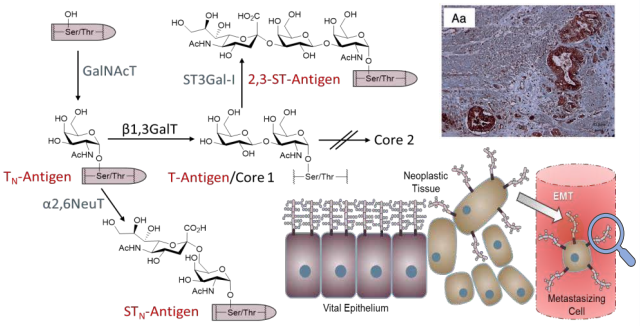

Tumor-associated (TA) MUC1 is a glycopeptide and diagnostic marker for different epithelial malignancies like mammary carcinoma, prostate, pancreatic or lung cancer. Besides its overexpression on tumor tissue, aberrant glycosylation due to dysregulation of glycosyltransferases is observed. This leads to truncated short glycan side chains resulting in the collapse of the peptide backbone. As a consequence of the defect glycan-shielding the peptide structure can be accessed and recognized by immune cells.

Immunological Evaluation

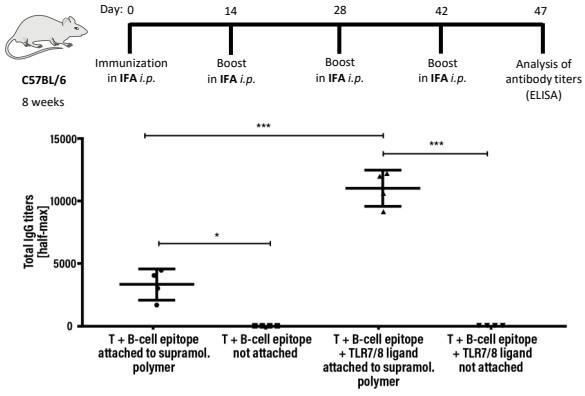

Five C57BL/6 mice were immunized with a vaccine comprising MUC1 B-cell epitope[4], Ttox p30 Th-cell epitope and TLR7/8 ligand decorated FM- together with SM+. After 3 boosts the sera were collected from the tail vein of the mice and analyzed for antibodies directed against TA MUC1. We found robust titers of all antibody classes whereas IgG memory-related type was dominating. Furthermore a significant level IgG2c antibodies was detected. The latter are capable to induce antibody dependent cell-mediated cytotoxicity (ADCC) due to the recruitment of NKs, Ms and DCs via Fc of the corresponding immunoglobulin. The application of unbound epitopes resulted in significantly lower IgG titers demonstrating the power of the supramolecular approach.

[1] H. Frisch, Y. Nie, S. Raunser, P. Besenius, Chem. - A Eur. J. 2015, 21, 3304–3309.
[2] D. Straßburger, N. Stergiou, M. Urschbach, H. Yurugi, D. Spitzer, D. Schollmeyer, E. Schmitt, P. Besenius, ChemBioChem 2018, 19, 912–916.
[3] B. Palitzsch, N. Gaidzik, N. Stergiou, S. Stahn, S. Hartmann, B. Gerlitzki, N. Teusch, P. Flemming, E. Schmitt, H. Kunz, Angew. Chemie Int. Ed. 2016, 55, 2894–2898.
[4] D. Straßburger, M. Glaffig, N. Stergiou, S. Bialas, P. Besenius, E. Schmitt, H. Kunz, ChemBioChem 2018, 19, 1142–1146.

Lloyd Jeffs

Strategies for producing clinical and commercial RNA-LNP drug products

L. Jeffs^, I. Johnston, D. Singh, A. Braun, B. MacDougall, B. Ma, A. Lazic, L. Yee, A. St. Quintin, C. Robin, F. Yuen, P. Harvie, S. Abraham, S. Clarke

^ presenting author
Precision Nanosystems ULC, Vancouver, Canada

Contact us at:
Precision NanoSystems, Vancouver, BC, Canada
info@precision-nano.com

Introduction

- The promise of messenger RNA (mRNA) lipid nanoparticle (LNP) therapies include prophylactic, rare disease, and oncology applications.
- However, encapsulation of mRNA drug substances by lipids is among the most difficult unit operation to bring to commercial-scales.
- In this work, we aim to demonstrate that the NanoAssemblr® commercial formulation system and NxGen™ commercial cartridge 48 L/h simplify this unit operation.

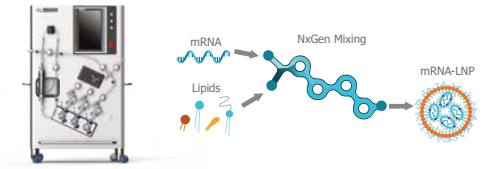

Figure 1. NanoAssemblr commercial formulation system (left) and NxGen microfluidic mixing system (right)

Objectives

- Demonstrate consistent mixing → The quality of mixing in the NxGen series of mixers was probed by formulating POPC:Chol liposomes at a range of flow rates
- Show scalability from pre-clinical to clincal/commercial → Increasingly large batches of plasmid DNA-LNPs were prepared with NxGen mixers
- Prepare consistent RNA-LNP drug products at all scales → Flow rates for saRNA-LNP production were stepwise increased by an order of magnitude

Methods and Results

Nanoparticle synthesis and purification:
POPC(1-palmitoyl-2-oleoyl-glycero-3-phosphocholine):Chol liposomes were prepared at a range of flow rates on NxGen mixers. Green fluorescent protein (GFP) plasmid DNA (pDNA) LNPs or self-amplifying mRNA (saRNA)-LNPs were prepared using NanoAssemblr® instruments and NxGen™ mixers. Specific formulation conditions are noted in the tables right and below.

RNA-LNP characterization and *in vitro* activity: RNA-LNP size and polydisersity index (PDI) were determined using DLS (Malvern Zetasizer Ultra). The encapsulation efficiency (EE%) of the RNA was determined using Ribogreen™ reagent.

***In vitro* and *in vivo* expression and immunogenicity:** *In vitro* potency was assessed with a kinase deficient baby hamster kidney cell (BHK 570) cell model. To determine the immunogenicity of the saRNA-LNPs, female BALB/c mice (n=5) were immunized by IM injection on day 0 with LNPs encapsulating 1µg nCoV saRNA and boosted at day 28. IgG levels in serum on day 21 and day 42 were measured by ELISA.

Condition	NanoAssemblr® system	NxGen mixer cartridge	Total flow rate [L/h]	Batch volume [mL]	RNA Encapsulated [mg]
1	Ignite+	NxGen	0.72	30	1.1
2	Ignite+	NxGen 500	6.9	30	1.1
3	Ignite+	NxGen 500	12	30	1.1
4	Blaze	NxGen 500	6.9	30	1.1
5	Commercial formulation system	NxGen commercial cartridge 12 L/h [Nxgen 500]	12	100	3.3
6	Commercial formulation system	NxGen commercial cartridge 48 L/h	48	100	3.3
7	Modular commercial formulation skid	NxGen commercial cartridge 48 L/h	48	150	5.0

Table 1. saRNA-LNP formulation conditions

1. NxGen Mixing Architecture Ensures Consistent Particles Across a Wide Range of Flow Rates

Figure 2. Controlled mixing using NxGen technology
Controlled mixing using NxGen technology allows for production of limit-size nanoparticles across a wide range of flow rates. **A)** computational fluid dynamic modeling with water and ethanol. **B)** Dye studies using the NxGen commercial cartridge 48 L/h. **C)** POPC:Chol liposome formation. The size of POPC:Chol liposomes prepared using the NxGen, NxGen 500, and NxGen commercial cartridge 48 L/h at a range of flow rates

2. Consistent LNP Formulation Conditions for >6g IVT Process

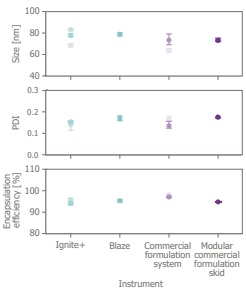

Figure 3. pDNA-LNPs prepared with the NxGen commercial cartridge 48 L/h in batches of up to 50 L in volume Size, polydispersity index and encapsulation efficiency of 3 pDNA-LNP formulations prepared using the NxGen commercial cartridge 48 L/h as a function of batch size (volume). Values are n = 1 for 5, 10 and 50 L batches while the 2 mL NxGen control sample is n =3.

Key Formulation Parameters for pDNA-LNPs	
Lipid Composition	Precision NanoSystems Custom Composition Ionizable lipid : Helper 1 : Helper 2 : Stabilizer
Initial Lipid Concentration	2x nominal concentration
Genetic Cargo	6.1 kb eGFP pDNA
N/P	8
Organic Solvent	Ethanol
Aqueous Phase	2x nominal pDNA concentration in acidic buffer
Flow Rate Ratio	3:1 aqueous to organic

3. Critical Quality Attributes of saRNA-LNPs Are Consistent Across NanoAssemblr Systems

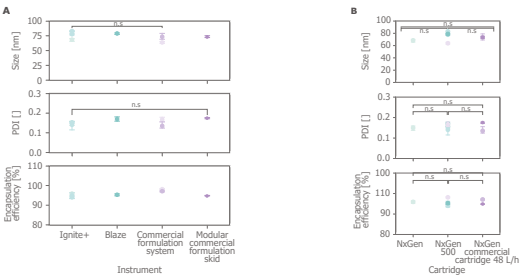

Figure 4. Physicochemical characterization of saRNA-LNPs prepared using NxGen Technology
A) Size, PDI, and encapsulation efficiency as a function of instrument system used to prepare the saRNA-LNP. **B)** Size, PDI and encapsulation efficiency as a function of NxGen mixer cartridge.

Key Formulation Parameters for pDNA-LNPs	
Lipid Composition	Precision NanoSystems Custom Composition Ionizable lipid : Helper 1 : Helper 2 : Stabilizer
Initial Lipid Concentration	2x nominal concentration
Genetic Cargo	6.1 kb eGFP pDNA
N/P	8
Organic Solvent	Ethanol
Aqueous Phase	2x nominal pDNA concentration in acidic buffer
Flow Rate Ratio	3:1 aqueous to organic
TFF Concentration and Diafiltration	Cytiva Delta cassette 30 kDa, 93 cm²
Cryopreservation Buffer	Precision NanoSystems custom
Sterile Filtration	Cytiva Acrodisc 0.22 µm

4. Commercial Scale saRNA-LNPs Are Biologically Potent *In Vitro* and *In Vivo*

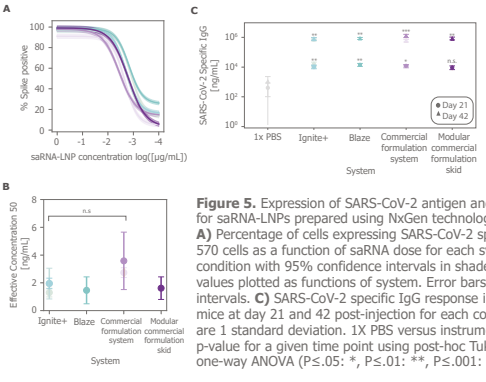

Figure 5. Expression of SARS-CoV-2 antigen and immune response for saRNA-LNPs prepared using NxGen technology
A) Percentage of cells expressing SARS-CoV-2 spike protein in BHK 570 cells as a function of saRNA dose for each system and mixer condition with 95% confidence intervals in shaded areas. **B)** EC50 values plotted as functions of system. Error bars are 95% confidence intervals. **C)** SARS-CoV-2 specific IgG response in serum from BALB/c mice at day 21 and 42 post-injection for each condition. Error bars are 1 standard deviation. 1X PBS versus instrument comparison p-value for a given time point using post-hoc Tukey test after one-way ANOVA (P≤.05: *, P≤.01: **, P≤.001: ***, P≤.0001: ****).

Conclusion

- Critical quality attributes of the saRNA-LNPs were maintained across all scales and flow rates for all analytical readouts.
- The NxGen commercial cartridge 48 L/h and NanoAssemblr commercial formulation system provide a scalable solution for production of RNA-LNP drug products under cGMP conditions.

Carina Jung

Achieving dendritic cell subset-specific targeting *in vivo* by site-directed conjugation of targeting antibodies to nanocarriers

C. Jung[1], M. Fichter[1,2], J. Simon[1], K. Landfester[1] and V. Mailänder[1,2]

jungc@mpip-mainz.mpg.de
[1] Max Planck Institute for Polymer Research, Ackermannweg 10, 55128 Mainz, Germany
[2] Department of Dermatology, University Medical Center Mainz, Langenbeckstraße 1, 55131 Mainz, Germany

MAX PLANCK INSTITUTE FOR POLYMER RESEARCH

SFB 1066

ABSTRACT

The major challenge of nanocarrier-based anti-cancer vaccination approaches is the targeted delivery of antigens and immunostimulatory agents to cells of interest, such as specific subtypes of dendritic cells (DCs), in order to induce robust antigen-specific anti-tumor responses. An undirected cell and body distribution of nanocarriers can lead to unwanted delivery to other immune cell types like macrophages, reducing the vaccine efficacy. An often-used approach to overcome this issue is the surface functionalization of nanocarriers with targeting moieties, such as antibodies, mediating cell type-specific interaction. Numerous studies could successfully prove the targeting efficiency of antibody-conjugated carrier systems *in vitro*, however, most of them failed when targeting DCs *in vivo*, which is partly due to cells of the reticuloendothelial system unspecifically clearing nanocarriers from the blood stream via Fc receptor ligation.
Therefore, we developed a surface functionalization strategy that site-specifically attaches antibodies in an orientated direction onto the nanocarrier surface. Different DC-targeting antibodies, such as anti-CD11c, anti-CLEC9A, anti-DEC205 and anti-XCR1, were conjugated to the nanocarrier surface at their Fc regions. Anti-mouse CD11c antibody-conjugated nanocarriers specifically accumulated in the targeted organ (spleen) over time. Additionally, antibodies against CD11c and CLEC9A proved to specifically direct nanocarriers to the targeted DC subtype, conventional DCs type 1.

SITE-SPECIFIC MODIFICATION OF NANOCARRIERS

Strain promoted azide-alkyne click reaction attaches modified antibody to nanocarriers.

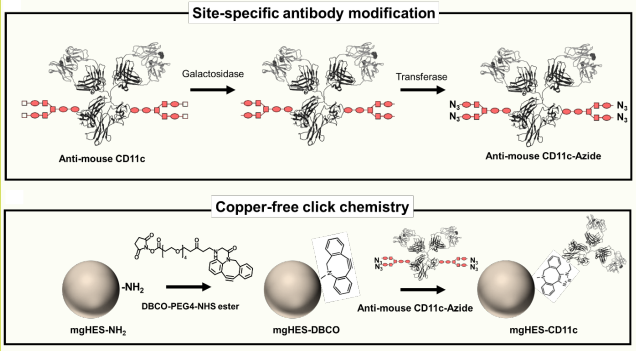

IN VIVO PROTEIN CORONA

Proteomic analysis of the protein corona on the modified nanocarriers, prepared *in vitro* and *in vivo*.

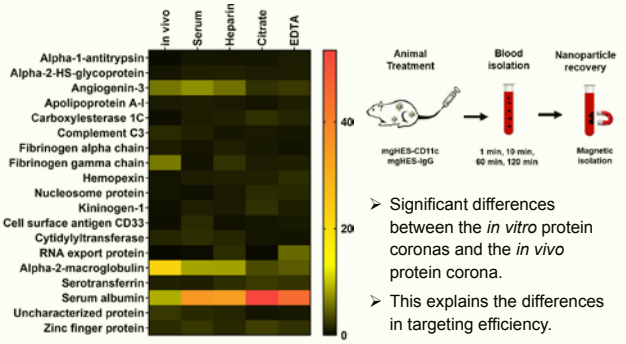

- Significant differences between the *in vitro* protein coronas and the *in vivo* protein corona.
- This explains the differences in targeting efficiency.

IN VITRO CELL UPTAKE OF THE MODIFIED CARRIERS

Dendritic cell uptake of CD11c- and IgG-modified nanocarriers with and without protein corona.

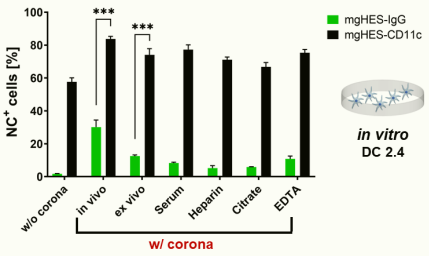

- Increased uptake of nanocarriers with protein corona.
- Efficient targeting of CD11c *in vitro*, no increased uptake of the isotype-conjugated carrier.

IN VIVO BIODISTRIBUTION OF THE MODIFIED CARRIERS

Uptake of anti-CD11c, -Clec9a, -XCR1 and -DEC205, as well as isotype (IgG) functionalized nanocarriers in splenocytes (isolated from the spleen 24h after injection in mice).

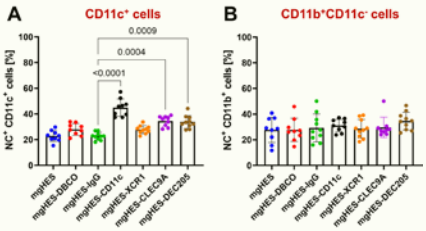

- No difference in uptake in CD11c$^-$ CD11b$^+$ cells.
- Highest uptake efficiency reached using anti-CD11c and anti-Clec9a.

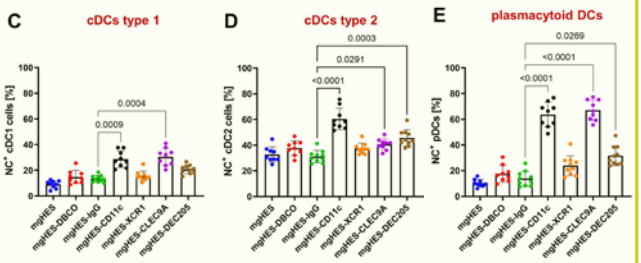

CONCLUSION

DC-targeting antibodies were successfully conjugated to magnetic nanocarriers in a site-specific manner, which is essential in order to avoid unspecific uptake by non-target cells while achieving a specific targeting of DC subsets. Proteomic analysis of the protein corona formed on the carriers during *in vitro* and *in vivo* incubation revealed major differences in composition, explaining the discrepancies in the targeting efficiency. The biomolecular protein corona did not prevent the binding towards cell surface receptors on CD11c$^+$ cells both *in vitro* and *in vivo*. An *in vivo* biodistribution assay revealed CD11c and Clec9a to be excellent candidates for DC targeting, with anti-Clec9a exhibiting a specific targeting towards cDC1 and pDCs. Consequently, this novel conjugation technique paves the way for the development of antibody-functionalized nanocarriers for DC-based vaccination approaches in the field of cancer immunotherapy.

J. Simon, M. Fichter, G. Kuhn, M. Brückner, C. Kappel, J. Schunke, T. Klaus, S. Grabbe, K. Landfester, V. Mailänder, *Nano Today* **2022**, *43*, 101375.

David Juriga

Effect of polyaspartamide-based polyelectrolytes on cellular uptake of Si nanoparticles

David Juriga[1], Krisztina Juriga-Toth[1], Nora Fekete[2], Anna Salvati[3]
E-mail: jurigad.16@gmail.com
[1]Laboratory of Nanochemistry, Department of Biophysics and Radiation Biology, Semmelweis University, H-1089. Budapest, Nagyvárad tér 4. Hungary
[2]Department of Genetics, Cell- and Immunobiology, Semmelweis University, Nagyvárad tér, 4, H-1089 Budapest, Hungary
[3]Department of Nanomedicine and Drug Targeting, Groningen Research Institute of Pharmacy, University of Groningen, A Deusinglaan 1, 9713 AV Groningen, The Netherlands

Introduction: Polyelectrolytes have been getting increasing attention for their potential applications for drug and RNA delivery since they are able to increase cellular uptake and also to achieve endosomal escape. Furthermore, polyelectrolytes exhibit various reactive groups that provide the opportunity for further modification whit targeting agents[1,2].
Polyaspartamide (PASP) based polyelectrolytes (PEs) are biocompatible and biodegradable polymers derived from polysuccinimide (PSI). Due to the high reactivity of the PSI, PASP-PEs can be modified with different biologically active molecules such as drugs or targeting agents (RGD tripeptide). Due to these features, the number of biomedical applications of PASP-PEs has increased significantly in the last decade [3].
In this present research, we aimed to coat silica nanoparticles (SiNP) with different PASP-PEs and investigate the effect of the coating on cell viability and uptake of HeLa cells.

Synthesis, nanoparticle coating, and characterization

Unpublished data

DLS and Zeta measurement

Sample name	Water (After 2X washing)		Complete Medium (10%FBS)
	Diameter (nm)	Zeta (mV)	Diameter (nm)
	Unpublished data		

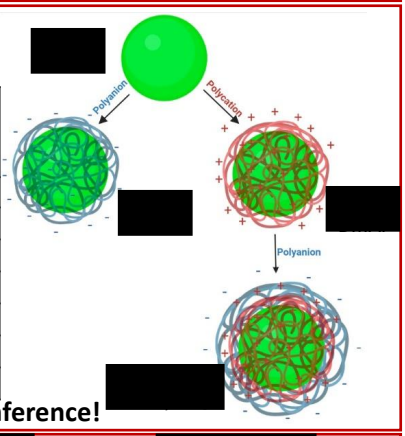

The complete poster will be presented at the conference!

Cytotoxicity

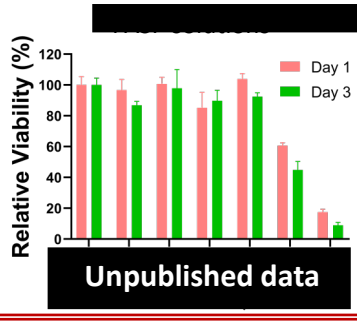

Unpublished data

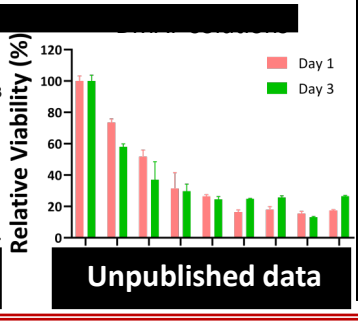

Unpublished data

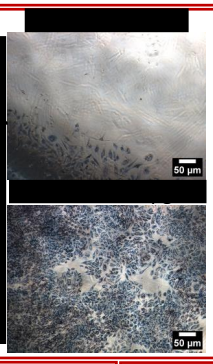

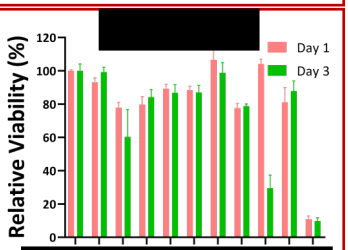

Unpublished data

Cell uptake

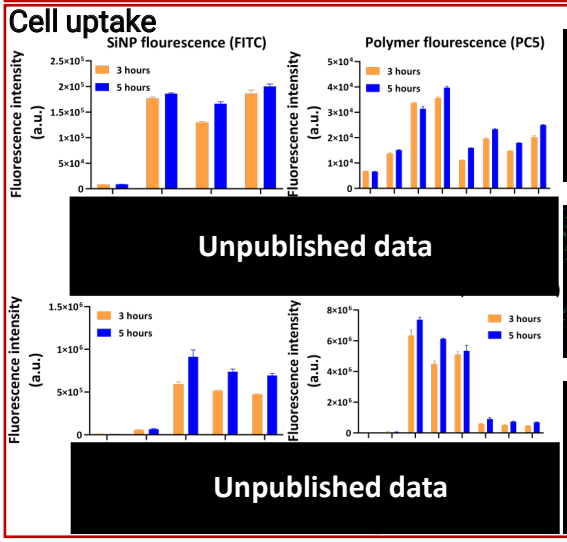

Unpublished data

Unpublished data

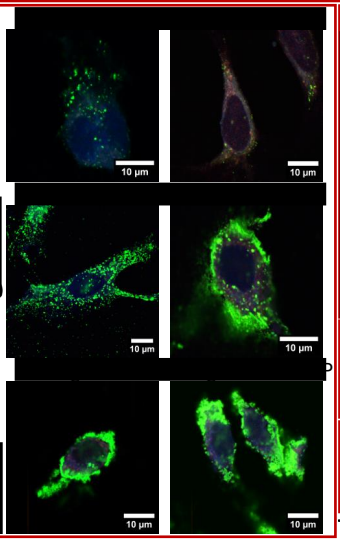

Conclusion

Unpublished data

Acknowledgment
This research was supported by the Eötvös Research fellowship (MAEO 2021-22 /166540) and the Erasmus+ program.

References

1 Vergaro, V. et al. Adv. Drug Deliv. Rev. 63, 847 (2011)
2 Meka, V. S. et al. Drug Discov. Today 22, 1697 (2017)
3 Yavvari, P. S. et al. J. Mater. Chem. B 7, 2102 (2019)

The complete poster will be presented at the conference!

Jinhong Kang, Pottanam Chali

Emulsion templated protein nanocapsule formation by interfacial denaturation for the efficient encapsulation and delivery of adjuvants for cancer immunotherapy

Jinhong Kang[1,2], Sharafudheen Pottanam Chali[1], Michael Fichter[1,2], Volker Mailaender[1,2], Katharina Landfester[1]

1 Max-Planck-Institut für Polymerforschung, Ackermannweg 10, 55128 Mainz, Germany
2 Universitätsmedizin der Johannes Gutenberg-Universität Mainz, D-55131 Mainz, Germany

ABSTRACT

Nanocapsules enable multicomponent encapsulation of therapeutic cargoes with high encapsulation content and efficiency, which is vital for cancer immunotherapy. In the past, complex chemical processes such as crosslinking has been used to synthesize nanocapsules, which can impede the regulatory approval process. Therefore, we developed a new class of protein nanocapsules by eliminating the need for chemical cross-linking by utilizing protein denaturation. A model antigen, Ovalbumin was incorporated in to the protein shell and two adjuvants, Toll-like receptor 7 (TLR7/8) agonist R848 and STING agonist diABZI were encapsulated in the protein nanocapsules. The studies on cytokine secretion by bone marrow derived dendritic cells (BMDCs) treated with adjuvant-loaded protein nanocapsules showed the synergistic activity of the adjuvants to enhance the immune response. Because there is no complex reactions or reagents involved in the synthesis, we anticipate an easier clinical translation of these nanocarriers compared to others.

PREPARATION OF PROTEIN NANOCAPSULES (PNC)

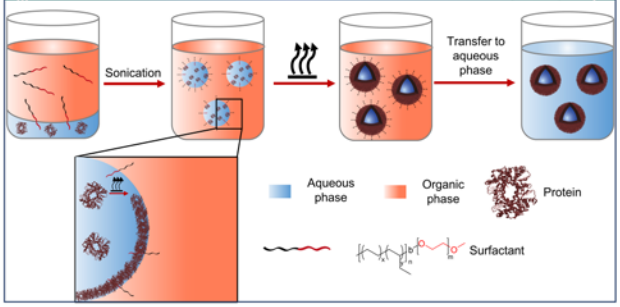

SCHEMATIC ILLUSTRATION: MECHANISM

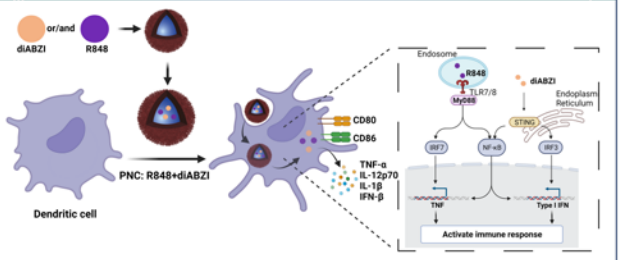

❖ Encapsulated single or combined adjuvants were released from PNC and upregulate the cytokines' secretion.

RESULTS

Characterization of PNC

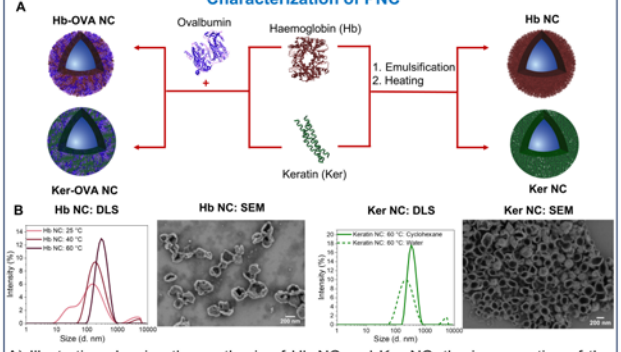

A) Illustration showing the synthesis of Hb NC and Ker NC, the incorporation of the antigen Ovalbumin to obtain Hb-OVA NC and Ker-OVA NC. B) Dynamic light scattering (DLS) and scanning electron microscopy (SEM) characterisation of the NC.

BMDC uptake and cytotoxicity of PNC

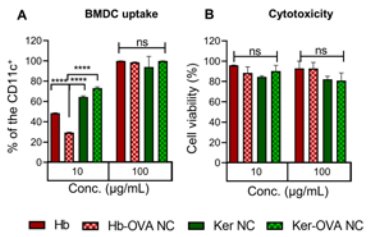

PNC A) uptake experiment and B) cytotoxicity experiment was performed on BMDCs with two different concentrations (10 and 100 μg/mL) for 24 hours (mean ± SD; n=3).

Cytokine secretion in BMDCs

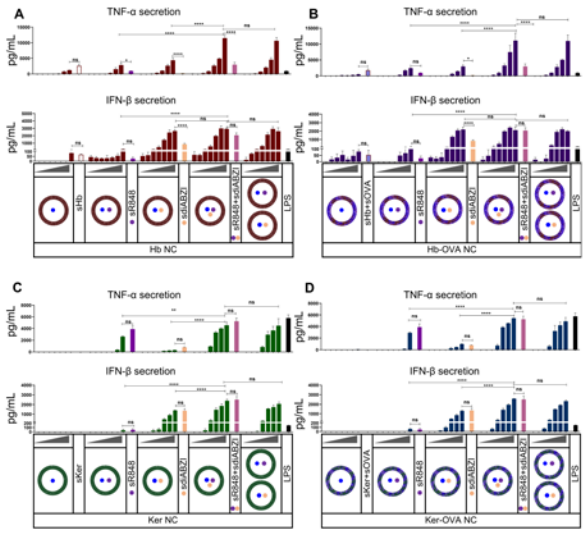

Evaluation of the efficacy of adjuvants loaded Hb NC and Hb-OVA NC in inducing cytokine secretion by bone marrow-derived dendritic cells (BMDCs). To achieve this, BMDCs were exposed to varying concentrations (0.1, 0.3, 1, 3, 10, 30, 100 μg/mL), soluble R848 (sR848, 600 ng/mL), soluble diABZI (sdiABZI, 1.1 μg/mL), or LPS (100 ng/mL) for 24 hours.A) Hb NC and B) Hb-OVA NC C) Ker NC and D) Ker-OVA NC.

SUMMARY AND CONCLUSIONS

- ❖ Protein nanocapsules (PNC) were synthesized from abundantly available proteins without any modifications or chemical reactions.
- ❖ PNC shell was formed by interfacial denaturation of proteins, which was also enhanced by thermal denaturation.
- ❖ PNCs exhibited excellent uptake in BMDCs while inducing only minute levels of cytotoxicity.
- ❖ Expression of TNF-α and IFN-β was significantly higher in all PNC loaded with both R484 and diABZI as compared to PNC loaded with single adjuvants.
- ❖ Dual adjuvant encapsulated PNC showed their capacity to enhance the immune response and opens up new possibilities in the field of nanomedicine.

Laurine Kaul

universität freiburg

Repurposing $Cu(DDC)_2$-liposomes as antibacterial agent for staphylococci infections

Laurine Kaul[1,2], Adrian Abdo[2], Andrew Zannettino[2], Katharina Richter[2], Regine Süss[1]

[1] University of Freiburg, Institute of Pharmaceutical Sciences, Department of Pharmaceutics, Sonnenstraße 5, 79104 Freiburg, Germany
[2] University of Adelaide, Faculty of Health and Medical Sciences, North Terrace, SA 5000 Adelaide, Australia

Background

- Staphylococci are pathogens associated with many clinical infections, e.g., surgical site infections.
- **Typically, an infection is treated with antibiotics, but standard medical care fails due to antibiotic resistance and biofilm formation.**
- Surgical site infections frequently lead to clinical complications and higher mortality [1]. More effective anti-bacterial strategies are needed.
- The antibacterial activity of copper-diethyldithiocarbamate $Cu(DDC)_2$ in combination with copper ions (Cu^{2+}) is limited by the poor water solubility of $Cu(DDC)_2$ [2].
- Investigation of the repurposed $Cu(DDC)_2$-liposomes [3] in combination with Cu^{2+}-liposomes or free Cu^{2+} against staphylococci biofilms.

Methods

- Determine the hydrodynamic diameter (d_h) and the polydispersity index (PDI) of Cu^{2+}-liposomes and $Cu(DDC)_2$-liposomes using ZetaPals.
- Determine *in vitro* antibiofilm activity against methicillin-resistant *S. aureus* (MRSA) and *S. epidermidis* using the alamarBlue cell viability assay (1-way ANOVA).
- Survival of uninfected and *S. epidermidis*-infected *Galleria mellonella* larvae over 4 days: determine toxicity and efficacy of the liposomes. Control = 0.9% NaCl. 30 larvae/group. Statistical analysis: log-rank test with Holm-Bonferroni adjustment of Kaplan-Meier survival curves.

Key findings

- **$Cu(DDC)_2$ are bigger than Cu^{2+}-liposomes**
- **$Cu(DDC)_2$-liposomes + Cu^{2+}-liposomes did not reduce biofilm viability *in vitro* but showed efficacy *in vivo*.**
- **$Cu(DDC)_2$-liposomes + free Cu^{2+} showed antibacterial activity *in vitro* and *in vivo*.**
- **All treatments were non-toxic *in vivo*.**

Liposome characteristics

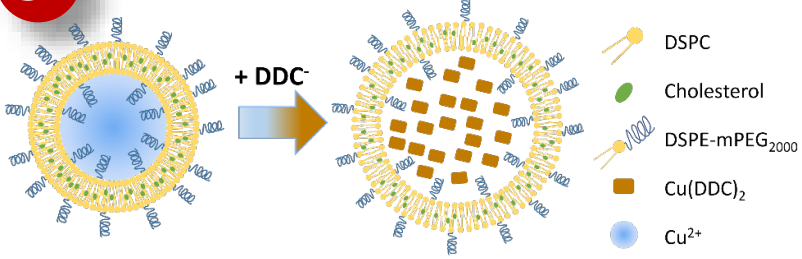

Cu^{2+}-liposomes
d_h = 104 ± 8 nm
PDI = 0.05 ± 0.01

$Cu(DDC)_2$-liposomes
d_h = 168 ± 12 nm
PDI = 0.14 ± 0.02

In vitro antibiofilm activity

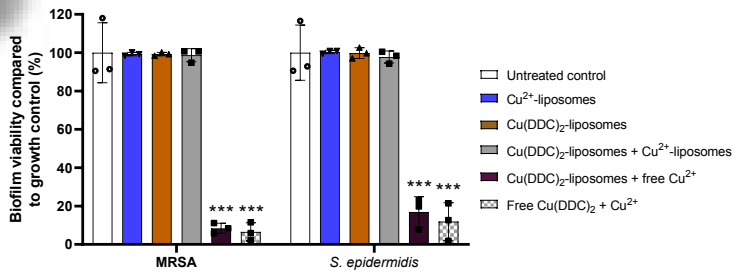

Only $Cu(DDC)_2$-liposomes + free Cu^{2+} and free $Cu(DDC)_2$ + Cu^{2+} significantly reduced biofilm viability by at least 90 % in MRSA biofilms and 80 % in *S. epidermidis* biofilms ($p < 0.001$)

Galleria mellonella larvae

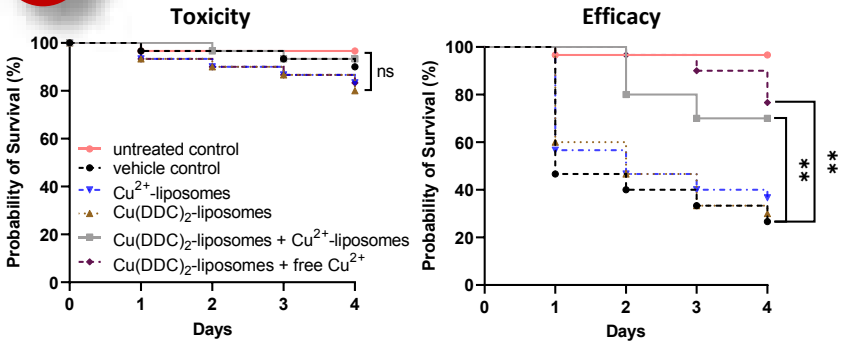

Living larvae

uninfected: all treatments ≥ 80% survival (ns = not significant)

***S. epidermidis*-infected**: 70% (21/30 larvae) and 77 % survival (23/30 larvae) when treated with $Cu(DDC)_2$-liposomes + Cu^{2+}-liposomes or $Cu(DDC)_2$-liposomes + free Cu^{2+}, respectively.

Dead larvae:

***S. epidermidis*-infected**: ≤ 40% survival rate when untreated or treated with $Cu(DDC)_2$-liposomes or Cu^{2+}-liposomes (8/30, 9/30, 11/30 larvae survived, respectively).

Acknowledgement & Disclosure

Thank you to Prof Hans-Georg Koch for the use of his laboratory facilities and Prof Tom Coenye for the larvae model.
Katharina Richter has a patent on the $Cu(DDC)_2$ + Cu^{2+} treatment against bacteria (PCT/AU2020/050661)

References: [1] Owens, C.D.; et al. *Surgical site infections: Epidemiology, microbiology and prevention*. J Hosp Infect 2008.
[2] Kaul, L.; et al. *In vitro and in vivo evaluation of diethyldithiocarbamate with copper ions and its liposomal formulation for the treatment of Staphylococcus aureus and Staphylococcus epidermidis biofilms*. Biofilm 2023.
[3] Hartwig, F.; et al. *Preclinical in vitro studies with 3D spheroids to evaluate $Cu(DDC)_2$ containing liposomes for the treatment of neuroblastoma*. Pharmaceutics 2021.

SCAN ME

Laurine Kaul, PhD
Postdoc
laurine.kaul@pharmazie.uni-freiburg.de

Designing nanomedicine libraries via custom-made 3D-printed microfluidics for applications in hematological malignancies

Shiva Khorshid[1,2,✉], Federica De Lorenzi[1,3], Julian Baumeister[3,4], Mattia Tiboni[2], Steffen Koschmieder[3,4], Twan Lammers[1], Luca Casettari[2], Alexandros Marios Sofias[1,3,5]
✉ s.khorshid@campus.uniurb.it

1. Department of Nanomedicine and Theranostics, Institute for Experimental Molecular Imaging (ExMI), Faculty of Medicine, RWTH Aachen University, Aachen, Germany
2. Department of Biomolecular Sciences, School of Pharmacy, University of Urbino Carlo Bo, Urbino, Italy
3. Mildred Scheel School of Oncology (MSSO), Center for Integrated Oncology Aachen Bonn Cologne Düsseldorf (CIO^{ABCD}), University Hospital Aachen, Aachen, Germany
4. Department of Hematology, Oncology, Hemostaseology and Stem Cell Transplantation, Faculty of Medicine, University Hospital Aachen, Aachen, Germany
5. Department of Circulation and Medical Imaging, Faculty of Medicine and Health Sciences, Norwegian university of science and technology (NTNU), Trondheim, Norway

Introduction. Conventional nanomedicine development relies on top-down approaches, i.e., manufacturing of one specific nanoparticle (NP) for one application. In this study, we designed an experimental framework for the bottom-up production of nanomedicine libraries, utilizing in-house 3D-printed microfluidics. Implementation of such concept can allow for **(i)** understanding the nanomaterial behavior at different conditions and compositions, and **(ii)** readily picking the most suitable nanoformulation for a given application.

Methods. The internal architecture and the tolerance of the microfluidic chips to different organic solvents, used for NP manufacturing, were evaluated via computed tomography (CT). Four different nanoparticles were included in the library: liposomes, lipid nanoparticles (LNP), polymersomes, and oil-in-water nanoemulsions. The composition and properties of each library were defined via a Design-of-Experiment (DoE) based on Box–Behnken Design (BBD), followed by their physicochemical characterization. The cytocompatibility was assessed by apoptosis assay, and cell uptake of the formulations was studied in hematological malignancies representative cell lines (K562, THP.1, MM.1S, and 32D) through FACS analysis (**Fig. 1**).

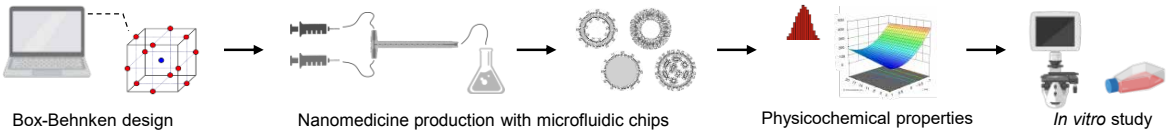

Figure 1. Study design: (i) design of experiment, (ii) nanoparticle preparation, (iii) characterization, (iv) modeling, (v) *in vitro study*

A. Microfluidic chips are compatible with organic solvents

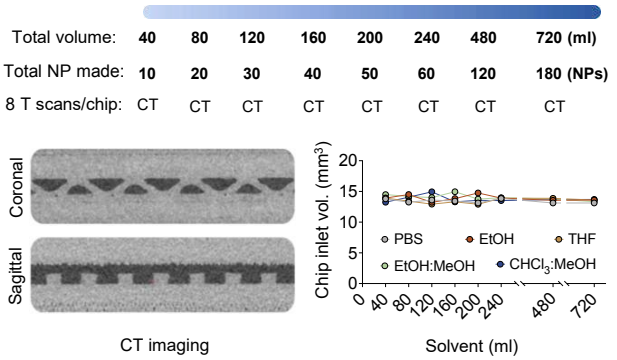

Figure 2. CT imaging verified the compatibility of the polypropylene-made chips with PBS, ethanol, methanol, chloroform, and tetrahydrofuran.

B. Size and dispersity of nanomedicine library

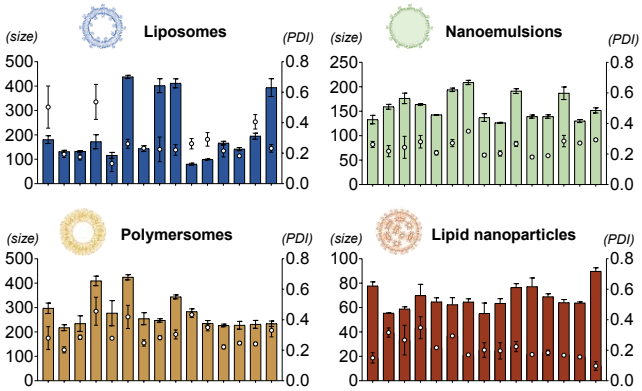

Figure 3. Size and dispersity variations were dependent on the selected manufacturing parameters in 15 individually made NP (n=3).

C. 3D plots shows the effect of input parameters on NP properties

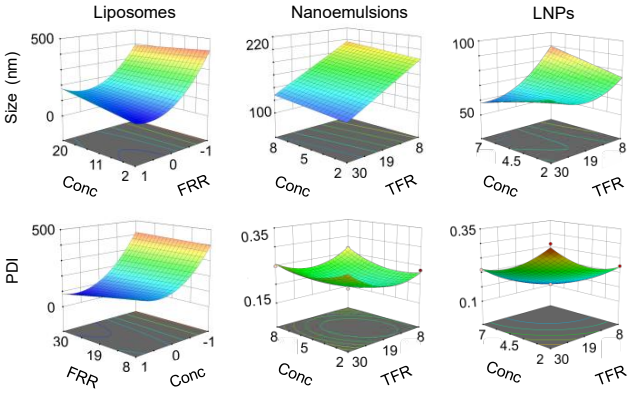

Figure 4. Subsequent modeling revealed the contribution and significance of each parameter [concentration (mM), total flow rate (TFR; ml/min), flow rate ratio (FRR)] in the characteristics of the final product.

D. *In vitro* study reveals NP uptake variability

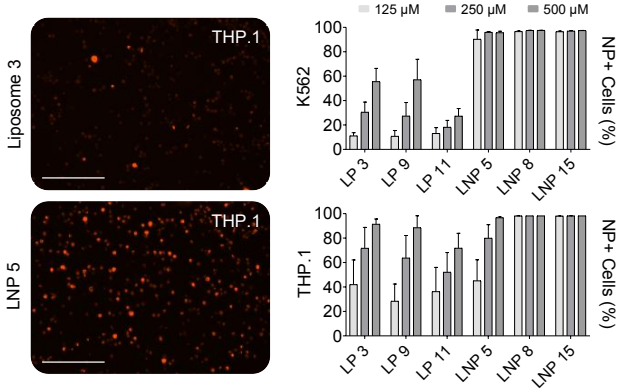

Figure 5. The cell uptake of the nanoformulations was influenced by the size of the formulations. Nanoparticles within the optimal size range demonstrated significantly higher uptake compared to the larger nanoparticles

Conclusions

- ✓ By utilizing a bottom-up manufacturing strategy, we achieved the rapid and versatile production of nanoparticle libraries in a reproducible and controllable manner.
- ✓ By utilizing mathematical modeling, we were able to predict nanoformulations properties
- ✓ By in vitro study, it becomes apparent that there exists a notable variability in the NP uptake.

Acknowledgements: German Research Foundation (AMS – DFG RWTH JPI Excellence Initiative grant 2021; AMS – DFG CRU344 grant for project P4; TL, AMS – SFB1066 grant for project B17), the German Cancer Aid (AMS, FD – SDK Postgraduate Program MSSO^{ABCD}), and the Euro-BioImaging (AMS – Mobility Grant for project PID1681). **COI:** None.

Bumjun Kim

Development and optimization of next-generation lipid nanoparticles for in-situ CAR-T production

Bumjun Kim[1] and Robert K. Prud'homme[1]
[1]Dept. of Chemical & Biological Engineering, Princeton University, Princeton, NJ, 08544
bumjunk@princeton.edu

Background & Challenges

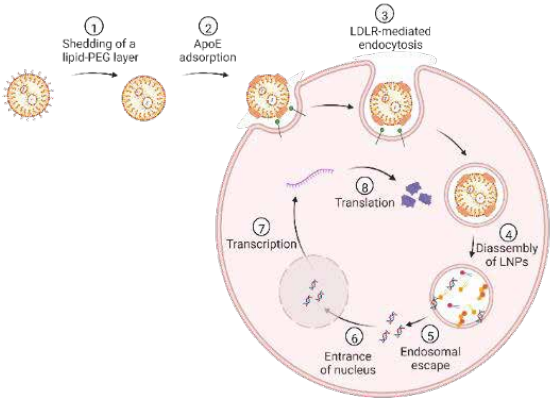

Scheme 1. Mechanism of LNP targeted to the liver. Created with BioRender.com

- Lipid nanoparticles (LNPs) targeted to the liver is primarily driven by shedding of lipid-PEG in the blood followed by adsorption of apolipoprotein E (ApoE) and uptake by hepatocytes.[1]
- Conjugation of antibodies (Abs) to the lipid-PEG will increase overall hydrophilicity, accelerating the 'shedding off' event.
- To improve the in-situ T cell engineering strategy, a next-generation LNP needs to be developed.

Approach

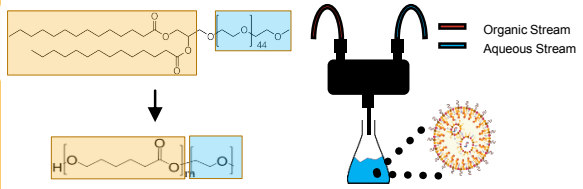

Scheme 2. Substitution of DMG-PEG to PCL-b-PEG and the production of LNP via Flash NanoPrecipitation (FNP).

- Lipid-PEG is replaced with three different Mw of poly(ε-caprolactone)-block-poly(ethylene glycol) (PLC-b-PEG); 1 kDa, 2.6 kDa, and 4.8 kDa of PCL block sizes are evaluated.
- Flash NanoPrecipitation (FNP), a scalable nanoprecipitation precipitation process, is used to formulate LNPs.

Results and Discussion

1) DOE approach for screening LNP formulations

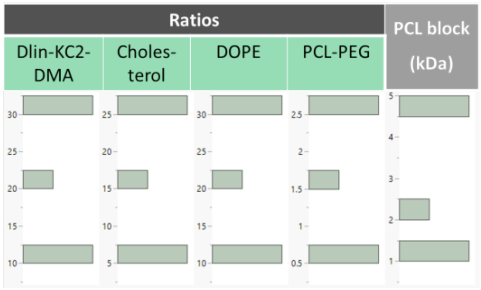

Design space: 3^5 = 243 formulations.
DOE approach: 26 formulations

Results and Discussion

2) Screening the transfection efficiency using an immortalized T cell line.

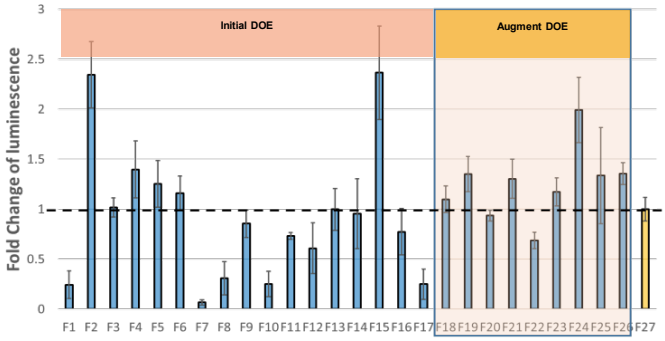

*F27 is the standard pDNA LNP formulation.
(50% Dlin-KC2-DMA/38.5% Cholesterol/10% DOPE/1.5% DMG-PEG)

3) Identification of design space

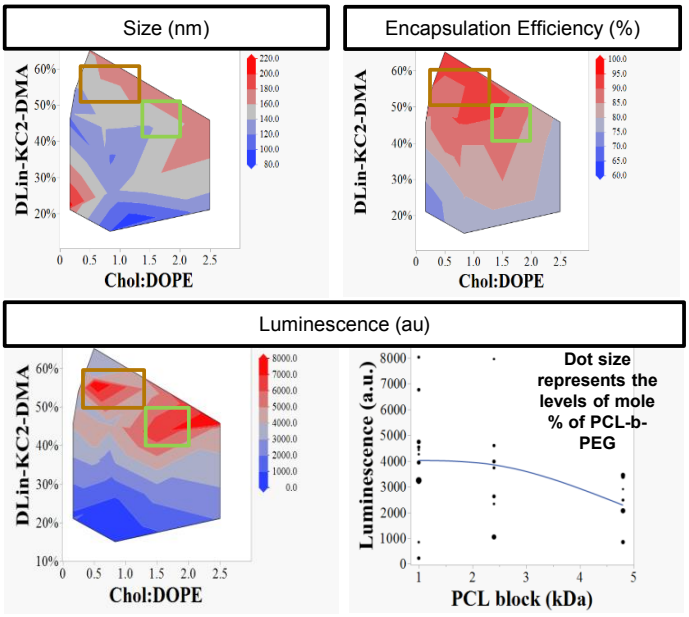

4) Optimization of freezing conditions

GROUP	CRYOPROTECTANT	mM
0	No	
1	Sucrose	250
2	Sucrose	500
3	Mannitol	250
4	Mannitol	500
5	Trehalose	250
6	Trehalose	500
7	Sucrose/Mannitol	250
8	Sucrose/Trehalose	250
9	Mannitol/Trehalose	250

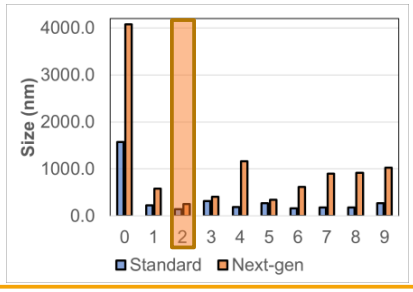

Acknowledgement

I would like to thank Dr. Robert Prud'homme for the guidance and Genentech and Bill & Melinda Gates Foundation for the financial support.

References

1. Chen et al., Influence of particle size on the in vivo potency of lipid nanoparticle formulations of siRNA. J Control Release 2016, 235, 236-244.

Jonas Koehler

Preparation of Small Multilamellar Vesicles Using Dual Centrifugation

Jonas Koehler[1], Meryl Moroni[1], Stefanie Schmager[1], Lars Gedda[2], Katarina Edwards[2], Heiko Heerklotz[1,3] & Ulrich Massing[1,4]

[1]Institute of Pharmaceutical Sciences, University of Freiburg, Germany
[2]Department of Chemistry - Ångström, Uppsala University, Sweden
[3]Leslie Dan Faculty of Pharmacy, University of Toronto, Canada
[4]Andreas Hettich GmbH & Co. KG, Tuttlingen, Germany

Abstract

We present a method for a highly reproducible preparation of a novel type of liposomes, small multilamellar vesicles (SMVs), which are in a size range of about 150 nm and are filled with membranes. The preparation of SMVs was achieved by in-vial homogenization of highly concentrated lipid/buffer mixtures by Dual Centrifugation (DC). This innovative liposome preparation technique is based on an additional rotation of the sample vial around its own axis during conventional centrifugation, which results in strong sample movements and thus efficient homogenization.
Liposome sizes, size distributions (PDI) as well as liposome morphology strongly depends on the viscosity of the lipid/buffer mixture and thus on the lipid concentration (m/V) during DC-homogenization. At optimal lipid concentration, which depends on the lipid composition used for DC-homogenisation (about 50 – 70%), predominantly small multilamellar vesicles (SMVs) are formed. SMVs are easily accessible by DC and appear to be a promising carrier for the delivery of lipophilic drugs.

Dual Centrifugation

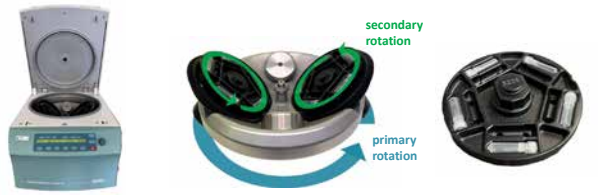

Dual Centrifuge (DC) ZentriMix 380 R | DC rotor | Centrifuge insert for 2 mL sample vials (horizontal vial positioning)

Why is DC so efficient?

1) Secondary rotation leads to strong sample movements

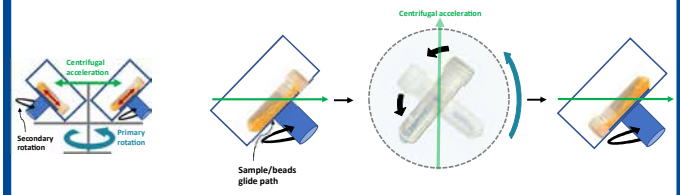

2) High performance friction and high impact events

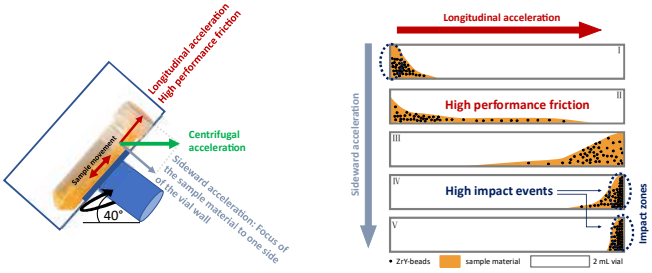

3) Large number of gentle homogenization events (about 50.000 times for a typical 30 min DC-homogenization at 2500 rpm)

Liposomes prepared by DC show much less lipid degradation substances in comparison to high-pressure homogenization. SMVs are even more stable during preparation than unilamellar vesicles

Morphology of DC-prepared liposomes

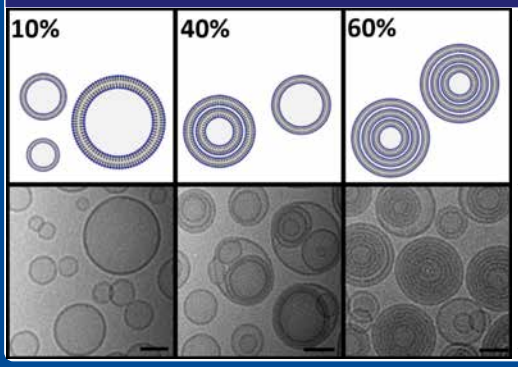

- Liposome morphology strongly depends on the lipid concentration during DC homogenization
- Predominantly SMVs are formed at 60% lipid concentration for HEPC/Chol 55/45 mol% liposomes
- Scale bar: 50 nm

HEPC/Chol (55/45 mol%) liposomes by DC

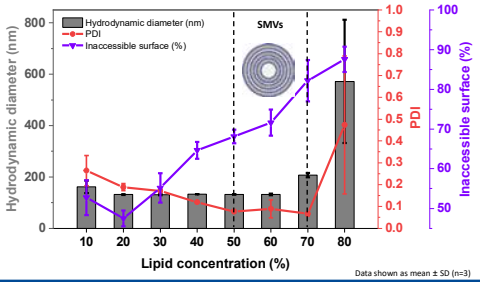

- Head-group fluorescence labeled lipid NBD-DSPE incorporated in the lipid-mixture
- Inaccessible surface determined by quenching of the accessible surface located NBD-DSPE by sodium dithionite

Take-home message

- Dual Centrifugation is a highly efficient method for liposome preparation in closed vials
- The lipid concentration during DC-homogenization strongly influences the resulting liposome morphology
- Small multilamellar vesicles (SMVs) are easily accessible through DC and appear as promising carriers for lipophilic drugs in the clinic

References

1. Massing, U.; Cicko, S.; Ziroli, V. Dual Asymmetric Centrifugation (DAC)--a New Technique for Liposome Preparation. *Journal of controlled release : official journal of the Controlled Release Society* **2008**, *125*, 16–24, doi:10.1016/j.jconrel.2007.09.010.
2. Koehler, J.K.; Schnur, J.; Heerklotz, H.; Massing, U. Screening for Optimal Liposome Preparation Conditions by Using Dual Centrifugation and Time-Resolved Fluorescence Measurements. *Pharmaceutics* **2021**, *13*, 2046, doi:10.3390/pharmaceutics13122046.
3. Koehler, J.K.; Gedda, L.; Wurster, L.; Schnur, J.; Edwards, K.; Heerklotz, H.; Massing, U. Tailoring the Lamellarity of Liposomes Prepared by Dual Centrifugation. *Pharmaceutics* **2023**, *15*, 706, doi:10.3390/pharmaceutics15020706.

European Foundation for Clinical Nanomedicine| CLINAM Summit 2023, Basel, Switzerland

Development of pH-responsive lipid-based nanotransporters aimed at effective siRNA delivery

Zdeněk Kratochvíl[1], Ganesh Selvaraj Duraisamy[1], Hana Michálková[1], Zbyněk Heger[1], Andrew David Miller[1 2]

[1]Department of Chemistry and Biochemistry, Mendel University in Brno, Zemědělská 1665/1, CZ-613 00 Brno, Czech Republic
[2]Veterinary Research Institute, Hudcova 296/70, CZ-621 00 Brno, Czech Republic

contact: zdenekkratochvil14@gmail.com

STRUCTURE AND PROPERTIES

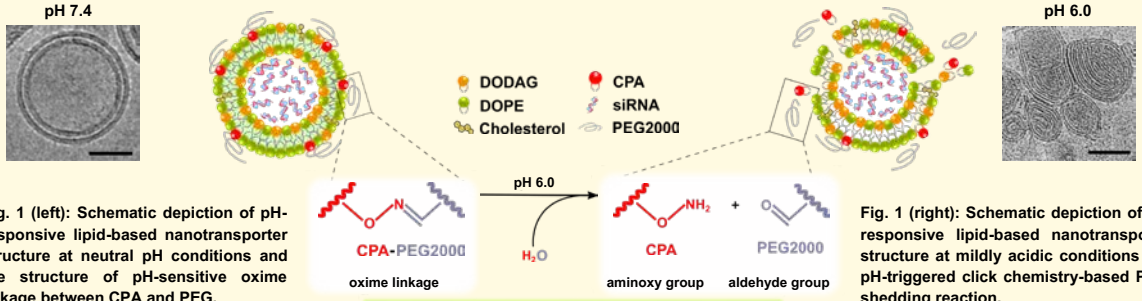

Fig. 1 (left): Schematic depiction of pH-responsive lipid-based nanotransporter structure at neutral pH conditions and the structure of pH-sensitive oxime linkage between CPA and PEG.
The cryo-TEM image displays stable bilamellar nanotransporter structure at physiological pH. Scalebar of cryo-TEM image: 50 nm

Fig. 1 (right): Schematic depiction of pH-responsive lipid-based nanotransporter structure at mildly acidic conditions and pH-triggered click chemistry-based PEG-shedding reaction.
The cryo-TEM image displays multilamellar fused nanotransporter structures at decreased local pH. Scale bar of cryo-TEM image: 50 nm.

Which intracellular fate will pH-responsive lipid-based nanotransporters get to choose?

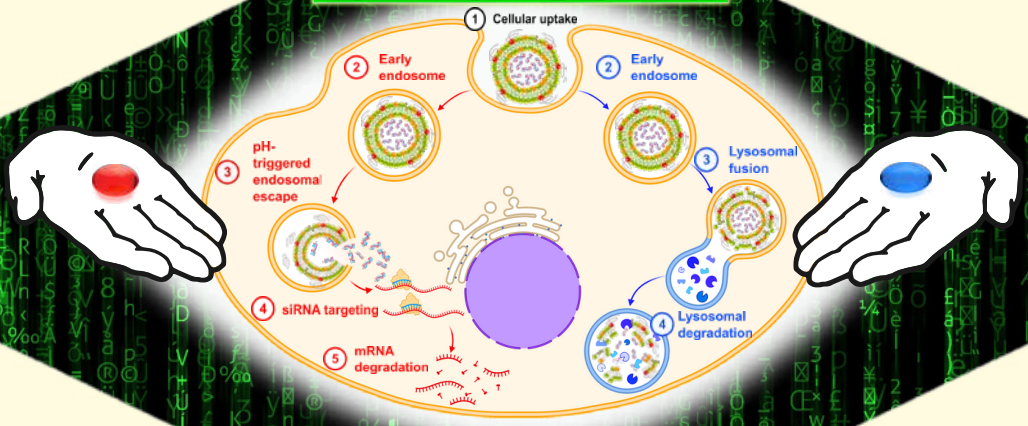

CELLULAR UPTAKE

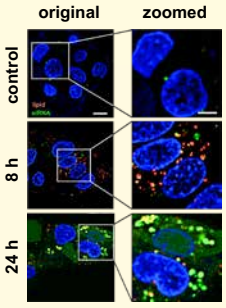

Fig. 2: Double-labelled siRNA-carrying lipid nanotransporters (Cy5-lipid – red, AF488-siRNA – green, colocalization – yellow, Hoechst-nuclei – blue) taken up by HepG2 cells are releasing siRNA cargo 24 h post transfection, based on increased AF488 diffusion fluorescence signal. Scale bar of the original images: 10 µm. Scale bar of zoomed cut-outs: 5 µm.

FUNCTIONALITY

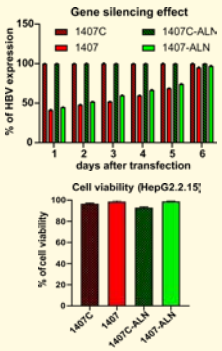

Fig. 3: HepG2.2.15 cells exhibit significant drop of the target HBV viral gene expression down to 40%/45% one day upon transfection with 1407/1407ALN siRNA-carrying lipid nanotransporters. The gene downregulating effect persists for the next four days.
HepG2.2.15 cells maintain high cell viability levels without cytotoxicity impacts after nanotransporter-mediated transfection.

CONCLUSIONS

- pH-dependent structural changes
- effective siRNA release into cytosol
- transporter-mediated gene silecing
- no cytotoxicity

PERSPECTIVES

- overcoming barriers in nanomedicine
- smart platform for *in vivo* use
- possible therapeutic versatility
- potential hybrid particles

CLINAM
European Foundation for Clinical Nanomedicine

Functionalised liposomes for automated fluorine-18 surface radiolabelling and *in vivo* PET imaging

Marcelo Kravicz[1‡]; Marco Nicola Iannone[2]; Stefano Stucchi[1,2]; Elisa Vino[2]; Elia Anna Turolla[1,2]; Antonia Antoniou[3]; Arianna Amenta[3]; Paolo Rainone[1,4]; Silvia Valtorta[4–6]; Sara Pellegrino[7]; Daniele Passarella[7]; Rosa Moresco[1,2,4,5]; Pierfausto Seneci[3]; Sergio Todde[1,2]; Francesca Re[1]

[1] School of Medicine and Surgery, University of Milano-Bicocca, via Raoul Follereau 3, 20854 Vedano al Lambro (MB), Italy.
[2] Tecnomed Foundation, University of Milano-Bicocca, Milan, Italy.
[3] Chemistry Department, University of Milan, Via Golgi 19, 20133 Milan, Italy.
[4] Nuclear Medicine Department, San Raffaele Scientific Institute IRCCS, Via Olgettina 48, 20132 Milan, Italy.
[5] Institute of Molecular Bioimaging and Physiology (IBFM), National Research Council (CNR), Via F.lli Cervi 93, 20054 Segrate, Italy.
[6] National Biodiversity Future Center (NBFC), Piazza Marina 61, Palermo, Italy.
[7] Pharmaceutical Sciences Department, University of Milan, Via Golgi 19, 201 Milan, Italy.

‡E-mail: **marcelo.kravicz@unimib.it**

Poster 48

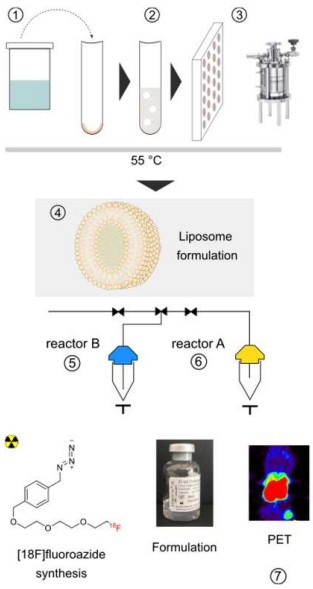

Figure 1. Scheme of the approach. From liposome formulation preparation to the final *in vivo* biodistribution evaluation and PET imaging.

Background

- Positron emission tomography (PET) enables the noninvasive tracking of labelled nanoparticles, allowing real-time analysis of their *in vivo* distribution and pharmacokinetics.
- Traditionally, metallic radionuclides have been introduced in the liposome's core or via surface radiolabelling using chelators to ensure in vivo stability. However, these methods are not automated and achieving sufficient radioactivity levels remains challenging.
- Fluorine-18 can be introduced onto lipid derivatives through a copper-catalyzed click chemistry approach via copper-catalyzed alkyne-azide cycloaddition (CuAAc) or copper-free approaches with fluorine-18 labelled azide.
- Radiolabeled liposomes functionalized or not with mApoE and MMP cleavable peptides were evaluated in a mouse model of GBM based on the intraparenchimal inoculation of an established cell line Gli36ΔEGFR-2 cells known to be resistant to TMZ.

Rational and Aim

- Liposomes were functionalised with a peptide derived from the receptor-binding domain of the apolipoprotein E (mApoE), useful to promote the blood-brain barrier (BBB) crossing, and with an MMP-sensitive lipopeptide (MSLP) for an MMP-triggered drug release [1].
- An automated liposome surface radiolabelling was performed both via CuAAC and copper-free cycloaddition, using a fluorine-18 labelled azide, on alkyne-DOPE constructs embedded in liposomes.

Results

- Radiosynthesis was entirely automated on a radiosynthesis system, from cyclotron-produced fluorine-18 to the final [^{18}F]-Lip product.
- High radiochemical purity and suitable yields (from 5 to 10% according to the cycloaddition approach) were obtained with [^{18}F]-Lip endowed with a hydrodynamic size smaller than 200 nm, low-medium dispersity, and negative ζ-potential.
- The intracranial and systemic biodistribution of radiolabeled liposomes functionalized or not with mApoE and MMP cleavable peptides has been evaluated with PET/CT up to four hours post injection (n=4) (**Figure 4A-D**).

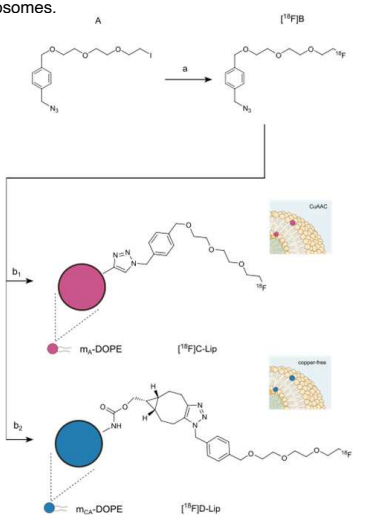

Figure 2. Scheme of CuAAC and copper-free reaction for [^{18}F]C-Lip radiolabelling. Reaction and conditions for CuAAc: (**a**) [18F]KF, kryptofix 2.2.2, ACN, 20 min, 100°C, (35%); (**b$_1$**) mA-Lip, CuSO4·5H2O, ascorbic acid, water, 20 min, rt, (76%). Reaction conditions for copper-free (**b$_2$**) [18F]KF, kryptofix 2.2.2, ACN, 20 min, 100°C, (35%). b) mCA-Lip, water, 30 min, 40 or 50°C, (40%).

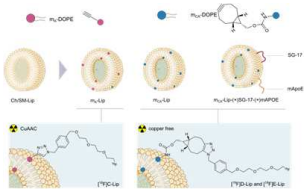

Table 1. Physicochemical properties of liposome formulations in the steps before and after radiosynthesis for the m_A-Lip and dual-functionalised m_{CA}-Lip liposome formulation after radiosynthesis.

	before radiolabelling			after radiolabelling		
COD	D_h [a]	PDI	ζ-pot [b]	D_h [a]	PDI	ζ-pot [b]
[^{19}F]C-Lip	120.6 ± 1	0.114 ± 0.003	-42 ± 2	125 ±2	0.133 ± 0.02	-30
[^{19}F]D-Lip	119 ± 1	0.122 ± 0.02	-36 ± 1	128 ±0.16	0.125 ± 0.017	-33 ± 1
[^{18}F]E-Lip	145.2 ± 2	0.203 ± 0.01	-27 ± 2	164 ±2	0.191 ± 0.02	-32 ± 2

[a] nm, determined by DLS; [b] mV.

Figure 3. Scheme of CuAAC and copper-free reaction and the final radiolabelling of dual-functionalized liposomes.

- On the same animals we performed also PET with [^{18}F]FLT to identify the area within the tumor with the highest cell proliferation.
- Tumor uptake of [^{18}F]D-Lip was similar to functionalized [^{18}F]E-Lip, interestingly the functionalization appears to prevent uptake into the contralateral healthy tissue (**Figure 4E-F**).

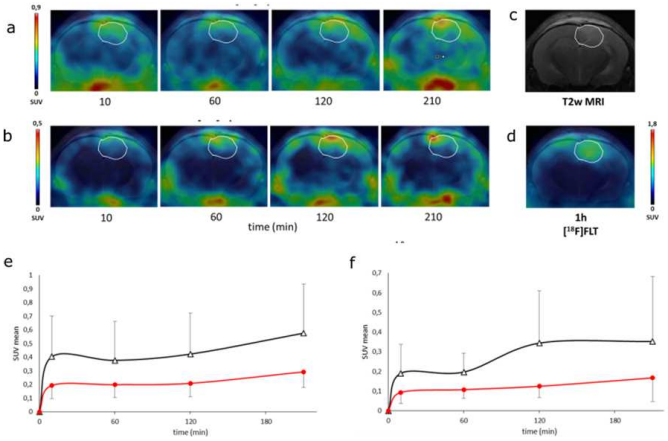

Figure 4. PET imaging. PET images of [^{18}F]D-Lip (**a**) and [^{18}F]E-Lip (**b**). Representative T2w MRI image (**c**). PET images of [^{18}F]FLT (**d**). The white line indicates the tumor area, depicted on MRI and transferred to PET images. [^{18}F]FLT PET imaging was used as a radiotracer clinical standard on orthotopic glioma model obtained with Gli36ΔEGFR cells. Tumour uptake quantification of [^{18}F]D- Lip (**e**) and [^{18}F]E-Lip (**f**). Data are expressed as SUV mean.

Table 2. Biodistribution. Radioactivity concentration expressed as standard uptake values (SUV) mean.

Tissue, SUV	[^{18}F]D-Lip				[^{18}F]E-Lip			
	10'	60'	120'	180'	10'	60'	120'	180'
Lung	0.77±0.08	0.4±0.09	0.35±0.11	0.51±0.04	0.35±0.06	0.31±0.04	0.29±0.05	0.26±0.04
Kidney	0.94±0.26	0.5±0.11	0.43±0.17	0.62±0.21	0.34±0.12	0.33±0.16	0.42±0.22	0.18±0.09
Heart	1±0.16	0.54±0.06	0.44±0.07	0.76±0.13	0.39±0.06	0.33±0.02	0.27±0.004	0.2±0.5
Liver	6.67±0.5**	3.76±0.3**	3.03±0.6*	4.87±0.75**	3.08±0.7	2.64±0.44	2.17±0.66	2.16±0.5
Muscle	0.26±0.08	0.26±0.07	0.22±0.08	0.33±0.04	0.1±0.02	0.11±0.01	0.09±0.02	0.1±0.02
Bone	0.94±0.28	1.23±0.2**	0.88±0.15	1.62±0.66	0.7±0.09	1.01±0.2	0.99±0.05	1.02±0.21
Spleen	3.69±1.7**	1.93±0.96	1.44±0.48	2.18±0.75	1.62±0.28	1.62±0.26	1.59±0.35	1.46±0.3
Intestine	5.31±0.4**	5.31±0.2**	4.62±0.8*	4.06±1.58**	2.08±0.17	2.81±0.1	3.65±0.57	1.46±0.23

*p<0.05, **p<0.001; 2-way ANOVA Bonferroni's multiple comparison test ([^{18}F]E-Lip).

- The uptake of non derivatized nanoparticle was higher and the wash-out rate lower than that of [^{18}F]E-Lip particularly in liver, intestine and spleen.
- Data indicate a general fast clearance rate of nanoparticles from peripheral organs and a lower uptake in presence of the peptides on liposome's surface.

Final remarks

- The high throughput radiolabelling of liposomes is most likely of interest to researchers working in the nanomedicine field due to the fluorine-18-labelled liposomes performance in visualising unhealthy tissues/areas such as glioblastoma, thus obtaining, for instance, short-term pharmacokinetics *in vivo*.
- Furthermore, access to an imaging tool with high performance is vital to support preclinical and future clinical phases for the development of nanoparticle-based products.

Reference. [1] Giofrè S., Renda A., Sesana S., Formicola B., Vergani B., Leone B.E., Denti V., Paglia G., Groppuso S., Romeo V., et al. *Dual Functionalized Liposomes for Selective Delivery of Poorly Soluble Drugs to Inflamed Brain Regions. Pharmaceutics.* 2022;14:2402. doi: 10.3390/pharmaceutics14112402.

Funding FRRB grant NEVERMIND (CP2_16/2018).

Joshua Krehan

UNIVERSITÄTSmedizin. MAINZ

Repolarizing Tumor-Associated Macrophages with pH-Modulating Liposomes for Enhanced Cancer Therapy

Joshua Krehan[1], Barbara Graefen[2], Andrea Tuettenberg[2], Andreas Walther[1]

Concept & Background

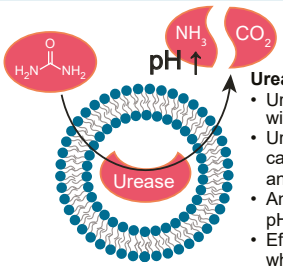

Urease-liposomes
- Urease encpasulated within liposomes.
- Urea, present in cells, is catalyzed into ammonia and CO_2.
- Ammonia increses the pH of the solution.
- Effective pH-modulator, while urease is protected from degradation.

TAM Repolarization
- Immunosuppressive tumor-associated M2 macrophages (TAM) play a critical role in the tumor microenvironment.
- Reprogramming M2 Macrophages: Shift from immunosup-pressive M2 state to pro-inflammatory M1 state.
- A pH Increase as Reprogramming Trigger: Elevating pH levels triggers M2 to M1 transition in macrophages.
- Activated macrophages stimulate innate immune response against tumor cells.

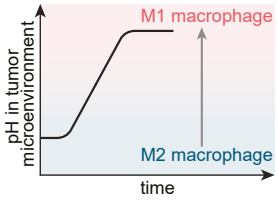

pH-Modulation Mechanism

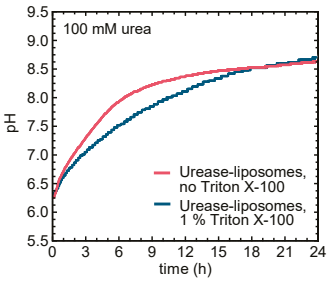

Liposomes are permeable to urea
- Comparison between urease-liposomes and urease released from liposomes using Triton X-100 reveals that the liposome's membrane is permeable to urea.
- This permeability obviates the requirement for an additional release mechanism.
- Simultaneously, the encapsulated urease remains safeguarded from degradation.

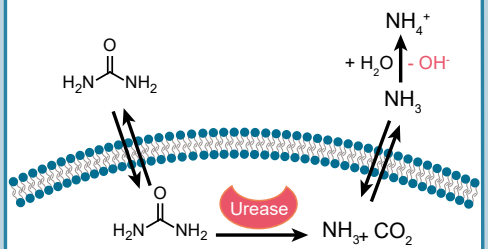

Liposome Formulation

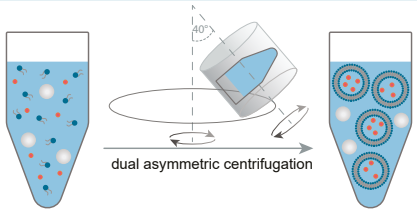

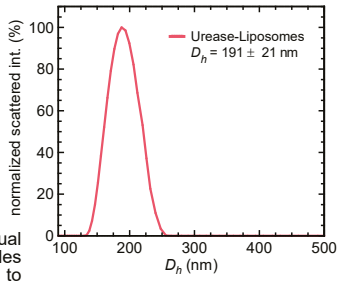

Liposome formation using dual asymmetric centrifugation provides high encapsulation effciency of up to 50%, a small volume of cargo solution, fast and high sample preparation.

Macrophage Repolarization Experiments

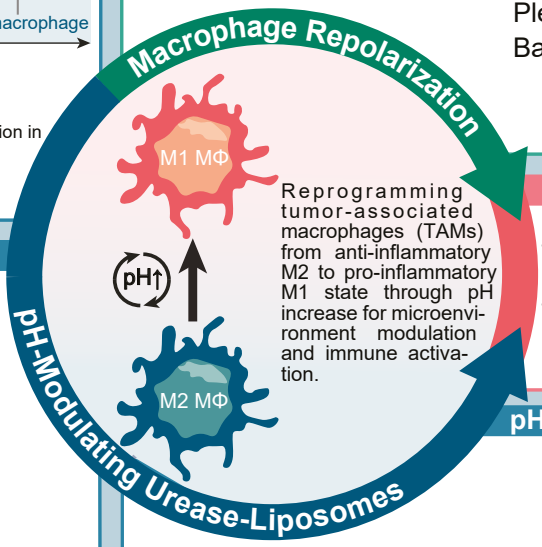

Reprogramming tumor-associated macrophages (TAMs) from anti-inflammatory M2 to pro-inflammatory M1 state through pH increase for microenvi-ronment modulation and immune activa-tion.

Please check out Barbara Graefen's Poster

Outlook

- Repolarizing M2 macrophages by pH-modu-lation using urease-liposomes.
- Surface funtionalization of urease-liposomes with GARP antibodies.

pH-Modulation of Buffers

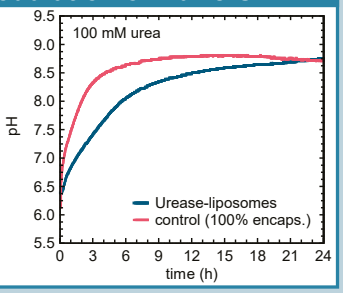

- pH elevation from 6.1 to 8.7 achieved within 24 hours at room temperature.
- pH 6.1, representative of solid tumor pH, serves as a suitable starting point for the experiment.
- Rapid pH increase highlights the efficiency of urease-liposomes in pH modulation.

pH-Modulation of Cell Media

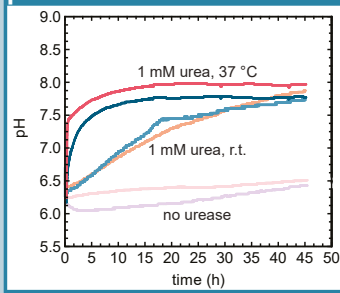

- TM10, 1 mM urea, 37 °C
- TM10, 1 mM urea, r. t.
- TM10, 1 mM urea, no urease
- X-Vivo, 1 mM urea, 37 °C
- X-Vivo, 1 mM urea, r. t.
- X-Vivo, 1 mM urea, no urease

- The rate of pH increase at 37 °C is approximately 4 times faster than at room temperature.
- Control: The pH remains constant in the absence of urease-liposomes.

Urease-liposomes effectively modulate the pH of cell culture media to a favourable physiological pH.

Funding

SFB 1066

These projects have received funding by the DFG through the collaborative research center 1066, project B14N.

References

[1] H. Wang, L. Burns, *PLoS ONE* **2008**.
[2] J. Dräger, H. Hahn, *Oncotarget* **2017**, 8, 3259-3273.
[3] N. Zimmer, A. Tüttenberg, *Int. J. Mol. Sci.* **2019**, 20, 3676.
[4] C. Cui, L. Becker, *Nature Nanotechnology* **2021**, 16, 1394-1402.
[5] B. Tian, H. Cao, *Bioconjugate Chem.* **2015**, 26, 1144−1155.

Contact

[1]Department of Chemistry, Johannes Gutenberg University Mainz
[2]Department of Dermatology, University Medical Center, Johannes Gutenberg University, Mainz
E-Mail: Joshua.Krehan@uni-mainz.de

www.walther-group.com

Nebulization of siRNA: Estimating the Impact of the Transition from Polyplex to Micelleplex

Adrian P. E. Kromer[1,*], Joschka Müller[1,*], Katharina Steinegger and Olivia M. Merkel[1,2]

[1] Department of Pharmacy, Ludwig-Maximilians-University Munich, Butenandtstrasse 5-13, Haus B, 81377 Munich, Germany
[2] Center for NanoScience (CeNS), Ludwig-Maximilians-University Munich, 80799 Munich, Germany
* Both authors contributed equallly to this work

contact: adkroph@cup.uni-muenchen.de
joschka.mueller@cup.uni-muenchen.de

Introduction

Respiratory diseases are a leading cause of death worldwide. Especially viral infection is a considerable health risk as shown by the emergence of SARS-CoV-19 but also asthma, COPD or lung cancer pose big challenges.
RNA interference has the potential to tackle all of these diseases. However, to be most efficient RNA molecules need to be directly delivered to the lungs. Nebulization is a widely accepted method for the gentle delivery of solutions to the lungs. Unfortunately, the integrity of most RNA delivery systems Is heavily impacted by nebulization.
In this work, we utilize poly(beta-amino ester)s (PBAE) as a tunable and easily synthesizable delivery agent [1] and PEI as a well-characterized comparison. We investigate the impact of the transition from polyplexes (PEI) to micelleplexes (PBAE) during nebulization.

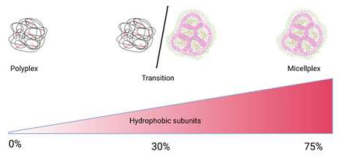

We characterize and investigate the structure of our nanoparticles with numerous methods, including transition electron microscopy (TEM), molecular dynamics simulations (MD), nano tracking analysis (NTA) and dynamic light scattering (DLS). We utilize two of the most commonly used nebulizers and show their impact on the integrity of our nanoparticle systems.

We further evaluate the in-vitro performance of the most stable formulations and the impact of nebulization.

Methods

Particle preparation and characterization

Particles were prepared by batch mixing. Briefly, siRNA solution in 10 mM Hepes at pH 5,4 was added to PBAE/PEI dissolved in the same buffer by pipetting up and down 30 times at constant speed. PBAE/PEI solutions were prepared in a concentration based on a ratio of protonated amines to phosphate groups of the siRNA backbone (N/P ratio) of 10. After mixing, solutions were incubated at room temperature for 90 minutes for micelleplexes and 30 minutes for polyplexes.

Nebulization stability

The impact of nebulization was determined by recollecting aerosol produced with an eFlow® Rapid (Pari, Starnberg, Germany) or an Aerogen Pro (Aerogen, Ratingen, Germany) vibrating mesh nebulizer with freshly prepared particle solution. Hydrodynamic diameter, polydispersity index (PDI) and Zeta potential were determined using a Zetasizer Ultra (Malvern Instruments Inc., Malvern, UK). Hydrodynamic diameter, particle dispersity and concentration were determined with a Nanosight 3000 NTA (Malvern Instruments Inc., Malvern, UK).

RNA encapsulation and loss assay

RNA encapsulation efficiency was determined using SYBR Gold dye with free siRNA as a reference and a plate reader (Tecan, Männedorf, Switzerland). To evaluate potential losses of RNA through nebulization, nebulized and non-nebulized nanoparticles were treated with Heparin and Triton-X to disrupt the nanoparticle structure. Afterwards, they were incubated with SYBR Gold to quantify the released siRNA.

Molecular dynamics

Molecular Dynamics simulations were run in Gromacs 2021.4 applying the Martini 3 force field. Polymers were newly parametrized based on an All-Atom model

Gene Knockdown

Knockdown experiments were conducted with H1299 stably expressing the enhanced green fluorescence protein. As nebulized formulations, only the most stable were tested meaning the Aerogen nebulizer for the 30% OA transition state micelleplex and the Pari eFlow rapid with the 75% OA micelleplex.

Micelleplex transition and structure

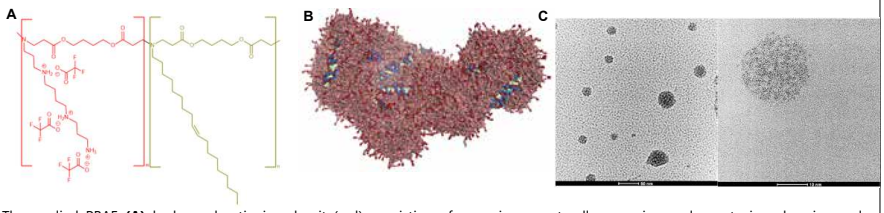

The applied PBAE **(A)** had a polycationic subunit (red) consisting of spermine, a naturally occurring and non-toxic polyamine and a hydrophobic oleylamine (OA) subunit (brown) which's proportions could be freely varied. By using a high ratio of hydrophobic subunits (75% OA) it was expected that the resulting nanoparticles would show a classical micellular structure with a hydrophobic core and an outer hydrophilic shell encapsulating the siRNA. Interestingly, molecular dynamics simulations (B) predicted the siRNA encapsulated into small micelles surrounded by our polymer that aggregated into larger structures with a homogenous siRNA distribution throughout the entire micelleplexe. A thin layer of free cationic spermine was oriented to the outside. Transmission electron microscopy (C) confirmed spherical monodisperse nanoparticles could be formed with the 75% OA polymer.

Nebulizer Characteristics

Nebulizer	Energy Input [J/g] [2]	Nebulization time [mL/min]	Residual Volume
Pari eFlow	35 +/− 12	0,54	1mL
Aerogen Pro	18 +/− 6	0,29	-

To compare the effects of the nebulizers, we initially assessed their key performance metrics. The Pari eFlow exhibited higher energy input, leading to faster nebulization but with a drawback of increased product loss. Additionally, the residual volume was shown to have a cooling effect. In contrast, the Aerogen Pro had lower energy input, resulting in longer nebulization times, but it effectively nebulized the entire sample due to its design, with no residual volume

Nebulization stability

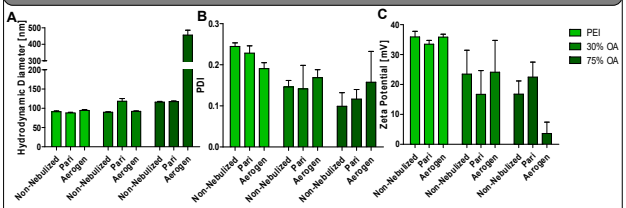

Our findings indicate that PEI Polyplexes remained stable when nebulized with all three nebulizers **(A, B, C)** (light green). Pari eFlow Rapid had a stable impact on transition state micelleplexes (green), while the Aerogen Pro had minimal impact, suggesting higher nebulization energies affect the transition state more. The micelleplexes (dark green) were unaffected by Pari eFlow Rapid but significantly impacted by the Aerogen Pro, possibly due to their higher susceptibility to temperature increases during nebulization.

Nebulization stability

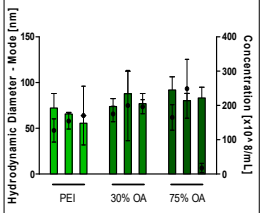

The NTA results highlighted our previous findings. Especially the lower concentration indicates aggregation

RNA loss assay

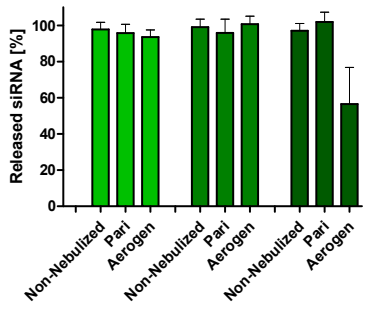

Heparin alone was not sufficient to release the encapsulated siRNA for the micelleplexes (data not shown), proving a transition from poly- to micelleplex. After treatment with Heparin and Triton-X almost all formulations released all their encapsulated siRNA indicating no loss through nebulization. Only the Aerogen Pro nebulized 75% OA Micelleplexes lost approximately 45% of their cargo.

Gene Knockdown

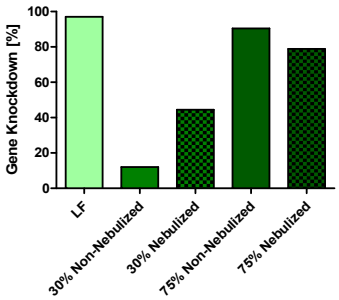

Surprisingly, even though the physicochemical characteristics of the 30% OA transition state micelleplex showed no difference after nebulization their in-vitro performance was improved. We hypothesize that this is due to a weakened association of polymer and siRNA facilitating the cargo release in the cells. The 75% OA micelleplex performed slightly worse after nebulization. This might be due to a decreased stability of the complex.

This project is funded by a European Research Council (ERC) grant and the Volkswagen Stiftung .

The poster comprises graphical items created with biorender and Prism 5.

[1] Tzeng et al., Expert Opin Drug Deliv. 2020 Oct; 17(10): 1395–1410

[2] van Rijn et al., Scientific Reports (2023) 13, article number: 8851

Adrian P. E. Kromer
Department of Pharmacy
Ludwig-Maximilians-University Munich
Butenandstr. 5, B2.027
81377 Munich, Germany
Email: adkroph@cup.uni-muenchen.de

Catia Lopes

Unravelling Gene Therapy's Potential in Alzheimer's Disease via the Brain-Blood Barrier

Cátia D. F. Lopes [1], Marco Basile [1,2], Alessandro Ronzoni [1,2], Giuseppe Battaglia [1,3,4]

1-Molecular Bionics Group, Institute for Bioengineering of Catalunya (IBEC), The Barcelona Institute of Science and Technology (BIST) Barcelona, (Spain). 2-Biomedicine Department, University of Barcelona, Barcelona, (Spain). 3-Biomedical Research Networking Center in Bioengineering, Biomaterials, and Nanomedicine (CIBER-BBN), Barcelona, (Spain). 4-Catalan Institution for Research and Advanced Studies (ICREA), Barcelona, (Spain).

clopes@ibecbarcelona.eu. @CatiaDLopes

Background: Alzheimer's disease (AD) is a genetic and sporadic neurodegenerative disorder, involving the accumulation of Amyloid-β (Aβ) in the blood and brain, with no cure available. The main clinical challenge remains the accomplishment of an efficient and safe therapeutic option that can arrest the disease progression and prevent cognitive failure. The decreased Aβ clearance is the most accountable process for AD development rather than the increased Aβ synthesis. From this point of view, Aβ clearance pathways are promising targets to lower Aβ levels and prevent or effectively change the clinical course of the disease. At the BBB, LRP1 acts as the main transporter for Aβ but its expression is declined in normal ageing and AD as well as the Aβ clearance across the BBB. Therefore, LRP1-mediated Aβ transport across the BBB and clearance from the brain is an important novel therapeutic target for Aβ clearance therapy.

Goal & Approach: This work aims to develop a brain endothelial-specific gene therapy that can improve the fast and efficient tubular mechanism for Aβ clearance from the brain.

The strategy is based on the establishing of super-selective polymersomes capable of targeting brain endothelial cells (BECs) and allow the modulation of the Aβ clearance mechanism across the BBB. The proposed Aβ lowering intervention relies on the re-establishment of proper expression levels of the LRP1 receptor - a key intervenient in the Aβ clearance across the BBB.

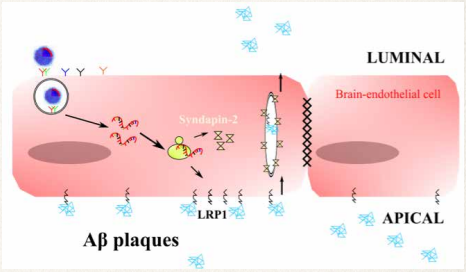

Super-selective BBB-targeted nanosystem

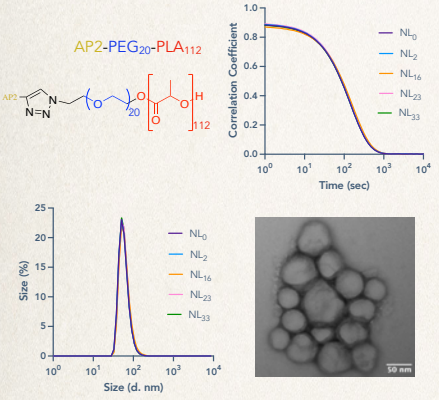

BBB properties are maintained after LRP1 up-regulation in BECs

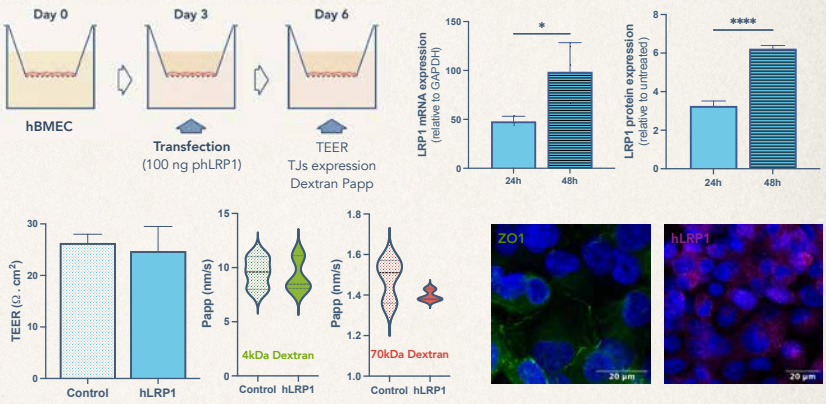

LRP1 up-regulation improves Aβ transcytosis across the BBB

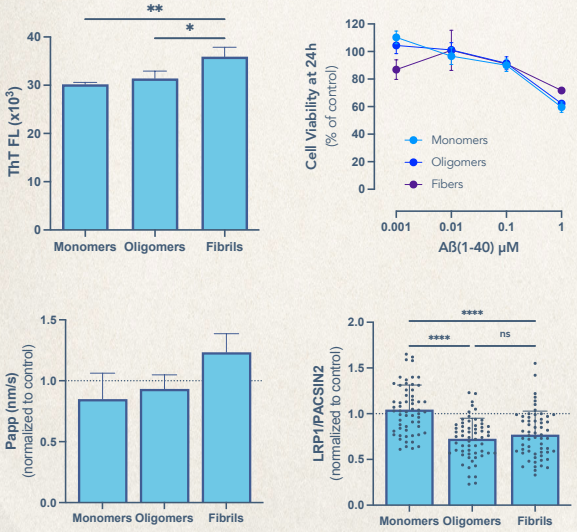

Main Findings

- Up-regulation of LRP1 in hBMEC do not interfere with the electrical resistance, tight junctions expression and dextran permeability.
- The different Aβ species showed to be non toxic in hBMEC at the concentrations tested.
- The apparent permeability of monomers and oligomers is not altered in comparison with the control, but the LRP1 up-regulation seems to be associated with higher transcytosis of Aβ fibrils.
- Previous work showed an increase in the association of LRP1/PACSIN2 (all Aβ species) during the first 15 min contact, with oligomers favouring the formation of PACSIN2 fast shuttling across BECs. Here, after 6h contact, the association of LRP1/PACSIN2 is significantly decreased for oligomers and fibrils indicating a possible time-dependent involvement of PACSIN2 in Aβ transport/clearance.

Acknowledgements:

Funded by the European Union

European Research Council

This work has received funding from the European Union's Horizon 2020 research and innovation programme under grant agreement No.101066836 and from the European Research Council (ERC) CoG CheSSTag (grant agreement No.769798).

Sandra López Cerdá

In vitro synergistic effect of dual-loaded budesonide and serpine1 siRNA lipid-polymer hybrid nanoparticles for the treatment of inflammatory tissue conditions

Sandra López Cerdá,[1,*] *Flavia Fontana,[1] Alexandra Correia,[1] Shiqi Wang,[1] Giuseppina Molinaro,[1] Rubén Pareja Tello,[1] Gonçalo Barreto,[2] Hélder A. Santos[1,3]*

[1] Drug Research Program, Faculty of Pharmacy. University of Helsinki, FI-00014 Helsinki, Finland
[2] Translational Immunology Research Program, University of Helsinki, FI-00014 Helsinki, Finland
[3] Department of Biomedical Engineering, University Medical Center Groningen, University of Groningen, 9713 AV Groningen, The Netherlands
**email: sandra.lopezcerda@helsinki.fi*

1. INTRODUCTION

Recent studies have proposed to enhance M2 macrophages activity to promote tendon healing. Budesonide is a small molecule drug that has been used for macrophage polarization toward the M2 phenotype (1). However, upregulation of TGF-β by M2 macrophages contributes to fibrosis. Hence, novel therapeutic strategies have been focused on supressing mediators of fibrosis. siRNA-mediated inhibition of key genes involved in the formation of adhesions and fibrotic tissue could potentially allow to increase the activity of MMPs involved in tissue remodelling. Hence, we hypothesise that co-delivery of budesonide and an anti-fibrotic siRNA would promote macrophage polarization toward the M2 phenotype while preventing fibrosis (2). Lipid-polymer hybrid nanoparticles (LPNs) were formulated to perform a controlled release of the drug molecules and to enhance the transfection efficiency in macrophages and tenocytes. The optimized LPNs displayed a suitable and homogenous size for intramuscular administration and encapsulated efficiently budesonide in the polymer core and siRNA in the lipid shell. In addition, LPNs were not toxic at the doses needed for therapeutic efficacy. LPNs were taken up more efficiently than the bare polymer core and displayed an efficient siRNA transfection efficiency even at low nanoparticle concentrations. The expression of pro-inflammatory and pro-fibrotic genes was modulated by the dual-loaded LPNs as preliminary indicator of a synergistic therapeutic efficacy.

2. METHODS

LPNs were prepared with a glass capillary microfluidics system using an optimized two-steps co-flow nanoprecipitation approach, and purification was achieved by ultracentrifugation. The size and size homgoneity was evaluated by dynamic light scattering (DLS) and transmission electron microscopy (TEM). The loading of budesonide and siRNA was assessed using a High Performance Liquid Chromatography (HPLC). HPLC and a fluorescent assay, respectively. The cell viability of the bare polymer core vs the hybrid NPs was assessed in RAW 264.7 macrophage cells and tenocytes using a luminiscent assay. The uptake was evaluated in RAW 264.7 murine cells and THP-1 human cells. The synergistic anti-inflammatory and anti-fibrotic potential of these LPNs was evaluated by RT-qPCR.

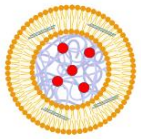

Figure 1. Shcematic representation of lipid-polymer hybrid nanoparticles (LPNs) loaded with budesonide in the polymer core and siRNA in the lipid shell.

3. RESULTS

1. Physicochemical characterization of BUD@siRNA@LPNs

A

NPs label	Size (nm)	PDI	ζ-potential (mV)
PLGA core	240 ± 6	0.11 ± 0.07	-23 ± 2
Empty LPNs	320 ± 8	0.19 ± 0.08	+25 ± 1
BUD@siRNA@LPNs	345 ± 7	0.22 ± 0.09	+25 ± 1

B

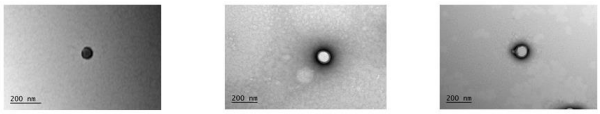

Figure 1. Dynamic light scattering (DLS) data (A) and transmission electron microscopy images of the dual-loaded LPNs (B).

2. Cell viability and uptake of LPNs in RAW 264.7 cells.

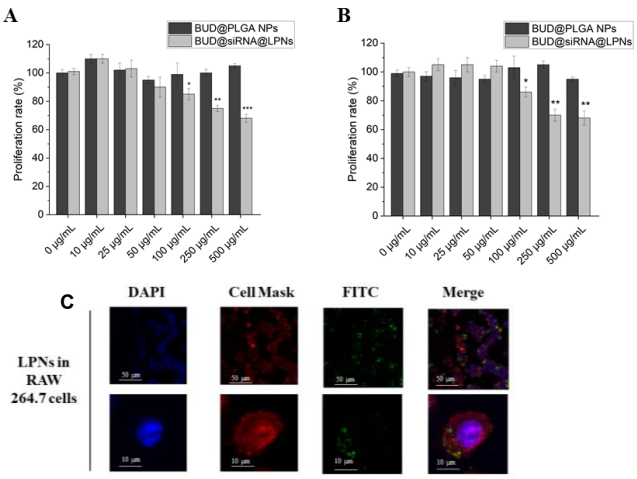

Figure 2. Cell viability of RAW 264.7 cells after 24 h (A) and 48 h (B) of incubation with LPNs at different concentrations. (C) Confocal microscopy images as qualitative uptake assessment of the internalisation of FITC-labelled LPNs in RAW 264.7 cells.

3. Anti-inflammatory and anti-fibrotic effect of BUD@siRNA@LPNs.

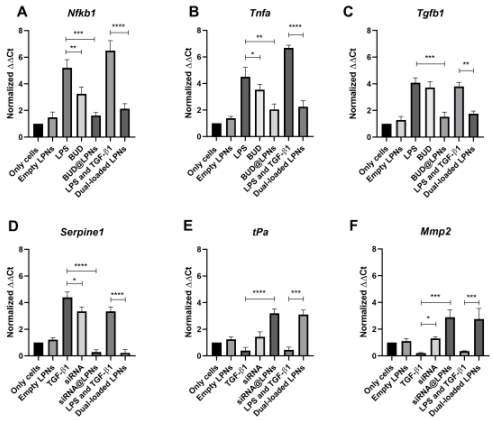

Figure 3. Modulation of the expression of different pro-inflammatory (A, B, C) and pro-fibrotic genes (D, E, F) in RAW 264.7 cells by BUD@siRNA@LPNs.

4. CONCLUSIONS

The optimized BUD@siRNA@LPNs optimized exhibit a core-shell structure, confirming the coating of the PLGA core by a lipid shell. LPNs had size homogeneity and colloidal stability had released the payloads ina sustained manner. The cell viability studies in macrophage cell lines demonstrated the cytocompatibility of the nanosystems. Quantitative and qualitatve uptake studies confirmed the internalization of LPNs in these cells lines, wiht a maximum uptake at 6 h after incubation. Finally, the synergistic anti-inflammatory and anti-fibrotic effect was demonstrated by analysing the expression of genes by RT-qPCR.

Acknowledgements:

P4FIT — PERSPECTIVES FOR FUTURE INNOVATION IN TENDON REPAIR

MARIE CURIE ACTIONS

This project has received funding from the European Union's Horizon 2020 research and innovation programme under the Marie Skłodowska-Curie grant agreement No 955685

P4 FIT ITN website:

To read more about this work:

Vacas Esther Loscertales

Chemoradiation therapy using lipid nanocarriers

E. Loscertales [1,2], J. Mateo [3], S. España [1,2,3]

[1]Grupo de Física Nuclear, EMFTEL & IPARCOS, Universidad Complutense de Madrid, CEI Moncloa, Madrid, Spain
[2]Instituto de Investigación del Hospital Clínico San Carlos (IdISSC), Ciudad Universitaria, Madrid, Spain
[3]Centro Nacional de Investigaciones Cardiovasculares (CNIC), Madrid, Spain

esloscer@ucm.es

Grupo de Física Nuclear @ UCM

INTRODUCTION

- Drug-loaded nanoparticles (liposomes) that respond to radiotherapy have emerged as a promising tool for enhancing the efficacy of cancer treatment[1–3]

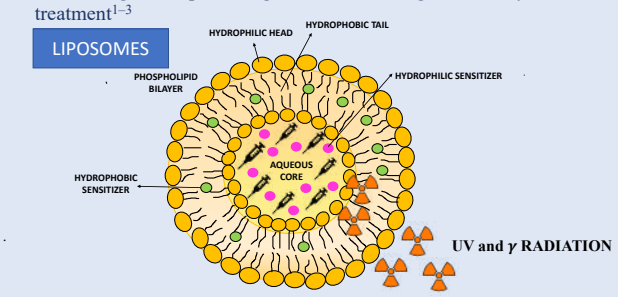

Fig 1. Nanocarrier based in liposomal systems containing the drugs and sensitizer agents that can be activated with ionizing radiation

- These nanoparticles can be designed to release therapeutic agents selectively within the tumor, exploiting the radiation-induced changes in nanoparticles for precise drug delivery.
- This integration of radiotherapy and nanoparticle-based drug release holds significant potential to improve the therapeutic outcomes in cancer patients while minimizing adverse effects, representing a promising advancement in cancer treatment strategies.

METHODS

- Liposomes were synthesized by a thin film hydration method followed by extrusion
- Molar ratio ➡ Lipid : Chol : DSPE-Peg 2000 ➡ 66.2 : 32.5 : 1.3
  - 1,2-dilinoleoyl-sn-glycero-3-phosphocholine (DLPC)
  - 1,2-dioleoyl-sn-glycero-3-phosphocholine (DOPC)
  - 1-stearoyl-2-linoleoyl-sn-glycero -3-phosphocholine (SLPC)
  - 1,2-distearoyl-sn-glycero-3-phosphocholine (DSPC).

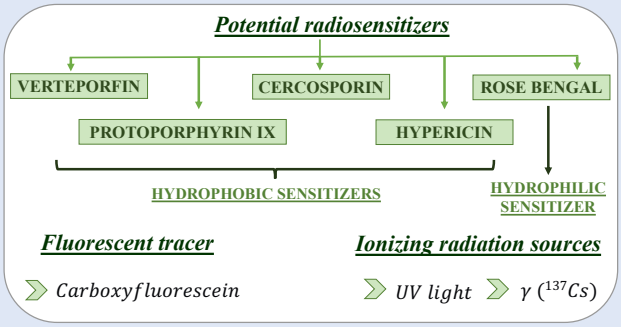

- *In vitro* studies were performed on HeLa cells in order to assess cellular uptake and radiosensitization effects when incubated with liposomes.

RESULTS

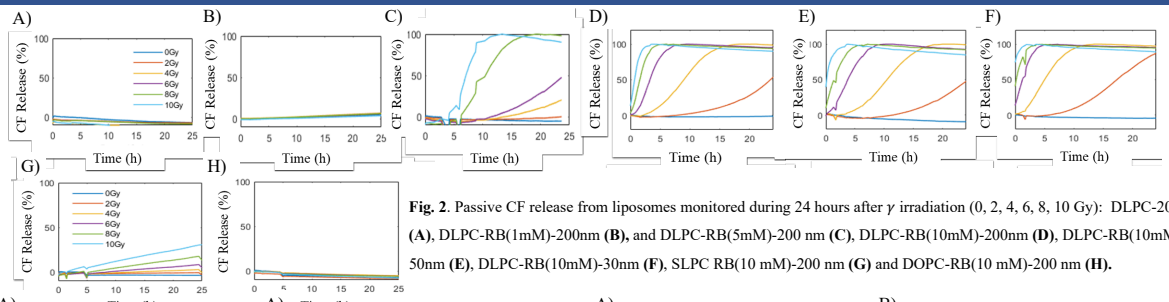

Fig. 2. Passive CF release from liposomes monitored during 24 hours after γ irradiation (0, 2, 4, 6, 8, 10 Gy): DLPC-200nm **(A)**, DLPC-RB(1mM)-200nm **(B),** and DLPC-RB(5mM)-200 nm **(C)**, DLPC-RB(10mM)-200nm **(D)**, DLPC-RB(10mM)-50nm **(E)**, DLPC-RB(10mM)-30nm **(F)**, SLPC RB(10 mM)-200 nm **(G)** and DOPC-RB(10 mM)-200 nm **(H).**

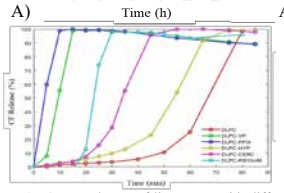

Fig. 3. CF release of liposomes with different radiosensitizer irradiated with UV light **(A)**

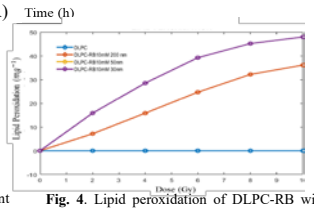

Fig. 4. Lipid peroxidation of DLPC-RB with different sizes irradiated with γ **(A).**

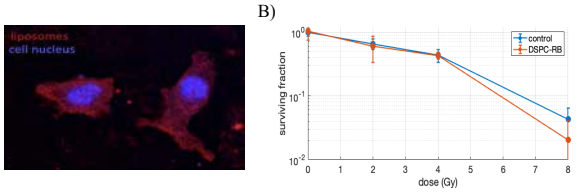

Fig. 5. Cell internalization **(A)** of DLPC-RB liposomes (544 nm/590 nm, red) in HeLa cells (24 h incubation). **(B)** Survival fraction of HeLa cells after γ irradiation (0, 2, 4, 8 Gy).

CONCLUSIONS

- ❖ RB was identified as a good radiosensitizer to induce lipid peroxidation in liposome membranes under radiotherapy leading to the synchronous release of their cargo.
- ❖ Minor differences on CF release was found for liposomes loaded with different RB concentrations when irradiated with UV light while large differences were obtained when irradiated with γ photons.
- ❖ Induced release is faster for smaller liposomes probably due to the higher curvature of the surface which leads to increased exposure of unsaturated lipids to reactive species.
- ❖ Polyunsaturated fatty acids like DLPC or SLPC are more sensitive to radiation damage.
- ❖ A minor radiosensitizing effect was obtained with RB liposomes on HeLa cells.

FUTURE WORK

Further work is needed to increase the radiosensitizing effect of the liposomes and to explore their chemoradiation capabilities on *in vitro* studies.

References

[1] Denkova, A. G., Liu, H., Men, Y. & Eelkema, R. Enhanced Cancer Therapy by Combining Radiation and Chemical Effects Mediated by Nanocarriers. Adv. Ther. 3, 1900177 (2020).
[2] Zhou, Z. et al. Synchronous Chemoradiation Nanovesicles by X-ray Triggered Cascade of Drug Release. (2019).
[3] Deng, W. et al. Controlled gene and drug release from a liposomal delivery platform triggered by X-ray radiation. Nat. Commun. 9, 2713 (2018).
[4] Grigalavicius, M. et al. Proton-dynamic therapy following photosensitiser activation by accelerated protons demonstrated through fluorescence and singlet oxygen production. Nat. Commun. 10, 3986 (2019).
[5]Clement, S. et al. Radiodynamic Therapy Using TAT Peptide-Targeted Verteporfin-Encapsulated PLGA Nanoparticles. Int. J. Mol. Sci. 22, 6425 (2021).

Acknowledgments

This work was funded by Comunidad de Madrid under ASAP project (S2022/BMD-7434) and Ministerio de Ciencia e Innovación under NANORADIOTHER Project (PID2021-127033OB-C22).

Anshika Maheshwari

Calcium phosphate nanoparticles as potential carriers for vaccines

Anshika Maheshwari, Rebecca Dookie, Birgitta Henriques-Normark and Georgios A. Sotiriou

Department of Microbiology, Tumor and Cell Biology, Karolinska Institutet, Stockholm, Sweden

Email: anshika.maheshwari@ki.se , lab website: https://sotirioulab.org/

Introduction

Subunit (protein/peptide) vaccines are preferred because of a safer profile and scalability. However, these antigens by themselves suffer from low immunogenicity and stability.[1]

Therefore, we propose the use of nanoparticles (NPs) as vaccine carrier since they can protect antigen against degradation, improve the immunogenicity and allow for targeted delivery.

[1] Nanishi E, Dowling DJ, Levy O. Current opinion in pediatrics. 2020 Feb;32(1):125.

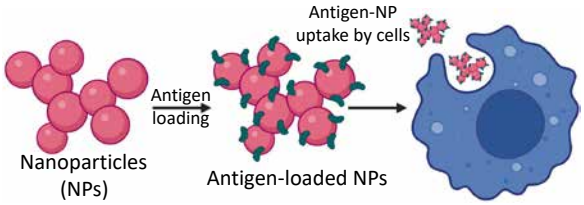

Nanoparticle synthesis and Characterization

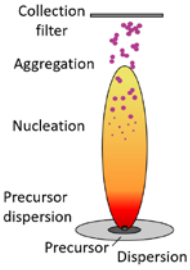

Flame Spray Pyrolysis

- Facile single step synthesis
- Highly scalable- gram/hr in lab
- Reproducible
- NPs with high specific surface area (SSA)

Calcium phosphate (CaP) NPs [Ca/P= 2.19]

Flame condition (p/d) Precursor flow (mL/min) / dispersion oxygen (L/min)	SSA (m^2/g)	d_{BET} (nm)	Mean hydrodynamic size (nm)	ζ potential (mV)
10/5 CaP (L)	78	24	1209	- 3.9
5/5 CaP (M)	132	14	1406	- 7
3/8 CaP (S)	231	8	2571	- 3.5

X-ray diffraction spectra of synthesised NPs

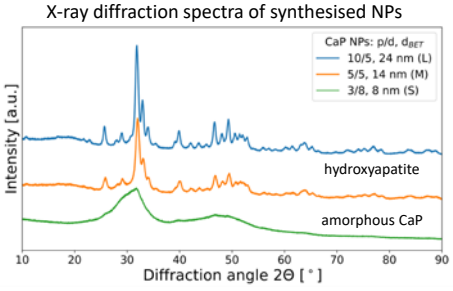

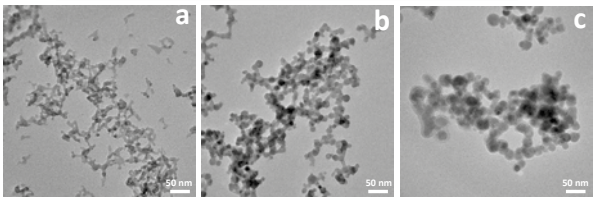

Transmission electron microscopy images of CaP NPs produced using different flame conditions- (a) 3/8 flame- small, (b) 5/5 flame- medium & (c) 10/5 flame- large

In vitro testing of NP-antigen conjugate

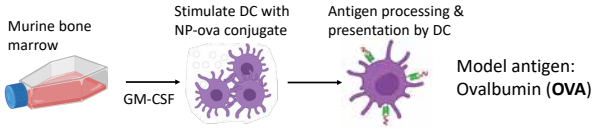

Bone marrow derived dendritic cells (BMDC)

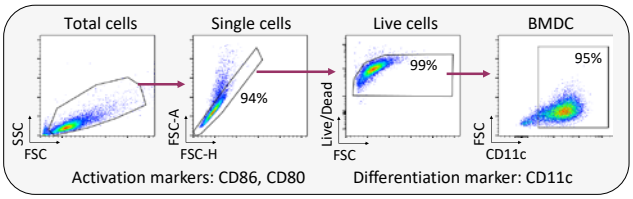

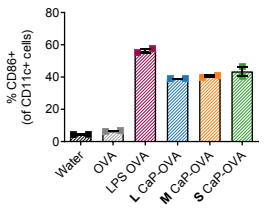

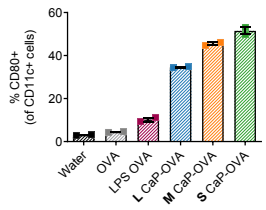

Antigen uptake by DCs (18hrs)

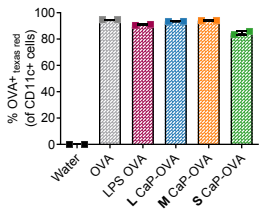

Antigen processing by DCs (30 min)

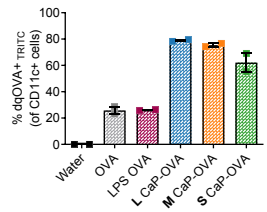

Cytokines produced

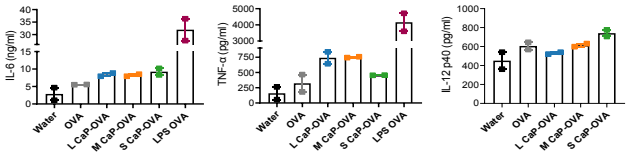

Acknowledgements

This research is funded by the Swedish Foundation for Strategic Research and European Research Council (ERC) under the European Union's Horizon 2020 research and innovation program.

Conclusion

- FSP allows facile synthesis of CaP NPs with good control over crystallinity and surface area.
- Both crystalline and amorphous CaP NPs have immunomodulatory effect on bone marrow derived dendritic cells.

Florian Meier

Multi-Detector Field-Flow Fractionation for Quality Assessment of Nano-Sized Drug Delivery Systems

POSTNOVA

The Postnova Nanomedicine Characterization Platform

Field-Flow Fractionation

Postnova AF2000 AF4 & EAF2000 EAF4

Postnova CF2000 CF3

Critical Quality Attributes

- Payload / Cargo Mass
- Encapsulation Efficiency
- Size / Molar Mass Distribution
- Particle Concentration / Virus Titer
- Particle Shape / Morphology
- Stability / Aggregation
- Zeta Potential / Surface Charge
- Corona Formation
- Composition / Conjugation
- Chemical Identity / Impurities

Multi-Detection

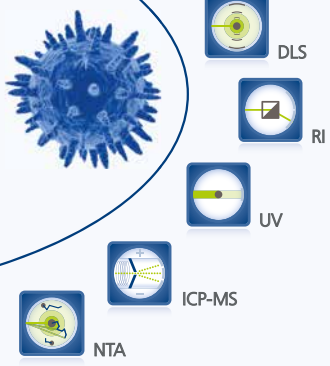

Field-Flow Fractionation - FFF

- Narrow ribbon-like channel without stationary phase
- Various external separation fields (e.g., Cross Flow, Centrifugal Field)
- Asymmetrical Flow FFF (AF4), Centrifugal FFF (CF3), Thermal FFF (TF3)...
- Gentle separation under physiological conditions
- Multi-detection capabilities
- Fraction collection

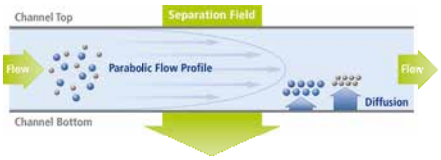

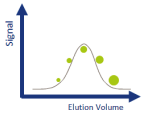

Schematic of the separation principle and elution order in Field-Flow Fractionation.

Liposome size distribution, concentration & Zeta potential by EAF4-MALS-NTA

- Commercial liposomal Doxorubicin (Doxil®)
- Diluted in 0.5 mM NaCl or DMEM + 10% fetal calf serum
- 1 x PBS as eluent

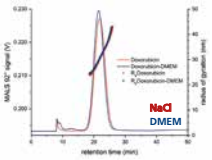

Doxil® fractionated under physiological conditions by EAF4-MALS.

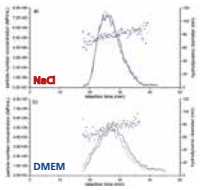

Size-resolved particle number concentration of Doxil® by EAF4-NTA.

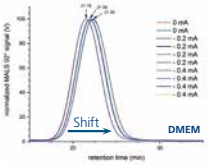

Shift of retention time of Doxil® observed during fractionation by application of different electrical field strengths.

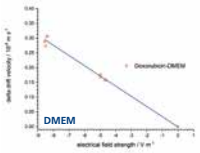

Plot of difference of retention times (drift velocity) against applied electrical field strengths.
slope = electrophoretic mobility; Zeta potential by Smoluchowski approximation.

- Size from MALS (Radius of Gyration R_g) and NTA (Hydrodynamic Diameter D_h)
  - R_g: 24-41 nm (NaCl and DMEM)
  - D_h: 65-95 nm (NaCl); 60-95 nm (DMEM)
- Particle number concentration from NTA
- Zeta potential from EAF4
  - -34.6 mV (NaCl); -45.2 mV (DMEM)
- No protein corona formation (?)

Further information: R. Drexel, A. Siupa, P. Carnell-Morris, M. Carboni, J. Sullivan and F. Meier, Molecules, 2020, 25(20), 4703.

Exosome-BSA cargo mass by CF3

- Empty and filled exosomes of similar size (BSA as cargo)
- 1x PBS as eluent
- Cargo mass quantification by CF3 theory
- Effective or buoyant mass m' ~ retention time

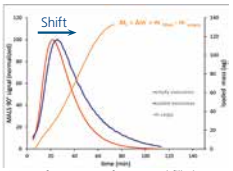

CF3-UV fractograms of empty and filled exosomes.

- CF3 ultrasensitive balance
  - 20 attogram (ag) BSA at detector peak maximum
  - 10-80 ag across full exosome size distribution
- Larger exosomes carry more cargo

mRNA-LNP payload by AF4-UV-MALS-RI-DLS

- mRNA-LNP synthesized at SINTEF Industry, Norway
- Frit-Inlet AF4 channel
- 1x PBS as eluent

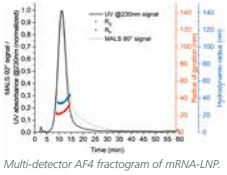

Multi-detector AF4 fractogram of mRNA-LNP.

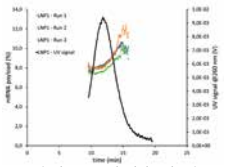

Determined mRNA payload plotted against UV-detector signal and LNP retention time. A priori knowledge: dn/dc & ε for mRNA and lipids.

- Figures of Merit
  - 90% recovery
  - SD (size) < 2.5%
  - SD (ret. time) < 0.6%
- Payload quantification
  - 6.0% mRNA
  - mRNA payload increases with increasing LNP size

Further information J. Parot, D. Mehn, H. Jankevics, N. Markova, M. Carboni, [...], F. Meier, R. Drexel, [...], F. Caputo, L. Calzolai, ACS Nano, 2023, under revision.

Postnova Analytics GmbH
86899 Landsberg, DE
T: +49 8191 985 688 0

Postnova Analytics Ltd.
Worcestershire, WR14 3SZ, UK
T: +44 1684 585167

Postnova Analytics Inc.
Salt Lake City, UT 84102, US
T: +1 801 521 2004

Postnova Northern Europe
00380 Helsinki, FI
T: +358 9 8545 510

info@postnova.com
www.postnova.com

Sophie Luise Meiser

Microneedle-Enhanced Delivery of Nanocrystalline Imiquimod for Transcutaneous Immunization – Manufacturing, Characterization and Permeation

Meiser SL[1,2] (smeise01@uni-mainz.de); Pielenhofer J[1,2]; Hartmann A[1,3]; Grabbe S[1,4]; Radsak M[1,3]; Langguth P[1,2]

[1]Collaborative Research Center 1066, Nanodimensional polymer therapeutics for tumor therapy, Mainz; [2]Biopharmaceutics and Pharmaceutical Technology, Johannes Gutenberg-University, Staudingerweg 5, Mainz, Germany; [3]3rd Department Internal Medicine, University Medical Center of the Johannes Gutenberg-University, Langenbeckstraße 1, Mainz, Germany; [4]Department of Dermatology, University Medical Center of the Johannes Gutenberg-University, Langenbeckstraße 1, Mainz, Germany

1 INTRODUCTION

Reaching the target destination within the body is one of the highest objective to achieve while formulating drugs. Focusing on the human skin as target site for drug delivery, we can take advantage of the high density of immune cells for implementing transcutaneous immunization [1]. However, the skin also acts as a strong barrier, providing a tough protective shield that drugs struggle to penetrate. To address this issue, we developed a solution using dissolving microneedle arrays (MNA) loaded with nanocrystalline imiquimod, a TLR-7 agonist. The MNA not only enhance drug permeation but also make the delivery process more effective. In our experiments, we conducted both *ex vivo* permeation tests using a Franz diffusion cell and *in vitro* release experiments. With the use of MNAs, we achieved the same level of drug permeation after 24 hours, using only 7% of the nanocrystalline imiquimod dose compared to that required in the semisolid formulations.

AIM OF THE PROJECT

Formulation development to establish of a platform strategy for transcutaneous vaccination

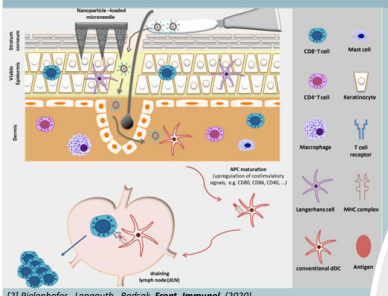

[2] Pielenhofer…Langguth…Radsak, ***Front. Immunol.*** *(2020)*

2 METHODOLOGY

PREPARATION OF MNA: SOLVENT CAST METHOD [3][4]

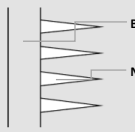

Backing layer: PVP K 30

Needles:
Matrix polymer: PVA 18-88
Imiquimod suspension
2:1 (v/v)

MIXING PROCESS OF MOULDING MASS USING STATIC MIXERS

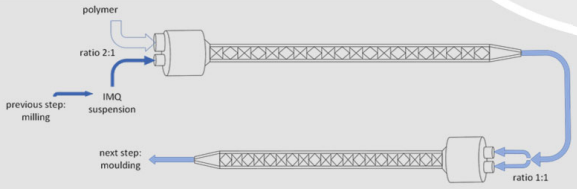

PROJECT WORKFLOW

MANUFACTURING
- Imiquimod nanoparticles
- Imiquimod suspension
- Moulding of MN

CHARACTERIZATION
- Particle size
- Optical appearance
- Insertion success
- Mechanical properties
- Loading dose

IN-VITRO/ IN-VIVO TESTING
- Franz diffusion cell: *ex vivo* skin permeation
- Release testing
- Mouse model: efficacy and immunological response

Fig. 1: A Imiquimod-loaded PVA microneedles **B** Insertion of PVA microneedles into porcine ear skin **C** Stereomicroscopical image of porcine ear skin after insertion of PVA microneedles stained with methylene blue solution

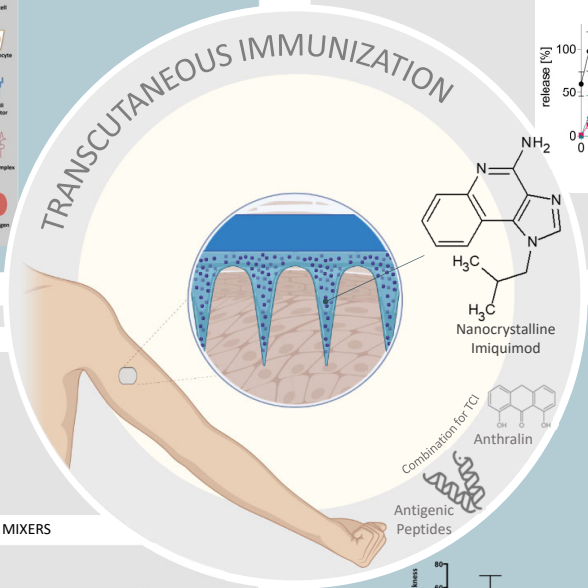

3 RESULTS

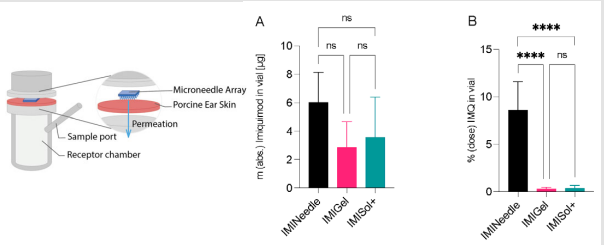

Fig. 2: Ex vivo permeation of imiquimod (IMQ) after 24 hours: MNA vs. semisolid formulations (IMIGel; IMISol+); **A** Absolute permeation (dose IMQ used: 70 µg (MNA); 1000 µg (IMIGel/ IMISol+)); **B** Relative permeation (% dose); showing means ± SD (n=5); one-way ANOVA followed by Tukey's post-hoc analysis (significant difference ($p<0.001$)

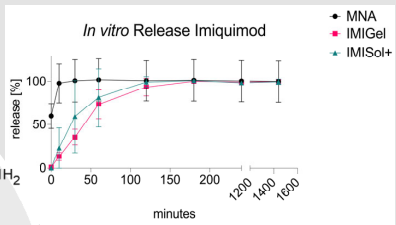

Fig. 3: In vitro release of imiquimod IMQ: MNA vs. semisolid formulations (IMIGel; IMISol+); dose IMQ used: 70 µg (MNA); 1000 µg (IMIGel/ IMISol+); showing means ± SD (n=3)

4 CONCLUSION

- We were able to manufacture dissolving microneedles containing nanocrystalline imiquimod in reproducible good quality
- MNA perform promising towards the insertion success and show advantages in drug permeation and release over semisolid formulations
- Promising results in preliminary tests in terms of immunological efficacy

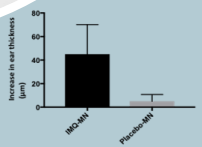

Fig. 4: Pilot experiment Imiquimod MN (left) or placebo MN (right) were applied to the ears of C57BL/6 mice and ear thickness was determined after 24 h (n=3 animals)

OUTLOOK

Preclinical proof of concept → Toxicity studies → GMP-compliant manufacture; Stability/ Quality control → Study design and protocol design

5 REFERENCES

1. Larrañeta, E.; Lutton, R.E.M.; Woolfson, A.D.; Donnelly, R.F. Microneedle arrays as transdermal and intradermal drug delivery systems: Materials science, manufacture and commercial development, Materials Science and Engineering R 104, 1-32, (2016)
2. Pielenhofer, J.; Sohl, J.; Windbergs, M.; Langguth, P.; Radsak, M.P. Current Progress in Particle-Based Systems for Transdermal Vaccine Delivery, Front. Immunol., (2020)
3. Abdelghany, S.; Tekko, I.A.; Vora, L.; Larrañeta, E.; Permana, A.D.; Donnelly, R.F. Nanosuspension-Based Dissolving Microneedle Arrays for Intradermal Delivery of Curcumin, Pharmaceutics 11(7), 308 (2019)
4. Kim, Y.K.; Park, J.; Prausnitz, M.R. Microneedles for drug and vaccine delivery, Adv. Drug Deliv. Rev. 64 (14), 1547-1568 (2012)

6 ACKNOWLEDGEMENTS

The support of the Deutsche Forschungsgemeinschaft (DFG CRC1066/3 TP B18 to MR, PL, SG und BMBF WIPANO (MR, Project No. *03THW13K04*) and SFB 1066 graduate school) is kindly acknowledged.

Víctor Mejías

Unleashing MR1's Potential: Peptide-functionalised Polymersomes for Targeted Tuberculosis Therapy

Víctor Mejías [1,2,3,*], **Joana Fort** [2,4,5], **Manuel Palacín** [2,4,5], **Giuseppe Battaglia** [1,6], **and Iris L. Batalha** [1,**]

[1]Institute for Bioengineering of Catalunya (IBEC), The Barcelona Institute of Science and Technology (BIST) Barcelona, (Spain). [2]Institute for Research in Biomedicine (IRB Barcelona), Barcelona Institute of Science and Technology (BIST), Barcelona (Spain). [3]Faculty of Medicine and Health Sciences, University of Barcelona, Barcelona, (Spain). [4]Centro de Investigación Biomédica en Red de Enfermedades Raras (CIBERER), Barcelona (Spain). [5]Department of Biochemistry and Molecular Biomedicine, Faculty of Biology, University of Barcelona, Barcelona (Spain). [6]Biomedical Research Networking Center in Bioengineering, Biomaterials, and Nanomedicine (CIBER-BBN), Barcelona, (Spain). [7]Catalan Institution for Research and Advanced Studies (ICREA), Barcelona, (Spain).

Presenting Author: *vmejias@ibecbarcelona.eu; ***Corresponding Author:*** **ibatalha@ibecbarcelona.eu

Graphical Abstract: **Development of a nanotherapeutic able to simultaneously deliver drug combination therapy and specifically target infected host cells through their unique metabolic profile.**

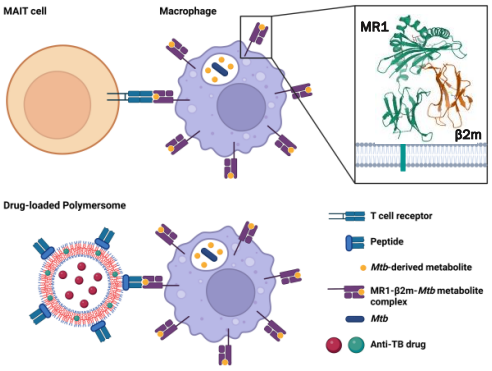

Fig 1. Antibiotic-loaded polymersomes functionalised with peptides will mimic the interaction between the MAIT cell receptor and human MR1 (hMR1). By recognising specific MR1-*Mtb* metabolite complexes, the polymersomes will target *Mtb*-infected host cells.

a. hMR1 Ectodomain (ED)–β2m heterodimer solubilisation and refolding

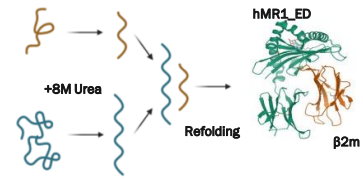

b. hMR1_ED–β2m DEAE Anion Exchange purification

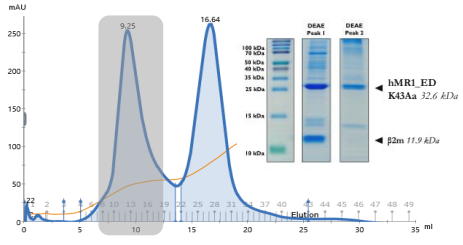

c. hMR1_ED–β2m Size Exclusion purification

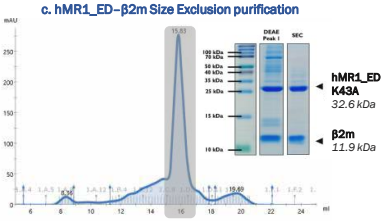

d. hMR1_ED-β2m native MS analysis

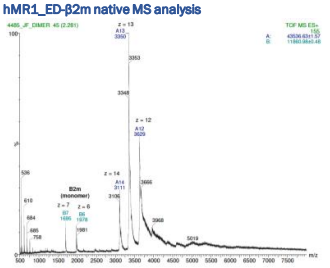

Fig 2. a. Mutant K43A hMR1 Ectodomain (hMR1_ED) and *β2m* inclusion bodies were denatured using 8M Urea and the proteins were refolded with a buffer containing 2mM EDTA and 0.4M of arginine. **b.** The refolded sample was loaded into a DEAE Anion Exchange column and fractions containing hMR1_ED and *β2m* were collected, analysed by SDS-PAGE, and concentrated. **c.** hMR1-β2m samples were further purified by Size Exclusion Chromatography (SEC) (Superdex 200 10/300 GL) and analysed by SDS-PAGE. **d.** Native Mass Spectrometry of hMR1-β2m purified samples.

a. Folic Acid photodegradation

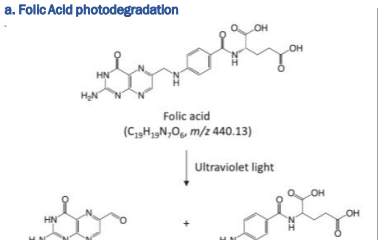

Immunology & Cell Biology (2018) 96:573–587

b. Folic Acid–hMR1_ED–β2m Size Exclusion purification

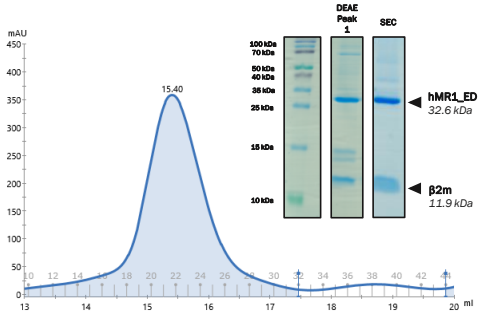

c. Folic Acid–hMR1_ED–β2m native MS analysis

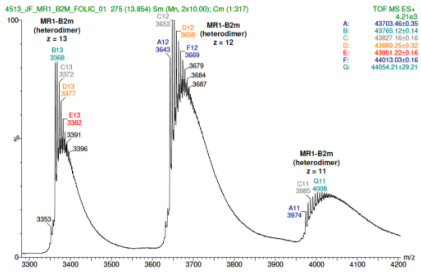

hMR1_ED	β2m	6-FP	Total
31,673.64	11,862.3281	-	43,535.9687
31,673.64	11,862.3281	190.04	43,726.01-18 = **43,708.01**

Fig 3. hMR1_ED and *β2m* were refolded in the presence of **a.** folic acid, which photodegrades into 6-formylpterin (6-FP), a metabolite known to bind MR1. **b.** The refolded sample was purified by DEAE and SEC and analysed by SDS-PAGE. **c.** Native Mass Spectrometry of 6-FP-hMR1-β2m confirming the accurate molecular mass of the metabolite-loaded complex.

a.

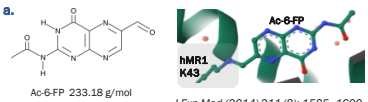

Ac-6-FP 233.18 g/mol

J Exp Med (2014) 211 (8): 1585–1600
PDB: 4PJF

b. Ac-6-FP–hMR1_ED–β2m Size Exclusion purification

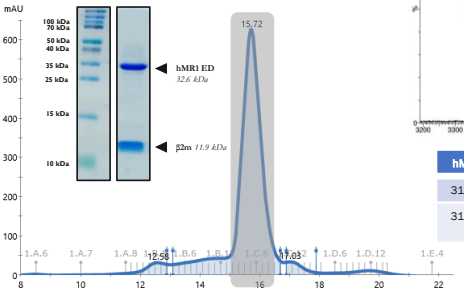

c. Ac-6-FP–hMR1_ED–β2m Native MS analysis

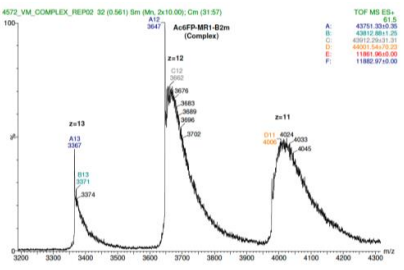

hMR1_ED	β2m	Ac-6-FP	Total
31,673.64	11,862.3281	-	43,535.9687
31,673.64	11,862.3281	233.18	43,769.14-18 = **43,751.14**

Fig 4. a. Acetyl-6-formylpterin (Ac-6-FP), a synthetic analogue of 6-FP (left). Ac-6-FP covalent binding to hMR1 lysine 43 (right) **b.** Refolded Ac-6-FP–hMR1_ED–β2m heterodimer was purified by DEAE and SEC and analysed by SDS_PAGE. **c.** Native Mass Spectrometry of Ac-6-FP–hMR1_ED–β2m confirming the accurate molecular mass of the metabolite-loaded complex.

Ongoing work

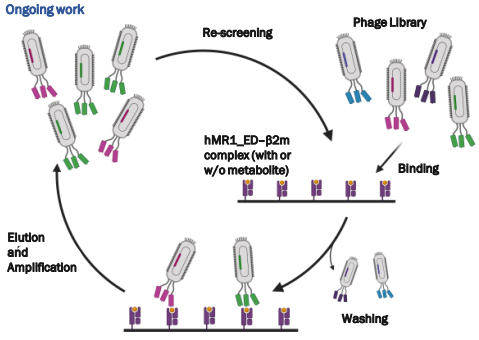

hMR1_ED(K43A)–β2m and Ac-6-FP–hMR1_ED–β2m heterodimers are currently being used as a target for phage display experiments to find peptides that selectively bind to these complexes.

Funding: The project that gave rise to these results received the support of a fellowship from 'La Caixa' Foundation (ID 100010434) and from the European Union's Horizon 2020 research and innovation programme under the Marie Skłodowska-Curie grant agreement No 847648. The fellowship code is LCF/BQ/PI21/11830004.

Raphael Mietzner

PEG hydrogel toolbox – Realizing various release timeframes of vaccine nanoparticles from hydrogels intended for improved quality of HIV immunization

Raphael Mietzner[1], Clara Barbey[1], David Peterhoff[2], Ralf Wagner[2], Achim Göpferich[1], Miriam Breunig[1]
[1]Department of Pharmaceutical Technology; [2]Department of Medical Microbiolgy and Hygiene; University of Regensburg, Universitaetsstrasse 31, 93053 Regensburg, Germany. ✉ raphael.mietzner@ur.de

Introduction

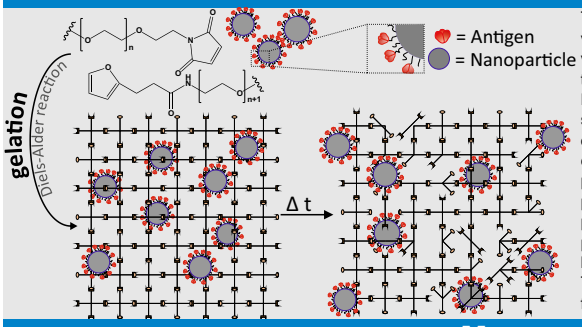

Today about 37.9 Mio people are living with the human immunodeficiency virus (HIV) [1]. An HIV-vaccine for prophylaxis would be the most effective approach to fight the global pandemic [2]. The viral envelope protein (Env) of HIV plays a key role in broadly neutralizing antibody elicitation and therefore protection against infection [3]. We and others have shown that the immobilization of Env on the surface of nanoparticles (NPs) is more effective compared to vaccination with the soluble antigen [4,5]. Another aspect is that a prolonged delivery of Env antigen e.g. from mini-osmotic pumps mimicking the kinetics of natural infections, elicit enhanced humoral responses compared to traditional bolus immunization [6]. Our goal is to combine both principles namely the particulate and prolonged delivery of Env antigen. Hydrogels have already proven to be a suitable platform for the release of proteins with different kinetics while maintaining the integrity of the proteins. [7-9]. Poly (ethylene glycol) (PEG) as material for the fabrication of hydrogels in particular has the immense advantage that it is easy to functionalize, and thus different release kinetics can be realized by varying the macromolecular chain length and the branching factor. Therefore, antigen carrying silica nanoparticles (SiNPs) were incorporated into PEG hydrogels for release over a prolonged period.

Methods and Results

Methods

Attachment of Ag to SiNPs: Env trimer (Env_{tri}), Env monomer (Env_{mono}) and human serum albumin (HSA) as a model were used for immobilization on fluorescein isothiocyanate (FITC)-labelled SiNPs (100 nm) as previously described [6]. **Polymer synthesis and hydrogel preparation:** 8armPEG10k/20k/40k, 4armPEG40k, and 4armPEG40k-Lysine-hexanoic acid (4armPEG40k-Lys-AHX) were functionalized with maleimide and furyl groups as previously described [10]. Hydrogels were fabricated by cross linking equal amounts of furyl and maleimide functionalized polymers. **Rheology and mechanical properties:** Oscillatory shear measurements were conducted at 37°C to study gelation time and Young's modulus of compression was determined on a material testing mashine. **Mesh size determination:** the average meshsize was determined as previously described [10]. **Antibody affinity measurements:** After release of Env_{tri}@SiNP and Env_{mono}@SiNP from a 4armPEG40k hydrogel, Microscale Thermophoresis (MST) was performed to measure binding affinities of the broadly neutralizing antibody VRC01 to the antigen.

Hydrogel Characterization

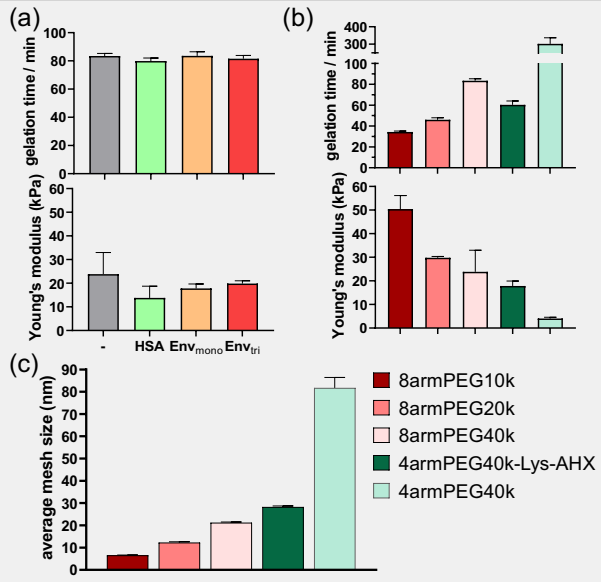

(a) Nanoparticle loading has no impact on gelation time as well as on hydrogel stiffness (expressed by Young's modulus). (b) With increasing polymer MW and decreasing branching factor, gelation time increases while hydrogel stiffness decreases. (c) With increasing polymer MW the meshsize increases

Release of antigen@SiNP

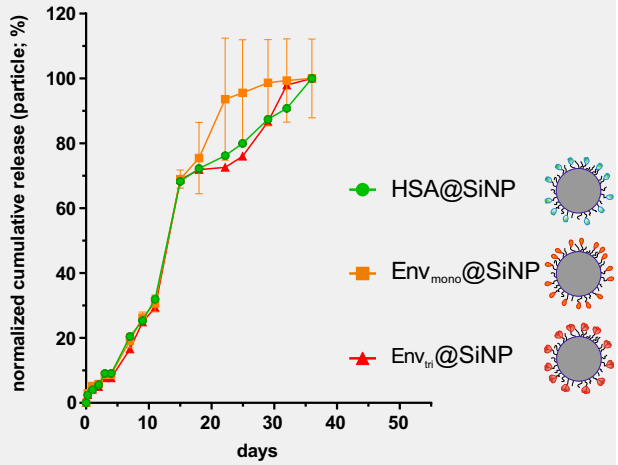

Representative release profile of antigen decorated SiNPs from an 8armPEG20k hydrogel. NPs were released in a controlled manner over a time frame of about 35 days. No differences were observed between the three types of antigen decorated NPs.

Antigen@SiNP Integrity after ReLease

		antigen@SiNPs (before hydrogel loading)		antigen@SiNPs (after release)	
antigen type	antibody		K_d (nM)		K_d (nM)
Env_{mono}	VRC01		4.5 ± 0.2		4.2 ± 1.7
Env_{tri}			13.5 ± 9.7		3.1 ± 2.6

Incorporation of decorated SiNPs could potentially lead to PEGylation of the antigen. Therefore, to test the integrity of the antigens before loading the SiNPs into the hydrogels and after their release, binding studies to antibodies were performed. The antibody affinity to Env_{mono}@SiNP and Env_{tri}@SiNP before loading and after release were quite similar and not negatively affected.

Conclusion

We believe that PEG hydrogels may serve as toolbox for the controlled release of vaccine NPs improving the immune response. An important step will be to demonstrate biological activity of released antigen carrying SiNPs in vivo.

References

[1] UNAIDS, Global HIV & AIDS statistics: 2019 fact sheet. (Vol. 2020). [2] UNAIDS, P.c., Geneva, Why the world needs an HIV vaccine. Press statement, 18 May 2017. UNAIDS. [3] Chung, A.W. et al. (2015) Cell 163 (4), 988-998. [4] Peterhoff, D. et al. (2021) Vaccines (Basel) 9 (6). [5] Tam, H.H. et al. (2016) Proceedings of the National Academy of Sciences of the United States of America 113 (43), E6639-E6648 [6] Thalhauser, S. and Breunig, M. (2020) European Journal of Pharmaceutical Sciences 155, 105520 [7] Gregoritza, M. et al. (2016) Journal of Control led Release 238, 92-102 [8] Gregoritza, M. et al. (2017). Biomacromolecules 18 (8), 2410-2418 [9] Schweizer, D. et al. (2013) J Control Release 172 (3), 975-982. [10] Kirchhof, S. et al., Journal of Materials Chemistry B 2013, 1 (37), 4855-4864.

Acknowledgement

Project "**HIV Vaccine Targeting via DNA Origami Nanoparticles to lymph nodes to promote Germinal Center formation (HIVacToGC)**" is funded by the Federal Ministry of Education and Research (BMBF) as part of program "Gezielter Wirkstofftransport" (grant no. 16GW0363K).

SPONSORED BY THE
Federal Ministry of Education and Research

Rahaf Mihyar

Evaluating Formulation and Process Parameters for Lyophilisation of Π-electron Stabilised Polymeric Micelles

Rahaf Mihyar,[1] **Armin A. Shalmani,**[1] **Tarun Ojha,**[1] **Marek Weiler,**[1] **Eva Miriam Buhl,**[2] **Fabian Kiessling,**[1] **Yang Shi,**[1]
Josbert M. Metselaar,[1] **Quim Peña,**[1] **Twan Lammers**[1]

[1]*Institute for Experimental Molecular Imaging, Uniklinik RWTH Aachen, Department of Nanomedicine and Theranostics, Forckenbeckstraße, Aachen, Germany.*
Email: rmihyar@ukaachen.de

Formulation Development

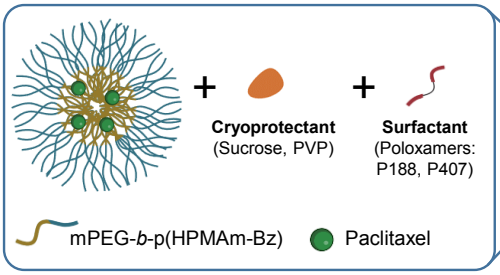

Lyophilisation Parameters

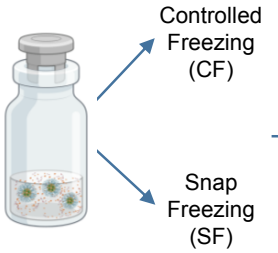

Formulation Characterisation

- Cake Structure
- Particle Size Analysis
- Drug Retention

1 Choice of Excipients

Only SF

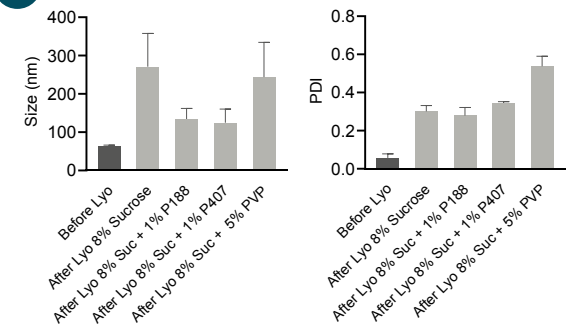

→ **Sucrose and poloxamer 188 combination provided the best protection of micelles size and polydispersity**

2 Cake Structure

Non-invasive μ-CT

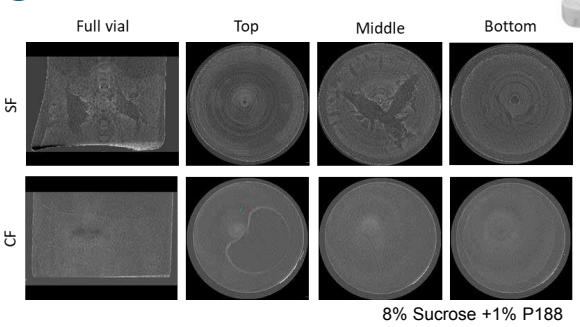

8% Sucrose +1% P188

→ **Controlled Freezing increased cake homogeneity compared to Snap Freezing**

3 Particles Size and Drug Retention Analysis

8% Sucrose +1% P188

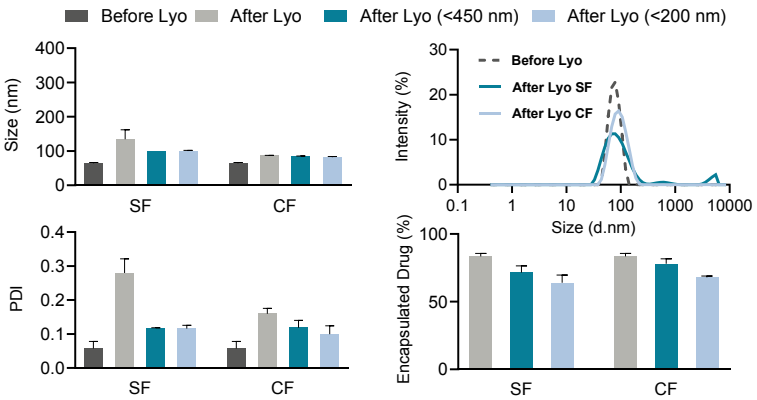

→ **Partial aggregation and partial increase in micelle size upon lyophilisation**

4 Morphology

8% Sucrose +1% P188

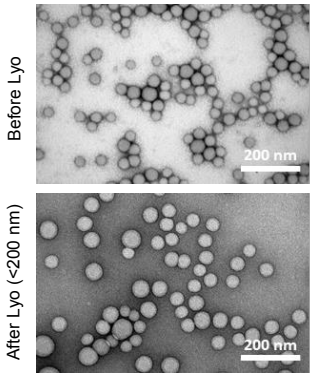

→ **The morphology of the micelles was preserved after lyophilisation**

- **The addition of stabilizing agents such as poloxamer 188 (surfactant) was crucial to preserve the properties of the formulation during lyophilization.**
- **The freezing step influences the homogeneity of the frozen sample as well as the pharmaceutical properties of the reconstituted formulations.**
- **Our work provides valuable insights into formulation and process parameters impacting on the lyophilisation process of non-crosslinked polymeric micelles, overall paving the way towards their pharmaceutical development and manufacturing.**

REFERENCES:
Metselaar J.M., Lammers T. *Drug Deliv Transl Res*, **2020**, 10:721-725.
Trenkenschuh E., Friess W. *Eur. J. Pharm. Biopharm.*, **2021**, 165:345–60.
Shi Y. et al. *ACS Nano*, **2015**, 9:3740-3752.

ACKNOWLEDGEMENT: The German Research Foundation (DFG: SH1223/1-1; LA2937/4-1; GRK / RTG 2735 (project number 331065168)), the German Federal Ministry of Research and Education (BMBF: Gezielter Wirkstofftransport, PP-TNBC, Project No. 16GW0319K), and the European Research Council (ERC: Meta-Targeting (864121)).

NANOTECHNOLOGIES FOR TARGETING THE TUMOR MICROENVIRNEMENT IN THE COLORECTAL CANCER

Agata Mlynska[1,2], Austeja Butkute[1], Evelina Voronovic[2,3], Vitalijus Karabanovas[2,3], Simona Steponkiene[2]

[1] Laboratory of Immunology, National Cancer Institute, Vilnius, Lithuania
[2] Department of Chemistry and Bioengineering, Vilnius Gediminas Technical University, Vilnius, Lithuania
[3] Biomedical Physics Laboratory, National Cancer Institute, Vilnius, Lithuania

Background

Colorectal cancer (CRC) is a complex disease characterized by a diverse tumor microenvironment (TME) comprising immune and non-immune components, with macrophages being the most abundant tumor-infiltrating cells that exhibit distinct phenotypic states, usually referred to as tumor-promoting M2 macrophages, or antitumoral M1 macrophages[1]. Macrophage polarization represents the activation state of a macrophage at a specific moment. However, their polarization status is dynamic and can be modified by integrating multiple signals from the neighboring milieu[2]. The dynamic interplay between tumor cells and macrophages plays a critical role in shaping the immunomodulatory properties of the TME, affecting tumor progression and therapeutic responses[3]. Moreover, the impact of both conventional and innovative therapies on the tumor microenvironment, where immune cells, including macrophages, play a crucial role, is often overlooked. The macrophage plasticity phenomenon allows for exploring novel therapeutic strategies aimed at reprogramming them from the M2 to M1 phenotype.

Aim

This study aims to explore potential nanotechnology- and drug-based strategies for targeting macrophages in the TME of CRC. The novelty of this work lies in its comprehensive approach to the heterogeneity and complexity of the TME.

Methodology

To address the need for innovative therapeutic strategies, nanotechnologies and photodynamic therapy were explored for their potential to target macrophages and cancer cells. A novel theranostic nanocomplex, composed of quantum dots and a photosensitizer, previously shown to accumulate in human skin mesenchymal cells[4], was tested for its efficacy in targeting macrophages and CRC cell lines. The induced transcriptomic changes, reflecting macrophage polarization state, were later compared to the gene expression profile induced by several small molecule inhibitors, designed for targeting the stemness pathways.

Results

We demonstrated that the theranostic nanocomplex accumulates uniformly in differenct CRC cell lines (Figure 1), regardless of their molecular subtype, as well as in macrophages. This suggests the potential utility of nanotechnologies for targeting tumor-associated macrophages in CRC.

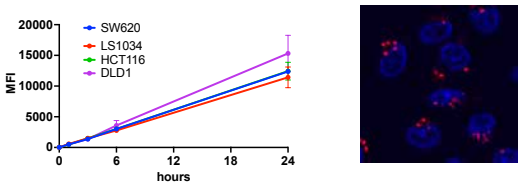

Figure 1. Dynamics (left) and representative confocal microscopy image (right) of theranostic nanocomplex accumulation in different CRC lines.

After prolonged incubation with nanocomplex, no major transcriptome changes were induced in the CRC cells on the molecular level. Macrophages, on the other hand, responded by downregulating their M2-related gene (e.g. *MRC1*) expression and upregulating the M1-related gene (e.g. *HLA-DR, CXCL8*) expression (Figure 2), suggesting the potential repolarization from the protumoral M2 type to the antitumoral M1 type.

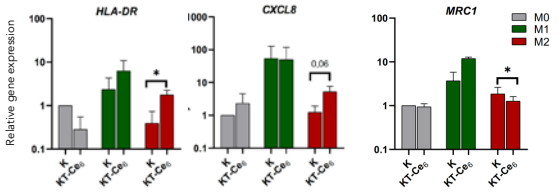

Figure 2. Gene expression changes in M0, M1, M2 macrophages after 24 hours incubation with theranostic nanocomplex (KT-CE$_6$) vs control (K).

Stemness inhibitors (salinomycin SAL, SB-431542, JIB-04, napabucasin NAPA) demonstrated ambiguous effects on macrophages, inducing changes in gene expression associated with both M1 and M2 phenotypes, and allowing for further combining several treatment strategies for obtaining the desired response.

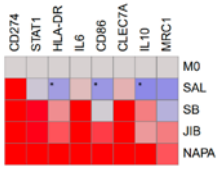

Figure 3. Gene expression profile of M0 macrophage polarization after 48 hours drug treatment. Blue – decrease, red – increase.

Summary

Novel therapeutic approaches, such as theranostic nanoparticles or stemness inhibitors, can act as immunomodulatory agents for repolarizing M2 macrophages towards an antitumor phenotype (Figure 4). These findings justify further investigation to elucidate the underlying mechanisms and explore potential combination therapies for improved clinical outcomes in CRC treatment.

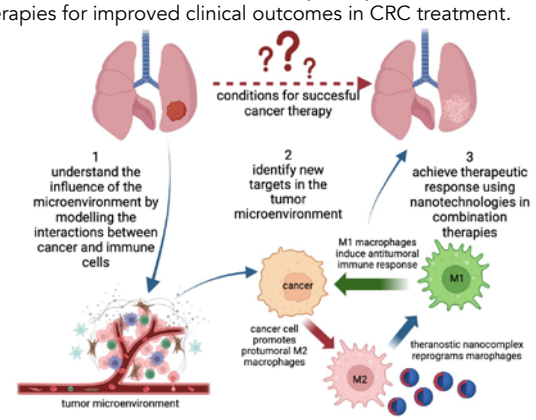

Figure 4. The conditions for successful cancer therapy might lie in the TME, composed of different host cell types. One of the most abundant populations – tumor-associated macrophages – are usually protumoral and M2-like. However, our initial findings suggest that theranostic nanocomplex can repolarize M2 macrophages into their antitumoral M1 state and consequently exert an active immune response.

Acknowledgements

This work was financially supported by the Research Council of Lithuania, Grant No. S-MIP-22-31.

Contact information

Interested in collaborations or discussing the topic? Contact us by email (agata.mlynska@nvi.lt) or LinkedIn (Agata Mlynska)

References

[1] PMID 34209703, 10.3390/ijms22136995
[2] PMID 31530089, 10.1146/annurev-pathmechdis-012418-012718
[3] PMID 36253762, 10.1186/s12929-022-00866-3
[4] PMID 34499462, 10.1021/acsami.1c10445

Local delivery of lipid liquid crystalline formulation of doxorubicin to cancer cells

CLINAM
European Foundation for Clinical Nanomedicine

Marzieh Mohammadi* [1], **Malihe Karimi** [1], **Hossein Kamali** [1], **Bizhan Malaekeh Nikuei** [2]

[1] Department of Pharmaceutics, School of Pharmacy, Mashhad University of Medical Sciences, Mashhad, Iran
[2] Nanotechnology Research Center, Pharmaceutical Technology Institute, Mashhad University of Medical Sciences, Mashhad, Iran

***Corresponding Author**: Mohammadimz@mums.ac.ir

Introduction

The serious challenges in cancer therapeutics are the low concentration of the cytotoxic agent at the tumor microenvironment and the systemic toxicity of the chemotherapeutics. With this in mind, we developed an injectable lipid liquid crystalline (LLC) based formulation of doxorubicin with sustained release pattern which provide sufficient dose of doxorubicin at the target tissue.

Methods

18 different formulations of LLC loaded with doxorubicin were synthesized via different ratios of phosphatidyl choline (PC): sorbitan monooleate (SMO), N-Methyl-2-pyrrolidone (NMP) and tween 80. Afterwards, physicochemical characteristics of the formulations were studied. Then, in vivo tumor inhibitory effect of the selected formulations in C26 tumor bearing mouse model was investigated.

Results

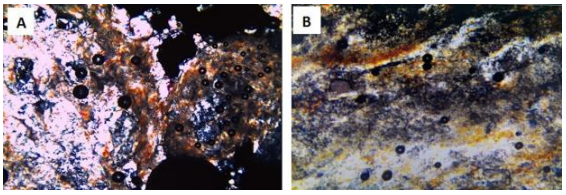

Figure 1. mage of LLC optimal formulations under polarized light microscopy (100X), F T (PC: SMO/NMP/Tween 80 (50:50/50/2 w/w%) (A), and F (PC: SMO/NMP (50:50/50 w/w%) (B).

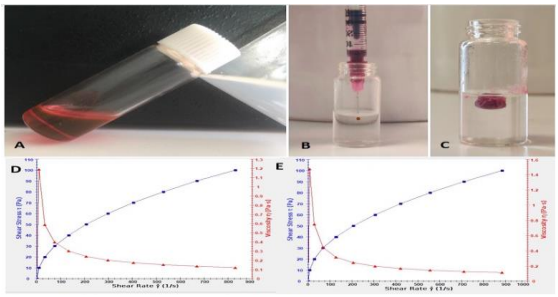

Figure 2. F_T Formulation (DOX loaded PC: SMO/NMP/Tween 80 (50:50/50/2 w/w%) was in sol state at room temperature (A). The syringeability of the formulation (B). The formation of gel state while injecting the formulation into phosphate buffered saline (pH:7.4) solution (C). Rheograms showing the pseudoplastic behaviors of F_T (DOX loaded PC: SMO/NMP/Tween 80 (50:50/50/2 w/w%) and F (DOX loaded PC: SMO/NMP (50:50/50 w/w%)(E&F).

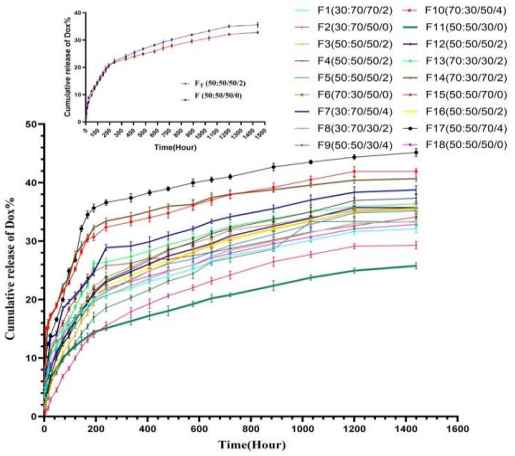

Figure 3. The release study of various formulations with different ratios of PC: SMO/NMP/Tween 80. Additionally, a separate chart showing the release pattern of the selected formulations is shown at the top.

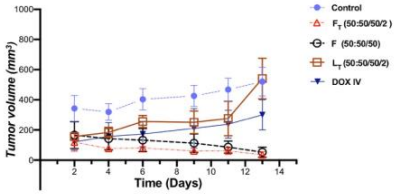

Figure 4. The tumor volume of Balb/c tumor bearing mice model after administration of PBS (control group), intravascular DOX (DOX IV), intratumoral F_T (DOX loaded PC: SMO/NMP/Tween 80 (50:50/50/2 w/w%), F (DOX loaded PC: SMO/NMP (50:50/50 w/w%) and L_T which is lipid liquid crystalline formulation made of PC: SMO/NMP/Tween 80 (50:50/50/2 w/w%).

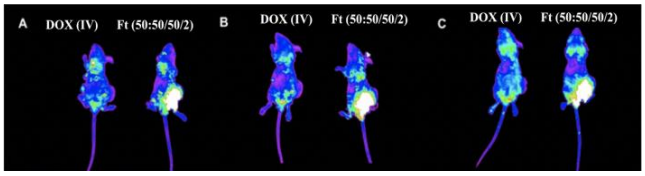

Figure 5. Animal imaging study of Balb/C tumor bearing mice after intravascular and intratumoral administration of DOX and F_T (DOX loaded PC: SMO/NMP/Tween 80 (50:50/50/2 w/w%).The study was done 4h (A) 24 h(B) and 72 h after the administration of the treatment.

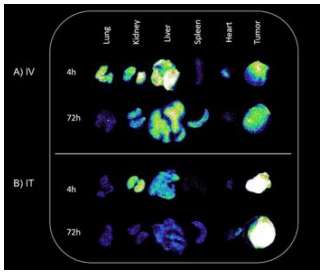

Figure 6. Ex vivo images of tumor and major organs (Lung, Kidney, liver, spleen and the heart). Tissues were excised from C26 tumor-bearing mice after (A) 4 h and (B) 72 h of IV injection of DOX and Intratumoral injection (IT) of FT (50:50/50/2).

Conclusion: We believe that doxorubicin loaded lipid liquid crystalline formulations could efficiently eradicate cancers cells in C26 tumor bearing mouse models without systemic cytotoxicity.

References:

1- Lim, J.-L., Ki, M.-H., Joo, M.K., An, S.-W., Hwang, K.-M., Park, E.-S., 2015. An injectable liquid crystal system for sustained delivery of entecavir. Int. J. Pharm. 490, 265–272.

2- Kamali, H., Karimi, M., Abbaspour, M., Nadim, A., Hadizadeh, F., Khodaverdi, E., Eisvand, F., 2022. Comparison of lipid liquid crystal formulation and Vivitrol® for sustained release of Naltrexone: In vitro evaluation and pharmacokinetics in rats. Int J Pharm 611, 121275.

Patricia Mora-Raimundo

The Louis Family Laboratory for Targeted Drug Delivery & Personalized Medicine Technologies

TECHNION Israel Institute of Technology

Active Targeting of Nanoparticles to the Brain for Treating Parkinson's Disease

Patricia Mora-Raimundo#1, Mor Sela#1, Maria Poley#1, Maya Kaduri1, Aviram Avital2, Omer Adir2, Shaked Kagan1, Adi Rozencweig1, Ifat Weiss3, Yael Bardoogo4, Jeny Shklover1, Janna Shainsky-Roitman1, Uri Ashery3, Ben Maoz4, and Avi Schroeder*1

[1]The Louis Family Laboratory for Targeted Drug Delivery and Personalized Medicine Technologies, Department of Chemical Engineering, Technion – Israel Institute of Technology, Haifa 32000, Israel
[2]The Norman Seiden Multidisciplinary Program for Nanoscience and Nanotechnology, Technion – Israel Institute of Technology, Haifa 32000, Israel
[3]School of Neurobiology, Biochemistry and Biophysics, George S. Wise Faculty of Life Sciences, Sagol School of Neuroscience, Tel Aviv University, 6997801 Tel Aviv, Israel
[4]Department of Biomedical Engineering, Sagol School of Neuroscience, The Center for Nanoscience and Nanotechnology, Tel Aviv University, Tel Aviv 6997801, Israel
# Contributed equally
patmora@campus.technion.ac.il

1.Introduction

One of the main causes of **Parkinson's Disease** (PD) is the massive **aggregation of alpha-synuclein** (AS) protein. A **potential treatment** could be the use of **monoclonal antibody** (mAb), such as SynO4, which prevents aggregation of AS. One of the **main challenges of mAb brain therapy is to reach the brain regions**. We have developed a **brain targeted delivery system** based on liposomes able to delivery this mAb for PD treatment. The system was conjugated to **transferrin** (TF) in its surface to **allow blood-brain-barrier crossing**.

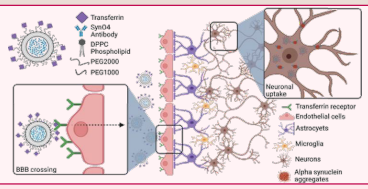

Why it Matters?

- PD has **not a cure**
- Particles allow to **cross the BBB**
- Loaded **mAb remains active**

2.Liposomal Fabrication

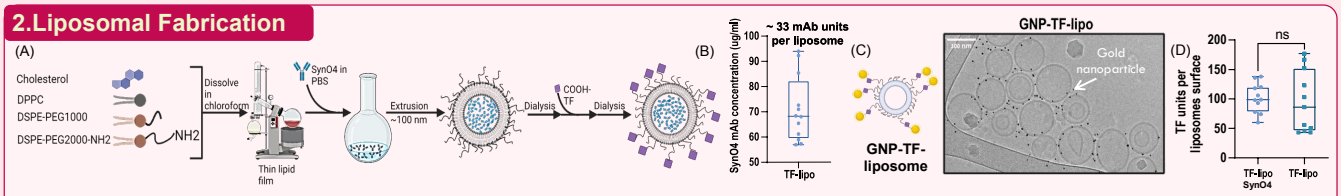

Schematic representation of the system, transferrin liposomes (TF-lipo) loaded with SynO4 antibody (A). We succeed in **encapsulating ~33 units of mAb** inside our liposomes (demonstrated by ELISA) (B); Cryo-TEM images of TF-liposomes shows the **functionalization of TF** (conjugated to 5 nm NHS activate gold nanoparticles (GNP) in the NH_2 group of the TF) and the shape and size of the system (C). The number of TF molecules conjugated on the liposomes surface was measured by BCA assay **(~100 units)**.

3.Crossing Through an *In Vitro* BBB Model

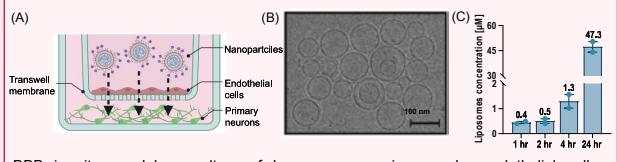

BBB in vitro model: co-culture of bone marrow microvascular endothelial cells (BMECs) and primary neurons (A). Liposomes cryo-TEM; **liposomes remain intact after BBB crossing** (B). **Liposomes cross the BBB** model over a period of **24 h** (C).

4.Neuronal Uptake and Efficacy *In Vitro*

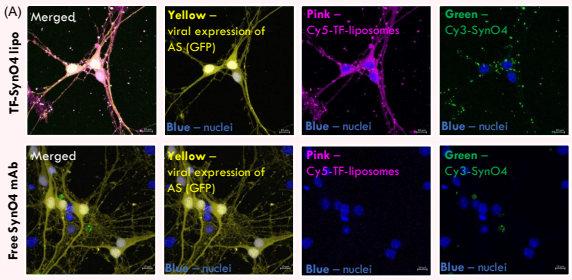

Neuronal uptake was evaluate in primary cortical neurons. The confocal images show a **higher uptake of the synO4 encapsulated liposomes** compared with free Ab (A).

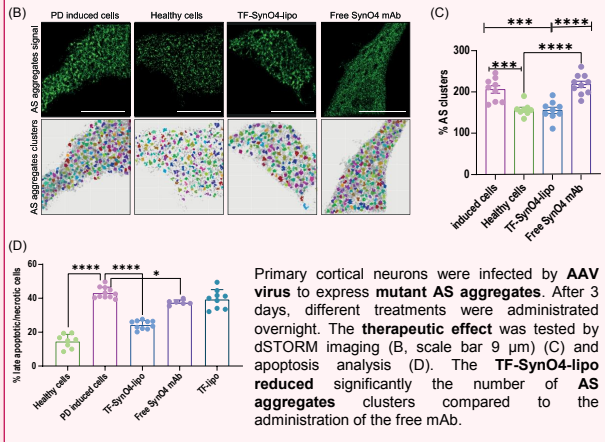

Primary cortical neurons were infected by **AAV virus** to express **mutant AS aggregates**. After 3 days, different treatments were administrated overnight. The **therapeutic effect** was tested by dSTORM imaging (B, scale bar 9 μm) (C) and apoptosis analysis (D). The **TF-SynO4-lipo reduced** significantly the number of **AS aggregates** clusters compared to the administration of the free mAb.

5.*In vivo* delivery and Therapeutic Efficacy

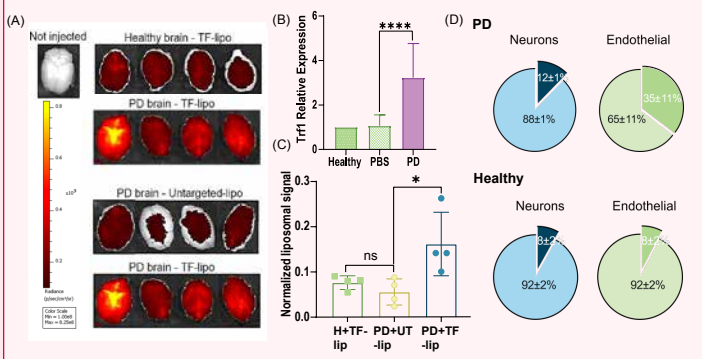

Brain uptake of untargeted (UT-lip) and transferrin modified liposomes (TF-lip) in healthy (H) and PD mice (A and C). Transferrin receptor gene expression in H and PD mice (B). **TF-lip uptake in neurons and endothelial cells was higher in PD mice** (D).

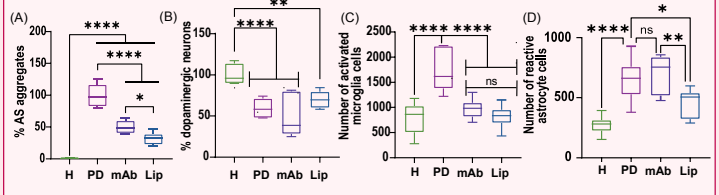

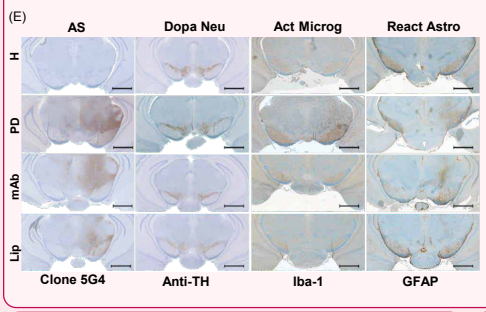

Therapeutic efficacy was evaluated after 4 weeks of treatment. Brain sections (E) were stained with different Ab to quantify AS aggregates (A), dopaminergic neurons (B), activated microglia (C) and reactive astrocytes (D) (scale bar 2 mm).
TF-liposomes reduced AS aggregation and neuro inflammation compared with free mAb treatment.

What we achieved?

Load mAb inside targeted liposome
Cross BBB, **Deliver** mAb in neurons
Reduce AS aggregation and **Neuroinflammation**

PLATFORM for BRAIN DRUG DELIVERY

Supported by

Acknowledgment - The National Fourm for BioInnovators (NFBI) program 2021 initiated by Teva; Israel Innovation Authority for the Nofar Grant; Teva Pharmaceutical Industries Ltd; Azrieli Foundation International Postdoctoral Fellowship.

Modulating the tumor microenvironment with nanomedicine and metronomic therapy to enhance treatment efficacy of immunotherapy

Fotios Mpekris [1], Chrysovalantis Voutouri [1], Myrofora Panagi [1], Rakesh K. Jain[2], Triantafyllos Stylianopoulos[1]

[1] *Cancer Biophysics Laboratory, University of Cyprus;* [2] *Edwin L. Steele Laboratories, Massachusetts General Hospital, USA*

Introduction: Recent preclinical studies suggest that metronomic therapy and nanomedicines **(Figure 1)** can cause similar changes in the tumor microenvironment including improvements in tumor perfusion, drug delivery and activation of the immune system. Here[1], we show experimentally in murine studies, that both approaches can serve as normalization strategies to enhance efficacy of immunotherapy.

Results: To test our hypothesis that nanoparticles have normalization effects similar to metronomic therapy and can improve efficacy of immunotherapy, we employed different doses of the clinically approved Doxil, **Figure 2**.

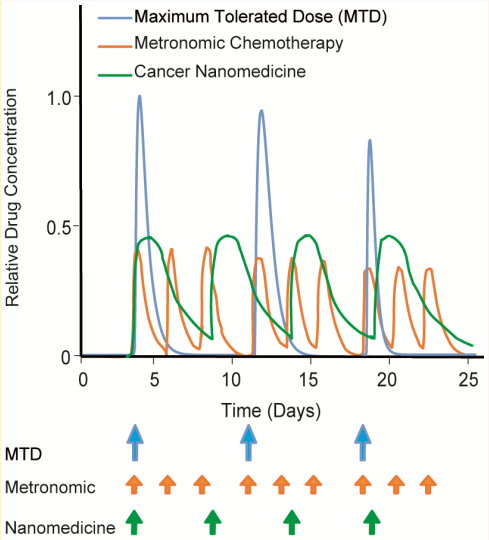

Figure 1. *Schematic of drug concentration as a function of time for MTD, metronomic chemotherapy and nanomedicine.*

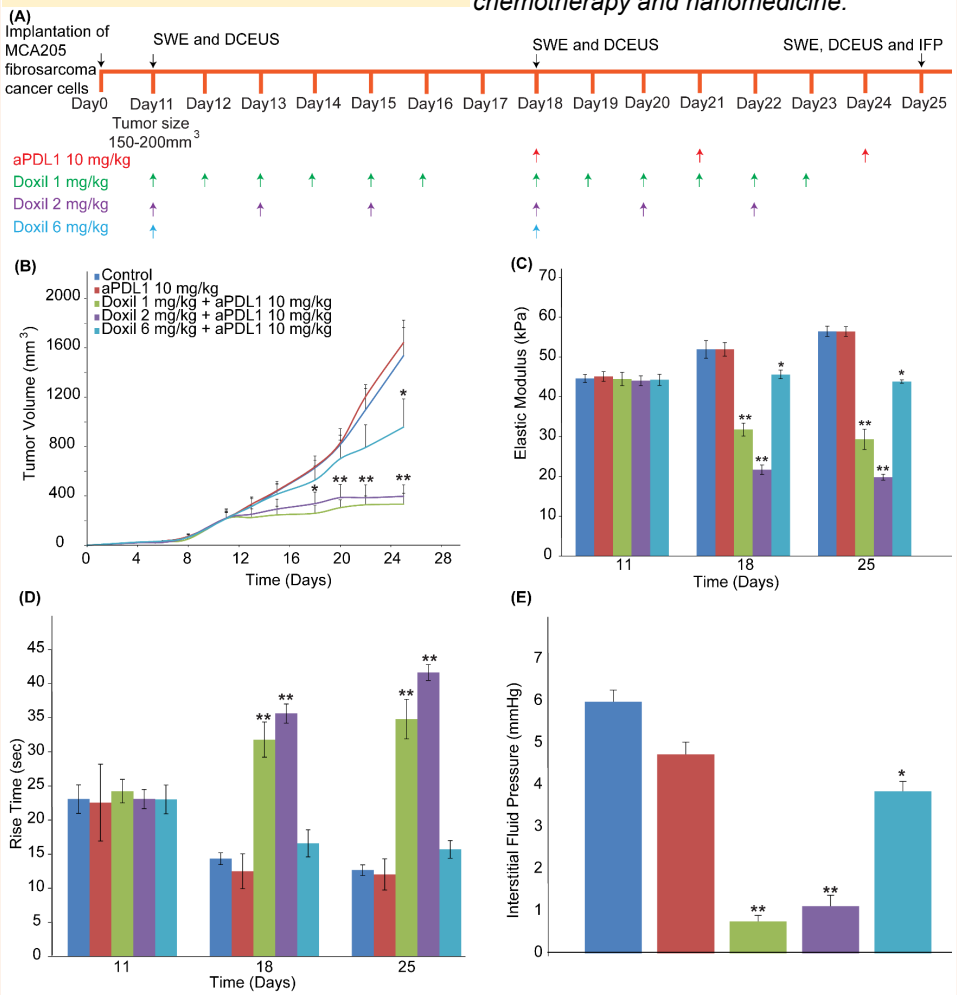

Figure 2. *(A) Treatment protocol. (B) Tumor volume. (C) Quantification of the elastic modulus of the tumors and (D) Time to peak of contrast agents. (E) Interstitial fluid pressure levels.*

References: *1.* Mpekris F. et. al., JCR, 2022.

HIERARCHIC POLYMERIC MICROPLATES FOR DELIVERY OF SMALL MOLECULES AND NANOPARTICLES

ISTITUTO ITALIANO DI TECNOLOGIA

Denise Murgia; Bianca Martins Estevão; Corinne Portioli; Roberto Palomba and Paolo Decuzzi

Laboratory of Nanotechnology for Precision Medicine, Italian Institute of Technology – Genoa (IT)

Presenting poster: denise.murgia@iit.it

INTRODUCTION

In the last decades**, polymeric microparticles** have found application in different biopharmaceutical fields, especially as a controlled drug delivery system [1]. The **top-down fabrication methodology,** one of the currently employed techniques to fabricate particles, allows for tuning the size, shape, particle density and surface area. Applying this procedure, we developed the **Microplates (µPL),** polymeric microparticles owing a peculiar shape, defined by a **square base of 20 × 20 µm and 10 µm height**, homogeneous in size, shape and surface area and developed to deliver a wide variety of payloads [2-4]. Recent optimizations of particle fabrication methods led us to develop a **novel porous version of µPL,** with different physiochemical and biopharmaceutical properties.

METHODS: µPL Fabrication

- **Composition** → Poly(D,L-lactide-co-glycolide) (PLGA) as main polymer and a copolymer
- **Implemented top-down fabrication methodology** → Production of porous µPL
- **Direct and post-production loading strategies** → Curcumin (CURC) directly loaded into the particle structure; fluorescent small molecules (such as Rhodamine B), polystyrene beads nanoparticles (50 and 200 nm) and fluorescent liposomes loaded after particle preparation.
- **µPL morphology** → Scanning Electron Microscopy (SEM), Confocal Microscopy and Fluorescence Microscopy (Fig. 1).
- **Size distribution and particle concentration** → Multisizer system.
- **Drug encapsulation** → HPLC and UV-Vis analyses.

RESULTS: µPL Characterization

✓ **Well-defined square-shaped porous particles.**

✓ **Homogeneous alveolar structure** → size range from 0.4 to 1.5 µm.

✓**Fluorescent CURC emission homogenously detected** → uniform distribution of the drug in the particle structure.

✓ **Distribution of signals from RhB, nanoparticles and fluorescent liposomes** → particles act as a hierarchic system able to housing different pharmaceutical entities.

✓ **Fabrication process yield** → 57.58 ± 4.96 %

✓ **Encapsulation Efficacy** → 12.53 ± 1.08 % CURC; 11.38 ± 1.08 % RhB; between 40-70% for beads of different sizes.

Strategic platform for the simultaneous delivery of drugs owning different physiochemical properties, or nanoparticles / liposomes for sustained drug releases. Further investigations required to role co-polymer and how the number, structure, and pore diameter, and affect the properties of the system.

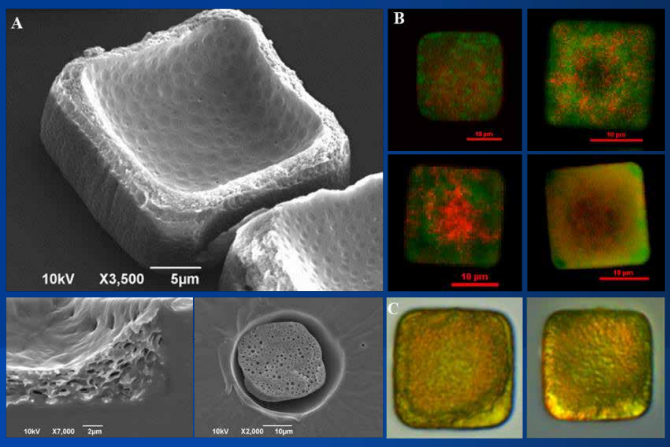

Figure 1: Geometrical characterization of porous µPL: A) SEM image; B) Confocal microscopy (40X) of µPL loaded by CURC and RhB, Beads 50 or 200nm and liposomes; C) Fluorescence microscopy image (40X).

CONCLUSIONS

In conclusion, novel µPL characterized by a peculiar porous structure have been obtained. The preliminary collected results define them as a promising hierarchic platform for multidrug delivery and suitable for various therapeutic applications.

ACKNOWLEDGMENT

This work was partially supported by the European Union's Horizon 2020 Research and Innovation Programme under the Marie Skłodowska-Curie grant agreement no. 754490 (COFUND 2018 "MINDED"), grant agreement no. 872648 (RISE2019 "MEPHOS") and the Fondazione Istituto Italiano di Tecnologia.

REFERENCES

[1] Vilos et al. J Biomed Biotechnol; 2012; 2012:672760.
[2] Di Francesco M, et al. J Control Release; 2020; 319:201-212.
[3] Bedingfield SK, et al. ACS Nano; 2021; 15(9):14475-14491.
[4] Bellotti E, et al. Drug Deliv Transl Res. 2022; 12(8):1829-1842.

Mariia Nesterkina

HIPS HELMHOLTZ Institute for Pharmaceutical Research Saarland

Thermoresponsive chiral-nematic liquid crystals as multifunctional nanostructured material for skin drug delivery

Mariia Nesterkina[1], Olga Vashchenko[2], Pavlo Vashchenko[2], Longin Lisetski[2], Iryna Kravchenko[1], Anna K. H. Hirsch[1,3], Claus-Michael Lehr[1,3]

[1] Helmholtz Institute for Pharmaceutical Research Saarland (HIPS), Campus Building E 8.1, 66123 Saarbrücken, Germany
[2] Institute for Scintillation Materials of National Academy of Sciences of Ukraine, Nauky Ave. 60, 61072 Kharkiv, Ukraine
[3] Department of Pharmacy, Saarland University, Campus Building E8.1, 66123 Saarbrücken, Germany

MAIN IDEA

The current work addresses an innovative strategy to implement the anisotropic properties of thermotropic liquid crystals (LCs) for extending their application in drug delivery. The distinctive feature of aforementioned systems is their temperature-induced on/off switchable permeability as result of their transition to the LC state at normal human skin temperature.

RESULTS

In this regard, we fabricated novel compositions with a thermosensitive core based on natural products – cholesteryl esters and mono-/bicyclic terpenoids (Fig. 1).

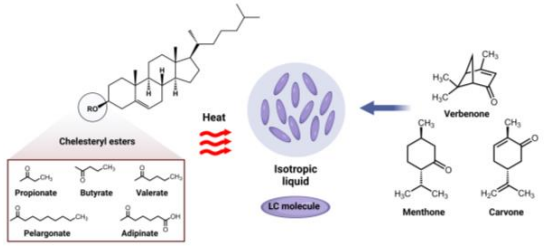

Figure 1. Schematic representation of liquid crystal (LC) system preparation based on cholesteryl esters and terpenoids.

LC mixtures were prepared by mixing of cholesteryl esters according to a multiplicity of mass ratios leading to the formation of four basic formulations – systems **S1**–**S4** (Fig. 2). The basic systems were optimized by doping with mono-/bicyclic terpenoids of 5% or 10% concentration. In total, 24 novel LC systems containing menthone, carvone and verbenone were designed as penetration/permeation enhancers for drug delivery.

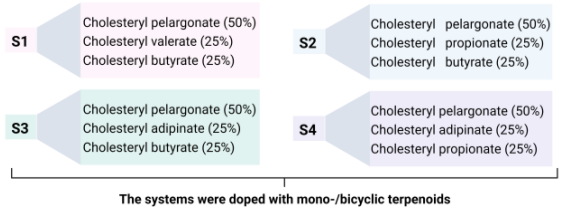

Figure 2. Compositions of liquid crystal systems.

Phase transition to LC state corresponding to human skin temperature was achieved when incorporating 10% of terpenoids into LC systems. This mesomorphic behavior is exemplified by LC properties of system **S1** comprising terpenoids as depicted in Fig. 3.

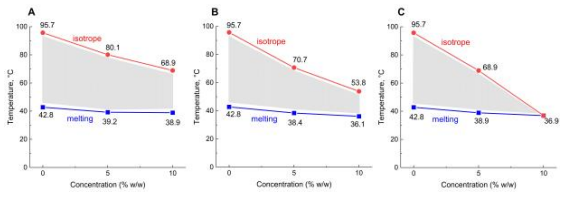

Figure 3. Temperatures of phase transitions "crystal – mesophase" (— squares) and "mesophase – isotropic liquid" (— circles) for system **S1** containing 5–10% of menthone (A), carvone (B) and verbenone (C); ··· liquid crystal state.

FUNDING

The study was performed under the program "Helmholtz-Initiative für Geflüchtete within the Impuls- und Vernetzungsfonds" supported by Helmholtz-Gemeinschaft Deutscher Forschungszentren e.V. This research was also supported by the Alexander von Humboldt Foundation.

To further explore the mesogenic behavior of LC systems, their optical texture was estimated when imaged with polarized optical microscopy (POM, Fig. 4). When pure systems **S1** and **S3** were heated to 43–45 ° C, the focal-conic texture of cholesteric phase began to appear indicating the birefringence properties of materials. When incorporating menthone (10%, w/w) in the LC systems **S1** and **S3**, a different colorful planar texture of the cholesteric phase was observed as illustrated by POM images.

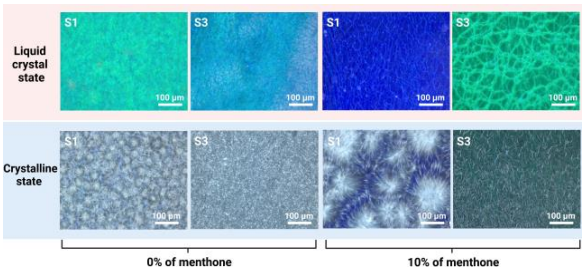

Figure 4. Optical polarizing microscope textures. Crystalline and chiral nematic liquid crystal structure of system **1** (**S1**) and system **3** (**S3**) in their pure form and after incorporation of 10% of menthone.

Furthermore, we describe the dependence of helical pitch on LC formulation for various ternary cholesteric systems doped with terpenoids, suggesting that these chiral dopants are nominally untwisting. Modification of cholesteric helical pitch leads to a visual color change of the LC systems upon their melting on the skin surface. In this context, we may propose that terpenoids are incorporated into quasi-nematic layers formed by cholesteryl esters contributing to the untwisting effect on the pitch (Fig. 5).

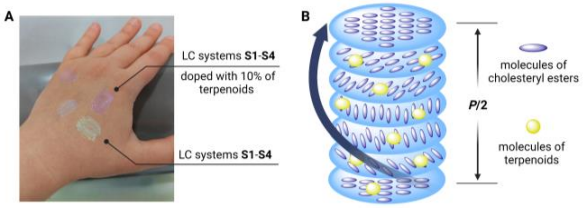

Figure 5. Phase transition of pure liquid crystal (LC) systems **S1**–**S4** and those containing 10% of terpenoids on the skin surface (A). Schematic representation of helical pitch in the cholesteric liquid crystals doped with terpenoids (B).

To prove the basic concept regarding the thermoresponsive LCs as drug-delivery systems for skin applications, we explored their potency by studying *in vitro* and *ex vivo* penetration across artificial Strat-M® membrane and full human skin, respectively. By incorporating model drugs with diverse molecular structures and physicochemical properties into such LC matrix, we explored their potential exploitation for both transdermal and intradermal drug delivery.

CONCLUSIONS AND OUTLOOK

This work provides key results on the stimuli-responsive and adaptive characteristics of LCs as a prerequisite to rationally design drug delivery systems for skin applications. For this purpose, novel thermoresponsive LC systems possessing the phase transition to the liquid-crystal state at normal human skin temperature were developed. We clearly demonstrated the suitability of LC formulations for transdermal drug delivery by in vitro and ex vivo penetration tests, using artificial membranes and full human skin. Prospectively, we intend to exploit these triggerable LCs for "smart" wound dressing that is anticipated to release antibiotics upon the increase of wound temperature as a sign of infection.

Emmanuel Okwelogu

Exploitation of the graphene oxide protein corona in secretome-based biomarker discovery

Emmanuel Okwelogu, Kostas Kostarelos, Sandra Vranic, Marilena Hadjidemetriou*

Nanomedicine Lab | Faculty of Biology, Medicine & Health | University of Manchester | UK

Email: emmanuel.okwelogu@postgrad.manchester.ac.uk; marilena.hadjidemetriou@manchester.ac.uk

INTRODUCTION

- The **cancer cell secretome** is a vital source of potential biomarkers as it consist of **proteins** release **directly from the cancer cells** into the extracellular space.[1]
- However, interference by **highly abundant FBS protein** still possess a **major challenge** to the analysis of **low abundance secreted proteins** in the conditioned media.[2]
- **Graphene oxide (GO)** is a 2-dimensional (2D) nanoparticle which forms a **protein corona** when in contact with biofluids.[3]
- The ability of the **Graphene Oxide (GO) protein corona to enrich low abundance proteins** is utilized here to provide **in-depth analysis of the secretome from different cancer cells grown in FBS-containing media.**

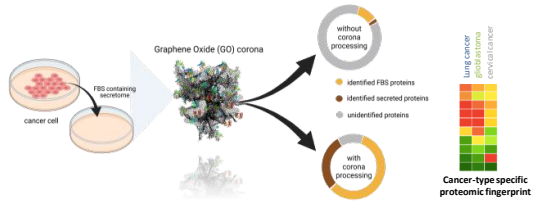

AIMS

- To exploit the graphene oxide protein corona formation in order to enrich the cancer cell secretome of **lung cancer (A549), glioblastoma (U251) and cervical cancer (HeLa) cell line in FBS media.**
- **Proteomically compare the cell secretome** of the three different cancer cell lines

EXPERIMENTAL

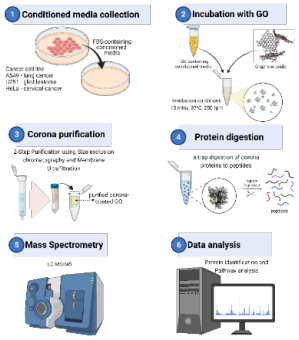

1. Cells were grown in FBS-containing media and the conditioned media was collected after 24 hours.
2. The conditioned media was concentrated and incubated with GO nanoparticles for 10 mins at 250 rpm/37°C to form the GO corona.
3. The GO corona was isolated using a 2-step purification process involving size exclusion chromatography and membrane ultrafiltration.
4. Proteins attached to the corona was dissolved in lysis buffer and digested by the s-trap trypsin digestion process to peptides.
5. Mass spectrometry analysis was performed on the peptides using the Q Exactive HF Orbitrap LC-MS/MS system
6. Raw data was processed using Proteome Discoverer software to identify the proteins from each corona sample and the proteomic pathway was analysis via KEGG pathway analysis

RESULTS

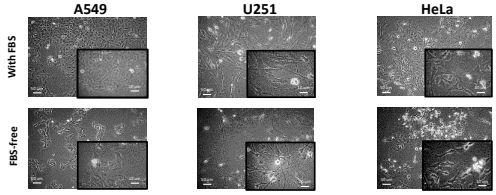

- **Cell images** show changes in cell morphology and confluence in FBS-free media

RESULTS

Enrichment of low abundance proteins

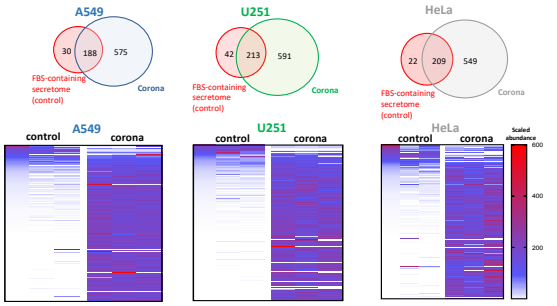

- **Mass spectrometry analysis of the GO corona** showed an increase in the number of **uniquely identified proteins** in comparison to control analysis of the FBS-containing secretome.
- Analysis of the GO corona **enriches** the identification of **low abundant** proteins.

Taxonomical identification of secreted proteins

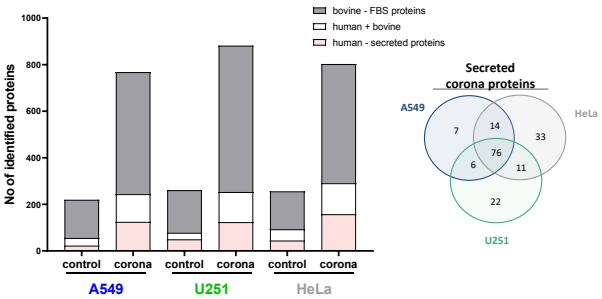

- Analysis of the GO corona **enriches** the identification of **human secreted proteins** among highly abundant FBS proteins
- Identified **unique secretome protein** for each cancer cell type

Pathway analysis

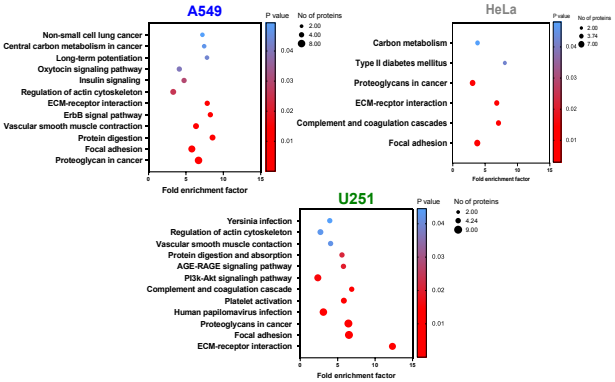

- **KEGG pathway analysis** revealed activation and enrichment of common cancer-related secretome pathways including ECM-receptor interaction, focal adhesion and proteoglycans in cancer.

CONCLUSIONS & FUTURE WORK

- Graphene oxide protein corona **enriched low abundance secretome proteins** in FBS containing media.
- Future study would utilize the graphene oxide enrichment protocol to compare the secretome from matched cancer vs healthy cells and identify potential biomarkers

References

1. Xue, H., Lu, B. & Lai, M. The cancer secretome: a reservoir of biomarkers. *Journal of Translational Medicine* **6**, 52 (2008).
2. Brandi, J. *et al.* Proteomic approaches to decipher cancer cell secretome. *Seminars in cell & developmental biology* **78**, 93–101 (2018).
3. Li, D. *et al.* When biomolecules meet graphene: From molecular level interactions to material design and applications. *Nanoscale* vol. 8 19491–19509 (2016).

Myrofora Panagi

Re-engineering the tumor microenvironment with polymeric micelles to improve the efficacy of nano-immunotherapy in breast cancer

Panagi M.[1], Mpekris F.[1], Chen C.[2], Voutouri C.[1], Martin J.D.[2], Michael C.[1], Kataoka K.[3], Cabral H.[2], Stylianopoulos T.[1]

[1] Cancer Biophysics Laboratory, University of Cyprus, Cyprus;
[2] Department of Bioengineering, The University of Tokyo, Japan;
[3] Innovation Center of NanoMedicine, Kawasaki, Japan

Introduction: Nano-drugs combined with immunotherapy has high potential to improve cancer patient outcomes. However, has a modest effect on survival due to abnormalities in the tumor microenvironment (TME) that inhibit drug delivery. Here[1], taking advantage of the TME-reprogramming capabilities of tranilast, we developed tranilast-loaded micelles (average size ~95nm) combined: (i) with Epirubicin micelles or (ii) with Doxil nanomedicine and immunotherapy (ICB) in mice bearing immunotherapy-resistant breast cancer.

Results: Tranilast micelles modulate mechanical forces and enhance homogeneous accumulation and antitumor efficacy of Epirubicin micelles (EPI/m) and decrease lung metastases **(Figure 1)**. Micelles combined with ICB and Doxil improve therapeutic outcomes as yield to a 100% survival and induce a long-term immune memory in mice **(Figure 2)**.

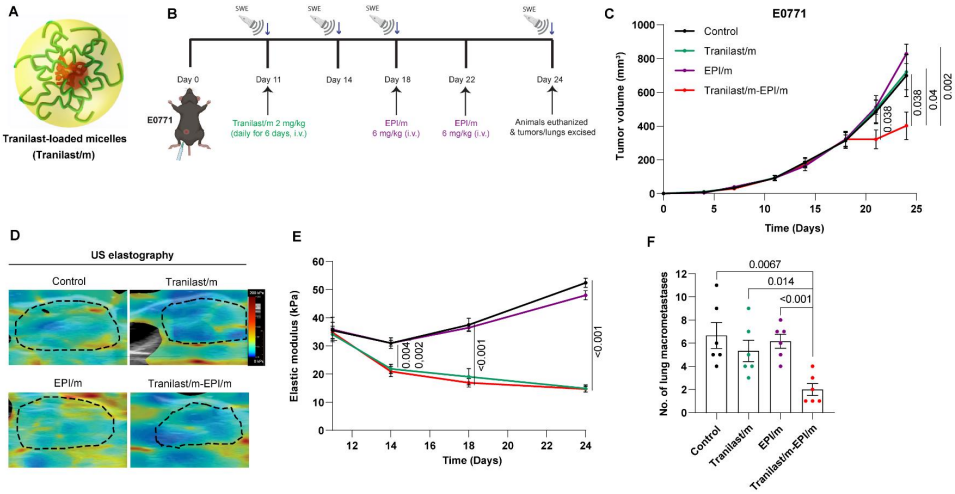

Figure 1. *(A)* Schematic of Tranilast/m. *(B)* Study treatment protocol. Animals received daily intravenous injections of Tranilast/m 2 mg/kg for 6 days and subsequently two doses of EPI/m 6 mg/kg (on days 18 and 22). *(C)* Orthotopic E0771 breast cancer primary tumor growth in mice treated with Tranilast/m, or EPI/m or combination of the two. *(D)* Representative ultrasound elastography heat maps of tumors with blue indicating compliant tissue and red indicating stiff tissue. The dashed black line denotes the tumor margin. *(E)* Elastic modulus values of tumors during treatment using ultrasound elastography. *(F)* Quantification of macroscopic spontaneous lung metastasis formation upon completion of the study.

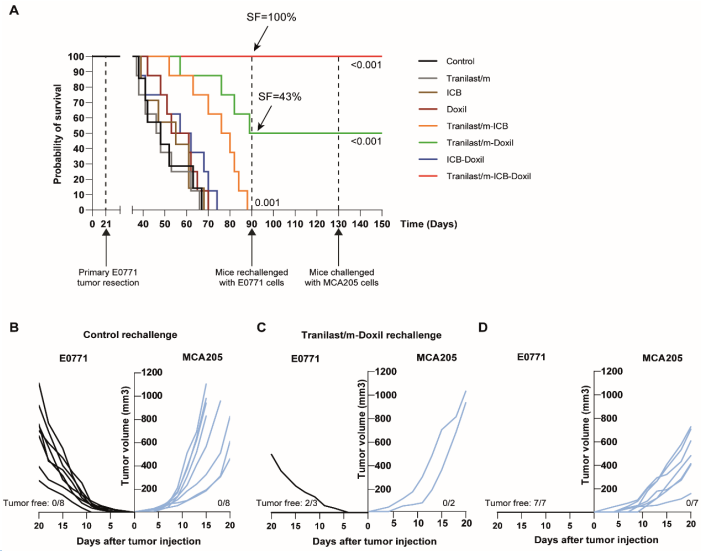

Figure 2. *(A)* Kaplan-Meier survival curves. *(B-D)* Individual growth curves of naïve mice *(B)*, cured mice of Tranilast/m-Doxil group *(C)* and Tranilast/m-ICB-Doxil group *(D)* challenged with E0771 and MCA205 tumor cells. The number of tumor free mice is demonstrated for each study.

References: *1.* Panayi M. et. al., *Nat. Commun.*, 2022, 13, 7165.

Alexandra Paul

A new aptamer delivery system transporting nucleic acids to T-cells for glioblastoma immunotherapy.

Alexandra R. Paul, Alaa Zam, Alessia Marrocu, Alexandra Moreno Mitchell, Nadia Rouatbi, Adam A. Walters & Khuloud T. Al-Jamal.

School of Cancer and Pharmaceutical Sciences, Institute of Pharmaceutical Science, King's College London, UK

alexandra_rosie.paul@kcl.ac.uk @alexandrarosiee

Introduction

- Glioblastoma (GBM) remains immensely difficult to treat, with most patients not surviving beyond 15 months after diagnosis.[1]
- Lipid nanoparticles (LNPs) can be used to deliver RNA therapies to their chosen target.[2] Challenges are delivering the LNPs to the correct locations and loss of therapeutics to non-desirable cells.
- Conjugating a specific targeting agent to the outside of the LNPs could be a way to tackle this, as the targeting agent guides the LNPs to the desired T-cell, such as aptamers.
- Aptamers are single-stranded oligonucleotides that bind strongly and specifically to diverse targets.[3] Aptamers can be targeted drug carriers or used as a targeting ligand, increasing efficacy and minimising side effects.

Aims

This research aims to create a therapeutic delivery system using novel T-cell targeting aptamers to improve the therapeutic effect of LNPs -mOX40 being delivered to immune cells in GBM *in vivo* models. Delivering mOX40 to T-cells will overexpress this marker and trigger an immune response with the T-cells and their reciprocal APC.

Methodology

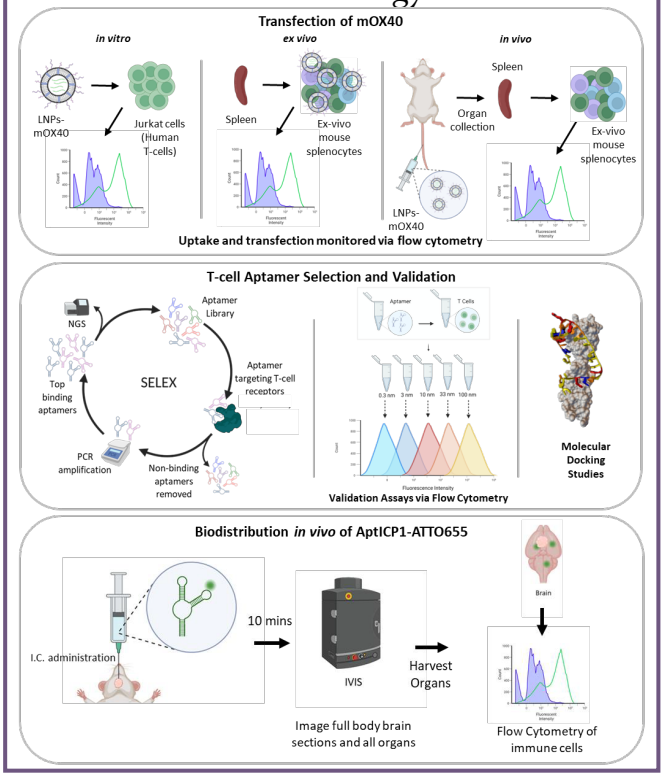

References

1. M. Koshy, J. L. Villano, T. A. Dolecek, A. Howard, U. Mahmood, S. J. Chmura, R. R. Weichselbaum and B. J. McCarthy, Improved survival time trends for glioblastoma using the SEER 17 population-based registries, *J Neurooncol*, 2012, **107**, 207–212.
2. J. C. Burnett, J. J. Rossi and K. Tiemann, Current progress of siRNA/shRNA therapeutics in clinical trials, *Biotechnol J*, 2011, **6**, 1130–1146.
3. M. R. Dunn, R. M. Jimenez and J. C. Chaput, Analysis of aptamer discovery and technology, *Nat Rev Chem*, 2017, **1**, 0076.

Results

In vitro, ex-vivo and *in vivo* transfection of mOX40

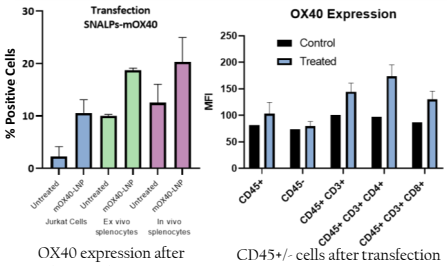

OX40 expression after transfection of LNPs-mOX40

CD45+/- cells after transfection of LNPs -mOX40 *in vivo*.

The transfection data shows a ~9% increase of OX40 expression across *in vitro*, *ex vivo* and *in vivo* T-cells after they had been transfected with LNPs -mOX40 (n = 3). Making these LNPs more targeted with a T-cell aptamer will hypothetically increase the uptake in these cells.

T-cell Aptamer Selection and Validation

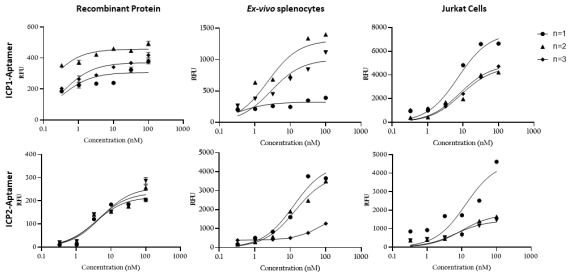

- Eight cycles of SELEX on ICP1 and ICP2 recombinant proteins, using a randomised DNA library (30 nucleotides) followed by Next Generation Sequencing.
- The 3 top aptamer candidates for each underwent validation studies: *in vitro* and *ex vivo* binding affinity assays across both human and mouse T-cells.
- These have produced K_ds ranging from 0.33- 16.66 nM.

Biodistribution *in vivo* of AptICP1-ATTO655

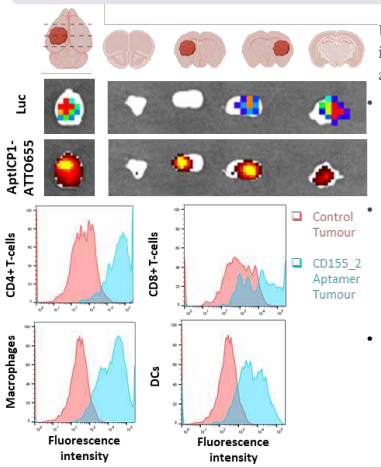

Uptake of ICP1-ATTO655 aptamer in GL261 tumours after I.C. administration for 10 minutes.

- The *in vivo* imaging results show co-localisation between the aptamer and the Luc+ tumours with distribution to CD45+/- cells.
- Histograms from the flow cytometry analysis showing the shift in fluorescence intensity between the control tumour and the tumour treated with AptICP1-ATTO655.
- The data of the tumour samples show uptake in all immune cells that were stained for (T-cells, Macrophages, DCs), with the highest accumulation in the CD4+ T-cells.

Future Work

- Run aptamer stability studies over time *in vivo*
- Conjugate AptICP1 to the surface of the LNPs -mOX40
- Compare transfection of OX40 with and without the aptamer on the LNP surface.

Ling Peng

Modular Self-assembling Supramolecular Dendrimers for Biomedical Applications

Dr Ling PENG

Biomolécules et Biomatériaux, Equipe Labellise par La Ligue
Centre Interdisciplinaire de Nanoscience de Marseille (CINaM), Aix-Marseille Université, CNRS, France

Background

Dendrimer: ideal material for nanomedicine

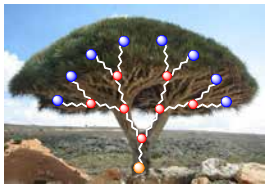

Synthetic macromolecule with dendritic structure

Lyu & Peng, *Nat Biomed Eng* **2017**, *1*, 686

well-defined structure
unique multivalency
inner cavities
nanosize *per se*

Nanocarrier for drug delivery

Bio-inspired dendrimers

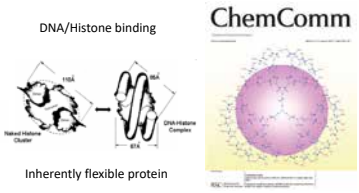

Wu J. et al, *Chem. Commun.* **2005**, 313.

Dendrimer for RNA delivery in cancer therapy

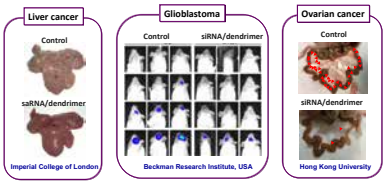

Hepatology **2014**, *59*, 216. *Nat Commun* **2016**, *7*, 10637. *Mol Ther* **2018**, *26*, 70.

Scheduled for clinical trials in USA and UK

Delayed due to the GMP production of dendrimer

Innovation Concept

Self-assembling supramolecular dendrimer

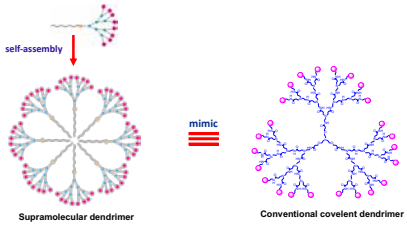

Yu et al, *Angew Chem Int Ed* **2012**, *51*, 8478
Liu et al, *Angew Chem Int Ed* **2014**, *53*, 11822

Modular and adaptive dendrimers for biomedical applications

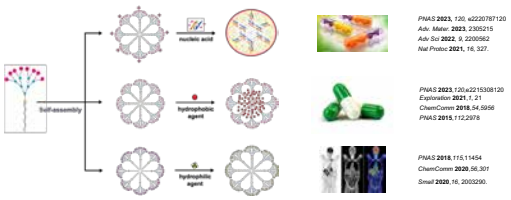

Lyu et al, *Acc Chem Res* **2020**, *53*, 2936
Chen et al, *Acc Mater Res* **2022**, *3*, 484

Proof-of-concept studies

Nucleic acid delivery : from self-assembly to gene silence

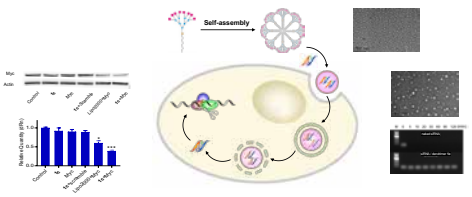

Chen et al, *Small* **2016**, *12*, 3667
Dhumal et al, *Nano Res* **2021**, *14*, 2247
Chen et al, *Nat Protoc* **2021**, *16*, 327.
Chen et al, *PNAS* **2023**, *120*, e2220787120

Drug delivery: overcome tumor heterogeneity and drug resistance

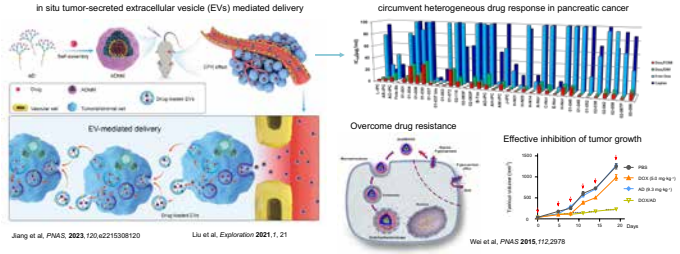

Jiang et al, *PNAS*, **2023**, *120*, e2215308120 Liu et al, *Exploration* **2021**, *1*, 21

Wei et al, *PNAS* **2015**, *112*, 2978

Bioimaging: detect otherwise undetectable tumor

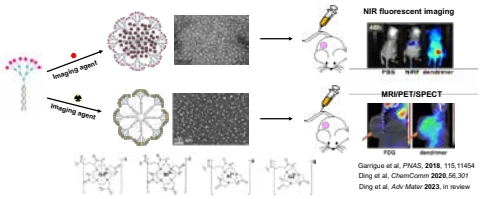

Garrigue et al, *PNAS*, **2018**, *115*, 11454
Ding et al, *ChemComm* **2020**, *56*, 301
Ding et al, *Adv Mater* **2023**, in review

Antibacterial agent: dynamic self-assembling to overcome multidrug resistance

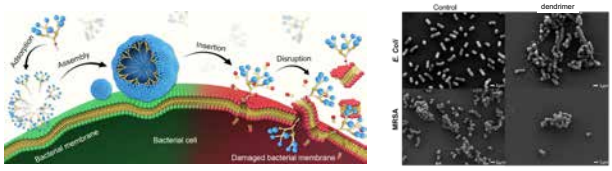

Dhumal et al, *Nanoscale*, **2022**, *14*, 9286 Galanakou et al, *Biomater Sci* **2023**, *11*, 3379.

Noah et al, *ACS Infectious Diseases* **2023**, in review.

Perspectives

Dendrimer engineering : from design concept to green, sustainable and intelligent synthesis
Biomedical application: from proof-of-concept to unmet medical need and precision medicine

supported by La Ligue and EU FP7, H2020 and Horizon Europe (DENANORNA, Target4cancer, NANOGLIO, TARBRAINFEC, NAN-4-TUM, iNanoGUN, antineuropatho, OLIGOMED, SAFE-N-MEDTECH)

Yannick Pilger

Julius-Maximilians-
UNIVERSITÄT
WÜRZBURG

Fakultät für Chemie und Pharmazie
MAKROMOLEKULARE
CHEMIE

Macromolecular immunodrug delivery guided by self-immolative nanobody modifications

Yannick A. Pilger,[1] Maximilian Scherger,[1,2]
Jo Van Ginderachter,[3] und **Lutz Nuhn**[1,*]

1: Institut für Funktionswerkstoffe und Biofabrikation, Lehrstuhl für Makromolekulare Chemie, Julius-Maximilians-Universität Würzburg
2: Max-Planck-Institut für Polymerforschung Mainz 3: VIB and Vrije Universiteit Brussek, Belgium

Antibodies, nanobodies and other antibody-derived immune proteins can play a vital role in targeted immunotherapeutic drug delivery. Because of their innate targeting capabilities they enable site-specific delivery of bioactive compounds.
However, to circumvent a reduction in biological acitvity for the conjugated active compounds, a reversibility of the covalent conjugation to the protein would be advantageous. Additionally, enhanced blood circulation can be achieved by reversibly decorating the protein surface with stealth polymer chains.
To address these needs, we present a package of strategies to reversibly modify proteins such as nanobodies by self-immolative linkers with bioactive compounds and Raft-polymerization derived stealth polymers. This assures a targeted delivery of the bioactive compound as well as prolonging the proteins' blood circulation properties.

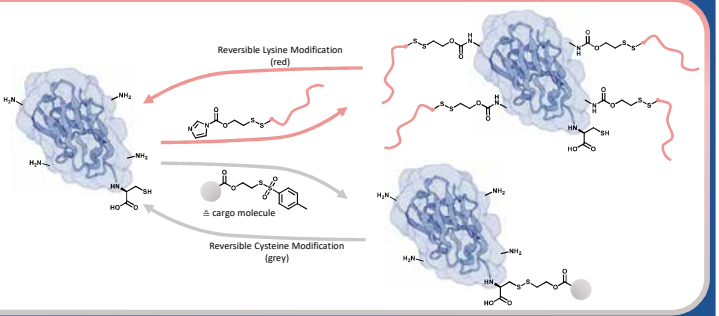

Self-Immolative Linker Conjugate Synthesis and Biomodification

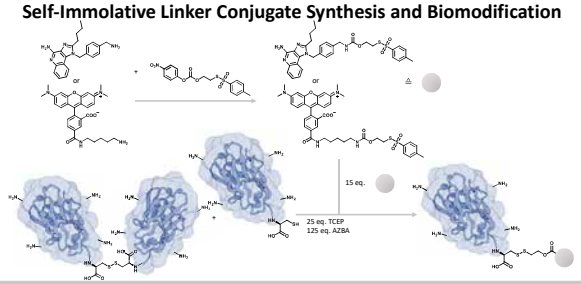

RAFT-Polymer Self-Immolative Linker Conjugate Synthesis

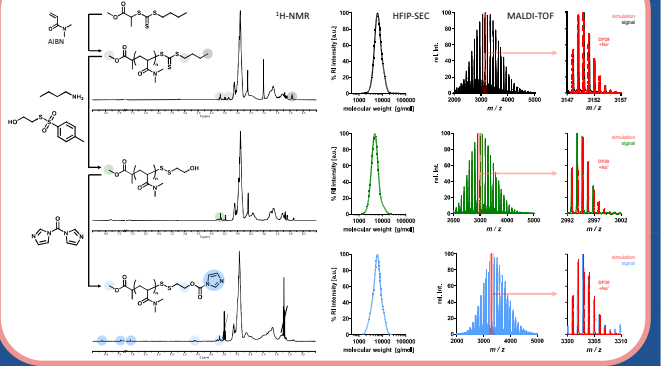

Cargo Conjugation and Reversibility Study

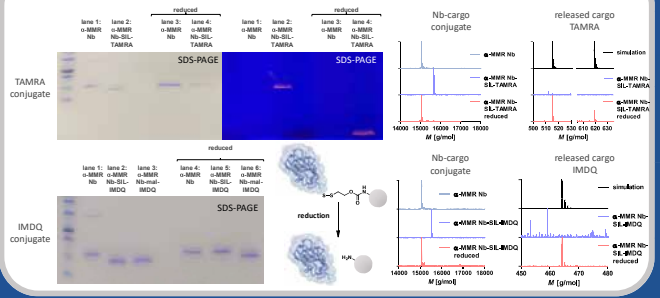

Protein-Polymer Conjugate Synthesis and Reversibility Study

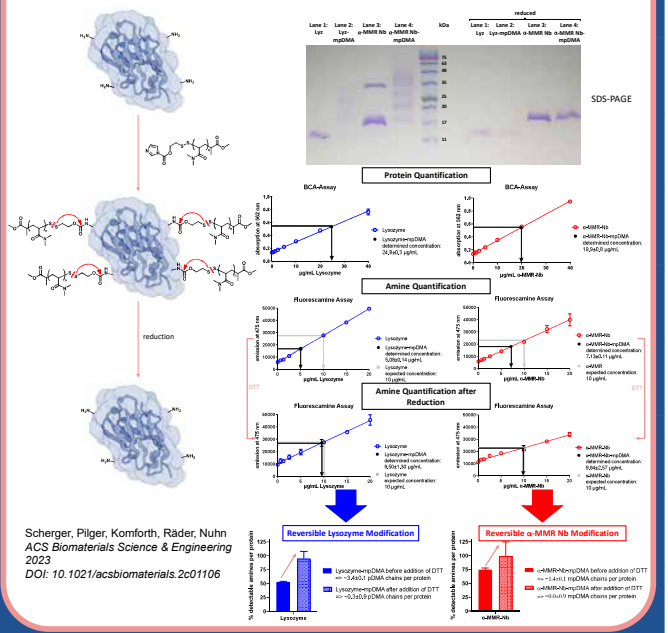

Cell Uptake and Plasma Stability

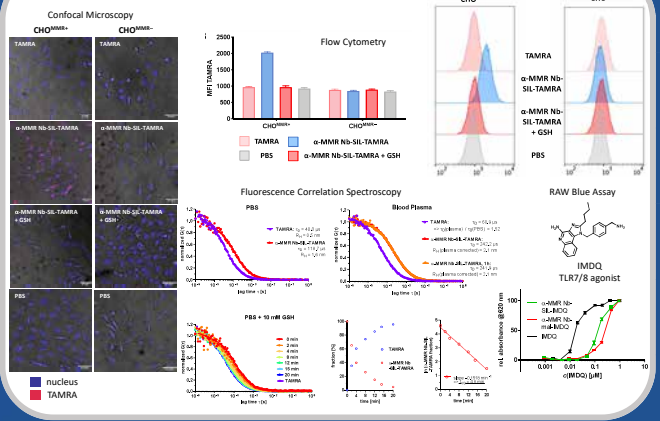

Scherger, Pilger, Komforth, Räder, Nuhn
ACS Biomaterials Science & Engineering 2023
DOI: 10.1021/acsbiomaterials.2c01106

Weitere Infos: www.chemie.uni-wuerzburg.de/mmc
Kontakte: lutz.nuhn@uni-wuerzburg.de
@NuhnLab @nuhnlab

UNI WÜ DFG Deutsche Forschungsgemeinschaft
Emmy Noether-Programm
SFB 1066
FCI FONDS DER CHEMISCHEN INDUSTRIE

Advanced Nano and Micro medicines to tackle Neurological Disorder

Corinne Portioli[1*], Raffaele Spanò[1], Denise Murgia[1], Bianca Martins Estevão[1], Anna Lisa Palange[1], Paolo Decuzzi[1]

[1]Laboratory of Nanotechnology for Precision Medicine, Italian Institute of Technology – Genoa (IT)

** Poster presenter:* ***corinne.portioli@iit.it***

Introduction

Poly(D,L-lactide-co-glycolide) (PLGA) is the main component of a plethora of drug delivery systems (in the form of nanoparticles, microparticles, and implants), that have been proposed for a variety of biomedical applications[1], including brain diseases[2]. Neurological disorders, which comprise developmental and degenerative diseases, ischemic stroke, and brain tumors, represent a major and increasing global health challenge that requires dedicated resources gathering[3]. **With the aim of finding new therapeutic approaches for those diseases, fast and efficient long-term treatments are needed to speed up the possibility of new cures. A platform based on square polymeric microparticles called PLGA-microPlates (μPL), has been developed to deliver a wide range of payloads**. They are characterized by homogeneous size, shape and surface area[4-7]. μPL loaded with the antipsychotic drug risperidone (RSP) have been use to treat schizophrenia[6] (*Fig.1A)*. Another PLGA-based technology has been developed for intra-vascular administration: Discoidal Polymeric Nanoconstructs (DPN) carrying the clinical formulation of the tissue plasminogen activator (tPA) were proposed as new thrombolytic agent (tPA-DPN)[7] (*Fig.1B*). Interestingly, a novel top-down fabrication process has been proposed to obtain square-defined PLGA μPL, as a versatile platform for the sustained drug delivery of new chemical entities for the treatment of neurodevelopmental disorders (NDDs) (*in preparation, Fig. 1C*).

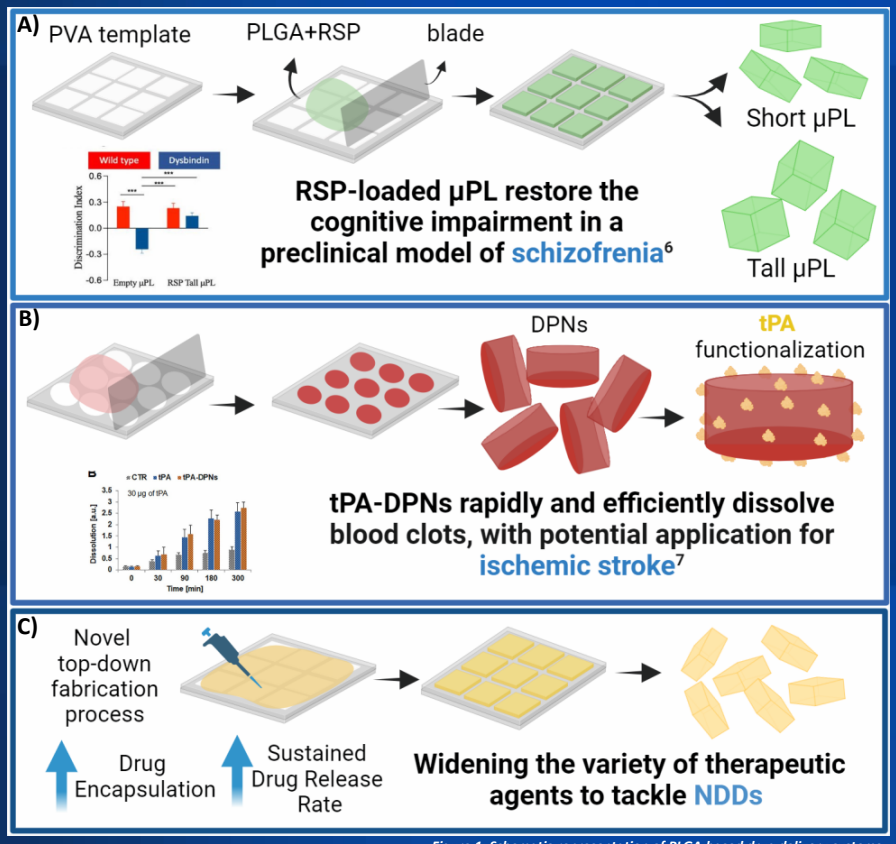

Figure 1: Schematic representation of PLGA-based drug delivery systems developed to tackle schizophrenia (A), ischemic stroke (B) and NDDs (C).

Methods

- ✓ Characterization of mechanical, physico-chemical, and pharmacological properties
- ✓ Morphology evaluation – SEM and fluorescence/confocal microscopy;
- ✓ Loading, encapsulation efficiency, and drug release profiles, under physiologically relevant conditions, by analytical and molecular assays – Multisizer system. HPLC and UV-Vis

Results

- μPL configurations have a well-defined shape and high fabrication yielding (50-70%). Drug release profiles were sustained for all the loaded drugs. Tall μPL have the slowest release up to 3months compared to short μPL. *In vivo*, In temporal order object recognition task, mice treated with a single *ip* injection of RSP loaded-μPL outperform those receiving the daily administration of free RSP.
- tPA-DPN preserved over 70% of the tPA original activity after 3h of exposure to serum proteins. Under dynamic conditions, tPA-DPNs dissolved clots more efficiently than free tPA. *In vivo*, tPA-DPN outperform the lytic activity of free-tPA in terms of recanalization events and clot area reduction.

Discussion and future prospective

RSP-loaded μPL are a promising platform for improving symptoms associated to schizophrenia, indeed the sustained release of antipsychotics from a single injection of μPL can rescue cognitive impairment up to several weeks. Moreover, the long-term efficacy with one single administration could be of clinical relevance in terms of patient's compliance and adherence to the treatment regimen.

tPA-DPN are promising nanotools for enhancing potency and safety of thrombolytic therapies, especially for those brain conditions already impaired. This is due to the conjugation of tPA with preserved lytic activity, the deformability and blood circulating time of DPN together with the faster blood clot dissolution. Further validation of this technology in a preclinical ischemic animal model is ongoing (*in preparation*).

We here propose a versatile platform obtained with fabrication process relying on soft lithographic techniques and leading to microsystems with a peculiar size, shape, surface, and tunable mechanical properties, critical aspects for the sustained delivery of new chemical entities, which could be effectively used in treating neurological conditions where small therapeutic doses can be provided continuously over weeks upon a single administration, increased compliance with the reduction of the administration's frequency, and lower side effects.

Acknowledgement *This work was partially supported by the European Union's Horizon 2020 Research and Innovation Programme under the Marie Skłodowska-Curie grant agreement no. 754490 (COFUND 2018 "MINDED"), and the Fondazione Istituto Italiano di Tecnologia.*

References: [1]Rocha et al., Int J Mol Sci. 2022 Feb 12;23(4):2034, [2]Pinto et al., Ageing Res Rev. 2022 Aug;79:101658, [3]Ding et al., Front Public Health. 2022 Nov 29;10:952161, [4]Di Francesco et al., J Control Release. 2020 Mar 10;319:201-212, [5]Bedingfield et al., ACS Nano. 2021 Sep 28;15(9):14475-14491, [6]Bellotti et al., Drug Deliv Transl Res. 2022 Aug;12(8):1829-1842, [7]Colasuonno et al., ACS Nano. 2018 Dec 26;12(12):12224-12237.

Lien Sabrina Reichel

Optimization of mixed micelles based on oppositely charged block copolymers for application in gene delivery

L. S. Reichel, K. Leer, J. Kimmig, S. Hoeppener, S. Zechel, U. S. Schubert, A. Traeger

Laboratory of Organic and Macromolecular Chemistry (IOMC)
Jena Center for Soft Matter (JCSM), Friedrich Schiller University Jena, Germany
nano-traeger.de

Motivation

- Non-viral, cationic polymer-based delivery systems provide easily adaptable composition and architecture.
- Hydrophobic moieties revealed superior efficiency in gene delivery due to membrane interaction, while stealth and anionic moieties reduce toxicity and serum interactions.[1]
- Combination of hydrophobic *n*-butyl acrylate (*n*BA), stealth monomer *N*-acryloylmorpholine (NAM) with positively charged guanidinopropyl acrylamide (GPAm)[2] or negatively charged carboxyethyl acrylamide (CEAm), resulting in oppositely charged diblock copolymers.
- Mixed micelles assembled at different charge ratios for effective transfection and high biocompatibility.

Results & Discussion

Assembly of oppositely charged block copolymers to mixed micelles

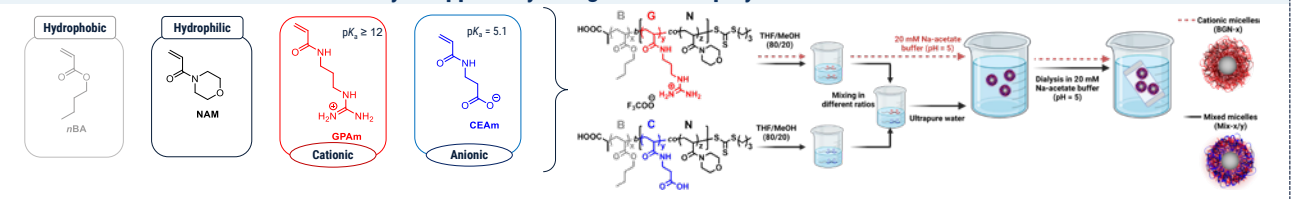

Figure1. Assembly of BGN- and Mix-micelles. Assembly method to generate cationic micelles (dashed red arrows) and mixed micelles (solid arrows) by solvent exchange. x: mol% GPAm and y: mol% CEAm).

Biological screening

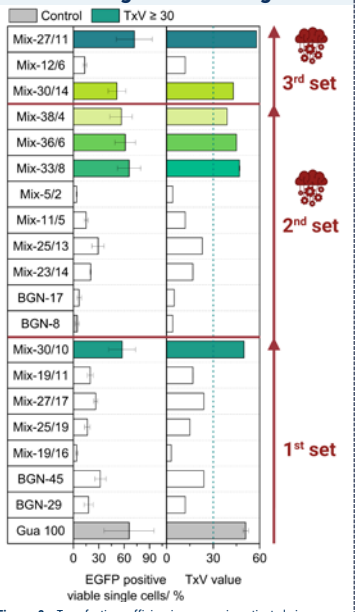

Figure 2. Transfection efficiencies were investigated in serum reduced medium with 2% serum (D2H). The 1st set was biologically investigated. The 2nd and 3rd were optimized by machine learning-based model to find the scope of the best performers and the boundary conditions. EGFP expression was analyzed via flow cytometry. The higher the TxV value (**T**ransfection efficiency x **V**iability), the more intense the color code.

Hit polymers

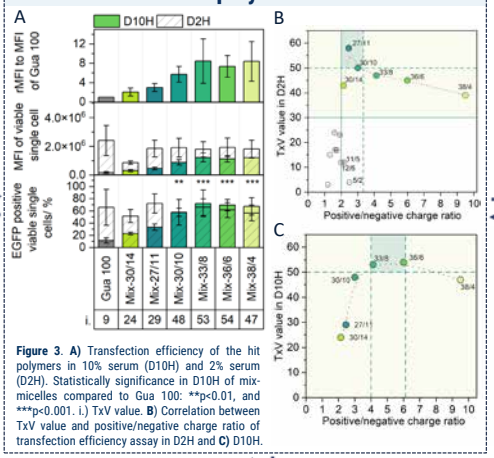

Figure 3. A) Transfection efficiency of the hit polymers in 10% serum (D10H) and 2% serum (D2H). Statistically significance in D10H of mix-micelles compared to Gua 100: **p<0.01, and ***p<0.001. i.) TxV value. **B)** Correlation between TxV value and positive/negative charge ratio of transfection efficiency assay in D2H and **C)** D10H.

Machine learning-based optimization

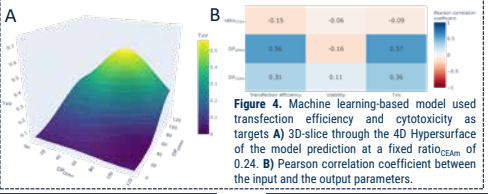

Figure 4. Machine learning-based model used transfection efficiency and cytotoxicity as targets **A)** 3D-slice through the 4D Hypersurface of the model prediction at a fixed ratio$_{CEAm}$ of 0.24. **B)** Pearson correlation coefficient between the input and the output parameters.

Characterization

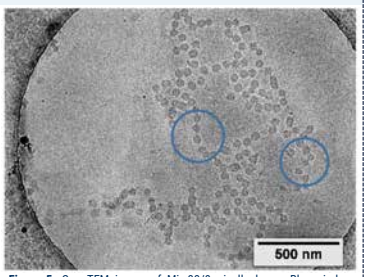

Figure 5. Cryo-TEM image of Mix-33/8-micelleplexes. Blue circles highlight the areas where the "beads-on-a-string" motif is visible.

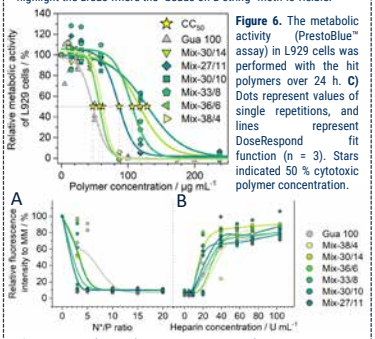

Figure 6. The metabolic activity (PrestoBlue™ assay) in L929 cells was performed with the hit polymers over 24 h. **C)** Dots represent values of single repetitions, and lines represent DoseRespond fit function (n = 3). Stars indicated 50 % cytotoxic polymer concentration.

Figure 7. The polymer-genetic material interaction was calorimetrically investigated. **A)** Decreased fluorescence intensity correlates with the ability of the polymer to complex genetic material. **B)** Increased in fluorescence intensity correlates with the release of genetic material.

Conclusion

- ✓ Oppositely charged guanidinium- and carboxy-based diblocks were assembled into mix-micelles at different charge ratios with sureplus of positive charge.
- ✓ Machine learning was successfully applied to optimize a complex polymer library for gene delivery.
- ✓ Optimal mixed micelle compositions successfully avoid strong serum interaction and trigger internalization yielding high transfection efficiency and viabily.

Acknowledgments

This work was supported by the Collaborative Research Center PolyTarget (SFB 1278—project B01 and Z01) funded by the German Research Foundation (DFG) and the Bundesministerium für Bildung und Forschung (BMBF, Germany, #13XP5034A PolyBioMik). Further fundings are supported by the Free State of Thuringia and the European Social Fund. Figures were created by BioRender.com

References:
[1] F. Richter, K. Leer, L. Martin, P. Mapfumo, J. I. Solomun, M. T. Kuchenbrod, S. Hoeppener, J. C. Brendel, A. Traeger, Nanobiotechnology 2021, 19, 292.
[2] F. Richter, L. Martin, K. Leer, E. Moek, F. Hausig, J. C. Brendel, A. Traeger, J. Mater. Chem. B. 2020,8, 5026-5041.
The poster is presenting the results of submitted manuscript: L. Leer, L.S. Reichel, J. Kimmig, F. Richter, S. Hoeppener, J. C. Brendel, S. Zechel, U.S. Schubert, A. Traeger. Optimization of Mixed Micelles Based on Oppositely Charged Block Copolymers by Machine Learning for Application in Gene Delivery. Small.

FRIEDRICH-SCHILLER-UNIVERSITÄT JENA

Susanne Resch

Cluster decorated functional DNA origami based biosensor: Towards safe nano-innovations

Susanne Resch*[1], Nerea Argarate[1], Clemens Wolf[1], Johanna K. Scheper[1], Andreas Falk[1]

[1]BioNanoNet Forschungsgesellschaft mbH, Graz, Austria

BioNanoNet Forschungsgesellschaft mbH
Kaiser-Josef-Platz 9, 8010 Graz, Austria
*susanne.resch@bnn.at
www.bnn.at

DNA origami based biosensor

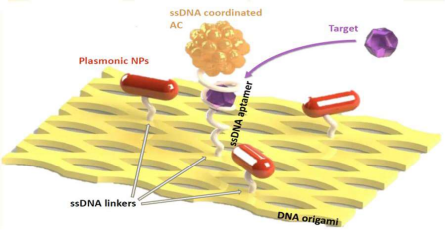

Figure 1. Cluster decorated DNA origami based biosensor.

The DeDNAed project intends to:

- Develop a **cutting-edge bioanalytical biosensor platform** with advanced sensitivity and versatility using **SERS** as an **ultrafast optical analysis method.**
- Assemble and integrate sensing elements using **DNA origami** as a **"nano-breadboard"**.
- **Use single-stranded DNA (ssDNA)** as "**solder**" to attach elements to DNA origami.
- Design and synthesize an appropriate DNA origami platform.
- Use atomic nanocluster decorated aptamers as bioreceptor elements for aflatoxin B1 detection and use atomic nanocluster decorated antibodies as bioreceptor elements.
- **Design appropriate plasmonic nanoparticles** for SERS and their surface functionalization.
- Integrate the DNA origami hybrids onto solid and flexible surfaces.
- **Integrate and validate** the DeDNAed SERS biosensor for potential application in the Biomedical and Food Safety sectors.

Aflatoxin B1 detection - A potent carcinogen

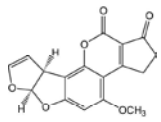

Figure 2. Aflatoxin B1 structure.

- Detection of Aflatoxin B1 (AFB1)
- Most potent genotoxic and carcinogenic mycotoxin
- Linked to hepatocellular carcinoma (HCC)
- High risk for grain mill workers
- Contaminant in food such as cereals
- MRL limits = 2 µg/kg in cereals

Nanomaterials in SERS readout strategies

- **Surface-enhanced Raman Scattering (SERS) enhancement**[1,2], **Raman hot spot,** is formed in the interparticle gaps of DNA origami functionalized with gold NPs specific spatial arrangement due to coupling of the surface plasmon resonance.
- However, nanocomponents' effects on humans and environment need to be studied using SbD actions during the product life-time.

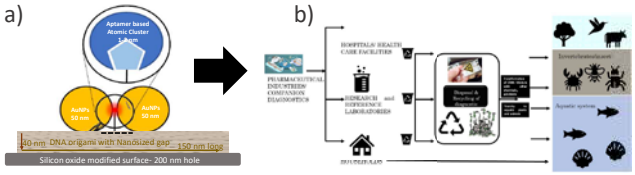

Figure 3. a) Integration of nanoscale components in DeDNAed biosensor, and (b) risks of nanoIVD devices life-cycle.

Safe-by-Design (SbD) actions

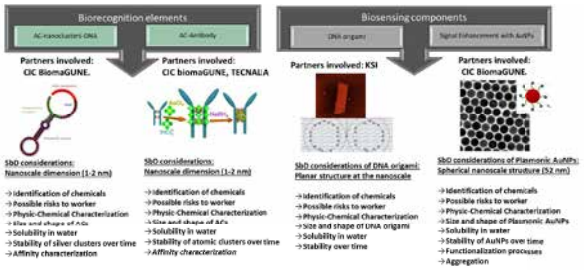

Figure 4. Suggested Safe-by-Design actions.

Risks of integrating nanoscale dimension materials:

Phase 1: Design, synthesis of nanoscale dimension materials

- **SbD assessment –** Several types of nanoscale materials are in development phase
  → Define complete Phys-Chem characteristics

Phase 2: Integration of nanoscale materials to DNA origami

- **SbD assessment –** Integration of nanoscale materials to DNA origami surface by complementary short oligo
  → Consider size, shape, stability

Phase 3: Integration of DNA origami hybrids on surfaces

- **SbD assessment –** Integration of DNA origami hybrids to SiO_2 modified wafer (nanometer surface 200 nm holes), stability of DNA origami hybrids on surface and risk of release
  → Check stability of the oligos binding and risk of release

Sustainability-by-Design considerations

Multiplexing consideration
- **SusbD consideration –** detection of multiple analytes in one device

Environmentally friendly components
- **SusbD consideration –** bio-based nanomaterials for SERS

Miniaturization: reduced reagents volumes and samples needed
- **SusbD consideration –** lower cost in reagents and samples

Designing sustainable surfaces
- **SusbD consideration –** recyclable, reusable and friendly design

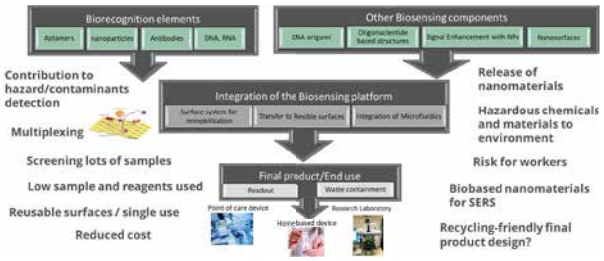

Figure 5. Sustainability-by-Design considerations during the different development stages and use phases.

CONCLUSION

DeDNAed will foster a safer nano-enabled biosensor considering the Safe-by-Design approach and sustainability aspects[3]. Several nanocomponents are in the development stage such as atomic nanocluster-decorated aptamers and antibodies as well as DNA origami and gold NPs. Unique and novel properties and materials attributes need to be checked for unanticipated hazard or exposure behavior. DeDNAed will define a preliminary hazard/risk assessment and control plans for the DNA origami biosensor nanocomponents.

[1] *J. Phys. Chem. Lett.* 2013, 4, 23, 4140–4145. DOI: https://doi.org/10.1021/jz402076b.
[2] *Nat Commun* 5, 3448 (2014). https://doi.org/10.1038/ncomms4448
[3] European Commission, Joint Research Centre, 2022, https://data.europa.eu/doi/10.2760/487955

Acknowledgements:

The research for this work has received funding from the project DeDNAed (grant agreement No 964248) under the European Union's Horizon 2020 research and innovation programme.

DEDNAED

Nadia Rouatbi

In vivo application of CRISPR/Cas9 gene editing using lipid nanocarriers for therapeutic immune target identification in Glioblastoma

Rouatbi, N.[1], Zam, A.[1], Lim, Y.[1], Costa, P.M.[1] , Walters, A.W.[1], Wang, J.T.[1], Grant, V.[2]
Arnold, J.[1] , Pollard, S.M.[2], J.[1] & Al-Jamal, K.T[1]

[1]Institute of Pharmaceutical Sciences, Faculty of Life Sciences and Medicine, King's College London
[2]MRC Centre for Regenerative Medicine, University of Edinburgh

INTRODUCTION

- Little progress has been accomplished in the clinical translation of immunotherapy for glioblastoma (GBM). The highly immunosuppressive tumour microenvironment (TME) and the presence of GBM stem cells (GSC) are major contributors to tumour growth and multi-treatment resistance. There is the need for a multitarget approach that can synergistically: disrupt multiple pathogenic pathways in GBM/GSC and enhance the antitumour immune response [1].
- CRISPR/Cas9 gene editing can correct mutations and delete pathogenic genes, like oncogenes and tumour-regulatory ones. However, its *in vivo* application can only occur if subsidised with an appropriate delivery system [2].

AIM

To develop lipid nanoparticles (LNPs) carrying CRISPR RNAs capable of *in vivo* gene editing of GSC tumours, for *in vivo* immune targets therapeutic target validation. CD47 and PDL1 were chosen as model targets.

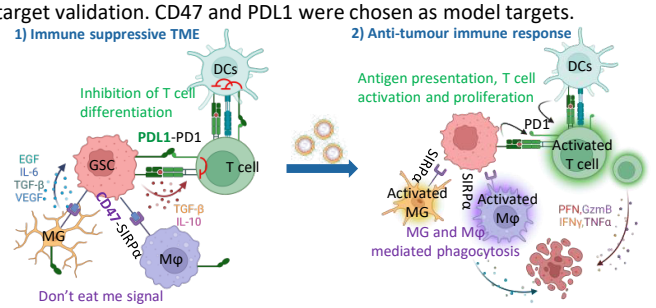

METHODS

LNPs formulation and characterization

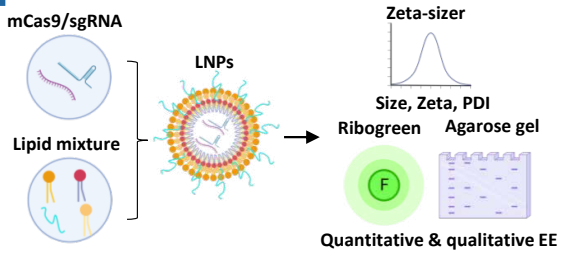

In vitro LNPs mediated gene editing

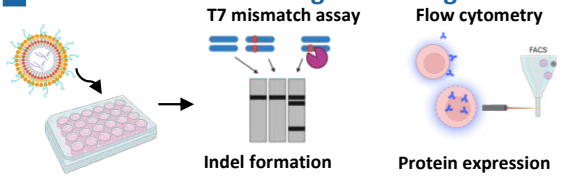

In vivo LNPs validation in GSCs model

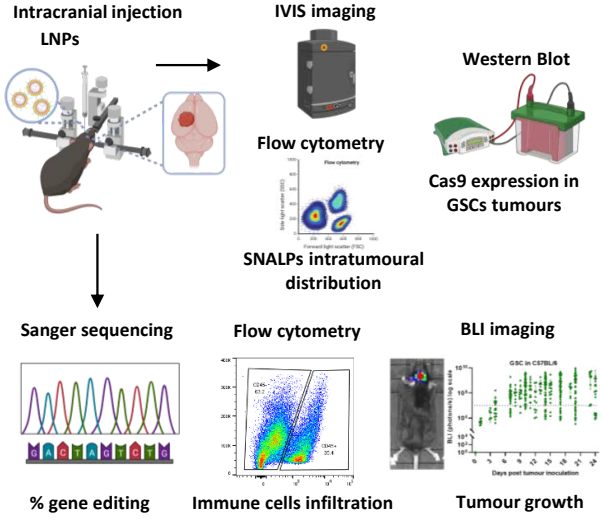

RESULTS

LNPs characterization

Size (d.nm)	PDI
143.44 ± 5.06	0.095 ± 0.03
Charge (mV)	**mCas9/sgRNA EE (%)**
4.35 ± 0.76	89. 95 ± 3.96

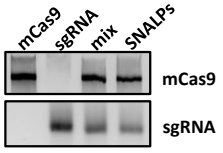

✓We formulated LNPs encapsulating mCas9/sgRNA (EE>80%) with particle size <150 nm, optimal polydispersity (PDI<0.1), and neutral surface charge under physiological conditions.

In vitro gene editing & protein knockout

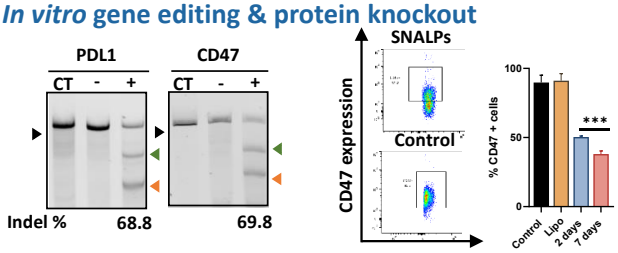

✓LNPs induced efficient CD47 and PDL1 gene editing *in vitro* cultured GSC.

In vivo SNALPs distribution & mCas9 transfection

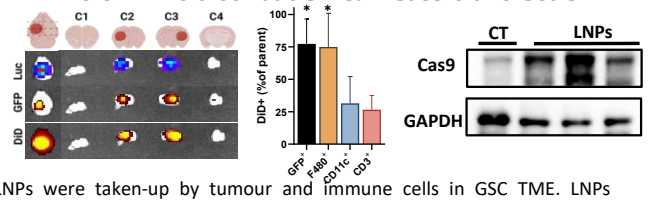

✓LNPs were taken-up by tumour and immune cells in GSC TME. LNPs efficiently transfected GSC tumours inducing Cas9 protein expression.

In vivo CD47 & PDL1 gene editing

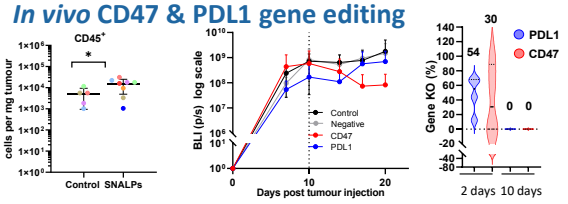

✓LNPs increased immune cells infiltration in GSC TME. While gene editing was confirmed for both CD47 & PDL1 groups 2 days post LNPs injection, only CD47 KO resulted in reduced tumour growth.

CONCLUSION

LNPs capable of *in vivo* gene editing of immune targets in GSCs were developed. CD47 targeting induced reduction in tumour growth in GSC orthotopic model suggesting that CD47 could be a potential therapeutic target for GBM immunotherapy .

References: [1] Nat Rev Cancer, 2020. 20(1): p. 12-25. [2] *Biomaterials Science*, 2022, 10.13: 3410-3432.

Anna Ruppl

Lyophilization of mRNA Lipid Nanoparticles

universität freiburg

Anna Ruppl[1], Denis Kiesewetter[1], Regine Süss[1], Andrea Allmendinger[1,2]

[1]University of Freiburg, Institute of Pharmaceutical Sciences, Department of Pharmaceutics, Sonnenstraße 5, 79104 Freiburg, Germany
[2]ten23 health AG, Mattenstr. 22, 4085 Basel, Switzerland
anna.ruppl@pharmazie.uni-freiburg.de

Introduction

mRNA lipid nanoparticles (LNPs) are typically stored at frozen conditions. Lyophilization is one approach to improve their stability due to the removal of water.
However, technical development of mRNA-LNPs requires large amounts of material. Therefore, we established polyA-LNPs as a surrogate for the formulation and process development of mRNA-LNPs.
The most promising formulation was tested with eGFP-mRNA. Green fluorescence protein (GFP) expression was maintained after lyophilization.

LNPs

	[mol-%]
SM-102	50
Cholesterol	38.5
DSPC	10
DMG-PEG2000	1.5
polyA / eGFP-mRNA	

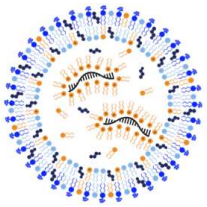

Manufacturing process

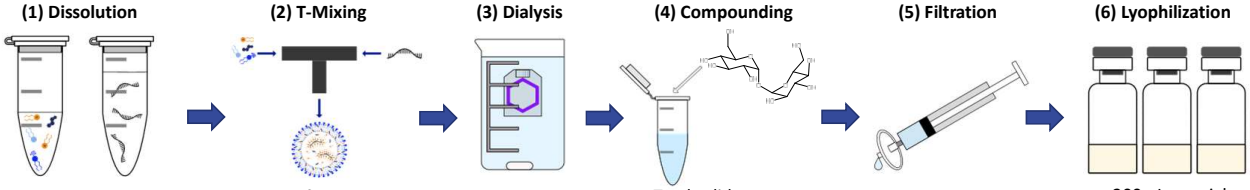

Results

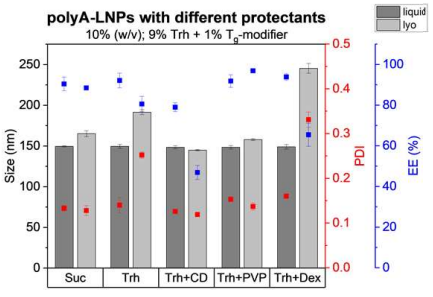

- Sucrose (Suc) is superior to trehalose (Trh)
- Addition of T_g-modifiers to reach higher T_g' (and T_g) values
  - Sucrose: -33.0 °C, trehalose: -29.5 °C
  - Trehalose + T_g-modifier: approx. -28 °C
- HP-β-CD (CD) causes leakage
- **Kollidon 12 PF (PVP)** shows good results
- Dextran 40 (Dex) leads to increase in size

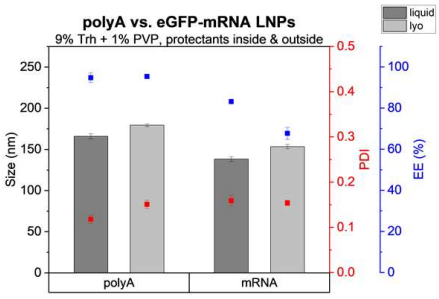

- **Same range in size and polydispersity index (PDI)**
- polyA-LNPs have a higher encapsulation efficiency (EE) than mRNA-LNPs
- polyA-LNPs maintain their EE after lyophilization
- mRNA-LNPs show a loss in EE after lyophilization

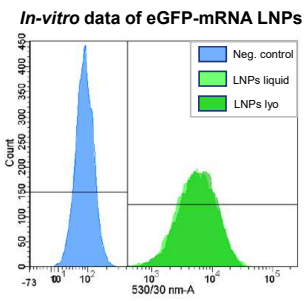

- Fluorescence Activated Cell Sorting (FACS)
- HeLa cells
- 60,000 cells/well in a 24-well plate
- 1 µg/mL eGFP-mRNA

- **No change in median fluorescence intensity (MFI) or GFP-positive cells [%]**

Conclusion

- Good stabilization with 10% sucrose or 9% trehalose + 1% PVP as protectants
- polyA can be used as a surrogate for mRNA during technical development
- eGFP-mRNA maintains activity during lyophilization

CLINAM 2023

14th European and Global Summit for Clinical Nanomedicine

Outlook

- Stability data formulation screening
- Stress testing
- Lyophilization process development

Acknowledgments

CHRIST · SCHOTT PHARMA · DATWYLER · Pfanstiehl · ROQUETTE · Lipoid

Enhancing the power of nanobodies through nanotechnology: reaching intracellular targets and extending half-life.

L Sanjurjo[1], G Berrecoso[2], AM López-Estévez[2], JA Simón[3] , S Blachon[4], JC Rain[4], I Peñuelas[3], MJ Alonso[1-2].

1 Health Research Institute of Santiago de Compostela (IDIS), Center for Research in Molecular Medicine and Chronic Diseases (CIMUS), Santiago de Compostela, Spain. 2 Department of Pharmacy and Pharmaceutical Technology, School of Pharmacy, University of Santiago de Compostela, Spain. 3 Radiopharmacy Unit, Department of Nuclear Medicine, Clinica Universidad de Navarra, University of Navarra, Pamplona, Spain. 4 Hybrigenics Services, Laboratories and Headquarters-Paris, Evry, France.

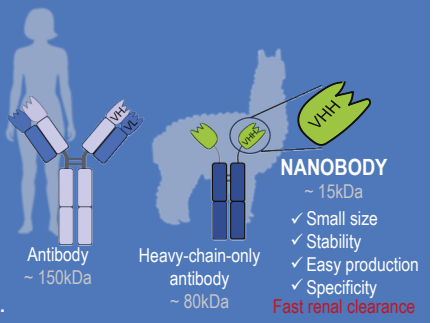

Nanobody-loaded nanocarriers (VHH-NCs)

Field Emission Scanning Electron Microscope (FESEM)

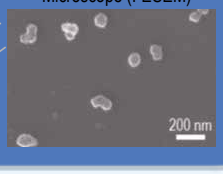

- Hydrodinamic size: ~ 100nm
- PDI < 0.2
- Neutral surface charge
- Functionalized with tumor penetrating peptide (TPP)
- Stable in physiological media and under storage
- High VHH association (up to 98%) and controlled release (20% at 24h)

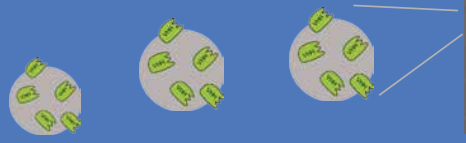

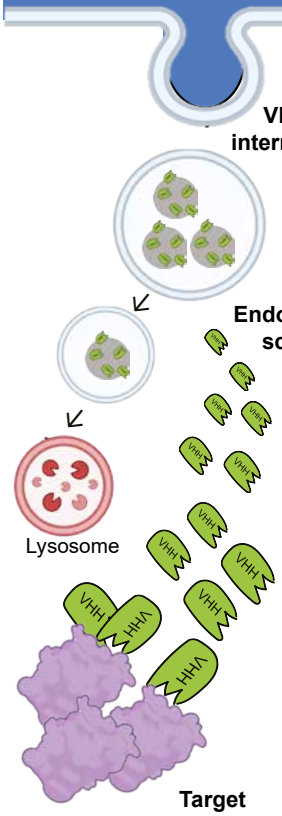

VHH-NCs are internalized by active uptake

VHH intracellular staining. Immunofluorescence HeLa cells.

Confocal microscopy

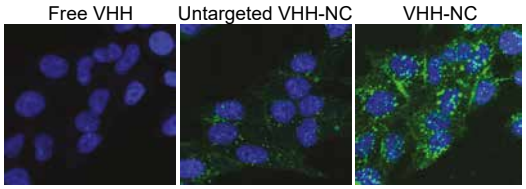

Flow cytometry

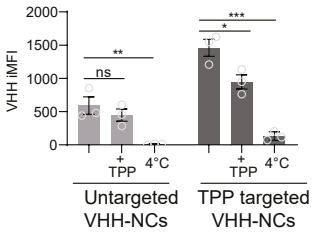

NCs allows nanobodies to scape hyperacidified endo/lysosomes and reach its intracellular target

VHH-Lysotracker colocalization. HeLa cells. Confocal microscopy.

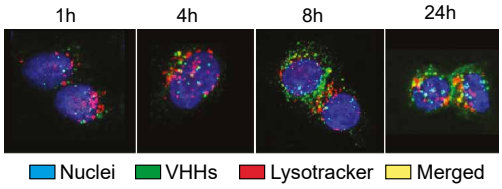

Target engagement. Hela-target expressing cells. Immunoprecipitation. VHH pull-down from cell lysates after VHH-NC uptake.

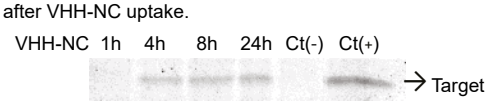

VHH-target colocalization (18h), microscopy.

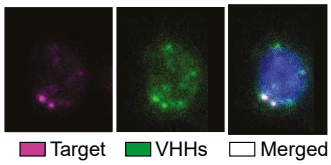

NCs preserve nanobody functionality

Functional assay. Target nuclear translocation. Hela-target expressing cells.

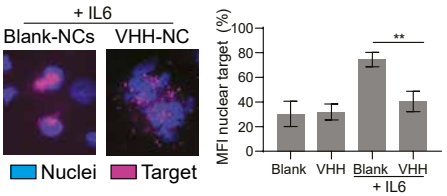

NCs modify nanobody biodistribution 4h

Radiolabeled VHH

Orthotopic lung cancer model

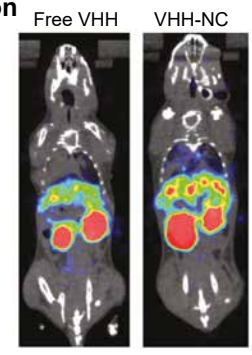

Acknowledgments
This work was supported by ERA-Net EuroNanoMed3 and the Spanish Ministry of Science, Innovation and Universities - Project Intracel (Ref. SAF2017-86634-R) and the Competitive Reference Groups (Consellería de Educación e Ordenación Universitaria, Xunta de Galicia, Ref: ED431C 2017/09). AMLE acknowledges a FPU18/00095.

Maximilian Schaaf

A versatile functionalization platform for liposomes and extracellular vesicles

Maximilian Schaaf[1], Ana Mateos-Maroto[1], Svenja Morsbach[1], and Katharina Landfester[1]

[1] Max Planck Institute for Polymer Research, Ackermannweg 10, 55128 Mainz, Germany

MAX PLANCK INSTITUTE FOR POLYMER RESEARCH

UNIVERSITÄTSmedizin. MAINZ

ABSTRACT

- We present a surface modification strategy for lipid-based carriers
- The functionalization can be divided into three main steps:

1. Azidation of the ligand of interest
2. Conjugation of a short linker containing a strained alkyne to the carrier surface
3. The final click chemistry reaction between the ligand's azide and the carrier's alkyne groups

- Emphasis on quantification and optimization of reaction parameters
- NHS-ester chemistry and bio-orthogonal copper-free click chemistry can be performed under physiological conditions
- Liposome membrane composition: 1:1:1 (eggPC : DOPE : cholesterol)
- The strategy will be transferred for example to extracellular vesicles (EVs)

APOA1-FUNCTIONALIZED LIPOSOMES

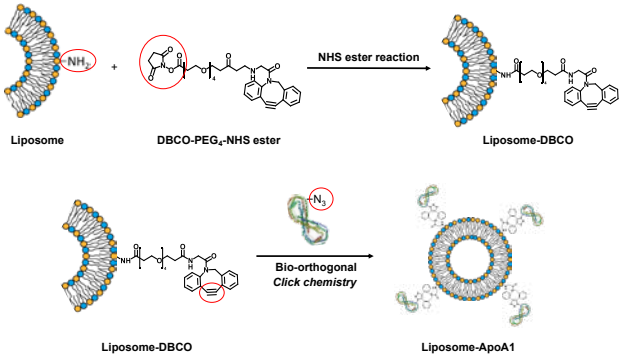

AMINE GROUP QUANTIFICATION - FLUORESCAMINE ASSAY

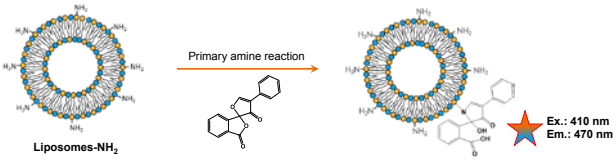

DBCO GROUP QUANTIFICATION - ANTHRACENE AZIDE ASSAY

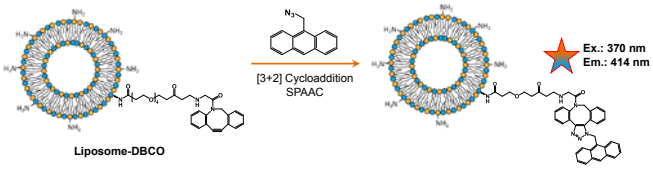

LINKER CONJUGATION OPTIMIZATION

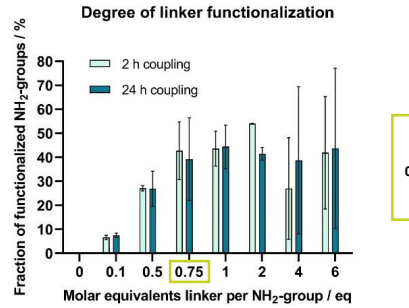

Linker conjugation parameters:
0.75 molar equivalents linker per NH_2-group
(2 h at room temperature)

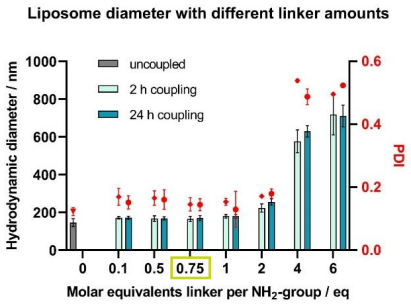

Linker conjugation observations:
Aggregation **above 2** molar equivalents linker per NH_2-group

APOA1 QUANTIFICATION - FLOW CYTOMETRY

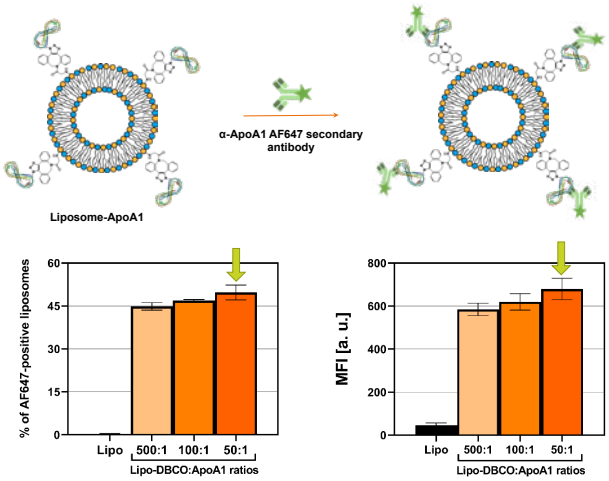

Robust functionalization strategy for lipid-based carriers

Every step can be quantified and controlled

Facile parameter screening allows rapid adaptation to applications

1. M. Gai, J. Simon, I. Lieberwirth, V. Mailänder, S. Morsbach and K. Landfester, Polymer Chemistry, 2020, 11, 527-540.
2. J. Wang, D. Chen and E. A. Ho, Journal of Controlled Release, 2021, 329, 894-906.
3. A. Paterna, E. Rao, G. Adamo, S. Raccosta, S. Picciotto, D. Romancino, R. Noto, N. Touzet, A. Bongiovanni and M. Manno, Frontiers in Bioengineering and Biotechnology, 2022, 10.
4. A. L. Zhou, S. K. Swaminathan, G. L. Curran, J. F. Poduslo, V. J. Lowe, L. Li and K. K. Kandimalla, Journal of Pharmacology and Experimental Therapeutics, 2019, 369, 481.

SFB 1066

This project has received funding from the FET Proactive programme under grant agreement Nº 952183 and the EU's Horizon 2020 research and innovation programme under grant agreement Nº 801338.

BOOW vesUS

Email: schaafm@mpip-mainz.mpg.de

Johanna K. Scheper

PHOENIX-OITB – A single entry point to develop or upgrade innovative nanopharmaceuticals

Johanna K. Scheper,[1,12]* Alba Cordoba,[2] Ariadna Padrós,[3] Nora Ventosa,[4] Jesus M. De la Fuente,[4] Ivana Vinković Vrček,[5] Hannes Bauer,[6] Mangala Srinivas,[7] Sabine Fleischer,[8] Robert Holzer,[9] Tommaso Serchi,[10] Nazende Günday-Türeli,[11]

[1] BioNanoNet Forschungsgesellschaft mbH, Graz, Austria, [2] Nanomol Technologies S.L, Barcelona, Spain, [3] Leanbio S.L, Barcelona, Spain, [4] Consejo Superior de Investigaciones Cientificas (ICMAB), Spain, [5] Institute for Medical Research and Occupational Health, Zagreb, Croatia, [6] Research Center for Pharmaceutical Engineering GmbH, Graz, Austria, [7] Cenya Imaging B.V., [8] Topas Therapeutics GmbH, [9] Research Center for Non-Destructive Testing GmbH, Linz, Austria, [10] The Luxembourg Institute of Science and Technology, Luxembourg, [11] MyBiotech GmbH, Überherrn, Germany, [12] Grace Bio S.L, Barcelona, Spain.

ABSTRACT

The PHOENIX Open Innovation Test Bed (PHOENIX-OITB) is focused on overcoming the challenges of production of novel and innovative nanopharmaceuticals (NPs) from lab scale to GMP quality and production, maximising bioavailability, stability and manufacturing to allow their implementation in the medicine field.

PHOENIX-OITB is a non-profit, open and self-sustaining legal entity that works as a Single-Entry-Point (SEP) providing its end-users transparent processes and procedures as well as easy access to services and expertise needed to bridge the gap between the bench and the bedside, i.e., providing them with high quality services, capable of Quality-Efficacy and Safety (QES) evaluation and production of nanopharmaceuticals at large scales meeting the regulatory and GMP requirements.

METHODS

The PHOENIX-OITB has been structurally conceived, designed and officially registered under the current on-going H2020 EU-funded project Phoenix (GA n° 953110)1. To test the operative capacity of PHOENIX-OITB, five demo-cases of different NP types, manufacturing methods and administration routes will be employed. Additionally, two pro bono demo-cases will be launched and granted to external users to test the services at relevant and operational environment.

1 HOW IT WORKS

PHOENIX concept & service strategies

PHOENIX offers solutions to overcome the biggest hurdle in the translation process of most nano-pharmaceuticals – the so-called "innovation valley of death" situation.

The Single Entry Point of the PHOENIX-OITB provides access to a consolidated network of facilities, technologies, services and expertise for all technology transfer aspects from characterization, testing, verification up to scale up, GMP compliant manufacturing and regulatory guidance. The OITB services include production and characterisation under GMP conditions, safety evaluation, regulatory compliance and commercialisation boost.

2 WORK PLAN

Implementing ideas into action

WP1: Overall Sustainability & Business Development (Exploitation) of the PHOENIX-OITB association

WP2: Quality Management

WP3: Research and Development

WP4: Production (Chemistry, Manufacturing, Control – CMC)

WP5: Regulatory Support

WP6: Marketing (Dissemination & Communication)

WP7: Project Management and Coordination

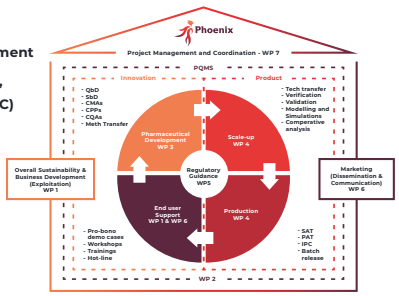

RESULTS

Process transfer and method development for all five demo-cases are ongoing while GMP production area is being constructed. The Pharmaceutical Quality Management System (PQMS) is being established and all exploitation activities are being managed and can be seen through: www.phoenix-oitb.eu. Furthermore, PHOENIX-OITB Open Call for the granting of two pro bono demo-cases to external end-users has been launched and applications are under evaluation.

3 DEMO CASES

Demonstrating scalability from prototype to industrial manufacturing

To establish the operative capacity of PHOENIX-OITB, five demo-cases representative of five different nano-pharmaceutical types, four different manufacturing methods and three different administration routes will be employed to demonstrate and verify the PHOENIX technologies in an industrially relevant environment.

1. **Polymer-based diagnostic agent**
2. **Polymeric particle conjugates loaded with small peptides**
3. **Oral formulation of nanocrystals**
4. **Nanoliposomes loaded with an enzyme for intravenous administration**
5. **Antimicrobial nanovesicles for topical administration**

4 PHOENIX-OITB SERVICE PORTFOLIO

The PHOENIX-OITB service portfolio is divided into 5 different categories. Each category includes a list of services, all of which together cover the different topics needed for the development of nano-pharmaceuticals from early stage to entry into clinical trials.

Physico-Chemical Characterisation
Surface properties, Moisture/Dry, Mass, Size & Distribution, Structure, Morphology, Composition, Chemical stability, Particle concentration, Drug (API) release kinetics, Free/Encapsuled API sterility

***in vitro* Characterisation**
Composition, Bioactivity, Immunocompatibility, Immunoresponse, Extraction of targeted cells, (A)cellular reactivity & cytotoxicity, Cell viability, Cellular structure, Uptake & localisation, Inflammatory response, Endocytosis/Exocytosis, Sensitization & Irritation, Cytotoxicity, Genotoxicity, Nanomechanical prop. of cells & tissues, Dose metrics, Microbial evaluation, Transcriptomics, Metabolomics, Proteomics, Gene expression

***in vivo* Characterisation**
Biodistribution, Hemocompatibility, Pharmacokinetics, Pharmacodynamics, Acute, Sub-acute & Repeated, Dose systemic toxicity, Reproductivity toxicity

Manufacturing
Manufacturing of liquid, semi-solid, solid nanoparticle formulations with a special focus on extended release parenterals; lipid based formulations and nanovesicles, liposomes, solid lipid nanoparticles, crystalline nanoparticles, polymeric nanoparticles, inorganic nanoparticles; On-site lyophilization and fill and finish capabilities.

Innovation
Training, Regulatory Support & Guidance, IPR & Business Support, QbD, SbD & SSbD support

OUR TEAM

The PHOENIX team consists of 12 international partners distributed across 6 countries. The partners are from the following countries: Austria, Croatia, Germany, Luxembourg, Netherlands and Spain. All partners contribute actively to the project to establish the service portfolio of PHOENIX to cover the whole supply chain leading to GMP manufacturing of nanopharmaceuticals.

GET IN TOUCH

info@phoenix-oitb.eu

To learn more visit:
www.phoenix-oitb.eu

PHOENIX project has received funding from the European Union's Horizon 2020 research and innovation programme under grant agreement No 953110.

A non-immunogenetic Polyethylene glycol derivative: Improved immune evasion by introducing sterically demanding side chains

Julian Schmidt[a], Fabian Fuß[a], Philip Dreier[a], Rebecca Matthes[a], Matthias Bros[b], Holger Frey[a]

[a]Department of Chemistry, Johannes Gutenberg University, D-55128 Mainz, Germany

[b]Department of Dermatology, University Medical Center of the Johannes Gutenberg University, D-55131 Mainz, Germany

Introduction:

PEGylation is the method of choice for improving the pharmacokinetics and pharmacodynamics of biomolecule therapeutics due to the unique properties of polyethylene glycol e.g. the stealth effect and biocompatibility.[1,2] As a direct consequence, PEG is indispensable for clinical nanomedicine. Nevertheless, a prevalence of up to 72 % for anti-PEG antibodies (APAs) was reported in the general population.[3] The immunogenicity of PEG leads to a growing concern about the safety and benefits of PEGylation.[4,5] This results in the mandatory development of alternatives to PEG for medical applications.

In our group, we developed a novel approach of preserving the polyether class while randomly incorporating side chains to prevent antibody recognition.[6] The side chains act as random "point mutations" in the highly regular PEG structure. In this work, we inserted isopropyl as a sterically demanding side chain to improve immune evasion while concurrently reducing the comonomer content. This can be achieved *via* AROP of ethylene oxide (EO) with isopropyl glycidyl ether (*i*PGE). Statistical P(EO-*co*-*i*PGE) copolymers (*i*PEG) with iPGE contents ≤ 20 mol-% and molecular weights up to 6000 g/mol, were obtained (Đ < 1.10). These *i*PEGs show significantly reduced affinities against backbone selective anti-PEG antibodies and feature a tailorable thermoresponsive behavior.

Biocompatibility

Cell Viability

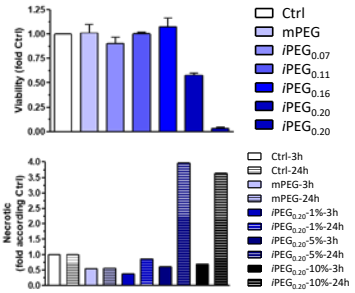

Immune Response

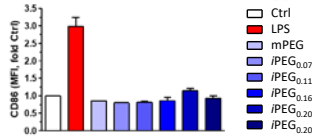

Thermoresponsive Behavior

Concentration Dependent

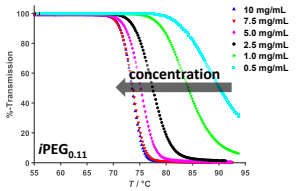

Comonomer Dependent

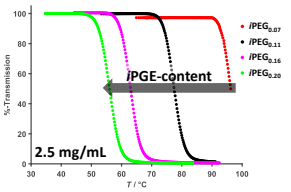

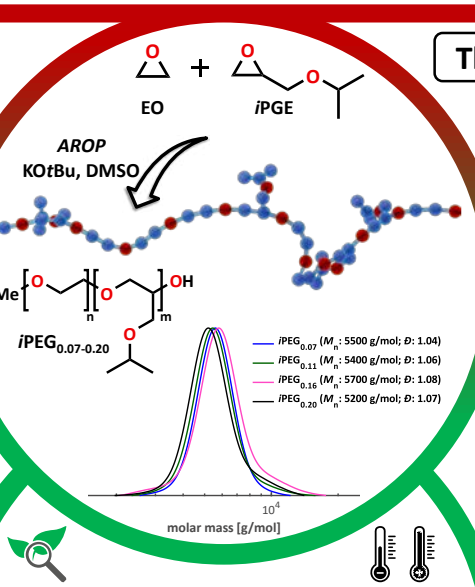

Fully biocompatible up to 20 mol-% *i*PGE

LCST above 56 °C

Conclusion

No immune recognition by anti-PEG antibodies

Improved immune evasion

Anti-PEG Antibody

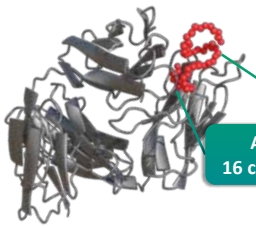

Anti PEG-epitope: 16 consecutive EO units[7]

Incorporation of *i*PGE side chains

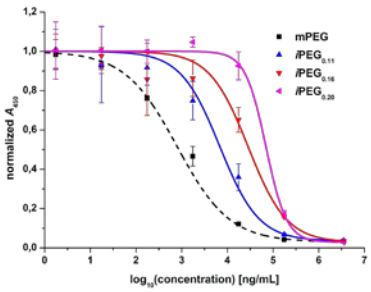

Immune Evasion

Steric Influence

Sample	M_n[a] [g/mol]	$B_{16,\ EO\%\ 100\%}$	n_{16EO}[b]	EC_{50} [µg/mL]
*i*PEG$_{0.20}$	5500	2.8 %	≥ 243	67.9
rPEG$_{0.24}$	5100	1.2 %	≥ 572	5.3

a: Determined *via* MALDI-TOF
b: Minimum probability = 99.9%

The sterical influence predominates the statistical one

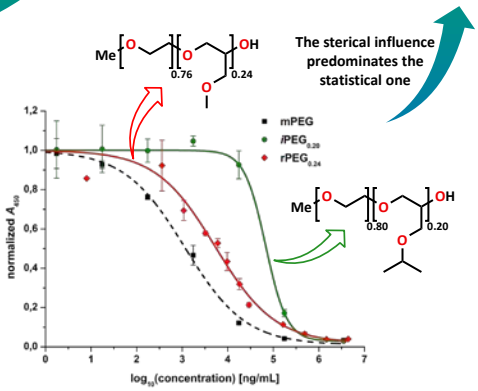

(1) Roberts *et. al. Adv. Drug Delivery Rev.* **2012**, 64, 116–127.
(2) Harris *et. al. Nat. Rev. Drug Discov.* **2003**, 2 (3), 214–221.
(3) Yang *et. al. Analytical Chem.* **2016**, 88 (23), 11804–11812
(4) Chen *et. al. ACS Nano* **2021**, 15 (9), 14022–14048.
(5) Chang *et. al. Nat. Commun.* **2017**, 8 (1), 522.
(6) Frey *et. al.* **2022** EP20210173944.
(7) Huckaby *et. al. Commun. Chem.* **2020**, 3 (1), 124.

Julian Schmidt
julian.schmidt@uni-mainz.de

CLINAM
European Foundation for Clinical Nanomedicine

JG|U THE FREY GROUP

JG|U JOHANNES GUTENBERG UNIVERSITÄT MAINZ

UNIKLINIK RWTH AACHEN | Institute for Experimental Molecular Imaging | RWTH AACHEN UNIVERSITY | DFG | SFB 1066 | UNIVERSITÄTSmedizin. First Department of Medicine MAINZ

Development and characterization of a syngeneic fibrotic hepatocellular carcinoma model

Karina Benderski[1], Paul Schneider[2], Panayiotis Kordeves[1] Federica De Lorenzi[1], Twan Lammers[1], Alexandros Marios Sofias[1], Leonard Kaps[2]

[1] Department of Nanomedicine and Theranostic, Institute for Experimental Molecular Imaging, University Hospital RWTH Aachen, Aachen, Germany; [2] First Department of Medicine , University Medical Center, Mainz, Germany

Development of a hepatocellular carcinoma model

Hepatocellular Carcinoma (HCC) accounts for 90% of all primary liver tumors [1]. Cirrhosis, due to chronic organ damage, is characterized by a massive accumulation of scared tissue in the liver and is the most frequent risk factor for HCC [2] [3]. But incidences of HCC are also increasingly observed in patients with metabolic-associated steatohepatitis (MASH) without cirrhosis [4]. Common murine models for HCC are lengthy and tumor load tends to be heterogeneous as tumor induction takes around 20 weeks and less than 50% of mice bear tumors [5]. In this work, we introduce a rapid and easy-to-handle injection model for HCC in cirrhotic and non-cirrhotic livers, which recapitulates histological and molecular key features of HCC in patients [6]. RNA-Seq analysis of HCC cells used in this work, namely Dt81Hepa 1-6, revealed that HCC hub genes (AFP, MCM3, SPATS2, NT5DC2, MCM6) were significantly upregulated and tumor cells showed a distinct clustering compared to healthy hepatocytes (**Fig. 1a**). For the non-cirrhotic model, mice were intrasplenically injected with Dt81-Hepa 1-6 tumor cells (HCC cells), while for the cirrhotic model, mice were gavaged with profibrogenic CCl_4 for 6 weeks prior tumor cell inoculation. (**Fig. 1b**). After 4 weeks, inoculated mice developed tumors exclusively in their livers. Interestingly, livers of the cirrhotic group had a significantly higher tumor load as indicated by higher liver weights (2.5-fold) and morphometric readouts of liver sections compared to non-cirrhotic mice (**Fig. 1c**).

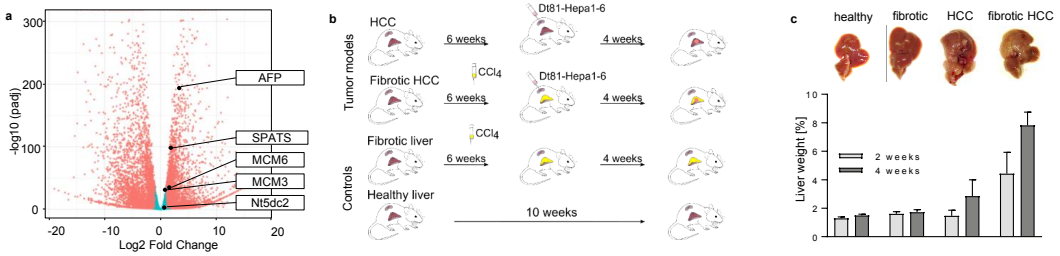

Figure 1. Development and initial assessment of HCC mouse models. (a) Dt81Hepa1-6 cells were sequenced and HCC keygenes were found to be upregulated. **b)** The HCC model was generated by intrasplenic injection of Dt81Hepa-1-6 cells. The fibrotic HCC model was generated by CCl_4 administration for 6 weeks and subsequent injection of Dt81Hepa-1-6 cells. Livers from healthy mice or mice only administrated with CCl_4 were used as controls. **(c)** Liver weight revealed tumor formation by substantial liver weight increase as compared to control livers. Furthermore, livers from the cirrhotic tumor group had a higher tumor load as compared to livers from the non-cirrhotic tumor group.

Analysis of the liver vs tumor microenvironment

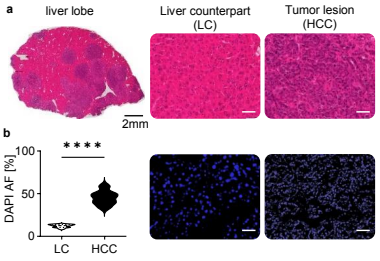

Figure 2. Development and initial assessment of HCC mouse models. (a) H&E staining of whole liver lobes reveales the difference between tumor lesions and the adjacent liver counterpart. **(b)** Quantification of cell density in tumor lesions versus non-malignant liver counterpart (scale bar = 50 µm). AF: Area fraction.

Clinical Relevance

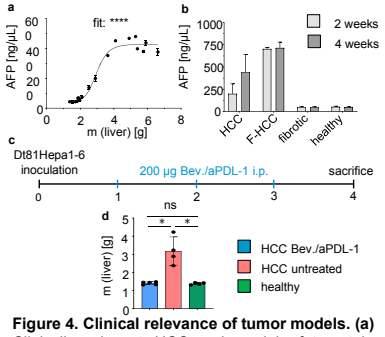

Figure 4. Clinical relevance of tumor models. (a) Clinically relevant HCC-marker alpha-fetoprotein (AFP) is expressed in sera of tumor-bearing mice and correlates with liver weight and tumorburden. **(b)** Fibrotic HCC mice displayed higher AFP concentrations after 2 weeks. **(c)** Experimental outline for Bevacicumab/anti-PDL1 treatment. **(d)** Standard first line medication against HCC inhibited development of tumor lesions.

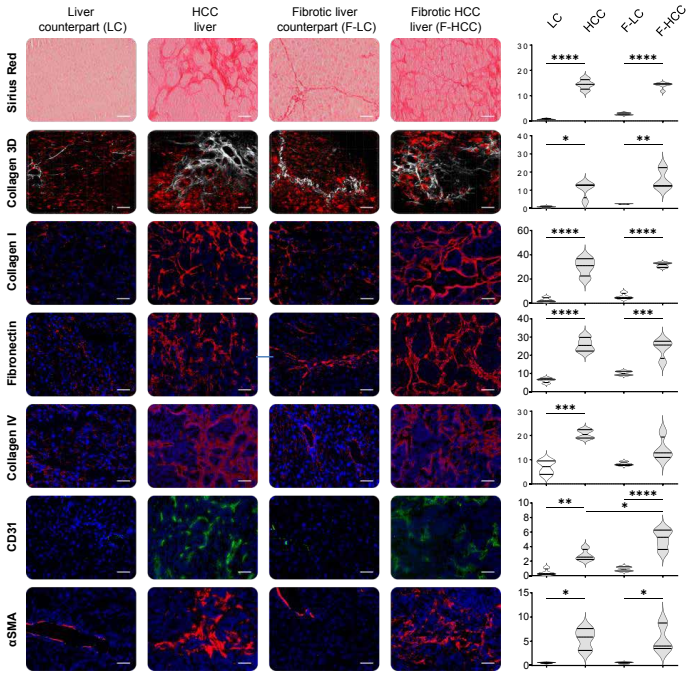

Figure 3. Quantification and analysis of tumor and adjacent liver ECM and vascular markers. A strong overexpression of ECM and vascular components was observed for HCC and fibrotic HCC, in comparison to their respective non-malignant liver counterparts. Compared to the surrounding tissue of HCC, the surrounding tissue of fibrotic HCC exhibits an overexpression of various ECM components, showcasing the ability of CCl_4 to provoke fibrotic reactions in livers. However, no change in vascular and fibroblast markers was observed between healthy and fibrotic livers. (scale bars = 50 µm; violin plots are expressed as area fraction % or volume fraction % for 2D microscopy and 3D multiphoton microscopy respectively).

Conclusions

We present two easy-to-handle murine models for HCC with high relevance for translational research. The two models resulted in robust cancer development and were proven more time-efficient in comparison to current models. Furthermore, CCl_4 administration along with HCC cell injection caused a fibrotic HCC model, which resembles how cirrhosis-derived HCC manifests in humans. The models reflect characteristics of human HCC and showed a positive antitumor response to AtezoBev.

References: [1] Llovet et al., Nat. Rev. Dis. Primers, 2021 [2] Sofias#, De Lorenzi# et al., Adv. Drug Deliv. Rev., 2021 [3] Kaps et al., Cells, 2020. [4] Xuancheng Xie et al, Nature Scientific Reports, 2022 [5] Galle et al., J. Hepatol, 2018. [6] Lacoste, Raymond et al., PLOS one, 2017.

Kathrin Schorr

Experimental approach for the quantitative characterization of multivalent ligand-receptor interactions of polymeric nanoparticles with target cells

Kathrin Schorr[1], Sebastian Beck[1], Max Keller[2], Achim Göpferich[1]
[1]Department of Pharmaceutical Technology, University of Regensburg, Universitätstrasse 31, 93053 Regensburg, Germany
[2]Department of Pharmaceutical/ Medicinal Chemistry II, University of Regensburg, Universitätsstrasse 31, 93053 Regensburg, Germany
✉ kathrin.schorr@ur.de

Research Interest

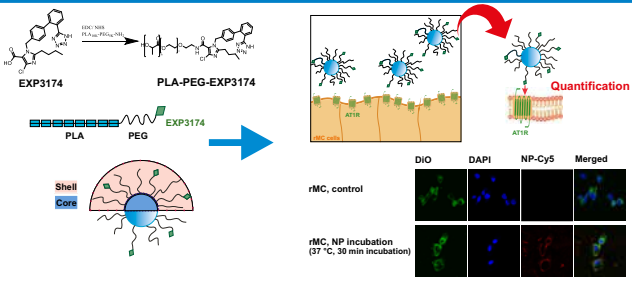

Figure 1. Design concept of the model nanoparticle with active targeting on the AT1R and CLSM images on the chosen target cell line (rat mesangial cells).

Polymeric nanoparticles have been explored for many years as innovative drug delivery and diagnostic systems, often equipped with complex targeting concepts on their surface to achieve the highest possible target specificity [1]. For this purpose, countless strategies for active targeting have been discussed in literature, relying on both small molecules and peptides as ligands [2]. Common to most of these targeting approaches is that the initial surface contact between ligand-functionalized nanoparticles and target or off-target cells represents a key moment in the concept of cell recognition and is decisive for the subsequent fate of the particles [3].
The aim of our work is to characterize this initial contact of ligand functionalized polymeric core-shell nanoparticles with the surface of their target cells.

Methods and Results

Quantifying the average number of ligands per nanoparticle binding simultaneously to cell surface receptors:

Number of binding ligands → $N_{bound} = \frac{0.5 \times N_{AT1R}}{N_{LR}}$

← Number of AT1R

← Number of nanoparticles attached to the cell membrane **if the applied NP concentration is equal to their K_i**

Quantification of nanoparticles on the cell matrix

Implementation of selenium as an ICP-OES tag:

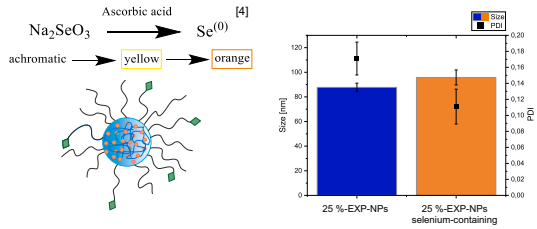

Recorded calibration lines with ICP-OES:

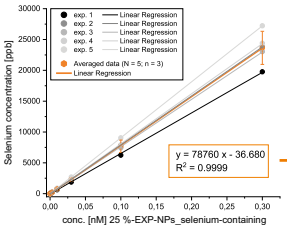

Confidence interval (level = 0.95)

	2.5 %	97.5 %
Intercept:	-49.823	-23.538
Gradient:	70769	86751

→ LoQ ~ 3 pM NP concentration

Figure 2. Illustration of the implementation of a selenium ICP-OES / ICP-MS tag via redox reaction. Size characterization of the NPs and demonstration of the uniformity of selenium-embedding.

K_i value of the nanoparticles

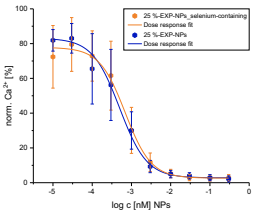

Cheng-Prusoff equation:

$$\frac{IC_{50}}{1+\frac{[L]}{K_D}} = K_i$$

→ K_i = 0.193 pM

K_i - Equilibrium dissociation constant of the ligand under investigation

K_D - Equilibrium dissociation constant of the competing ligand

[L] - Competing ligand concentration

Figure 3. Binding curves derived from Fura-2 AM-based Ca^{2+} mobilization assay in competition with the agonist Lys-Ang II and conversion of IC_{50} value via Cheng-Prusoff equation into K_i value.

Number of AT1R per cell

Radiochemical saturation binding assay ([^{3}H]UR-MK292 / a = 3.44 Tbq/mmol) [5]:

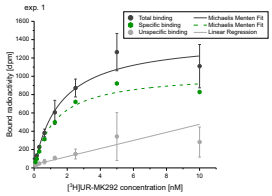

	$N_{cells/well}$	B_{max} [dpm]	Calculated $N_{AT1R/cell}$
exp. 1	258878	1034 ± 70	23000
exp. 2	250364	899 ± 31	21000
exp. 3	250465	993 ± 292	23000
exp. 4	250465	851 ± 80	20000

→ 22000 AT1R/ cell

Figure 4. Radiochemical saturation binding assay to determine the number of AT1 receptors per cell performed on rat mesangial cells.

References

[1] S. Maslanka Figueroa *et al.*, Advanced science **7**, 1903204 (2020).
[2] Y. Zhong *et al.*, Biomacromolecules **15**, 1955-1969 (2014).
[3] S. Zhang, H. Gao and G. Bao, ACS Nano **9**, 8655–8671 (2015).
[4] Y. Luo *et al.*, International journal of biological macromolecules **143**, 393 (2020).
[5] M. Keller *et al.*, Journal of medicinal chemistry **59**, 1925 (2016).

Acknowledgements

The authors like to acknowledge the excellent technical assistance by Renate Liebl, Brigitte Wenzl and Vanessa Tomanek and the scientific support by Prof. Axel Dürkop. We would also like to kindly thank the German Research Foundation (DFG) for financial support, grant GO 565/20-1.

Conclusion

We succeeded in developing an interlocking experimental set-up to determine the K_i value of our model particles and to quantify the receptor number on the surface of the target cells. Currently, we are working on the direct quantification of polymeric nanoparticles on the cell matrix. Assuming complete binding of the nanoparticles to the cell surface in the concentration of their K_i value, as previous experiments indicate, a preliminary value for the number of binding ligands could already be calculated: 84 binding ligands per nanoparticle as lower threshold of the average number. We expect to be capable of deriving a final result from the overall view of the experiments.

SYNTHESIS AND FUNCTIONALIZATION OF POLYETHYLENE GLYCOL (PEG) ISOMERS: REINVENTING A WELL-KNOWN POLYMER

Dominik Schulz, Philip Dreier, Rebecca Matthes, Holger Frey*

Department of Chemistry, Johannes Gutenberg-University Mainz, Duesbergweg 10-14, D 55128 Mainz, Germany

*Email: hfrey@uni-mainz.de

JOHANNES GUTENBERG UNIVERSITÄT MAINZ

THE FREY GROUP

Polyethers, particularly polyethylene glycol (PEG), play a crucial role in modern medicine due to their non-toxicity and biocompatibility.[1] PEGylation, the functionalization of active pharmaceutical ingredients (APIs) with PEG, reduces immune reactions and extends API circulation time in the bloodstream.[2] This phenomenon is known as the "stealth effect."[3] However, anti-PEG antibodies (APAs) have been known since the 1980s, causing adverse reactions to PEG in some individuals - ranging from accelerated blood clearance (ABC), negating the stealth effect of the PEGylation, to hypersensitivity in the form of "pseudo-anaphylaxis".[4 - 6]

To address this problem, we would like to introduce "rPEGs," random copolymers of ethylene oxide (EO) and glycidyl methyl ether (GME). These copolymers have statistically distributed side chains containing ethylene glycol units which could significantly reduce the immune response to PEGylated APIs while preserving important properties like biocompatibility and aqueous solubility. Furthermore, by synthesizing rPEGs through classic anionic ring-opening polymerization (AROP), the need for toxic catalysts is eliminated, making them suitable for medical utilization.

These advancements in rPEG synthesis and characterization offer promising materials for various medical and chemical applications. The hope is that rPEGs could replace PEG in PEGylation processes, reducing immune reactions and encouraging safe use in medical settings. Still, further research is required to fully assess their safety and efficacy.

SCAN ME

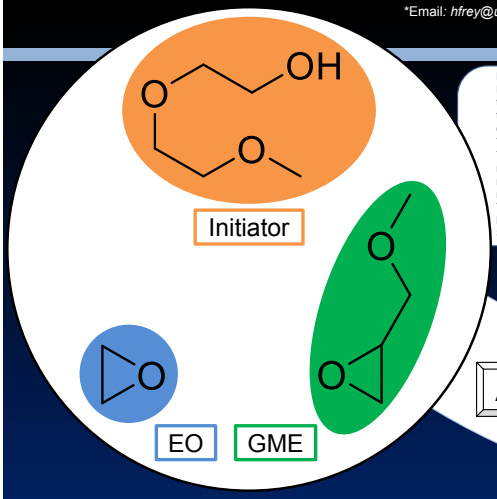

AROP

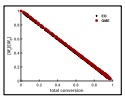

Figure 1: Kinetic data – conversion of EO/GME during AROP in DMSO at 55 °C

rPEG

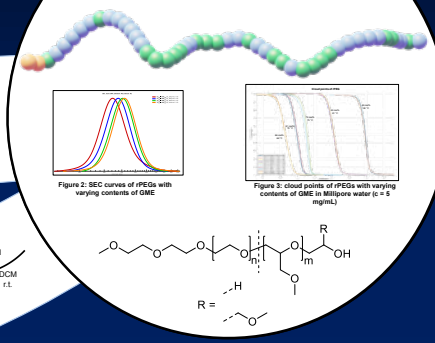

Figure 2: SEC curves of rPEGs with varying contents of GME

Figure 3: cloud points of rPEGs with varying contents of GME in Millipore water (c = 5 mg/mL)

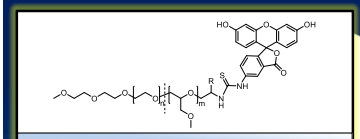

rPEG-FITC

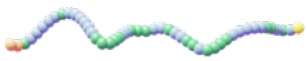

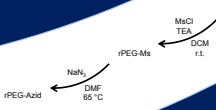

rPEG-Fluorescein

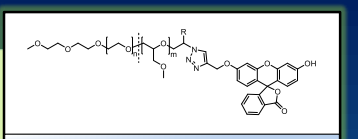

Functionalization with FITC

Polymer	$M_{n,theo}$ g·mol^{-1}	$M_{n,MALDI}$ g·mol^{-1}	$^{a}M_{n,SEC}$ g·mol^{-1}	$^{a}Đ_{SEC}$
P(EG$_{0.60}$-co-GME$_{0.40}$)	5,010	5,160	4,200	1.05
P(EG$_{0.60}$-co-GME$_{0.40}$)-Ms	5,089	5,220	4,260	1.04
P(EG$_{0.60}$-co-GME$_{0.40}$)-N$_3$	5,035	5,200	4,110	1.04
P(EG$_{0.60}$-co-GME$_{0.40}$)-NH$_2$	5,010	5,190	4,030	1.07
P(EG$_{0.60}$-co-GME$_{0.40}$)-FITC	5,398	5,470	4,190	1.05

Table 1: Characterization data of the functionalized copolymers

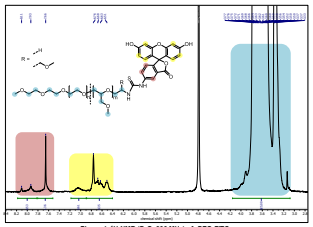

Figure 4: ^{1}H-NMR (D_2O, 300 MHz) of rPEG-FITC

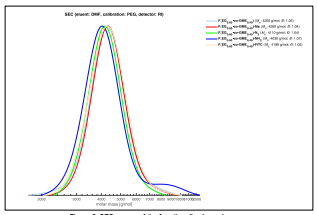

Figure 5: SEC curves of the functionalized copolymers

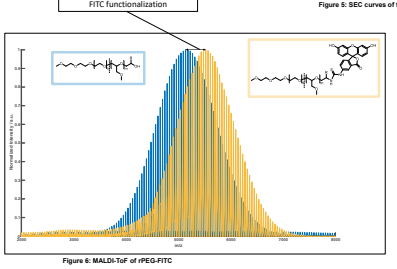

Figure 6: MALDI-ToF of rPEG-FITC

Functionalization via Click reaction

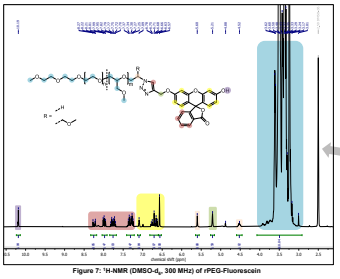

Figure 7: ^{1}H-NMR (DMSO-d_6, 300 MHz) of rPEG-Fluorescein

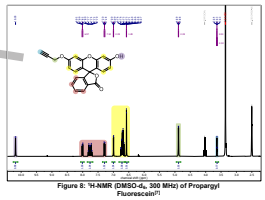

Figure 8: ^{1}H-NMR (DMSO-d_6, 300 MHz) of Propargyl Fluorescein[2]

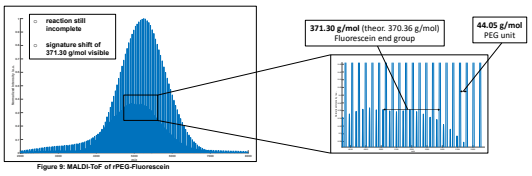

Figure 9: MALDI-ToF of rPEG-Fluorescein

References

[1] Veronese, F.M., Mero, A., *BioDrugs*, **22**, 315–329 (**2008**)
[2] Herzberger, J., Niederer, K., Pohlit, H., Seiwert, J., Worm, M., R. Wurm, F.R., and Frey, H., *Chemical Reviews*, **116** (4), 2170-2243 (**2016**)
[3] Abuchowski, A., McCoy, J.R., Palczuk N.C., van Es, T., Davis, F.F., *J Biol Chem*., **252** (11), 3582-3586 (**1977**)
[4] Richter A.W., Åkerblom E., *Int Arch Allergy Appl Immunol*., **74** (1), 36-39 (**1984**)
[5] Szebeni, J. et al., *World Allergy Organization Journal*, **13** (8), 9315-9325, (**2019**)
[6] Ehlinger, C., Spear, N., Doddareddy, R., Shankar, G., Schantz, A., *Journal of Immunological Methods*, **474**, (**2019**)
[7] Derbré, S., Roué, G., Poupon, E., Susin, S.A. and Hocquemiller, R., *ChemBioChem*, **6**: 979-982 (**2005**)

CLINAM
European Foundation for Clinical Nanomedicine

SFB 1066

Jenny Schunke

UNIVERSITÄTSmedizin. Department of Dermatology MAINZ

Antigen nanocapsule-based combinatorial delivery of STING and TLR7/8 agonists induces effective anti-tumor immune responses

MAX PLANCK INSTITUTE FOR POLYMER RESEARCH

Jenny Schunke[1], Natkritta Hüppe[2], Michael Fichter[1,2], Michael Kuske[1], Vanessa Bolduan[1], Paul Schneider[1], Katharina Landfester[2], Volker Mailänder[1,2]

1. Department of Dermatology, University Medical Center of the Johannes Gutenberg University Mainz 2. Max Planck Institute for Polymer Research Mainz

Introduction

Nanocarrier-based vaccines enable the simultaneous transport of antigens and adjuvants for specific activation of the immune system for cancer therapy. In this context, the targeting of dendritic cells (DCs), whose maturation can be induced and directed by specific adjuvants and which can prime naïve T cells in an antigen-specific manner, is particularly relevant. To induce complete B16 tumor remission, R848, a Toll-like receptor 7/8 agonist, was encapsulated in combination with the potent STING agonist diamidobenzimidazole (diABZI, compound 3), in OVA nanocapsules. This adjuvant combination induced synergistic effects *in vitro* with respect to the expression of DC maturation markers as well as the production of a broad spectrum of pro-inflammatory cytokines and chemokines. In particular, the induction of type I interferons, which are required for an efficient anti-tumor immune response, by diABZI offered an advantage over the previously established adjuvant combination. In subsequent tumor studies, animals with OVA-expressing B16/F10 melanomas were cured by triple injection of diABZI- and R848/diABZI-loaded nanocapsules. The nanovaccine was evolved by supplemental encapsulation of the melanoma-specific antigen tyrosinase-related protein 2 (TRP2). This melanoma-specific nanovaccine elicited a significant reduction of wild-type B16/F10 melanomas. Another focus was set on the characterization of the NC-induced immune response. The infiltration of different immune cells into tumor-draining lymph nodes and the tumor tissue *in vivo* was demonstrated. In particular, the anti-tumor immune response was shown to be mediated by antigen-specific activation of $CD8^+$ cytotoxic T cells.

Material and Methods

Nanocapsules:
OVA-NC: Ovalbumin crosslinked by click chemistry (containing Cy5-Oligo).

Primary immune cells of bone marrow and spleen:
All primary immune cells were obtained from C57BL/6J mice, cultured and treated in specific cell culture media and maintained at 37 °C, 7.5% CO_2. In all experiments the cells were handled under sterile conditions.

Mice:
Wildtype C57BL/6J were obtained from Charles River Laboratories.

B16 cells:
The melanoma cell line was provided by TRON and cultured in DMEM enriched with 10% FCS and Blasticidin (10 µg/ml). The cell line was tested negative for mycoplasma. $5*10^5$ cells resuspended in 100 µl were injected s.c. into the flanks.

Flow cytometric analysis:
Single cell suspensions were incubated with Fc-block (2.4G2) for 10 min at 4 °C and with monoclonal Abs for 30 min at 4 °C (eBioscience: αCD11c-PE-Cy7, αMHC-II-eFl450, αCD80-PE, αCD86-FITC). Data were acquired with Attune NxT (Life Science) and analyzed using Attune NxT software.

Cytometric Bead Array (CBA):
The LEGENDplex Anti-Virus Response Kit (Biolegend) was used to quantify the amount of secreted cytokines/chemokines.

Results

A-D: NC treatment of B16/OVA tumors and determination of effective NC dose

E-H: Comparison of different NC injection routes and proof of antigen-specific immunity induced by T cells

I-K: Analyses of lymph node- and tumor-infiltrating immune cells

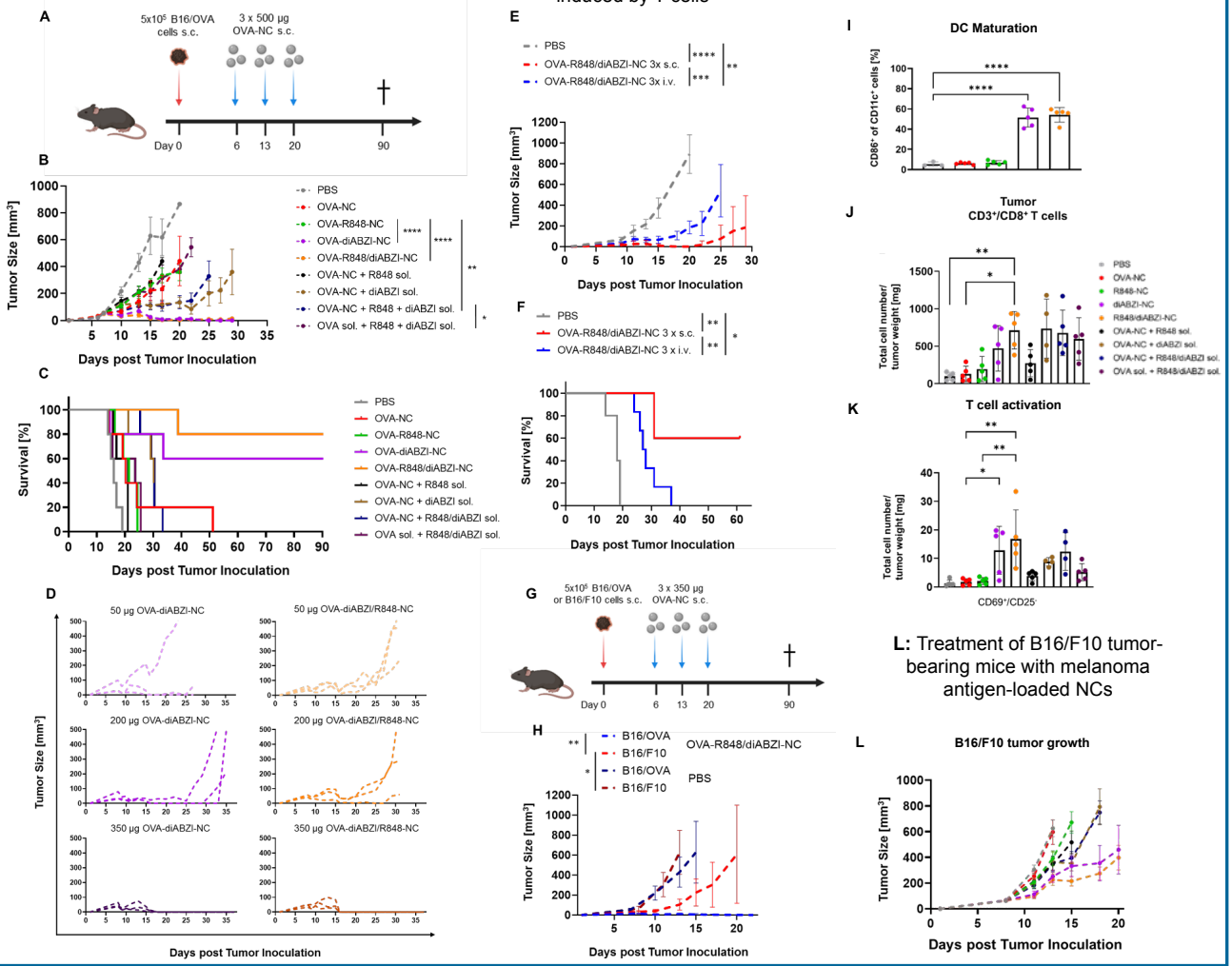

L: Treatment of B16/F10 tumor-bearing mice with melanoma antigen-loaded NCs

Outlook

- Encapsulation of other tumor-specific antigens (e.g. TRP1, MelanA/MART-1, gp100)
- NC surface modifications for DC targeting (antibodies or nanobodies)
- Combination with immune checkpoint inhibitors to enhance anti-tumor immunity (anti-PD1-Ab, anti-CTLA-Ab, anti-TIM-3-Ab)

Armin Azadkhah Shalmani

Polymeric micellar platform with controlled release kinetics for taxane and corticosteroid cancer combination therapy

Armin Azadkhah Shalmani[1], Zaheer Ahmed[1], Maryam Sheybanifard[1], Alec Wang[1], Eva Miriam Buhl[2], Josbert M Metselaar[1], Yang Shi[1], Twan Lammers[1], Quim Peña[1]

[1] Institute for Experimental Molecular Imaging, RWTH Aachen University Hospital, Germany
[2] Electron Microscopy Facility, Institute of Pathology, RWTH University Hospital, Germany
Email: ashalmani@ukaachen.de

Introduction

Nanomedicine-based combination therapy has demonstrated great potential in cancer treatment.[1] Combining tumor microenvironment priming agents, such as corticosteroids, with taxane chemotherapeutics has been recently shown to improve therapy outcome. [2] Here, we used mPEG-*b*-p(HPMAm-Bz) block copolymers of different MW[3] to prepare micelles of different sizes, and employed them for co-loading taxanes and corticosteroids, with primary focus on paclitaxel (PTX) and dexamethasone (DEX) combination.

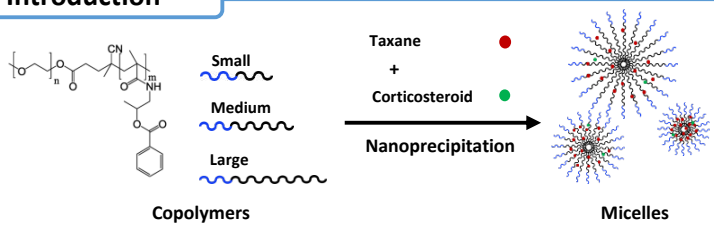

Results

Polymer

Polymer	Mn $_{NMR}$ (kDa)	Mn $_{GPC}$ (kDa)	Đ
Small	15	13	1.5
Medium	23	19	1.5
Large	28	20	1.6

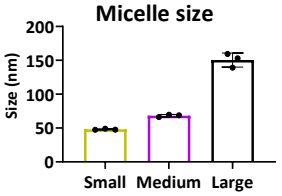

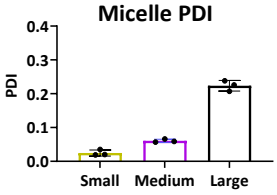

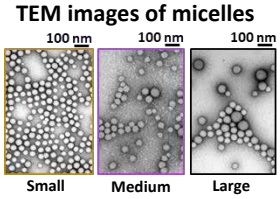

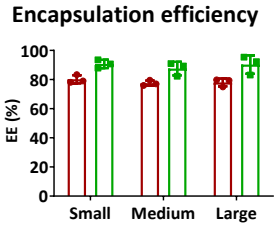

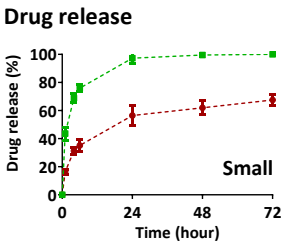

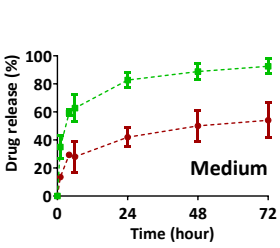

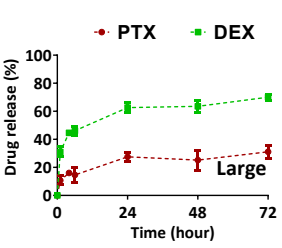

Polymers of 3 different sizes (namely, small, medium, and large) were synthesized and employed to prepare PTX and DEX co-loaded micelles. Size of the micelles showed a positive trend as the molecular weight of the polymers increased. All micelles demonstrated narrow size distribution (low PDI) and spherical shape. Both drugs were efficiently loaded in all the micelles (EE of 80 % and 90 % for PTX and DEX, respectively). Release studies under sink conditions revealed higher drug retention in micelles constituted of larger polymers and an overall faster release of DEX as compared to PTX in all the cases.

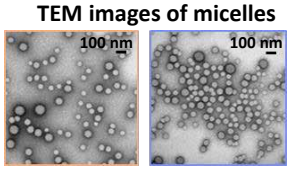

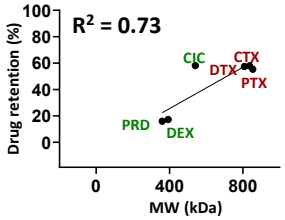

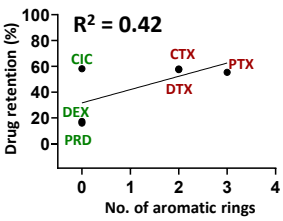

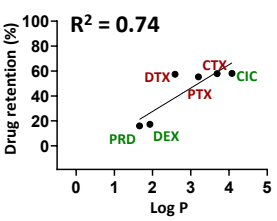

Two other pairs of taxanes and corticosteroid, *i.e.,* docetaxel with prednisolone (DTX+PRD) and cabazitaxel with ciclesonide (CTX+CIC), were also efficiently loaded into the micelles. Using micellar drug retention data from all three different pairs of taxanes and corticosteroids, we evaluated the association between different structural and physicochemical properties of the encapsulated drug and its retention in the micelles. Our findings suggested that hydrophobicity (log P) and molecular weight (MW) were found to be the main contributing properties.

Conclusions

- In all the micelles, regardless of their size, DEX was released faster than PTX which is pharmacologically favorable.
- Hydrophobicity and molecular weight of the encapsulated drug strongly contribute to its retention in the micelles.
- The [mPEG-*b*-p(HPMAm-Bz)]-based micellar platform exhibits high tuneability and versatility for codelivery of taxanes and corticosteroids.

Reference

[1] Sofias AM, Lammers T, et al. Nat. Nanotechnol. **2023**
[2] Martin JD, Panagi M, et al. ACS Nano **2019**
[3] Shalmani AA, Ahmed Z, et al. ACS Biomacromolecules **2023**

Acknowledgement

This work was supported by the German Research Foundation (DFG: LA 2937/4-1), German Federal Ministry of Research and Education (BMBF: PP-TNBC, Project No. 16GW0319K), and the European Research Council (ERC Consolidator grant; Meta-Targeting: 864121).

Isabelle Florence Silvestre

Multicomponent Supramolecular Platform for the Design of Glycoconjugate Antitumor Vaccines

SFB 1066

Nicole Hutter[1], Isabelle Silvestre[2], Jessica Erlenbusch[1], Moritz Urschbach[1], Riem Attariya[2], David Straßburger[1], Natascha Stergiou[2], Tobias Bopp[2], Edgar Schmitt[2], Pol Besenius[1]
[1] Department of Chemistry, Johannes Gutenberg-University Mainz, Germany, [2] Institute of Immunology, University Medical Center Mainz, Germany

Abstract

Classical synthetic vaccine approaches commonly utilize immunogenic carrier proteins of biological origin to immobilize antigens or haptens. These bioconjugation approaches suffer from problems like low reproducibility and poor characterizability of the products. Deviations in the antigen loading are inevitable and may cause issues in biomedical applications. An ideal fully synthetic vaccine should only contain chemically well-defined molecules that are bound in a controlled and multivalent manner onto the carrier.
Supramolecular polymers are a promising scaffold for the presentation of antigenic structures to the immune system due to the dynamic nature of the underlying polymerization process.[1] Each monomer can be individually functionalized and comprise a targeting structure,[2] immunostimulant or antigen. Simple mixing in aqueous solution results in the formation of co-polymers which harbor all desired features on their surface and are able to trigger an antigen-specific humoral immune response.
We present the synthesis and immunological evaluation of a novel modular and fully synthetic antitumor vaccine. The supramolecular platform is employed for versatile multivalent presentation of different epitopes and capable of inducing a strong immune response directed against tumor-associated MUC1, comprising a Tn and 2,3-ST antigen, in C57BL/6 mice.

Nanoplatform For Vaccine Development

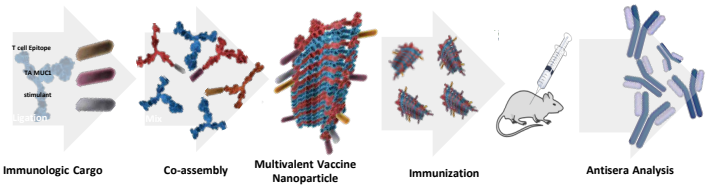

The human immune system is a powerful machinery, evolutionary specialized on recognizing and eliminating nano-scaled pathogens of viral, bacterial or xenobiotic origin. For the design of fully synthetic vaccines, supramolecular polymers can serve as well-defined scaffold to present relevant tumor-associated structures to immune cells on their surface. Bioorthogonality of the conjugation chemistry enables convenient, "last step" attachment of relevant pharmacological structures which was successfully demonstrated for peptidic B-cell and T-cell epitopes as well as heterocyclic immunostimulants. No effects of cytotoxicity or immunogenicity of the self-assembling scaffold were seen in the mouse model. The fact that each monomer bears only one cargo gives the chemists full control on the total amount of active ingredients in the vaccine. Blending diversely loaded monomers with different functional moieties and subsequent copolymerization in physiological media is a promising and modular approach to construct multivalent fully synthetic antitumor vaccines.

Self-Assembling Peptide Motifs

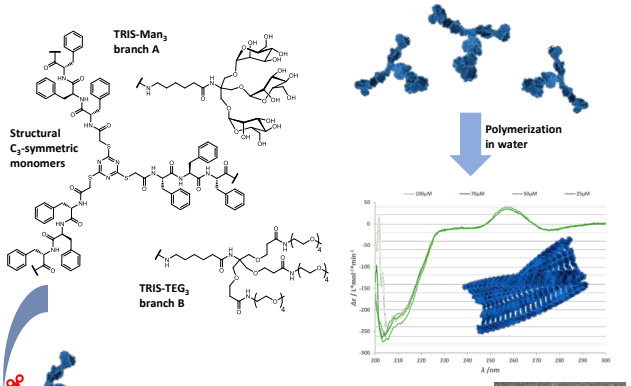

Triazine branched nonaphenylalanine based monomers bearing tetra(ethyleneglycol) or mannose functionalized solubilizing dendrons direct supramolecular polymerization into anisotropic particles up to 300 nm in length.[4] The structures are characterized *via* CD-spectroscopy and TEM.

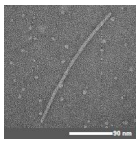

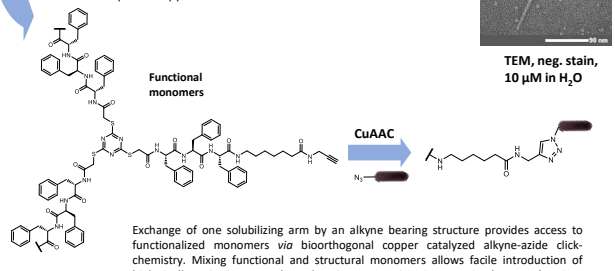

Exchange of one solubilizing arm by an alkyne bearing structure provides access to functionalized monomers *via* bioorthogonal copper catalyzed alkyne-azide click-chemistry. Mixing functional and structural monomers allows facile introduction of biologically active compounds, such as immunogenic epitopes, stimulants or dyes into self-assembled structures.

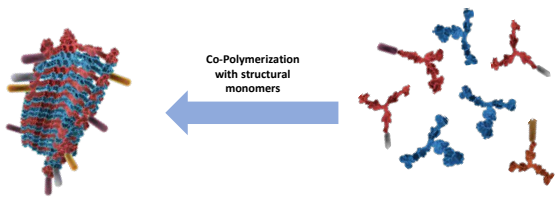

Mucin 1 Glycopeptide

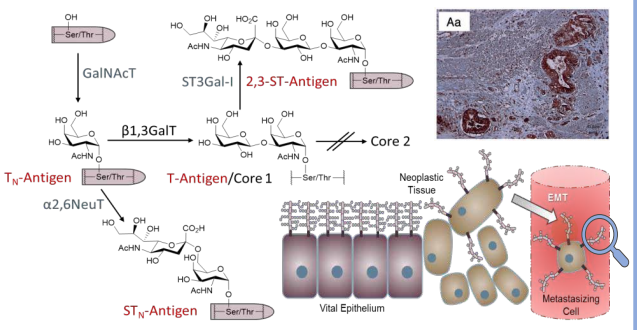

Tumor-associated (TA) MUC1 is a glycopeptide and diagnostic marker for different epithelial malignancies like mammary carcinoma, prostate, pancreatic or lung cancer. Besides its overexpression on tumor tissue, aberrant glycosylation due to dysregulation of glycosyltransferases is observed. This leads to truncated short glycan side chains resulting in the collapse of the peptide backbone. As a consequence of the defect glycan-shielding the peptide structure can be accessed and recognized by immune cells.

Immunological Evaluation

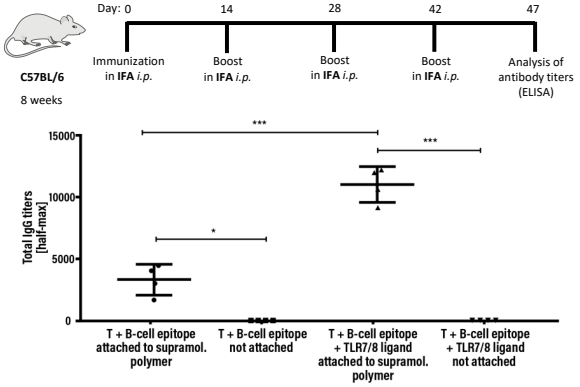

Five C57BL/6 mice were immunized with a vaccine comprising MUC1 B-cell epitope[4], Ttox p30 Th-cell epitope and TLR7/8 ligand decorated FM- together with SM+. After 3 boosts the sera were collected from the tail vein of the mice and analyzed for antibodies directed against TA MUC1. We found robust titers of all antibody classes whereas IgG memory-related type was dominating. Furthermore a significant level IgG2c antibodies was detected. The latter are capable to induce antibody dependent cell-mediated cytotoxicity (ADCC) due to the recruitment of NKs, Ms and DCs via Fc of the corresponding immunoglobulin. The application of unbound epitopes resulted in significantly lower IgG titers demonstrating the power of the supramolecular approach.

[1] H. Frisch, Y. Nie, S. Raunser, P. Besenius, Chem. - A Eur. J. 2015, 21, 3304–3309.
[2] D. Straßburger, N. Stergiou, M. Urschbach, H. Yurugi, D. Spitzer, D. Schollmeyer, E. Schmitt, P. Besenius, ChemBioChem 2018, 19, 912–916.
[3] B. Palitzsch, N. Gaidzik, N. Stergiou, S. Stahn, S. Hartmann, B. Gerlitzki, N. Teusch, P. Flemming, E. Schmitt, H. Kunz, Angew. Chemie Int. Ed. 2016, 55, 2894–2898.
[4] D. Straßburger, M. Glaffig, N. Stergiou, S. Bialas, P. Besenius, E. Schmitt, H. Kunz, ChemBioChem 2018, 19, 1142–1146.

Kai Speth

Proteomics-guided intracellular trafficking analysis reveals time-dependent protein corona changes and the intracellular pathway

Richard da Costa Marques [a,b], Natkritta Hüppe [a], Kai R. Speth [a,b,+], Jennifer Oberländer [a,b], Ingo Lieberwirth [a], Katharina Landfester [a] and Volker Mailänder [a,b,*]

a Max Planck Institute for Polymer Research, Ackermannweg 10, 55128 Mainz, Germany.
b Dermatology Clinic, University Medical Center of the Johannes Gutenberg-University Mainz, Langenbeckstr. 1, 55131 Mainz, Germany.
+ Poster Presenter
* Corresponding author (Email: mailaend@mpip-mainz.mpg.de, Phone: +49 6131 378-248)

INTRODUCTION

Upon the contact of a nanocarrier with a biomolecule-containing fluid, biomolecules can adsorb spontaneously to a nanocarriers´ surface, forming a so called biomolecular corona, also described as protein corona when investigating adsorbed proteins [1, 2]. The intracellular protein corona (IC-PC) remains poorly investigated within the field of nanotechnology-biology (nano-bio) interactions.
Here, we established a protocol to isolate the IC-PC of two different iron-oxide nanocarrier, namely commercial hydroxyethyl starch nanoparticles (HES-NPs) and in-house produced human serum albumin nanocapsules (HSA-NCs) and compared its evolution after the uptake in the murine dendritic cell line DC2.4. Besides using conventional methods to investigate the uptake and intracellular trafficking of the nanocarriers, such as flow cytometry, transmission electron microscopy (TEM) and confocal microscopy (cLSM), we highlight the use of quantitative LC-MS proteomics as a powerful tool to study the IC-PC profile in detail. We demonstrate a time-dependency of the IC-PC formation that served as an effective fingerprint to reconstruct the intracellular trafficking routes. Since the IC-PC defines the direct molecular contact partners of the nanocarriers, its detailed characterization may provide new targets for further drug development.

METHODOLGY & RESULTS

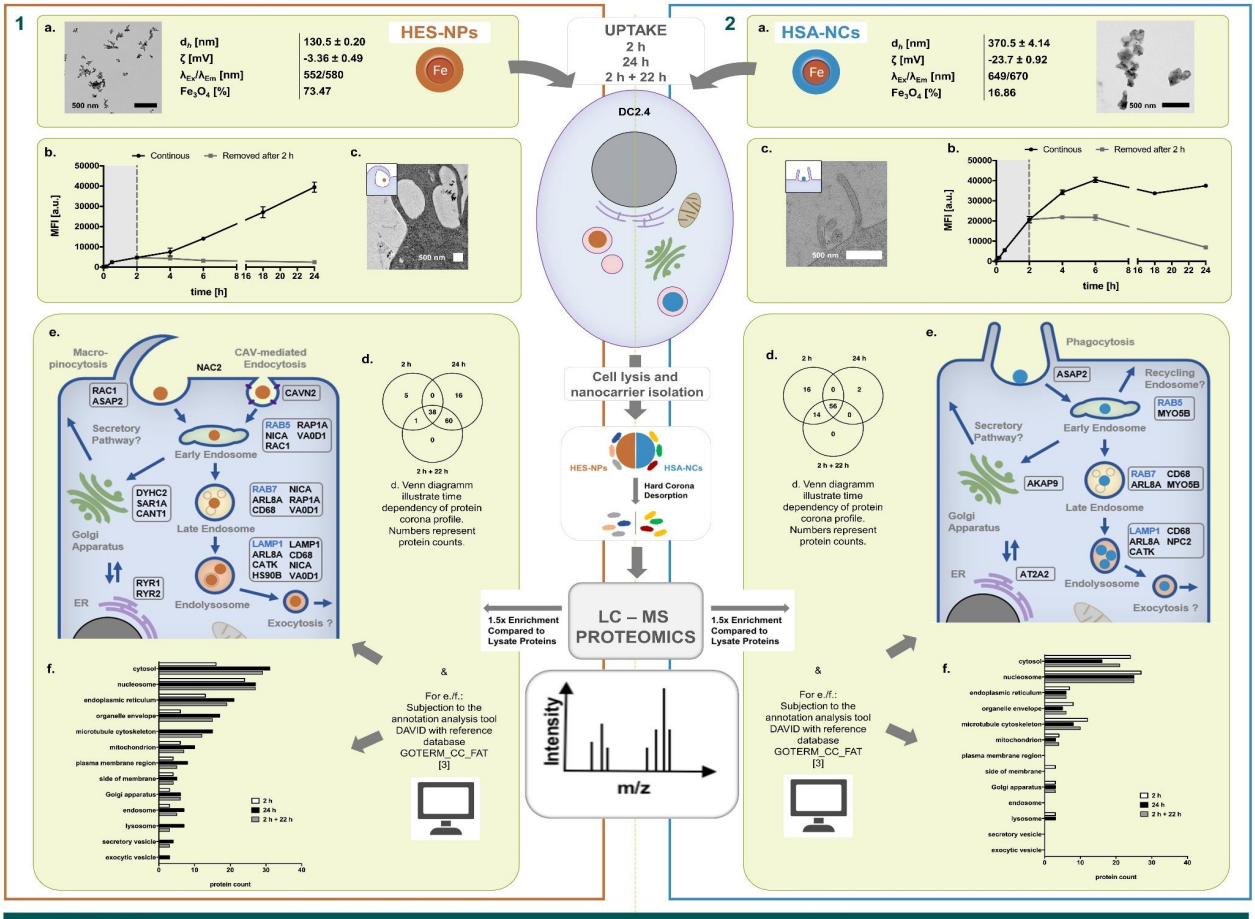

CONCLUSIONS

- Successfull **establishment of a workflow** to isolate the **intracellular protein corona (IC-PC)** from two different magnetic ironoxide nanocarriers.
- By **LC-MS assisted proteomics** we demonstrated a **time dependency** of the IC-PC profile with a more stable IC-PC for the HSA-NCs compared to HES-NPs. This is in accordance with the rather fast uptake for HSA-NCs compared to HES-NPs as measured by flow cytometry.
- The enriched proteins were subjected to **annotation analysis** to extent the proteomic dataset in the context of **intracellular trafficking**. We found that some proteins served as an **effective fingerprint** to allow for a detailed intracellular pathway reconstruction that complement the results from the conventional methods (cLSM, TEM, flow cytometry).
- The experimental strategy, as presented in this study, will prove beneficial when **investigating altered intracellular routes** through nanomaterial modification and targeting.

[1] M.P. Monopoli, C. Åberg, A. Salvati, K.A. Dawson, Biomolecular coronas provide the biological identity of nanosized materials, Nature Nanotechnology 7(12) (2012) 779-786.
[2] N.D. Donahue, H. Acar, S. Wilhelm, Concepts of nanoparticle cellular uptake, intracellular trafficking, and kinetics in nanomedicine, Advanced drug delivery reviews 143 (2019) 68-96.
[3] B.T. Sherman, M. Hao, J. Qiu, X. Jiao, M.W. Baseler, H.C. Lane, T. Imamichi, W. Chang, DAVID: a web server for functional enrichment analysis and functional annotation of gene lists (2021 update), Nucleic Acids Res (2022).

Rene Stein

Department of Otorhinolaryngology -
Head and Neck Surgery

Universitätsklinikum
Erlangen

Gold-coated Superparamagnetic Iron Oxide Nanoparticles for Cardiovascular Applications

René Stein[1], Hatice Genç[1], Harald Unterweger[1], Christoph Alexiou[1], Iwona Cicha[1*]

[1] Department of Otorhinolaryngology-Head and Neck Surgery, Section of Experimental Oncology and Nanomedicine (SEON), Else Kroener-Fresenius-Stiftung- Professorship, Universitätsklinikum, 91054 Erlangen, Germany

Abstract

Surface-functionalized gold-coated superparamagnetic iron oxide nanoparticles (Au-SPIONs) may be a useful tool in intravascularly delivering drugs towards atherosclerotic plaques. To obtain Au-SPIONs, gold salt was precipitated onto citrate-stabilized SPIONs (Cit-SPIONs) using a simple, aqueous one-pot technique inspired by the Turkevich method of gold nanoparticle synthesis. By the further stabilization of the Au-SPION surface with additional citrate (Cit-Au-SPIONs), controllable and reproducible Z-averages enhanced long-term dispersion stability and moderate dispersion pH values were achieved. Cit-Au-SPION concentrations of up to 25 µg Fe/mL for 48 h showed only minor cytotoxic effect on HUVEC cells. Furthermore, HUVEC cells avidly internalized the gold-coated SPIONs in large quantities. Thus, we were able to magnetically guide and accumulate the cells under arterial-like flow conditions.

Gold-coating of citrate-stabilized SPIONs

1

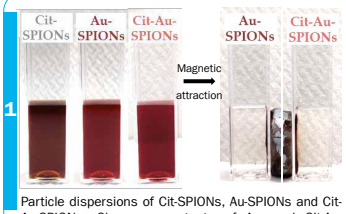

Particle dispersions of Cit-SPIONs, Au-SPIONs and Cit-Au-SPIONs. Clear supernatants of Au- and Cit-Au-SPIONs after magnetic attraction indicate the formation of nano-sized gold only on the SPION surface.

2

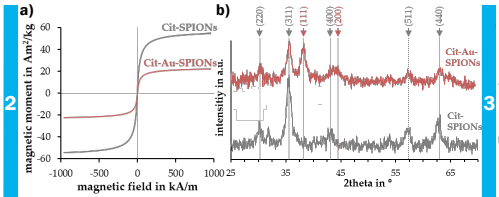

(a) Superparamagnetic behavior of Cit- and Cit-Au-SPIONs.
(b) XRD measurements confirm nano-sized gold on Cit-Au-SPIONs and a magnetite/maghemite structure of Cit-SPIONs.

3

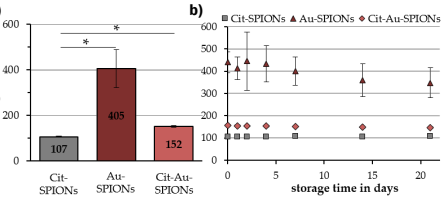

(a) Mean Z-averages over 21 days, (b) Z-averages for different time points during storage of Cit-SPIONs, Au-SPIONs and Cit-Au-SPIONs indicate enhanced dispersion stability of Cit-Au-SPIONs due to citrate-stabilization.

SPION parameter summary

4

	Cit-SPIONs	Au-SPIONs	Cit-Au-SPIONs
Z-Avg. in nm	107 ± 3	405 ± 83	152 ± 5
PDI in a.u.	0.15 ± 0.03	0.25 ± 0.06	0.19 ± 0.01
ζ-Potential @ pH 7 in mV	–48.0 ± 6.3	–43.5 ± 0.6	–48.6 ± 0.3
pH Value in a.u.	8.27 ± 0.07	2.89 ± 0.14	6.21 ± 0.14
Rel. Susceptibility in a.u.	100%	94% ± 2%	89% ± 2%

Z-avg.: Z-average; PDI: polydispersity index; Rel.: relative; Cit: citrate; Au: gold; SPIONs: superparamagnetic iron oxide nanoparticles

Cit-Au-SPIONs influence on proliferation of HUVECs

5

Enhanced storage stability of Cit-Au-SPIONs.

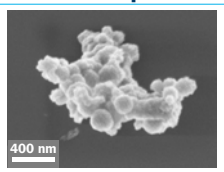

SEM image of Cit-Au-SPION (3 keV).

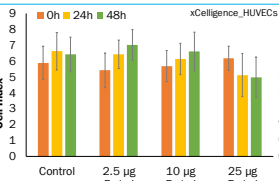

In vitro cell proliferation profile of HUVECs treated with different Cit-Au-SPION concentrations.

Particle uptake by HUVEC cells

6

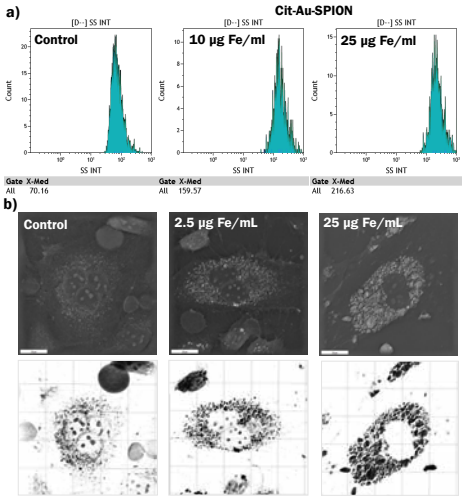

(a) Analysis of Cit-Au-SPION particle uptake via FACs measurement, (b) Label-free detection of particle accumulation in HUVECs using Nano-Live 3D cell imaging system. Both analyses, (a) and (b), were done after 24 h of particle treatment.

Magnetic accumulation under flow conditions in vitro

7

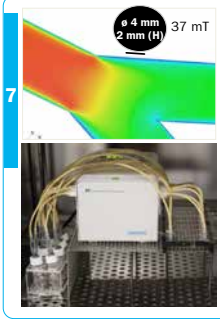

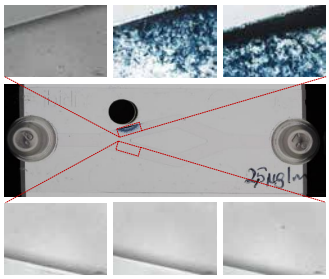

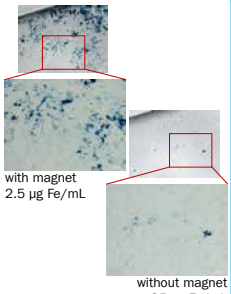

with magnet
2.5 µg Fe/mL

without magnet
25 µg Fe/mL

Flow rate: 9.6 mL/min
Shear stress in straight channel: ~10 dyne/cm²

Conclusion

- SPIONs were coated by gold and stabilized by citrate resulting in Cit-Au-SPIONs with reproducible size as well as enhanced stability.
- Cit-Au-SPIONs show low cytotoxicity on HUVEC cells after 48 h at up to 10 µg Fe/mL.
- HUVEC cells take up Cit-Au-SPIONs in large quantities.
- Loaded cells can be magnetically guided and accumulated under flow conditions.
- Outlook: Usage of thiol binding motif on gold to develop a magnetic drug targeting (MDT) system which carries drugs towards atherosclerotic plaques.

Acknowledgements

This research was supported by the Margarete Ammon Foundation (Munich, Germany), the Manfred-Roth-Stiftung (Fürth, Germany) and the Forschungsstiftung Medizin am Universitätsklinikum Erlangen (Erlangen, Germany) and funded in part by EraNet Magna (project number 01DJ21004).

Nanoparticle-loaded Mesenchymal Stem Cells for Tumor-tropic Delivery of Theranostic Agents

Simona Steponkiene[1], Dominyka Dapkute[1], Evelina Voronovic[1,2], Greta Jarockyte[1,3], Aleja Marija Daugelaite[1,3], Artiom Skripka[4,5], Vitalijus Karabanovas[1,2]

[1] Biomedical Physics Laboratory, National Cancer Institute, Vilnius, Lithuania
[2]Department of Chemistry and Bioengineering, Vilnius Gediminas Technical University, Vilnius, Lithuania
[3] Faculty of Natural Sciences, Vilnius University, Lithuania
[4]Centre Énergie, Matériaux et Télécommunications, Institut National de la Recherche Scientifique, Université du Québec, Varennes, QC, Canada
[5]Nanomaterials for Bioimaging Group, Departamento de Física de Materiales, Facultad de Ciencias, Universidad Autónoma de Madrid, Madrid, 28049 Spain
simona.steponkiene@nvi.lt

Introduction

In the past decade, mesenchymal stem cells (MSCs) have been derived to track down and destroy malignant cells taking advantage of their tumor-tropic property. However, the cargo for such transportation is not that easy to construct. Only non-toxic bio-friendly and trigger-activatable materials could be used as cargo, including photosensitizers (PSs), core-shell quantum dots (QDs), and rear-earth doped upconverting nanoparticles (UCNPs).

Aim of the study

To evaluate the capability of MSCs' to transport the theranostic cargo (QDs-PS and UCNPs-PS) towards human breast cancer cells MDA-MB-231.

Tumor Tropism

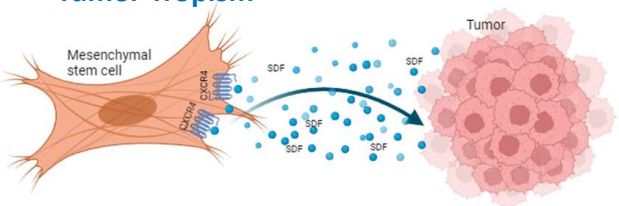

Mesenchymal stem cells have specific receptors for binding chemokines released by tumors. After the chemokine signaling mesenchymal stem cells migrate towards the chemokine gradient (tumor).

Materials

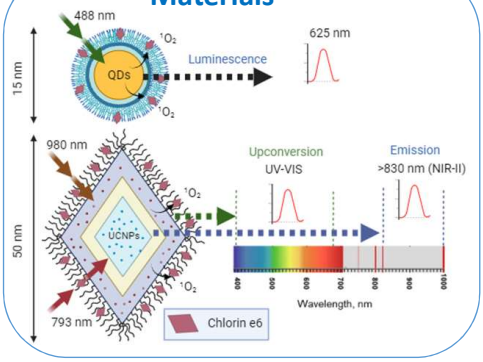

Methods

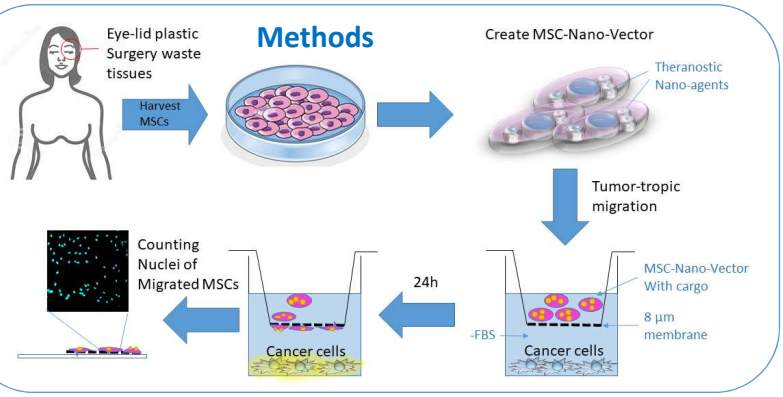

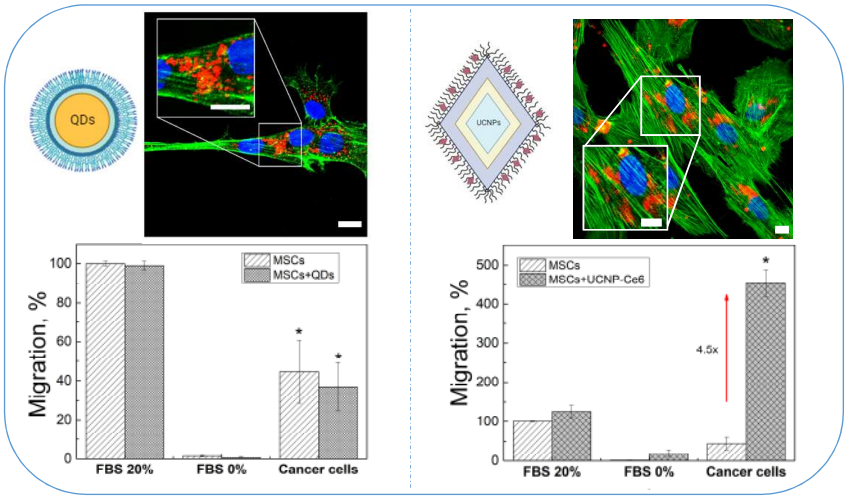

Conclusion

- Theranostic MSC-Nano-Vector was created by the natural 24-hour uptake of QDs and UCNP-Ce6.
- MSCs are capable of QDs and UCNPs-Ce6 transport toward MDA-MB-231 cancer cells.
- UCNP-Ce6 changes the migratory potential of MSCs by a 4.5-fold increase compared to unlabeled cells.

This work was financially supported by the Research Council of Lithuania, Grant No. S-MIP-22-31.

CLINAM 2023
European Foundation for Clinical Nanomedicine
Switzerland

Yael Suarez

Microfluidic device for the investigation of nanoparticle dynamics in the healthy and diseased state of the gastrointestinal tract

Yael del Carmen Suárez López and Alexandra Teleki

Department of Pharmacy, Science for Life Laboratory, Uppsala University, Uppsala, Sweden

E-mail: yael.suarez@farmaci.uu.se Website: https://telekilab.org

Objective Development of a microfluidic device that mimics the healthy and diseased states of the gastrointestinal tract (GIT) to study the impact of fluid composition on nanoparticle (NP) stability, aggregation, and protein corona formation in different GIT regions.

Nanoparticle synthesis and characterization

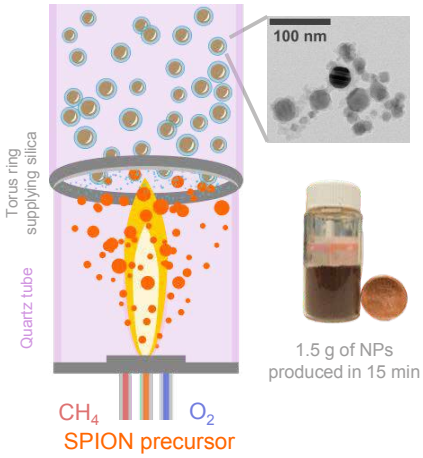

Figure 1. Flame spray pyrolysis synthesis of silica-coated superparamagnetic iron oxide (γ-Fe_2O_3) nanoparticles (SPION).

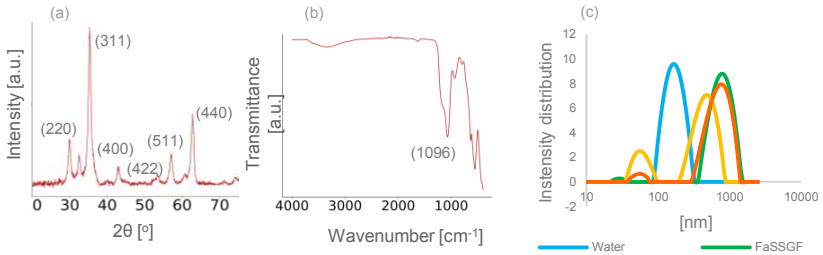

Figure 2. (a) X-ray diffraction pattern confirms a maghemite crystalline phase. (b) Fourier-transform infrared spectroscopy spectrum of SPION. The peak at 1096 cm^{-1} confirms the coating with SiO_2. (c) Hydrodynamic diameter measured by dynamic light scattering of SPION in water (blue), fasted simulated gastric media (FaSSGF, green), small intestinal media (FaSSIF, yellow), and colonic media (FaSSCoF, orange).

Table 1. ζ-Potential of γ-Fe_2O_3 NPs in different simulated media.

Media	ζ-Potential (mV)
Water	- 35.6
FaSSGF	-8.5
FaSSIF	-18
FaSSCoF	-25.7

Development of a microfluidic device to mimic the GIT

1 Micromixer selection

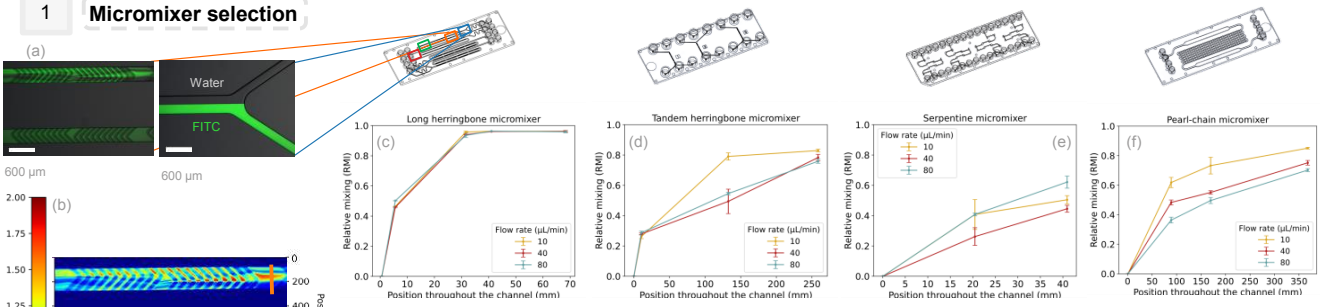

Figure 3. (a-b) Quantification of fluorescence intensity to calculate the relative mixing index (RMI)[1]. (c-f) RMI vs channel position throughout 4 different commercially available micromixers at equal input flow rates (10, 40, and 80 µL/min)

$$RMI = 1 - \frac{\sigma}{\sigma_0} = 1 - \frac{\sqrt{\frac{1}{N}\sum_{i=1}^{N}(I_i - \bar{I}^2)}}{\sqrt{\frac{1}{N}\sum_{i=1}^{N}(I_{0i} - \bar{I}_0^2)}}$$

σ = standard deviation
σ_0 = standard deviation of the unmixed state
N = number of pixels
I = Intensity of pixels

2 Proof of concept

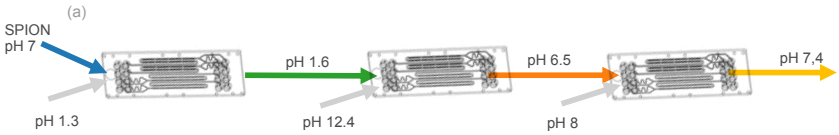

Figure 5. (a) Sketch of modular microfluidic device. (b) Hydrodynamic diameter measured by dynamic light scattering of polysterene nanoparticles through the modular microfluidic device.

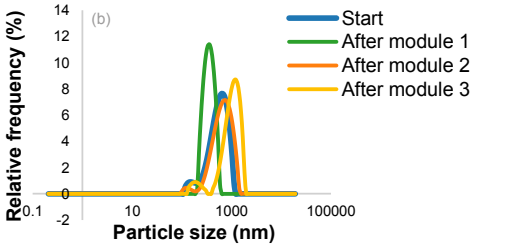

Conclusions

- SiO_2–coated γ-Fe_2O_3 NPs were produced in a single step by FSP.
- According to the relative mixing index, the long herringbone micromixer had the best mixing efficiency (>96%).
- The behaviour of SPION in more complex simulated media in the healthy and diseased state will be tested in future experiments.

[1]Hashmi, A., & Xu, J. (2014). SLAS Technology, 19(5), 488–491.

Malin Svensson

Comparative study of adjuvants and their synergistic potential for the stimulation of dendritic cells (DC) and liver non-parenchymal cells

Malin Svensson[1], Yanira Zeyn[2], Maria-Jose Limeres[1], Maximiliano Caceido[1], Stephan Gehring[1] and Matthias Bros[2]

[1] University Medical Center, Children's Hospital, Germany
[2] University Medical Center Mainz, Department of Dermatology, Germany

Background

Liver non-parenchymal cells (NPCs), comprising Kupffer cells (KC), dendritic cells (DC) and liver sinusoidal endothelial cells (LSEC) exert tolerogenic activity by default.

Liver NPCs express receptors to which nano-particles (NP) can bind:

- Fc receptors (antibodies)
- CD206 (mannose)
- CD209 homologs (trimannose)
- Scavenger receptors

Systemically applied NP most often bind to tolerance-inducing liver NPCs,which may counteract the induction of **anti-tumor responses** (by DC) in spleen/lymph nodes.

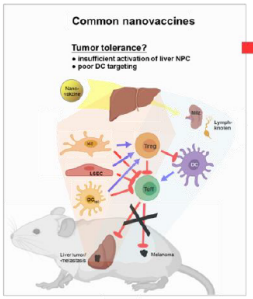

Aim

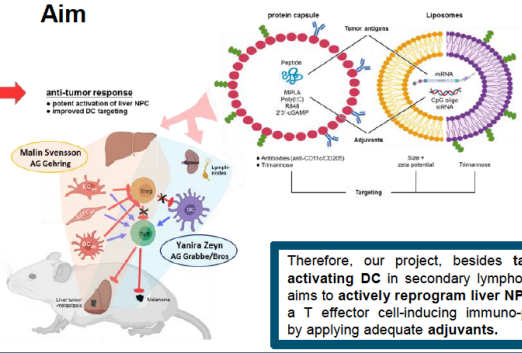

Therefore, our project, besides **targeting / activating DC** in secondary lymphoid organs, aims to **actively reprogram liver NPC** towards a T effector cell-inducing immuno-phenotype by applying adequate **adjuvants.**

Adjuvant Screening

Nucleic acid-based Adjuvants

- synthetic oligonucleotides that contain unmethylated CpG dinucleotides (CpG motifs)
- such motifs are present at a 20-fold greater frequency in bacterial DNA compared to mammalian DNA
- CpG motifs are recognized by TLR9

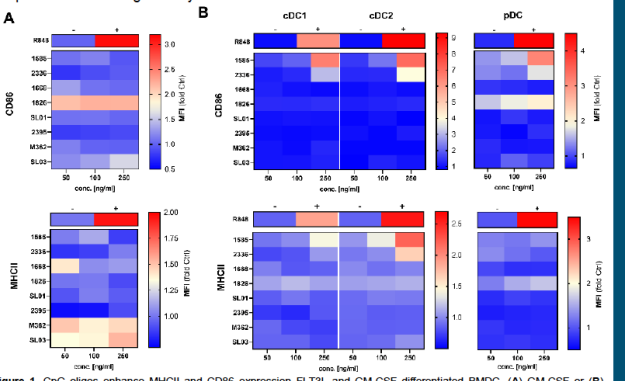

Figure 1. CpG oligos enhance MHCII and CD86 expression FLT3L and GM-CSF differentiated BMDC. (**A**) GM-CSF or (**B**) FLT3L differntiated BMDC were incubated with different concentrations of CpG oligos (50, 100 or 250 ng/ml) or the TLR 7/8 ligand R848 (1 µg/ml). On the next day, expression of MHCII and CD86 was assessed by flow cytometric analysis. Graphs denote the fluorescence intensities (**MFI**) (mean±SEM of **4** experiments) of marker expression.

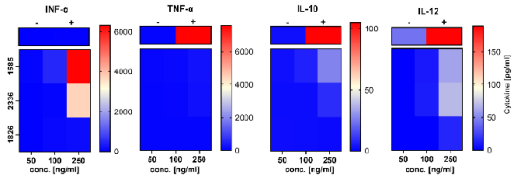

Figure 2. CpG oligos enhance proinflammatory cytokine release of FLT3L differentiated BMDC. BMDC were incubated o.n. with CpG oligos. Cytokine concentrations of culture supernatants were determined by CBA (mean±SEM of **2-3** experiments).

Other Adjuvants

Adjuvant	Agonist
R848	TLR7/8
cGAMP	STING
Poly(I:C)	TLR3

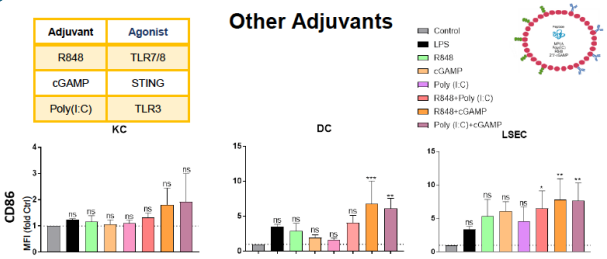

Figure 3. Adjuvant combinations enhance CD86 expression in dendritic cells (DC) and in liver sinusoidal endothelial cells (LSEC). Liver non-parenchymal cells (NPC) were incubated o.n. with adjuvants (5 µg/ml). On the next day, expression of CD86 was assessed by flow cytometric analysis. Data represented are the means ± SEM (n = 4). Significant different compared to the control: no significant difference (ns); * p < 0.05; ** p <0.01; *** p <0.001; **** p <0.0001. (One-way ANOVA).

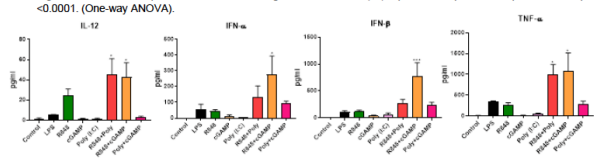

Figure 4 . Cytokine concentrations were assayed by CBA. Data represented are the means ± SEM (n = 4). Significant different compared to the control: no significant difference (ns); * p < 0.05; ** p <0.01; *** p <0.001; **** p <0.0001. (One-way ANOVA).

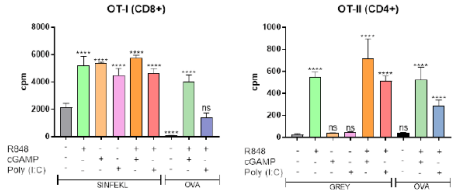

Figure 5. DC and T-cell co-cultures stimulated with adjuvant/combinations and OVA-peptide/protein led to enhanced levels of T-cell proliferation. Data represented are the means ± SEM (n = 6). Significant different compared to the control: no significant difference (ns); * p < 0.05; ** p <0.01; *** p <0.001; **** p <0.0001. (One-way ANOVA).

Conclusion

Nucleic acid-based adjuvants

- Functionally active CpG oligos (ODN1585 and ODN1826) were identified for dendritic cell populations
- In case of liver NPC and splenocytes (not shown) ODN1585, ODN2336 and ODNSL03 enhanced upregulation of activation markers

➢ SL03 was identified as optimal performer

Other adjuvants:

- R848, cGAMP and Poly (I:C) were the most potent adjuvants once incubated with NPC population. Combinations of these adjuvants showed synergistic effects both regarding activation markers (CD86, CD80) and cytokine secretion.

Outlook

- Test CpG oligos in combination with OVA as model antigen in co-cultures with T cells from OT-I and OT-II animals.
- Development of lipid-based nanocarriers for the encapsulation of OVA-encoded mRNA in combination with selected adjuvants

SFB 1066

Nikolaos Tagaras

Intelligent single-atom nanozymes for effective and safe therapy of inflammatory diseases in pregnancy

Nikolaos Tagaras[1], Haihan Song[2], Weijun Tong[2], Zhengwei Mao[2], Tina Buerki-Thurnherr[1]
[1]Empa, Swiss Federal Laboratories of Materials Science and Technology, Laboratory for Particles-Biology interactions, Lerchenfeldstrasse 5, 9014 St. Gallen, Switzerland
[2]Department of Polymer Science and Engineering, Zhejiang University, China

Contact

Introduction

Gestational inflammation is pivotal for an uncomplicated pregnancy. Nevertheless, **aberrant inflammation** can lead to **obstetric complications** (1). Large body of evidence demonstrates a significant contribution of the **placenta** in the development of many pregnancy disorders (2). **Conventional therapies** (NSAIDs, antibiotics) to treat inflammatory diseases during pregnancy raise **questions** about their **safety** and **efficacy**. In addition, there is increasing concern that such therapies can be drivers of obstetric complications or induce adverse health effects in later life.

Aim: Development of safe and effective nanotherapeutics to treat gestational inflammatory diseases. We will engineer nanoparticles bearing enzymatic activities (nanozymes) with antioxidant properties and further endow them with a micro-environment responsive antimicrobial coating.

Single-atom Nanozyme (SAzyme) Synthesis and Characterization

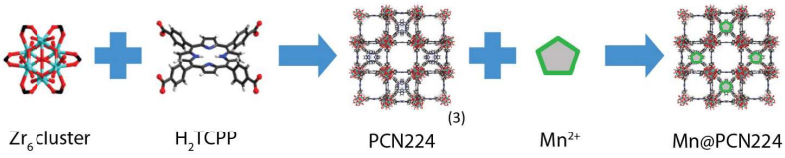

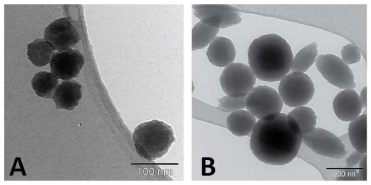

Figure 1: TEM images of Mn@PCN224 A) 90 nm, B) 208 nm.

Table 1: Physicochemical properties of Mn@PCN224 SAzymes.

SAzymes	Size ± SD (nm) in ddH_2O	Zeta potential (mV) in ddH_2O	SOD activity (%)
Mn@PCN224 1.7	90 ± 2	18	80
Mn@PCN224 2.4	208 ± 8	24	84

Placenta Barrier Integrity

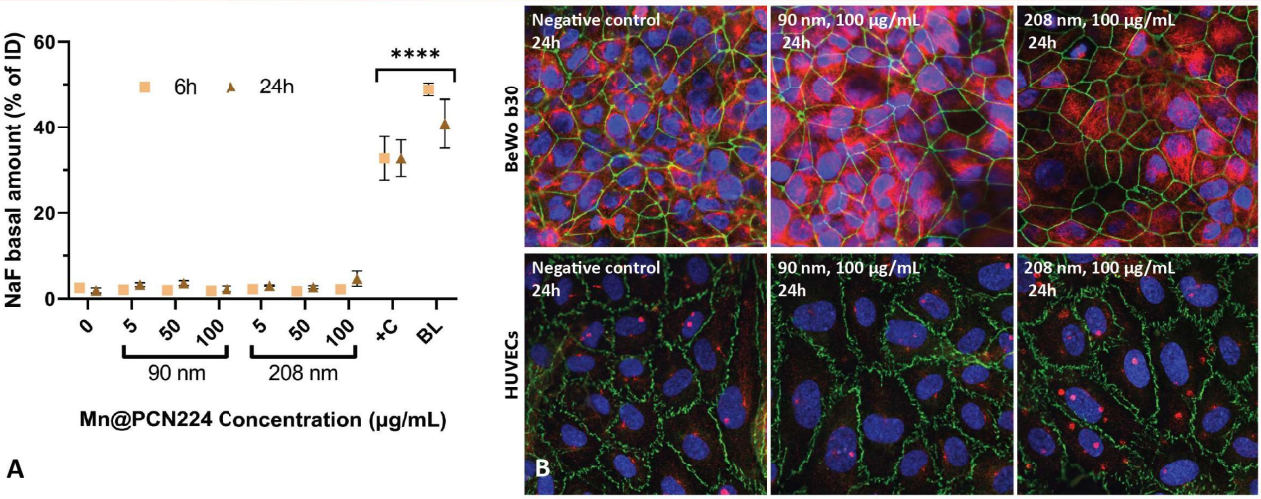

Figure 2: *In vitro* placental barrier integrity (BeWo b30 – HUVECs co-culture model) after exposure to 90 nm and 208 nm Mn@PCN224 for 6 and/or 24h, assessed with **A)** NaF exclusion assay and **B)** Immunocytochemistry. **A)** Cell medium and Triton-X 100 (0.2%) were used as negative (0 µg/mL) and positive control (+C), respectively. The results are presented as the mean of minimum three independent experiments ± SEM. ID: Initial Dose. **B)** Confocal micrographs of BeWo b30 / HUVECs on microporous inserts stained for DAPI (blue, nuclei), tubulin (red, microtubules) and ZO-1 (green, tight junctions). Magnification: 63x.

Cell Membrane integrity

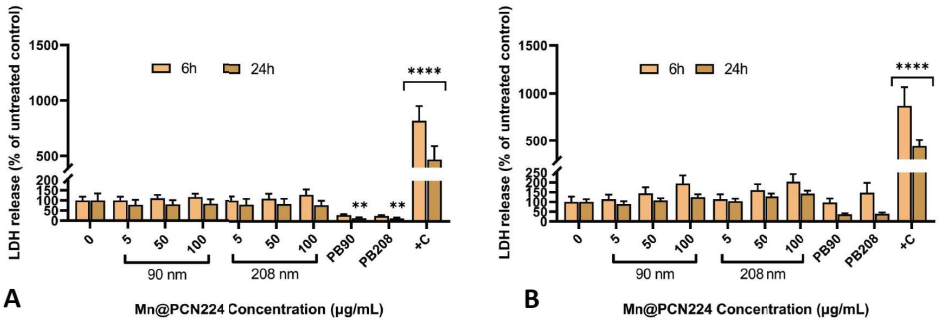

Figure 3: Membrane integrity of A) BeWo b30 and b) HUVEC mono-cultures after exposure to 90 nm and 208 nm Mn@PCN224 for 6 and 24h, assessed with LDH assay. The negative control (0 µg/mL - cell medium) was set to 100% LDH release. Triton-X 100 (0.2%) was used as positive control (+C). PB: Particle blank: cell-free inserts with 100 µg/mL of SAzymes. Results are presented as the mean of three independent experiments ± SEM.

Conclusion

Our first SAzyme product is a Porous Coordination Network 224 (PCN224) nanomaterial with encapsulated Mn^{2+} (**Mn@PCN224**) displaying **Superoxide Dismutase (SOD)-activity**. Preliminary toxicity studies demonstrated **no barrier integrity or cell membrane impairment** by Mn@PCN224 in ***in vitro*** trophoblast-endothelial cell co-cultures. These preliminary results suggest a **high cytocompatibility** profile of SAzymes ***in vitro***. **Further research** is ongoing to investigate sub-lethal and long-term effects of Mn@PCN224 on **placenta functionality** and along with the assessment of **cell uptake**, **accumulation** and **translocation** patterns across the **feto-placental interface**.

References
1. Negishi Y, Shima Y, Takeshita T, Morita R. Harmful and beneficial effects of inflammatory response on reproduction: sterile and pathogen-associated inflammation. Immunol Med. 2021
2. Burton GJ, Fowden AL. The placenta: a multifaceted, transient organ. Philos Trans R Soc Lond B Biol Sci. 2015
3. Park J, Jiang Q, Feng D, Mao L, Zhou HC. Size-Controlled Synthesis of Porphyrinic Metal-Organic Framework and Functionalization for Targeted Photodynamic Therapy. J Am Chem Soc. 2016

ETH zürich

This research project is funded by the Swiss National Science Foundation (Grant no. IZLCZ0_206059)

Empa

Self-assembling nasal gel for enhanced delivery of ghrelin to the central nervous system for amyotrophic lateral sclerosis therapy

Rifka Nurul Utami[1], Shunping Han[1], Julie Wang[1], Jemeen Sreedharan[2], David K. Smith[3], Jeffrey S. Davies[4], Khuloud T. Al-Jamal[1]

[1]Institute of Pharmaceutical Science, Faculty of Life Sciences & Medicine, King's College London; [2]Institute of Psychiatry, Psychology, and Neuroscience, King's College London; [3]Department of Chemistry, University of York; [4]Molecular Neurobiology Group, Institute of Life Sciences, School of Medicine, Swansea University

INTRODUCTION

- Current available treatments for ALS are limited to increased survival with minimum improvement in patients' quality of life.
- The 'hunger hormone' ghrelin has attracted attention for ALS therapy due to its neurogenic and neuroprotective effects.
- Nose-to-brain (N2B) route has been shown to increase brain uptake of therapeutics; beneficial for treating CNS diseases.
- Smart self-assembling and shear-thinning hydrogel may increase brain uptake of ghrelin using the nasal route.

OBJECTIVES

To formulate ghrelin into self-assembling nasal gel system and assess brain uptake following intranasal administration as a potential therapy for ALS.

METHODS

1 Hydrogel formulation

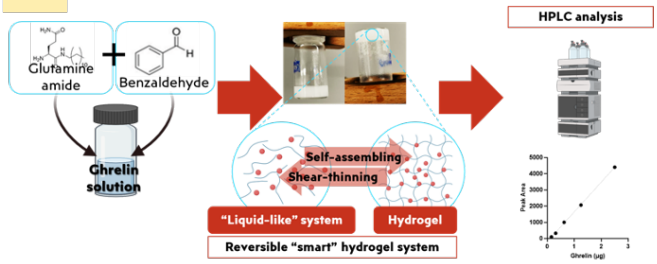

2 *In vivo* brain uptake and spatial distribution studies

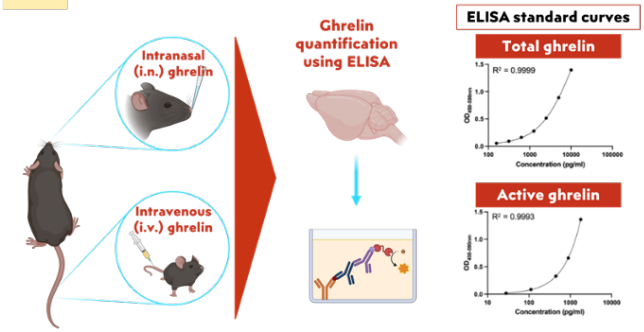

3 Therapy studies on ALS-FTD TDP43 *knock-in* mice

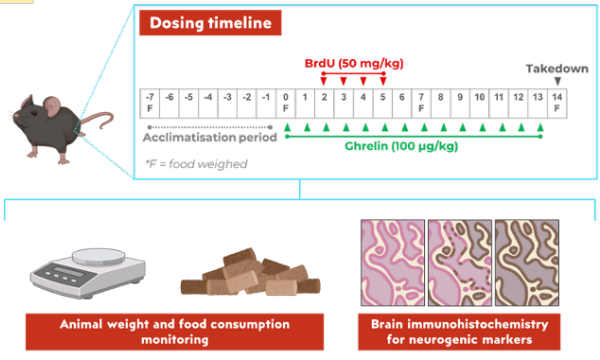

References:
Wang, JT et al. Advance Science, 2021; 8(14): 2101058.
Ngo ST et al. Journal of Neuroendocrinology, 2021; 33(7).

RESULTS

1) HPLC chromatograms showing that ghrelin remains stable after incorporation into the nasal gel formulation

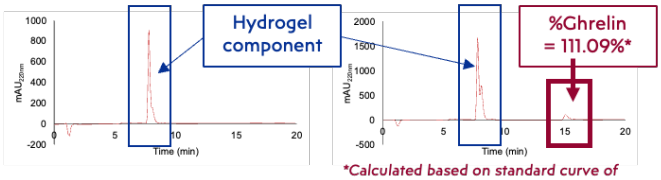

**Calculated based on standard curve of ghrelin*

2) Brain uptake of ghrelin at 10 min following different routes of administration

3) Time-function brain up-take of ghrelin following intranasal administration of Ghr-HG

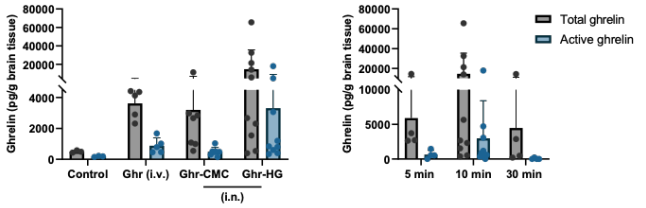

4) Brain region-specific distribution of total and active ghrelin following different administration routes after 10 minutes

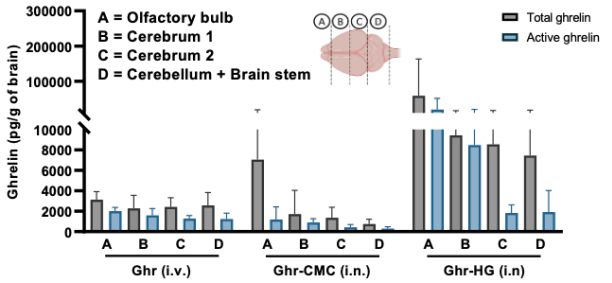

5) Percentage of body weight changes and food consumption from different treatment groups following ghrelin multiple administrations on ALS-FTD mouse model

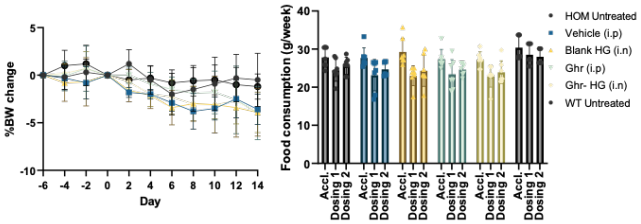

CONCLUSIONS

- ✓ "Smart" self-assembling hydrogel system for i.n. administration containing ghrelin was successfully prepared.
- ✓ I.n. administration of Ghr-HG resulted in higher brain accumulation compared to i.v. Ghr and i.n. Ghr-CMC at 10 minutes post administration.
- ✓ Brain region-specific distribution results showed accumulation in olfactory bulb in the i.n. groups, proving the occurrence of nose-to-brain transport.
- ✓ Brain level of ghrelin following i.n. Ghr-HG administration peaked at 10 minutes, but the activity diminished after 30 minutes.
- ✓ Multiple administration of Ghr-HG on ALS-FTD mouse model for two weeks was well-tolerated.

PROTEIN CORONA STUDY OF TUNABLE LIPID BILAYER COATED NANOPARTICLES

Mireia Vilar-Hernández [1,2] *, Pedro Veloso [3], Giorgio Arrigoni [3], Emanuele Papini [3], Pascal Jonkheijm [1,2]
1. LipoCoat B.V, Enschede, Netherlands. 2. Molecular Nanofabrication Group, University of Twente, Enschede, Netherlands.
3. Department of Biomedical Sciences, Università di Padova, Padova, Italy.
*e-mail: m.vilarihernandez@utwente.nl

Introduction

Research has shown that the complement activation pathway caused by liposomes is different depending on the charge (anionic or cationic)[1]. Moreover, the molecular group seems to be relevant regarding the immune activation profile[2]. For that reason we coated silica nanoparticles with different charged phospholipids to see the differences in protein corona formation.

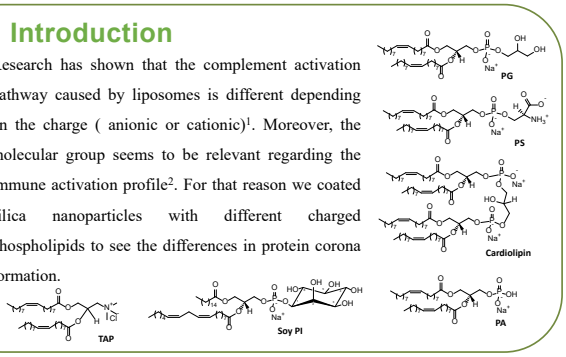

Coating SiNP with Lipids

Synthesis

Solvent Gradient Assisted Method

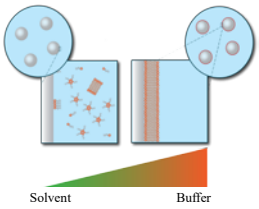

Characterization

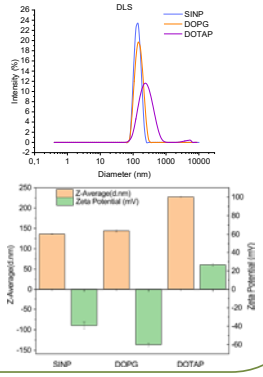

Fig 1. SiNP Coated synthesis scheme. On the upper right, intensity graph. Bottom right, representation of Z-Average and Z-Potential values of the different particles measured with DLS.

Protein Corona Studies

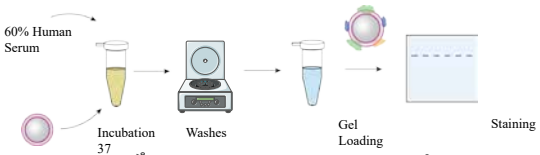

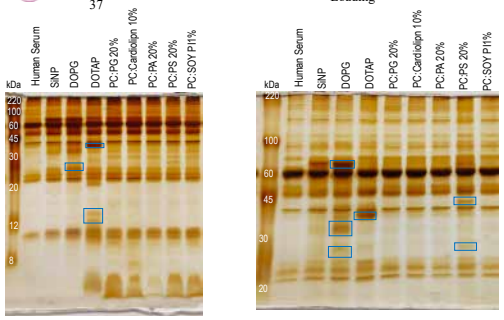

Fig 2. Protein gel of the particles' corona with silver staining. On the left, 15% Acrylamide gel and a 10% Acrylamide gel on the right. The blue boxes highlight the differences in the protein profile.

Proteomics

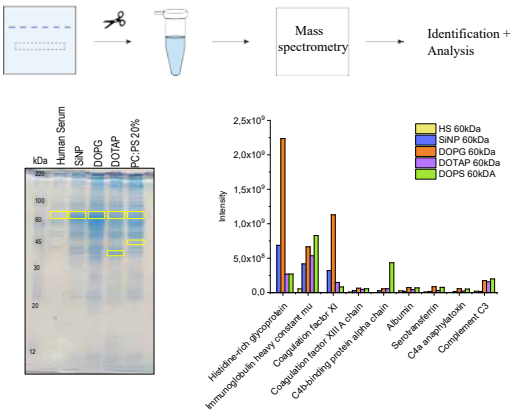

Fig 3. On the left, the protein gel of the particles' corona with Coomassie blue staining. The bands that were cut to perform in-gel proteomics are indicated in yellow. On the right, representation by intensity of the most predominant proteins in the 60kDa band.

Histidine-rich glycoprotein as dysopsonin

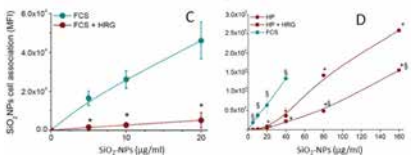

Fig 4. Image from Fedeli C. et al. *Nanoscale* **2015**, *7(42) , 17710.* Macrophage uptake of silica nanoparticles pre-incubated with FCS and FCS + HRG. In graph D, the nanoparticles are incubated with Human Plasma (HP), HP + HRG and FCS.

- The presence of a protein corona around the nanoparticle decreases the uptake by the macrophages.
- When added HRG the uptake is highly decreased compare to just FCS

Conclusions

- The cationic coating (DOTAP) presents different protein profile than the anionic one (DOPG).
- Between the negatively charged coatings, DOPS shows more differences in their protein corona profile.
- DOPG coating might shield the nanoparticle from the macrophages due to the HRG presence in the protein corona.

Future Work

- Coat silica fluorescent nanoparticles for internalization studies.
- Shotgun proteomics to determine the identity of different corona proteins.
- Further studies of different coating and their influence on the immune response.

References

1. Choon, A. J. Immunol. **146**, 4234-4241.
2. Sou, K. Biochim. Biophys. Acta-Biomembr. **1778**, 1035-1041.

Acknowledgments

This project has received funding from the european union's horizon 2020 research and innovation programme under the marie skłodowska-curie grant agreement no 956544.

Theranostic Bimodal Lipid-based Nanomedicines for Effective Cancer Treatment

Michaela Vojnikova[1,2], Ladislav Sivak[2], Andrew D. Miller[2], Zbynek Heger[2]

[1]Central European Institute of Technology, Brno University of Technology, Brno, Czech Republic
[2] Department of Chemistry and Biochemistry, Mendel University in Brno, Brno, Czech Republic

Theranostics enables the simultaneous detection, drug distribution, and therapeutic response evaluation, ultimately leading to the development of **precise medicine.** We aim to develop **highly stable theranostic LNPs** (TNPs) with the incorporated hydrophobic **drug ellipticine** (Elli@TNPs) for real-time tracking using MRI. Ellipticine has high efficacy against various cancer types, minimal toxic side effects, and absence of haematological toxicity.

RESULTS

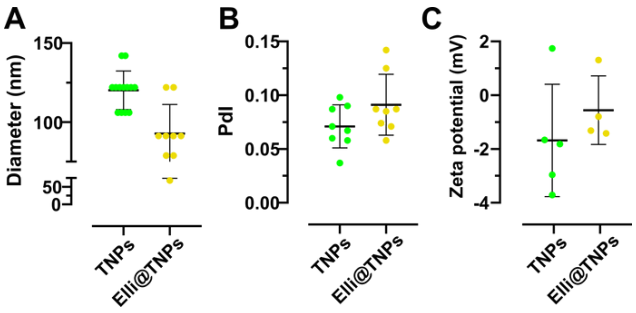

Physicochemical characterisation of theranostic Elli@TNPs and imaging TNPs: Fig. A-B) combination of injection method with extrusion provide uniform (PdI < 0.1) TNPs with diameter around 125 nm and Elli@TNPs up to 100 nm and have neutral charge (Fig. C).

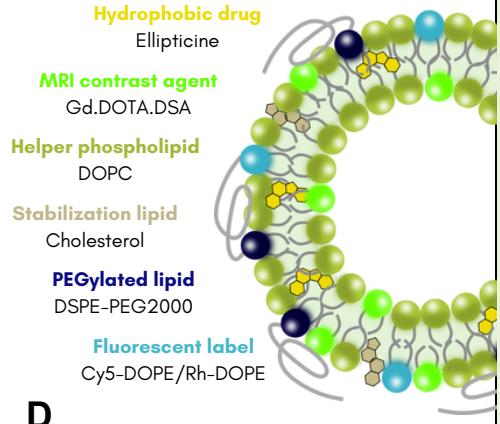

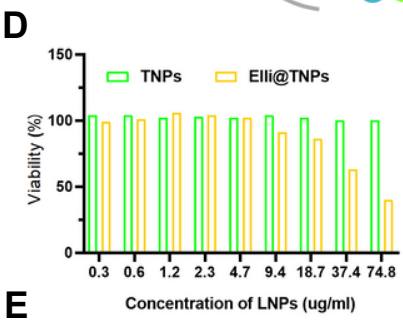

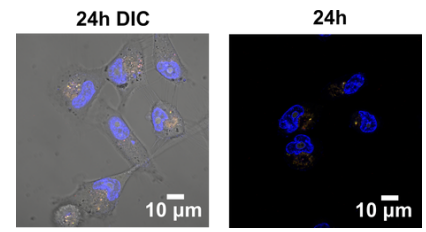

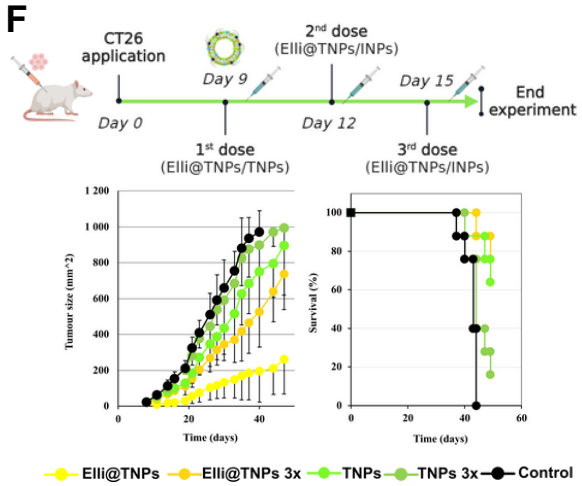

***In vitro* and *in vivo* evaluation of Elli@TNPs as drug carrier:**
Fig. D) MTT assay revealed cytotoxic profile of Elli@TNPs, while TNPs were fully non-toxic. Therefore, cytotoxicity can be fully attributed to the payload (Ellipticine). Fig. E) cellular uptake of Elli@TNPs by MDA-MB-231 cells, Fig. F) Elli@TNPs have therapeutical potential for treatment of CT26 tumours. Survival of mice were prolongated compared to control or empty TNPs.

CONCLUSIONS

- Elli@TNPs and TNPs have **uniform size** and **neutral charge**.
- TNPs are highly **biocompatible** and toxicity of Elli@TNPs is related to Ellipticine.
- Our TNPs proved to be **promising drug carrier**.
- MRI biodistribution studies are ongoing.

Shiqi Wang

A biomimetic dual-drug loaded lipid nanocarrier enhances apoptosome assembly for cancer therapy

Shiqi Wang*, Huijie Han, Jie Chen, Jiachen Li, Alexandra Correia, Raquel Bártolo, Mohammad-Ali Shahbazi, Tambet Teesalu, Wenguo Cui, Hélder A. Santos

*Division of Pharmaceutical Chemistry and Technology, Faculty of Pharmacy, University of Helsinki. Email: shiqi.wang@helsinki.fi

Background and Aim

- Cancer cells develop various mechanisms to escape apoptosis via interrupting apoptosome assembly, a key step to initiate apoptosis. This promotes tumorigenesis and drug resistance, and thus, poses a great challenge in cancer treatment.
- **Our goal is to promote apoptosome formation and the subsequent cancer apoptosis by developing a biomimetic liposomal formulation**, co-loaded with a pro-apoptotic protein Cytochrome C (Cyt C) and a glycolysis inhibitor lonidamine (LND). Cyt C is a major component of apoptosome, while LND modulates the metabolic activity to sensitize the cells to Cyt C-induced apoptosis. We further conjugated a tumor homing peptide, LinTT1 on the liposome, to increase tumor accumulation and the efficacy of pro-apoptosis cancer therapy.

Project Design

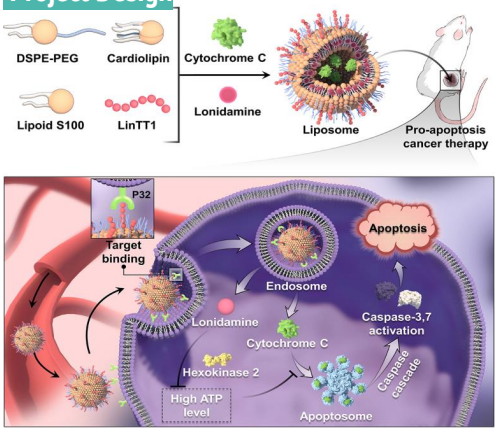

Liposomal Formulation Characterization

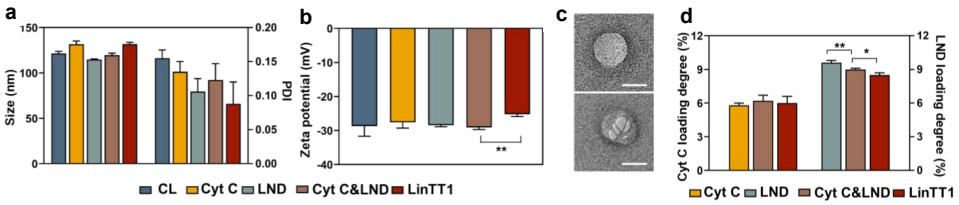

(a, b) The size, PDI and Zeta potential of liposomal formulations with or without drug loading. (c) TEM images of blank liposome (above) and CytC&LND liposome (below). (Scale bar: 100 nm). (d) Cyt C and LND loading degree (wt %) in different liposomes.

In vitro Pro-apoptotic Mechanisms and in vivo Anti-tumor Efficacy

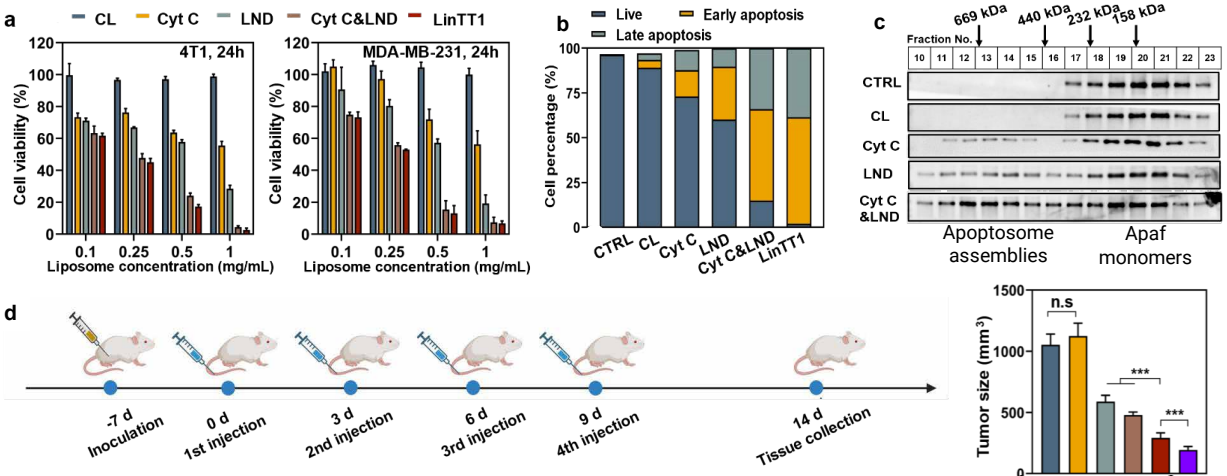

(a) The cytotoxicity, and the apoptosis level of different liposomes treated cells based on annexin V-FITC/PI staining (b) , and by Apaf-1 Western Blot analysis (c). (d) The average tumor volume after 14 day treatment on 4T1-mice model. CL: blank liposome; Cyt C: Cyt C loaded liposome; LND: LND loaded liposome; Cyt C&LND: Cyt C and LND co-loaded liposome; LinTT1: LinTT1 modified Cyt C&LND co-loaded liposome.

Acknowledgements: Travel expenses were partially covered by the Travel Award sponsored by the open access journal published by MDPI.

More details in: Advanced Functional Materials, 2305316. https://doi.org/10.1002/adfm.202305316

Christoph Wilhelmy

Polysarcosine-Functionalized mRNA lipid nanoparticles tailored for immunotherapy

CLINAM
European Foundation for Clinical Nanomedicine

Christoph Wilhelmy[1,2](cwilhelmy@uni-mainz.de), Isabell Sofia Keil[1,3,4], Lukas Uebbing [1,2], Matthias Barz [1,5], Ugur Sahin [1,4], Heinrich Haas [1,2], Mustafa Diken[1,3], Peter Langguth[1,2]

[1] Collaborative Research Center 1066, Nanodimensional polymer therapeutics for tumor therapy, Mainz, Germany; [2] Department of Biopharmaceutics and Pharmaceutical Technology, Johannes Gutenberg University, Mainz, Germany; [3] TRON–Translational Oncology at the University Medical Center of the Johannes Gutenberg University, Mainz, Germany; [4] Department of Immunology, University Medical Center of the Johannes Gutenberg University Mainz, Germany; [5] LACDR – Leiden Academic Centre for Drug Research, Leiden, The Netherlands

Background & Objectives

Lipid nanoparticles (LNPs) are designed to deliver various types of RNA for therapeutic purposes and induce an antigen specific immune response. They have shown promising results, not only with the success during the pandemic, but for a wide range of applications. However, many structural features and their implications on *in vitro* and *in vivo* efficacy still remain unclear. In this study, small angle X-ray scattering (SAXS) and other physicochemical characterization methods were utilized to elucidate structural changes induced by variation in particle composition. Permutations from combinations between two different well-established ionizable lipids (DODMA vs. Dlin-MC3-DMA (MC3)) together with phospholipids comprising either a -PE or a -PC headgroup (DOPE vs. DOPC) and two different stealth moieties (PEG vs. polysarcosine (pSar)) were investigated. To correlate structural and functional properties, the biological efficacy of those formulations was tested with different *in vitro* assays on human peripheral mononuclear blood cells (hPBMCs).

Structural characterization of LNP formulations with SAXS

Methodology

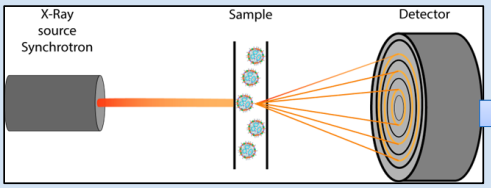

Basic concept of SAXS measurement: X-Ray beam is emitted from synchrotron and is scattered by the LNP sample in a flow-through capillary. Scattered light is detected and converted in a scattering profile (as shown right).

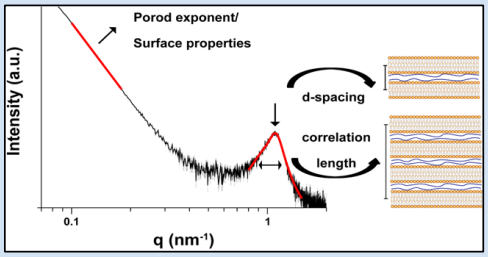

Analysis of SAXS data: SAXS patterns are dominated by a single peak at around 1 nm^{-1}. Lorentzian fitting allows insight in repeating unit length (d-spacing) and long range order (correlation length). Analysis of exponential decay in low q region indicates overall particle shape and surface properties.

Results

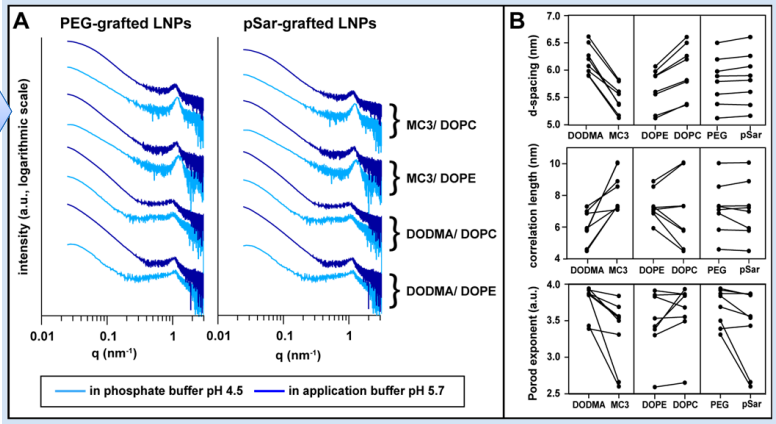

Results of structural investigation via SAXS:
A. SAXS patterns of different LNP formulations in phosphate buffer (pH 4.5, light blue) and application buffer (pH 5.7, dark blue). Formulations are displayed according to their composition with PEG-grafted LNPs (left) and pSar-grafted LNPs (right) and their ionizable and helper lipid being displayed right to the scattering patterns. Scattering patterns are vertically shifted for better visualization. **B.** Comparison between LNP formulations in d-spacing, correlation length and Porod exponent. Investigated pairs generated with formulations only differing in one lipid component (ionizable lipid (left), helper lipid (middle), stealth lipid (right)). While DOPE and MC3 containing LNPs show denser internal packing, functionalization with pSar leads to lower Porod exponents and therefore higher surface roughness, without influencing internal structure.

In vitro studies: screening of different LNP formulations in hPBMC

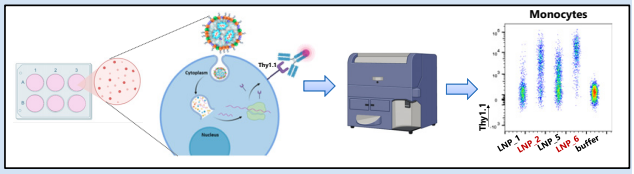

Methodology of transfection studies: LNP formulations, containing Thy1.1 encoding mRNA were added to hPBMCs. Transfected cells express Thy1.1, a highly conserved membrane glycoprotein. Flow cytometry analysis is used to screen the transfection efficiency of each LNP formulation.

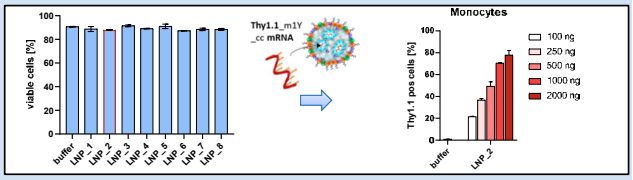

***In vitro* tolerability and dose-dependency of LNP formulations:** All LNP formulations show cell viabilities at or above 90% in all tested doses (10-2000 ng). Dose-dependent transfection of monocyte sub cell population was observed for all formulations.

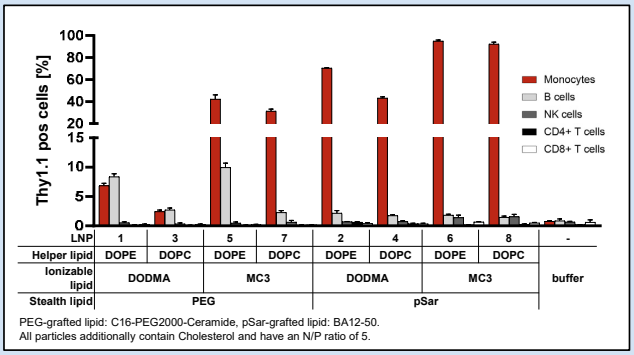

PEG-grafted lipid: C16-PEG2000-Ceramide, pSar-grafted lipid: BA12-50.
All particles additionally contain Cholesterol and have an N/P ratio of 5.

Transfection studies on hPBMCs:
In vitro transfection efficacy of LNP formulations at a dose of 1000 ng in hPBMC cell populations. Monocytes show highest transfection rates. Respective lipid composition is displayed in the table at the bottom. MC3 and DOPE containing LNPs show better transfection than DODMA and DOPC containing counterparts. Also pSar as stealth moiety leads to higher transfection than in PEG counterparts for monocytes.

Conclusion

SAXS analysis enabled a sensitive determination of the influence of respective lipids on LNP internal and overall structure. We observed certain compositional and structural 'fingerprints' of LNPs which led to improved transfection efficacy in the investigated cells. LNPs comprising MC3 as an ionizable lipid, DOPE as helper lipid and pSar as a stealth moiety showed increased fractal dimension and packing density. Interestingly, these formulations obtained the highest activity *in vitro*. A deeper understanding of these relationships can be highly valuable for development of safe and efficient delivery systems and implementation of quality control measures.

This work is supported by the CRC1066 B12 project funded by the Deutsche Forschungsgemeinschaft (DFG). Access additional information related to the research in Wilhelmy, C., et al. Polysarcosine-Functionalized mRNA Lipid Nanoparticles Tailored for Immunotherapy. Pharmaceutics 2023, 15, 2068; or by scanning the QR code shown above.

SFB 1066 · Johannes Gutenberg Universität Mainz · TRON Science in Translation · Universitätsmedizin Mainz · Universiteit Leiden

Yu Xiaodong

Targeted Regulation of Ceramide Synthesis Ameliorates Non-alcoholic Fatty Liver Disease

Xiaodong Yu[1,2], Chenyuan Huang[1], Martijn Evers[3], Sitong Zhang[1,2], Hui Jun Ting[1], Mark D. Muthiah[4], Liang Gao[5], Federico Torta[5], Raymond Schiffelers[3], Gert Storm[1,2,6], Jiong-Wei Wang[1,2]

[1]Department of Surgery, Yong Loo Lin School of Medicine, National University of Singapore, Singapore 119228, Singapore (surwang@nus.edu.sg)
[2]Nanomedicine Translational Research Program, Centre for NanoMedicine, Yong Loo Lin School of Medicine, National University of Singapore, Singapore 117609, Singapore
[3]CDL Research, UMC Utrecht, Utrecht, the Netherlands
[4]Division of Gastroenterology and Hepatology, Department of Medicine, Yong Loo Lin School of Medicine, National University of Singapore
[5]Singapore Lipidomics Incubator, Life Sciences Institute, NUS, Singapore 117456, Singapore
[6]Department of Pharmaceutics, Faculty of Science, Utrecht University, Universiteitsweg 99, 3584 CG Utrecht, The Netherlands

Introduction & Method

Non-alcoholic fatty liver disease (NAFLD) is a spectrum of chronic liver disease caused by excessive fat accumulation in the liver, with a prevalence of up to 40% in the United States and in Singapore. NAFLD can progress to a more severe form known as non-alcoholic steatohepatitis (NASH), which is characterized by liver inflammation and fibrosis, and can ultimately lead to cirrhosis and liver cancer. Currently, efficacious drugs reversing the various forms of this disease are not yet available. Clinical studies have linked ceramides, a type of sphingolipids, to the development of NASH, however, their pathogenic contribution to NASH remains largely unexplored. In this study, we identified a ceramide synthesis pathway that is highly upregulated in a cohort of NASH patients and several clinically relevant NASH animal models. Employing the DLin-MC3-based lipid nanoparticles (LNP) for siRNA delivery, we achieved effective knockdown of ceramide synthesis enzymes in the liver and lowered both hepatic and circulating ceramides in animals. Intravenous administration of LNP-siRNAs on a regular basis remarkably improved animal lipid profiles and ameliorated NASH disease progression, including steatosis (hepatic lipid accumulation), inflammation and fibrosis. Apart from biochemical and histological evidence, the therapeutic efficacy was also confirmed by our recently developed myeloperoxidase-responsive T_1 and T_2 switchable magnetic resonance imaging (MRI) approach. To conclude, this proof-of-concept study demonstrates the feasibility of LNP siRNA system for the treatment of metabolic diseases.

Results

1. Liver Ceramide Production Increases in NASH

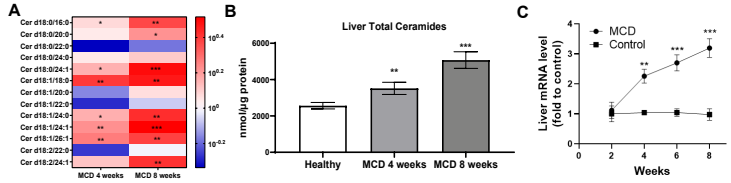

Figure 1. Liver ceramide production increases in NASH. (A) Alteration in specific ceramide species in NASH liver (Heat map presented as LOG 10 of fold change vs Ctrl group). (B) Liver total ceramides increase in MCD NASH mice. (C) Liver Ceramide synthesis associated mRNA expression in NASH liver. *P < 0.05, **p < 0.01, ***p < 0.001, N=3

2. LNP-siRNA Knockdown in NASH Liver

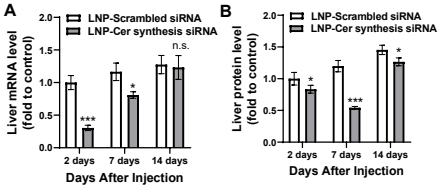

Figure 2. LNP-siRNA knockdown in NASH liver. Time response of Ceramide synthesis associated gene knockdown evidenced by the expression of targeted mRNA (A) and protein (B). *P < 0.05, **p < 0.01. ***p < 0.001, N=3.

3. Lowering Ceramides Prevents NASH Development

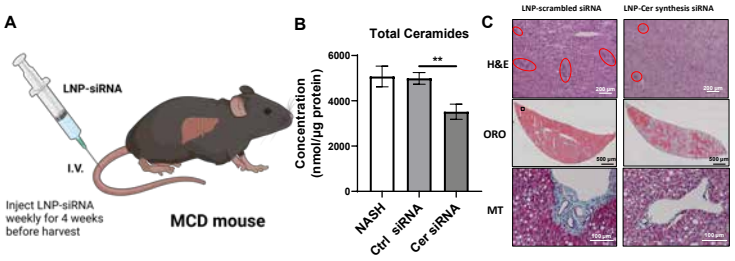

Figure 3. Lowering ceramides prevents NASH development. (A) *In vivo* experimental design. (B) Total ceramides decreased in NASH Liver. (C) Lowering liver ceramides production reduces liver inflammation (H&E staining), lipid deposition (ORO staining) and fibrosis (Masson's trichrome staining). **P < 0.01, N=7.

4. Therapeutic Efficacy Confirmed by T_1 and T_2 Switchable MRI

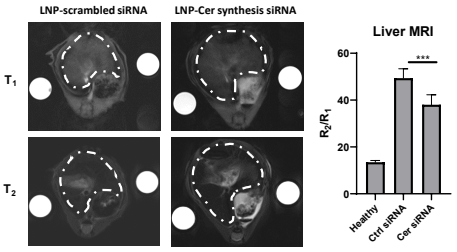

Figure 4. Therapeutic efficacy confirmed by T_1 and T_2 switchable MRI. (A)The T_1 and T_2 MR imaging of mice at horizontal plane 24 hours post injection. (B) R_2/R_1 of the livers reduced with LNP-Ceramide synthesis associated siRNA treatment. **P < 0.01, N=3.

Conclusion

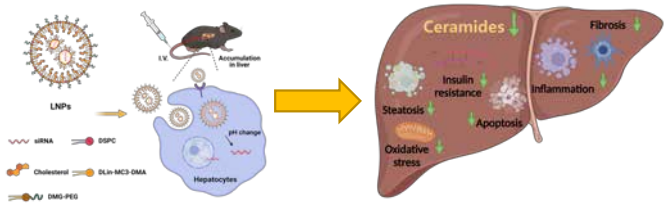

Lowering hepatic ceramides via LNP mediated siRNA knockdown prevents NASH progression in mice.

In addition, the therapeutic efficacy was also confirmed by our recently developed myeloperoxidase-responsive T1 and T2 switchable MRI approach

Acknowledgment: We acknowledge funding from the National University of Singapore NanoNASH Program (NUHSRO/2020/002/NanoNash/LOA) and the Ministry of Education MOE AcRF Tier 1 grant (NUHSRO/2021/113/T1/Seed-Sep/06).
Reference: Jingjing Liu, Xiaodong Yu, *et al.* Myeloperoxidase-Sensitive T1 and T2 Switchable MR Imaging for Diagnosis of Nonalcoholic Steatohepatitis. **ACS Nano** 2023 17 (4), 3324-3333

Assessing brain targeting efficiency of lipid nanoparticles encapsulating CRISPR following different routes of administration in mice

Meiling Yu, Nadia Rouatbi, Jemeen Sreedharan and Khuloud T Al-Jamal
Institute of Pharmaceutical Sciences, Faculty of Life Science and Medicine, King's College London

❑ INTRODUCTION

- Gene therapy works by introducing a stable and inducible transgene that will correct or delete the defective gene leading to a correction in the disease status.
- The clustered regularly interspaced short palindromic repeats (CRISPR)/Cas9 technology has recently emerged as a powerful tool for targeted genome editing [1].
- Non-viral system, such as lipid nanoparticles (LNPs), has become an attractive delivery platform for CRISPR-mediated genome editing due to its cost-effectiveness, low immunogenicity and application flexibility.
- LNPs capable of efficient gene-editing can be potentially used in multiple brain disorders which currently lack effective therapies, for improving drug delivery to cellular targets both at and across the blood–brain barrier (BBB) [2].

❑ AIM

To study brain distribution and gene-editing efficiency of Stable nucleic acid lipid particles (SNALPs) after intravenous (*i.v.);* intracranial *(i.c.)* and intranasal (*i.n.)* routes of administration to Rosa26-Cas9 knock-in mice expressing GFP.

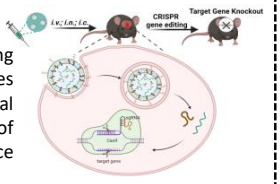

❑ METHODOLOGY

SNALPs formulation & characterization

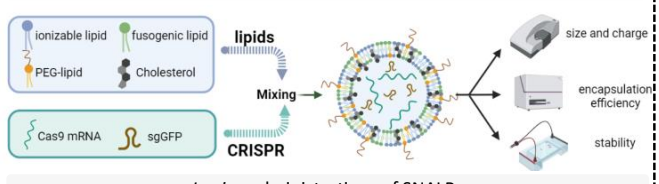

In vivo administrations of SNALPs

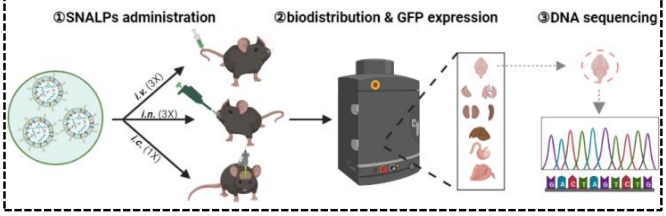

❑ RESULTS

SNALPs characterization & stability

Table 1. Physicochemical characterisation of SNALPs formulations

size (d.nm)[a,d]	PDI[a,d]	Charge at pH7.4 (mV)[a,b,d]	% RNA encapsulation (%)[c,d]
125.68±3.14	0.17±0.021	-1.46±5.10	91.26±2.31

[a] Measured 3.14 by Dynamic Light Scattering.
[b] Measured in phosphate buffer 0.1M (pH7.4)
[c] The encapsulation efficiency (EE %) was measured with the RiboGreen assay
[d] Expressed as mean ± SD (n=3).

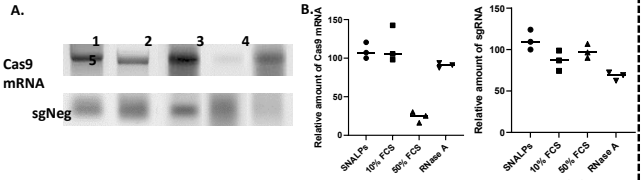

Figure 1: CRIPSR loaded SNALPs are stable in 10% FCS and RNase A for at least 48h. (A) RNA agarose gel electrophoresis: Free Cas9 mRNA & sgRNA (lane 1), encapsulated Cas9 mRNA & sgRNA from SNALPs (lane 2), encapsulated Cas9 mRNA & sgRNA recovered from SNALPs after 48h exposure to 10% FCS; 50% FCS and RNase A (lanes 3, 4, 5). **(B)** Relative amount of Cas9 mRNA & sgRNA from SNALPs without exposure or with 48h exposure to 10% FCS; 50% FCS and RNase A.

✓ SNALPs produced were <140 nm in diameter, < 0.2 polydispersity and near neutral Zeta potential. Nucleic acid loading efficiency ~90%.
✓ SNALPs were serum stable under *in vitro* testing conditions.

In vivo biodistribution of fluorescent SNALPs

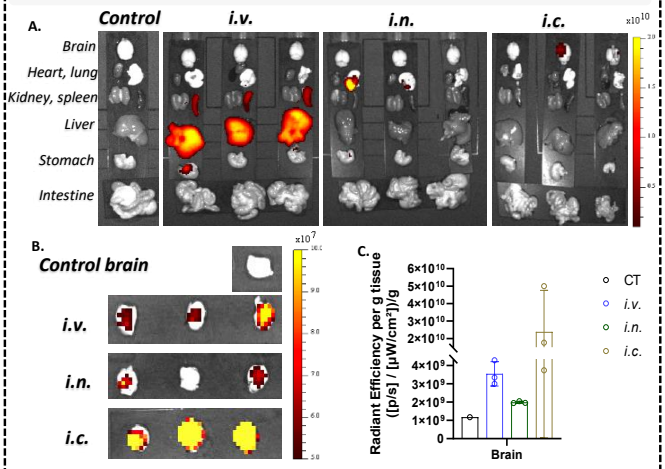

Figure. 2: Biodistribution of DiR labelled SNALPs following single *i.v.; i.n.* and *i.c.* administration. Organs were imaged at 24 hours post-administration **(A).** Brains were imaged separately **(B)** and semi-quantified **(C)** using IVIS Lumina Series III.

✓ SNALPs could reach and stay in brain for up to 24h following *i.v.; i.n.* and *i.c.* administration.

In vivo GFP knockout (KO) in mouse brain

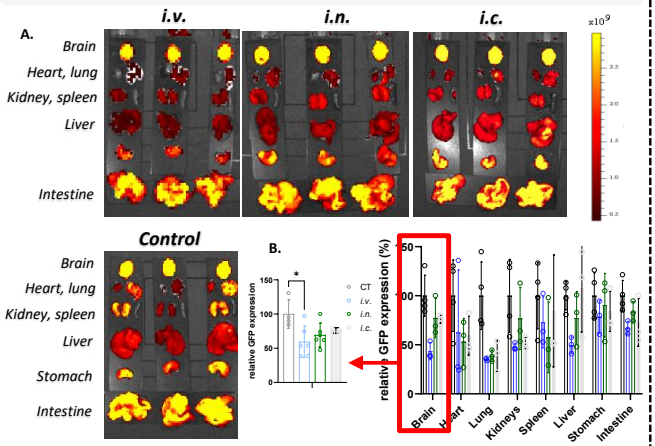

Figure. 3: GFP expression in organs following administration of GFP SNALPs. (A) optical imaging of GFP and **(B)** semi-quantify following *i.v. (3x); i.n. (3x)* and *i.c. (1x)* administration for 7 day's treatment.

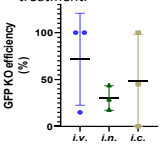

Figure. 4: GFP KO in mouse brain. DNA were extracted from treated brains. KO was assessed after 7 days using Sanger Sequencing and Inference of CRISPR Edits (ICE) analysis.

✓ *i.v.* administration achieved the most potent KO efficiency (50-60%) compared to *i.c.* and *i.n.* (<20%) as confirmed by optical imaging and ICE.

❑ CONCLUSIONS AND FUTURE WORK

- All routes of administration achieved KO in mouse brain but *i.v.* appeared to be the most promising followed by *i.c.* and *i.n.*
- *i.v.* injection resulted in KO in other organs which may not be desired.
- A limitation of *i.c.* administration was limited to a single administration due to the invasive nature of the procedure.
- Future work will involve assessing gene-editing efficiency in wildtype mice and replacing GFP as a model target with therapeutic target genes.

❑ REFERENCES

[1] Wright AV, Nunez JK, Doudna JA. *Cell* 2016; 164:29-44.
[2] Jiang, Yihang, et al. *Biomaterials Science* (2022).

❑ ACKNOWLEDGEMENT

Meiling Yu is funded by China Scholarship Council (K-CSC) and Sanofi iAward.

Alaa Zam

Developing nucleic acid-based therapies targeting immune checkpoints in glioblastoma microenvironment using lipid nanoparticles

Alaa Zam, Nadia Rouatbi, James Arnold, and Khuloud T. Al-Jamal
School of Cancer & Pharmaceutical Sciences, King's College London, UK

cara — a lifeline to academics at risk

INTRODUCTION

Immunotherapy strategies have revolutionised the treatment of many cancers, increasing the hope for Glioblastoma Multiforme (GBM) therapy [1].
One viable strategy is the use of nucleic acid (NA)-based therapies to manipulate the expression of positive and/or negative immune checkpoints (ICPs) in GBM microenvironment [2]. Lipid nanoparticles (LNPs) represent the most clinically advanced non-viral vector for the delivery of NAs [3].

AIM

To optimise LNPs for mRNA delivery (mOX40L) by changing the type of ionisable and PEG-lipids to improve transfection efficiency of brain cancer (GL261) and brain cancer stem (BL6) cell lines *in vitro* and *in vivo*.

METHODS

Preparation and physico-chemical characterisation of LNPs

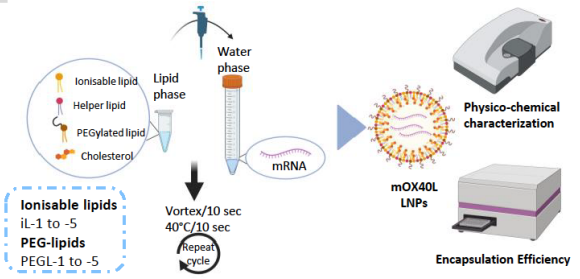

In-vitro assays: Transfection, MTT assay, and fluorescence imaging

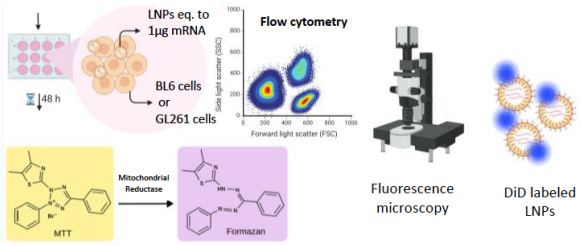

Tumour models: mRNA modification and in-vivo transfection

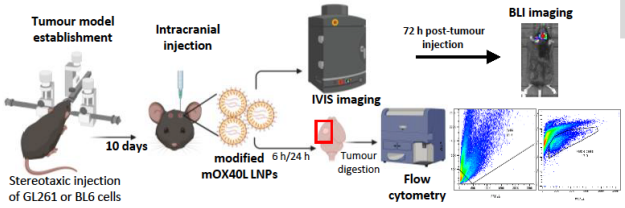

RESULTS

Physicochemical characteristics

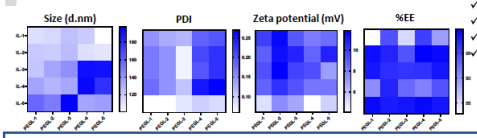

Physicochemical characteristics in the acceptable range:
- ✓ hydrodynamic size <200 nm
- ✓ PDI <0.27
- ✓ zeta potential 4 – 12 mV.
- ✓ EE% >85%.

LNPs Cytotoxicity

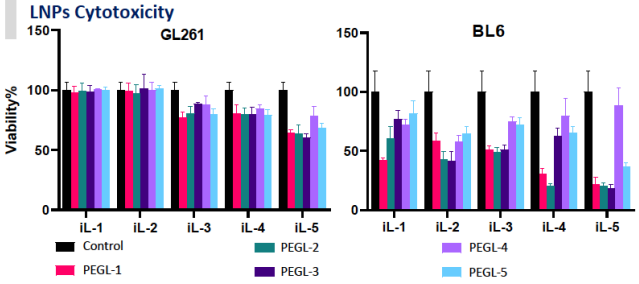

✓ Results show that LNPs formulations were more toxic when incubated with BL6 cells. PEGL-1 and PEGL-2 showed consistent toxicity with all ionizable lipids. PEGL-4 offered safest profile.

Transfection efficiency

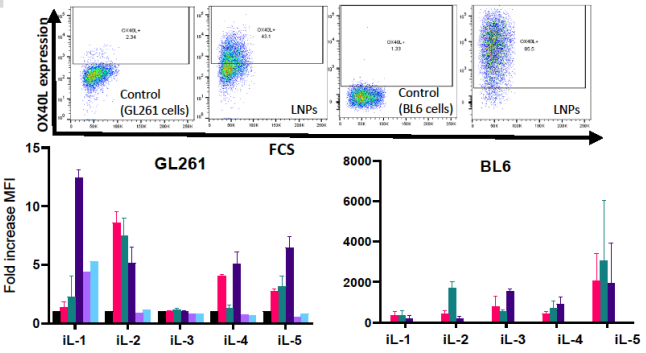

✓ GL261 seemed to be harder to transfect than BL6. Different lipids combinations offered different transfection efficiency profiles.

Fluorescence imaging

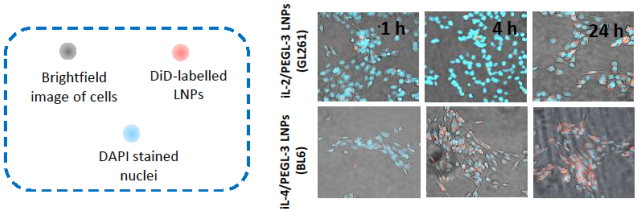

✓ Results show more efficient and time-dependent uptake in BL6 cells, which agrees with transfection results as previously shown.

mRNA delivery in-vivo transfection

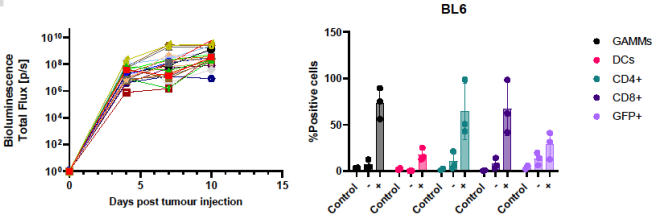

✓ LNPs were successful in transfecting different immune cell populations in BL6 tumour models. Transfection was higher in macrophages and T cells. (Control=Untreated, - = mLuc LNPs, + = modified mOX40L LNPs).

Conclusions

- GL261 cells were harder to transfect than BL6 cells. The commercial reagents, lipofectamine failed to transfect both cell types.
- IL-1/PEGL-3 and iL-5/PEGL-2 showed the best transfection efficiencies in GL261 and BL6 respectively. However, due to the high toxicity of iL-5, iL-1/PEGL-3 offers a safer and more effective alternative.
- mOX40L LNPs were efficient in transfecting different cell populations in GL261 and BL6 in-vivo models. Higher levels of transfections were observed in BL6 model which correlates with our in-vitro data.

References
[1] Bausart M, et al. Immunotherapy for glioblastoma: the promise of combination strategies. J Exp Clin Cancer Res. 2022 Jan 25;41(1):35.
[2] Buonfiglioli A, Hambardzumyan D. Macrophages and microglia: the cerberus of glioblastoma. Acta Neuropathol Commun. 2021 Mar 25;9(1):54.
[3] Yan Y, et al. Non-viral vectors for RNA delivery. J Control Release. 2022 Feb;342:241-279.

Yanira Zeyn

Comparative study of adjuvants and their synergistic potential for the stimulation of dendritic cells (DC) and liver non-parenchymal cells

Malin Svensson[1], Yanira Zeyn[2], Maria-Jose Limeres[1], Maximiliano Caceido[1], Stephan Gehring[1] and Matthias Bros[2]

[1] University Medical Center, Children's Hospital, Germany
[2] University Medical Center Mainz, Department of Dermatology, Germany

UNIVERSITÄTSmedizin. MAINZ

CLINAM European Foundation for Clinical Nanomedicine

Background

Liver non-parenchymal cells (NPCs), comprising Kupffer cells (KC), dendritic cells (DC) and liver sinusoidal endothelial cells (LSEC) exert tolerogenic activity by default.

Liver NPCs express receptors to which nano-particles (NP) can bind:

- Fc receptors (antibodies)
- CD206 (mannose)
- CD209 homologs (trimannose)
- Scavenger receptors

Systemically applied NP most often bind to tolerance-inducing liver NPCs,which may counteract the induction of **anti-tumor responses** (by DC) in spleen/lymph nodes.

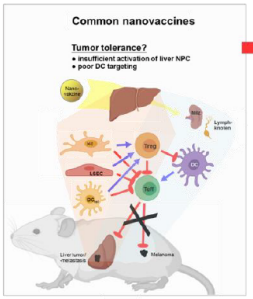

Aim

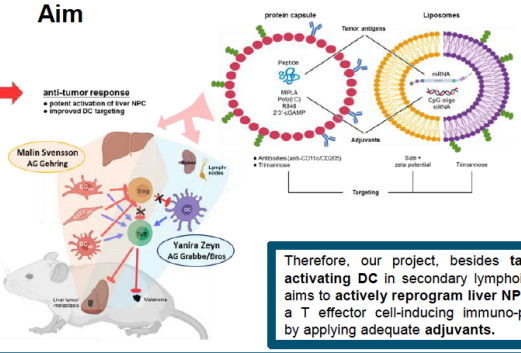

Therefore, our project, besides **targeting / activating DC** in secondary lymphoid organs, aims to **actively reprogram liver NPC** towards a T effector cell-inducing immuno-phenotype by applying adequate **adjuvants.**

Adjuvant Screening

Nucleic acid-based Adjuvants

- synthetic oligonucleotides that contain unmethylated CpG dinucleotides (CpG motifs)
- such motifs are present at a 20-fold greater frequency in bacterial DNA compared to mammalian DNA
- CpG motifs are recognized by TLR9

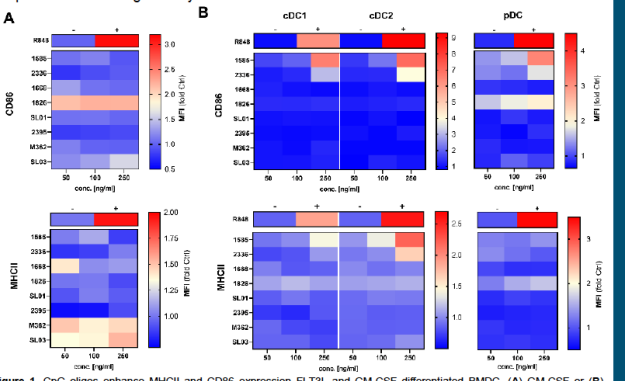

Figure 1. CpG oligos enhance MHCII and CD86 expression FLT3L and GM-CSF differentiated BMDC. (**A**) GM-CSF or (**B**) FLT3L differntiated BMDC were incubated with different concentrations of CpG oligos (50, 100 or 250 ng/ml) or the TLR 7/8 ligand R848 (1 µg/ml). On the next day, expression of MHCII and CD86 was assessed by flow cytometric analysis. Graphs denote the fluorescence intensities (**MFI**) (mean±SEM of **4** experiments) of marker expression.

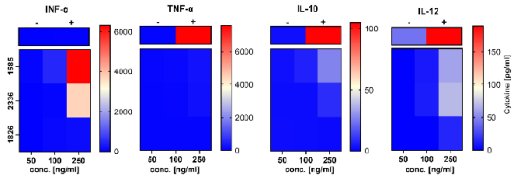

Figure 2. CpG oligos enhance proinflammatory cytokine release of FLT3L differentiated BMDC. BMDC were incubated o.n. with CpG oligos. Cytokine concentrations of culture supernatants were determined by CBA (mean±SEM of **2-3** experiments).

Other Adjuvants

Adjuvant	Agonist
R848	TLR7/8
cGAMP	STING
Poly(I:C)	TLR3

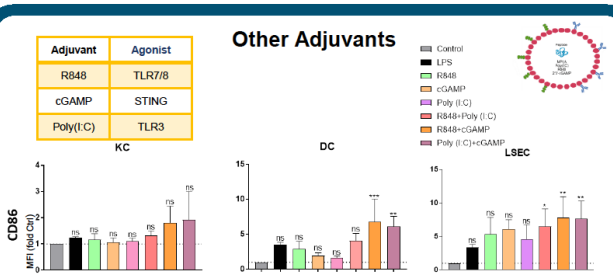

Figure 3. Adjuvant combinations enhance CD86 expression in dendritic cells (DC) and in liver sinusoidal endothelial cells (LSEC). Liver non-parenchymal cells (NPC) were incubated o.n. with adjuvants (5 µg/ml). On the next day, expression of CD86 was assessed by flow cytometric analysis. Data represented are the means ± SEM (n = 4). Significant different compared to the control: no significant difference (ns); * p < 0.05; ** p <0.01; *** p <0.001; **** p <0.0001. (One-way ANOVA).

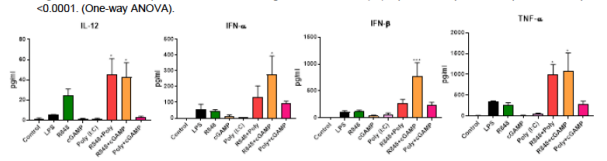

Figure 4 . Cytokine concentrations were assayed by CBA. Data represented are the means ± SEM (n = 4). Significant different compared to the control: no significant difference (ns); * p < 0.05; ** p <0.01; *** p <0.001; **** p <0.0001. (One-way ANOVA).

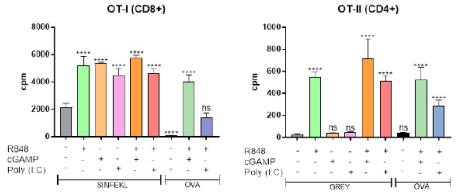

Figure 5. DC and T-cell co-cultures stimulated with adjuvant/combinations and OVA-peptide/protein led to enhanced levels of T-cell proliferation. Data represented are the means ± SEM (n = 6). Significant different compared to the control: no significant difference (ns); * p < 0.05; ** p <0.01; *** p <0.001; **** p <0.0001. (One-way ANOVA).

Conclusion

Nucleic acid-based adjuvants

- Functionally active CpG oligos (ODN1585 and ODN1826) were identified for dendritic cell populations
- In case of liver NPC and splenocytes (not shown) ODN1585, ODN2336 and ODNSL03 enhanced upregulation of activation markers
  ➢ SL03 was identified as optimal performer

Other adjuvants:

- R848, cGAMP and Poly (I:C) were the most potent adjuvants once incubated with NPC population. Combinations of these adjuvants showed synergistic effects both regarding activation markers (CD86, CD80) and cytokine secretion.

Outlook

- Test CpG oligos in combination with OVA as model antigen in co-cultures with T cells from OT-I and OT-II animals.
- Development of lipid-based nanocarriers for the encapsulation of OVA-encoded mRNA in combination with selected adjuvants

Bonan Zhao

Precise AMPK Activator Delivery and Antibody Conjugation via Novel Core-Shell Polymer Brush for Enhanced Combined Immunotherapy

Bonan Zhao[1], Ramon Arens[2], Matthias Barz[1]

[1] Division of BioTherapeutics, LACDR, Leiden University, the Netherlands

[2] Department of Immunology, Leiden University Medical Center, the Netherlands

Introduction and aim

*Combining monoclonal antibodies and small molecule drugs has shown promise as an effective approach for cancer therapeutics. However, challenges persist in optimizing the activities of monoclonal antibodies and ensuring precise delivery of small molecule drugs to tumor cells[1,2].

* To address this, we focus on designing and synthesizing a novel core shell brush(CSB) based on polysarcosine to facilitate the precise delivery of a potential drug, Compound 991, into the benzyl core through π-π interactions.

* This approach aims to enhance Compound 991's water solubility and enable its co-delivery alongside conjugated antibodies.

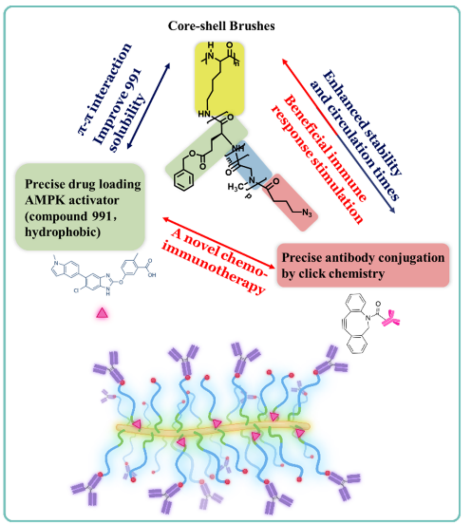

Methods and results:

Synthesis steps of CSB by ROP

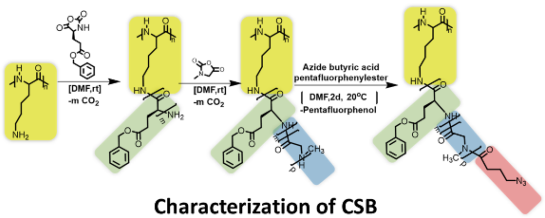

Characterization of CSB

^{1}H NMR

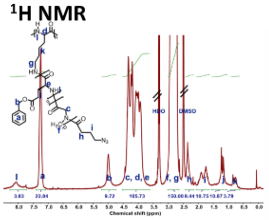

HFIP GPC

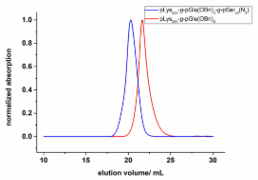

^{1}H NMR spectroscopy calculated the DP of side chains and GPC showed the narrow distribution of CSB.

References:

1. C. Kappel, M. Barz, et al. ACS Nano, 2021, 15, 9, 15191–15209.
2. T. Sluis, R. Arens, et al. Cell Rep Med, 2023, 4, 100939.

Single-angle dynamic light scattering (DLS)

V_{CSB}/V_{991} (μL/μL)	loading capacity (μg/mL) / (μM)	Size diameter (nm)	Đ (Size)
500	/	29.9±0.44	0.09
495/5	10/23	26.8±0.16	0.16
490/10	20/46	27.6±0.21	0.17
480/20	40/92	31.1±0.23	0.19
475/25	50/115	35.0±0.53	0.19
450/50	100/230	93.3±3.25	0.34

Size distribution changes showed the drug capacity of CSB.

UV/Vis

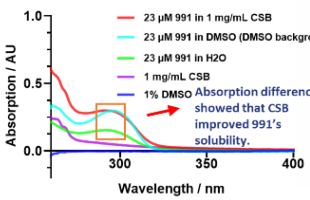

Multi-angle DLS and SLS

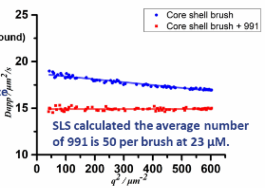

Diffusion-ordered spectroscopy (DOSY)

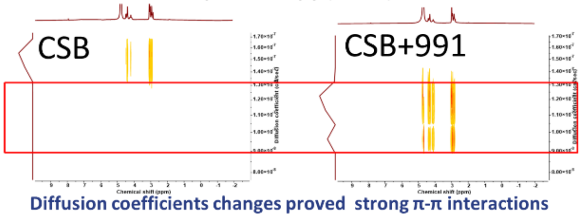

Diffusion coefficients changes proved strong π-π interactions between 991 and CSB.

Atomic force microscopy (AFM)

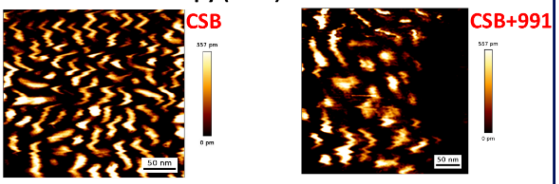

AFM visualized morphology of brushes before and after drug loading.

Biology test

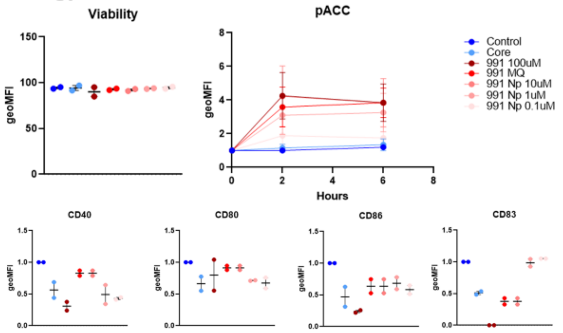

The pACC expression test indicated a strong dosage dependency of 991 loaded by CSB.

Conclusion:

* A novel core-shell brush based on polysarcosine was developed.
* The π-π interactions between drugs and brushes was proved and number of drugs per brush can be calculated.
* 991 loaded by CSB had strong dosage dependency to activate AMPK expression.

Contact information:
Email: b.zhao@lacdr.leidenuniv.nl
Web: https://barzlab.com
LinkedIn: Scan QR-code on the right

Discover the world at Leiden University

CAN WE TARGET CANCER WITH SOUND AND NANOMEDICINE?

Glucosylated Hybrid TiO_2/Polymer Nanomaterials for Targeted Sonodynamic Therapy of Cancer

TECHNION Israel Institute of Technology

Department of Materials Science and Engineering

Ivan Zlotver ✉, Alejandro Sosnik

Department of Material Science and Engineering, Technion – Israel Institute of Technology, Haifa, Israel

✉ ivan@campus.technion.ac.il

Application overview

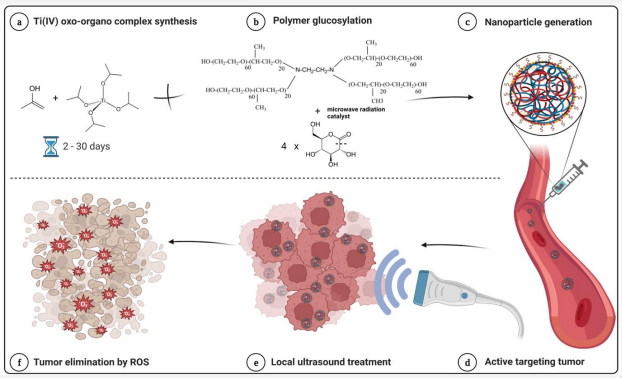

Synthesis

Size controlled synthesis of nanoparticles using mathematical model

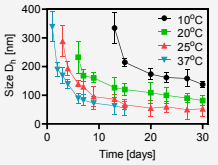

$$D = 745.27 - 51.30t - 0.05t^2 + 2.04t^3 - 0.13T - 1.09T^2 - 0.03T^3$$

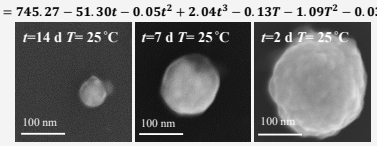

HR-TEM/EDS analysis of nanoparticles

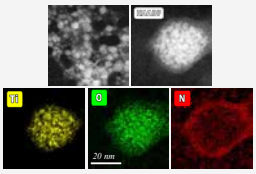

ROS generation in suspension

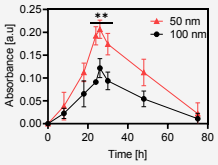

In-vitro 2D

Rh30 uptake of NPs analysis by ImageStream FACS

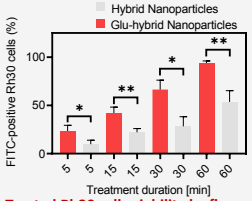

ROS levels in treated Rh30 cells

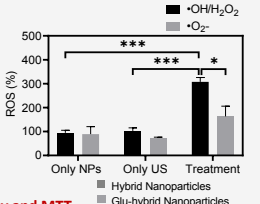

Treated Rh30 cells viability by fluorescence microscopy and MTT

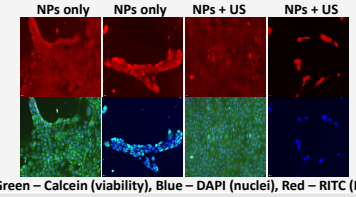

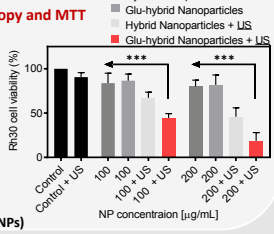

Green – Calcein (viability), Blue – DAPI (nuclei), Red – RITC (NPs)

In-vitro 3D

Rh30 spheroids uptake of NPs

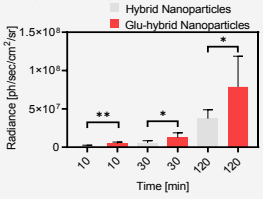

Treated Rh30 spheroids viability by ATP levels

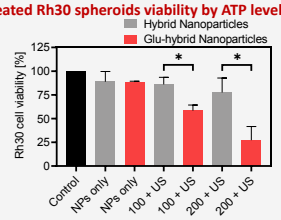

Rh30 spheroids uptake of NPs and their viability by LSFM

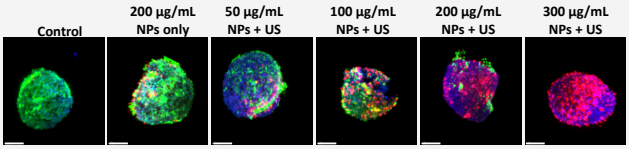

Green – Calcein (viability), Blue – DAPI (nuclei), Red – RITC (NPs)

In-vivo targeting

Biodistribution of NPs post-IV administration in mice bearing Rh30 tumors

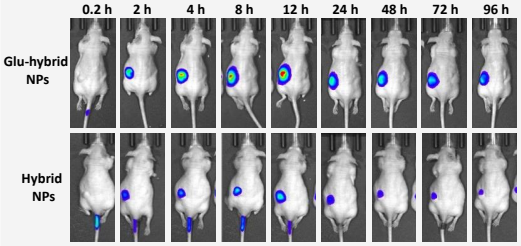

NPs accumulation in tumor

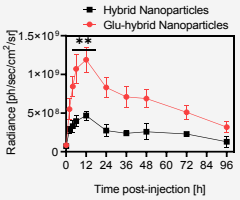

NPs accumulation in liver

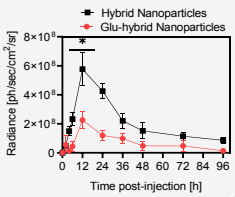

In-vivo efficacy

Survival of Rh30 tumor-bearing mice post-treatment

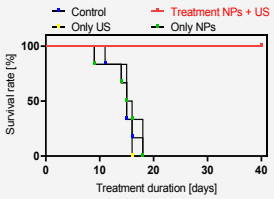

Histological examination of Rh30 tumors

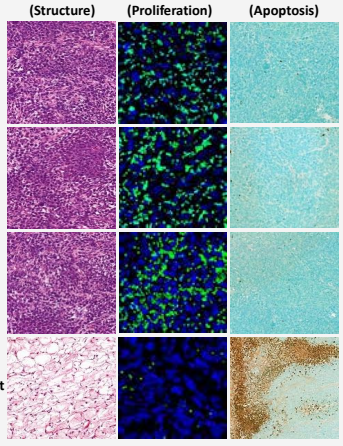

Progression of Rh30 tumors volume

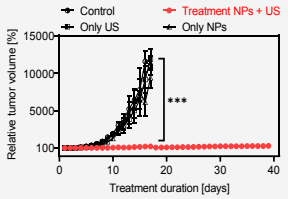

Ivan Zlotver & Alejandro Sosnik, 2023 (in press)

Conclusions

- ❑ **Modular Synthesis:** Flexible synthetic method allowing precise adjustments of nanoparticle size and surface features.
- ❑ **Surface Glucosylation :** Surface conjugation of glucose moieties boosts cancer cell targeting and further sonodynamic efficacy.
- ❑ **In Vitro 2D and 3D Efficacy:** Enhanced targeting precision and anticancer efficacy demonstrated in both 2D and 3D cell models.
- ❑ **In Vivo Tumor Efficacy:** Excellent tumor targeting demonstrated. Dramatic lifespan prolongation observed, with induced apoptosis within the tumor.
- ❑ **Therapeutic Potential:** Confirmed efficacy of the sonodynamic therapy platform, offering a foundation for solo and combination anticancer therapies.

Acknowledgments

ISRAEL SCIENCE FOUNDATION
Fundació Sant Joan de Déu
RBNI
Technion Israel Institute of Technology